GEOLOGIC AND PETROLOGIC EVIDENCE FOR GRANULITE FACIES PARTIAL MELTING IN THE GARIES-PLATBAKKIES SUPRACRUSTAL GNEISS BELT, NAMAQUALAND METAMORPHIC COMPLEX, SOUTH AFRICA.

by Franciscus Jacobus Baars

Department of Mineralogy and Geology
University of Cape Town
January 1990

Supervisors: Dr. D.J. Waters, Department of Earth Sciences,
Oxford University, United Kingdom
Dr. J.M. Moore, Department of Mineralogy and Geology
University of Cape Town, South Africa

Thesis submitted in fulfilment of the requirements for the degree of Master of Science at the University of Cape Town, South Africa

" ... and de rocks, dey will be meltin' "

Bob Marley

CONTENTS

ABSTRACT

The Namaqua Province of southwestern Africa is comprised of a number of distinct tectonostratigraphic subprovinces and terranes, which have in common a 1100-1200Ma structural and metamorphic imprint. In the western Bushmanland Subprovince, E-W-trending belts of supracrustal gneisses are intruded by and infolded with granitic gneisses of varying ages. A central zone of rocks metamorphosed in the granulite facies is bordered to the north and south by amphibolite facies rocks.

A portion of the Garies-Platbakkies supracrustal gneiss belt has been mapped on a 1:15 000 scale. The supracrustal succession was deposited on an unconfirmed basement. It is structurally juxtaposed and infolded with three different granitic augen gneisses. Large bodies of orthopyroxene-bearing granite are syntectonically emplaced in the succession. A wide variety of anatectic granites crop out as sills, dykes and pods varying in size between a few metres and a few hundred metres. These bodies commonly truncate pre-existing foliations.

The metamorphosed supracrustal succession contains gneissic equivalents of felsic, mafic and intermediate volanics; pelitic, semi-pelitic, magnesian and granitic composition sediments; feldspathic quartzites; and subordinate quartzites, banded iron formation and calc-silicates. The mineral assemblages of all the rocks indicate metamorphism in the granulite facies. A variety of field evidence exists which suggests that the metamorphic peak

was responsible for generating significant quantities of partial melt.

The rocks of the study area contain an early D1 fabric. This is refolded in tight, E-plunging D2 crenulation folds. D2 mineral fabrics pre-date the metamorphic peak. D3 open, asymmetric folds are N-vergent and fold the crystalline products partial melting. The southern limbs of D3-folds are attenuated in D4 shear zones. The whole belt is cut by steep, N-S-trending faults.

A wide variety of thermobarometers are tested for their applicability to mineral assemblages in the supracrustal rocks. The results of this application suggest that the metamorphic peak occurred at 780 $\pm$ 30^{o}C and 5.0 $\pm$ 0.4 kbar. Assemblages in shear zones indicate an isobaric retrograde cooling path.

The phase relations of melting near the solidus are reviewed with reference to common assemblages in the leucosomes of rocks with granitic and peraluminous bulk compositions. Isobaric T-a(H_2O) sections are constructed from available experimental and thermochemical data. Biotite dehydration and dehydration melting reactions are balanced using natural mineral compositions. The predicted results are compared with the modal abundances of natural product assemblages. The results suggest that dehydration melting was responsible for migmatization, and the consequent reduction of water activity. The amount of melt produced was

controlled by the amount of water available from the dehydration of biotite. There is no evidence for the control of water activity by an external fluid reservoir.

Limited amounts of water-undersaturated melts were extracted from their sites of generation. This process was responsible for the depletion of some leucosome assemblages with respect to K_2O, H_2O and in peraluminous rocks Na_2O. The partial melts were emplaced locally in developing shear zones.

LIST OF ABBREVIATIONS

Minerals (after Kretz, 1983)

Ab = albite
Alm = almandine
An = anorthite
Ap = apatite
Bt = biotite
Cal = calcite
Chl = chlorite
Cld = chlortoid
Crn = corundum
Czo = clinozoisite
Di = diopside
Dsp = diaspore
En = enstatite
Ep = epidote
Fs = ferrosillite
Fsp = feldspar
Grs = grossularite
Grt = garnet
Hbl = hornblende
Hc = hercynite
Hem = hematite
Ilm = ilmenite
Kfs = K-feldspar
Mag or Mgt = magnetite
Ms = muscovite
Opq = opaque
Opx = orthopyroxene
Or = orthoclase
Phl = phlogopite
Pl = plagioclase
Py = pyrope
Qtz = quartz
Rt = rutile
Scp = scapolite
Sil = sillimanite
Spr = sapphirine
Srp = serpentine
Ts = tschermakite
Wo = wollastonite
Zrn = zircon

Other

The Periodic Table

S.I. units

a = activity

Fig = figure

K_D = distribution coefficient

MF = 100Mg/(Mg + Fe)

nd = not detected

P = pressure

Pers. comm. = personal communication

T = temperature

Unpubl. = unpublished

Wt.% = weight percent

X = mole fraction

LIST OF FIGURES

Legend for Figs. 2.2, 2.3, 2.4, 2.5:

Coarse stipple - garnet; close stipple - hercynite-magnetite; fine stipple - cordierite; edge stipple - feldspar; dashed - biotite; small euhedra - sillimanite; clear - quartz.

Fig. 2.2a Poikiloblastic garnet in aluminous quartzofeldspathic gneiss FB266C.

2.2b Poikiloblastic garnet, overgrown by radiating skeletal garnet-quartz and biotite-quartz intergrowths, surrounded by orthopyroxene in garnet-biotite-orthopyroxene anatectic granite FB71.

Fig. 2.3a Coarse garnet poikiloblasts with refoliated biotite flakes in garnet-biotite metapelitic gneiss DWN 673.

2.3b Sillimanite rims around magnetite-hercynite-quartz associations in cordierite-bearing metapelitic gneiss FB109.

2.3c Acicular sillimanite overgrowths on cordierite and hercynite in shear foliations of metapelitic gneiss DWN679.

Fig. 2.4a Vermicular hercynite-magnetite intergrowths with orthopyroxene and cordierite, near garnet porphyroblast and blocky hercynite-magnteite association with cordierite rim in magnesian gneiss FB26.

2.4b Cordierite-orthopyroxene association with phlogopite in magnesian gneiss FB10.

Fig. 2.5a Equant orthopyroxene grains truncating biotite foliation biotite-orthopyroxene leucoparagneiss FB170.

2.5b Skeletal biotite-quartz intergrowths surrounding orthopyroxene in biotite-orthopyroxene leucoparagneiss FB256.

Fig. 3.1 Composite plot on a Schmid steroenet of structural elements measured in the study area. See text for discussion.

Fig. 4.1 P-T conditions of stability of the assemblage

Grt-Pl-Sil-Qtz in FB210

using the geothermobarometer calibrations of

A - Ghent (1976)

B - Newton and Haselton (1981)

C - Powell and Holland (1988);

and of the assemblage Grt-Hc-Sil-Qtz in FB210

using the calibration of

D - Perkins and Chipera (1985).

Dashed arrow indicates possible retrograde P-T path.

Fig. 4.2 P-T conditions of stability, with errors, of the assemblage

Grt-Opx-Pl-Qtz in FB71

using the geothermobarometer calibrations of

A - Newton and Perkins (1982)

B - Powell and Holland (1988)

C - Harley and Green (1982)

D - Harley (1984b);

and using the Fe-Mg exchange thermometer of

E - Sen and Bhattacharya (1985).

Fig. 4.3 Pressures calculated for a cordierite-hercynite pair co-existing with quartz in FB210, using the calibration of Bhattacharya (1986). This calibration is sensitive to $X(H_2O)$(Crd).The dashed line at relatively low P shows the P-T conditions of stability of Fe-Mg exchange of the same pair using the calibration of Vielzeuf (1983).

Fig. 4.4 Ternary feldspar and mesoperthite compositions from magnesian gneisses DWN552 and RW4. Solid curves are the isotherms of Lofgren and Gooley (1977). Dashed curves are the approximate isotherms of Fuhrman and Lindsley (1988).

Fig. 4.5 Summary of the P and T estimates of the peak of Namaqua metamorphism in the study area. Numbers indicated alongside each bar refer to the T or P bracket in which each barometer and thermometer was calibrated, respectively. The shaded regions are the estimated peak conditions using all these results. See overleaf for list of author abbreviations.

Fig. 4.6 The variation of pressure and temperature estimates of the peak of metamorphism along an approximately N-S traverse across the western Bushmanland Subprovince (c.f. text and Fig. 1.2)

Fig. 5.1 Projection from quartz, plagioclase and H_2O in the system CNKFMASH of the compositions of biotite and orthopyroxene in rocks with granitic bulk compositions.

Fig. 5.2 The variation of F(Bt) and Ti(Bt) with X_{Mg}(Bt) in rocks with granitic bulk compositions. The annotations refer to the rocks of Fig. 5.1. Best-fit straight lines of the data are given with correlation coefficients.

Fig. 5.3 Projection from quartz, plagioclase, K-feldspar and H_2O in the system CNKFMASH of the compositions of biotite and garnet in FB266A and DWN673, rocks with peraluminous bulk compositions.

Fig. 5.4 The variation of F(Bt) and Ti(Bt) with X_{Mg}(Bt) in rocks with peraluminous bulk compositions FB266A and DWN673. Best-fit straight lines of the data are given with correlation coefficients.

Fig. 5.5 The phase relationships involving the assemblage Bt-Opx-Qtz-Kfs-Pl-H_2O-L shown schematically in P-T space after Luth (1967), Bohlen et al. (1983a), Grant (1986a, b).

Fig. 5.6 Experimental and thermodynamic constraints on the phase relationships in an isobaric T-a(H_2O) section at 5 kbar through Fig.5.5. See overleaf for a list of the references used and an explanation of reaction names. The numeric prefix to each reference is the X_{Mg}(Bt) used.

Fig. 5.7 A best-fit calibration of the data shown on Fig. 5.6, in terms of Fe- (light lines) and Mg- (heavy lines) end-member reactions in T-a(H_2O) space. Dashed lines of reaction (L) indicate that it is metastable with respect to melting. Reaction (V) is calibrated in terms of X_{Mg}(Bt). See text for discussion.

Fig. 5.8 Phase relationships involving the assemblage Bt-Grt-Sil-Qtz-Kfs-Pl-L-H_2O shown schematically in P-T space after Grant (1973, 1985a, b), Thompson (1976, 1982), Vielzeuf and Boivin (1984) and Speer and Cheney (1988).

Fig. 5.9 Experimental and thermodynamic constraints on the phase relationships of an isobaric T-a(H_2O) section at 5 kbar through Fig. 5.8. See overleaf for a list of the references used and an explanation of the reaction labels. The prefix number to each reference refers to the X_{Mg}(Bt) used.

Fig. 5.10 A best-fit calibration of the reaction constraints shown on Fig. 5.9 in terms of $X_{Mg}(Bt) = 0.4$ (light lines) and $X_{Mg}(Bt) = 0.8$ (heavy lines). Dashed curves of reaction (L) indicate that it is metastable with respect to melting. Reaction (V) is calibrated in terms of $X_{Mg}(Bt)$.

Fig. 5.11 A simplified outcrop map of migmatitic garnet-biotite metapelitic gneiss FBM2. The marked off areas indicate matrix- and leucosome-dominated, and intermediate geometric portions of the outcrop. See Appendix 2 for an explanation of the method of estimation of the modal proportions of this rock.

Fig. 5.12a Plot of the ratios of modal proportions G/M against L/M in the different zones of FBM2 on Fig. 5.11. The points define a straight line with slope G/L = 0.14. Point T, the total modal proportions of the sample, is shown for reference.

Fig. 5.12b Logarithmically scaled plot of the ratios of modal proportions G/M against L/M in the different zones of FBM2 shown on Fig. 5.11. The circle radii of each data point are propotional to the sample size in each zone. The best-fit straight line through these points is strongly weighted to larger sample sizes, and has a slope of +1.0. This confirms the constant G/L ratio indicated on Fig. 5.12a.

Fig. 5.13a An 'isochon' diagram (Grant, 1986a) comparing the observed modal proportions of a leucosome in Bt-Opx leucoparagneiss FB256against those predicted by mass balance calculations on the biotite-rich matrix (Appendix 3B). Gains and losses refer to those of the leucosome relative to the matrix.

Fig. 5.13b An 'isochon' diagram (Grant, 1986a) comparing the observed modal proportions of a leucosome in Grt-Bt meta-pelitic gneiss DWN673 against those predicted by mass balance calculations on the biotite-rich (Appendix 3D). Gains and losses refer to those of the leucosome relative to the matrix.

Fig. 6.1 A semi-quantitative P-T-time path for the granulites of the field area, adapted after Waters (1989). The numbers refer to events summarized in section 6.2. Their order indicates the direction of the path The letters in the P-T boxes are the different metamorphic facies of western Bushmanland (Fig. 1.2, from Waters, 1986).

LIST OF TABLES

LIST OF PLATES

Plate 6. Discordant leucosome, containing orthopyroxene (light green-brown), clinopyroxene (dark green-black) and plagioclase (white to pale blue), in hornblende-pyroxene granulite gneiss. Hammer shaft is 83 cm.

Plate 7. An ovoid leucosome patch, containing rhombododecahedra of garnet intergrown with quartz, and surrounded by an anhydrous, quartzofeldspathic halo, in garnet-biotite quartzofeldspathic gneiss. Compass pouch is 8 cm wide.

Plate 8. Garnetiferous and entirely quartzofeldspathic leucosomes occurring as crenulated compositional bands in garnet-biotite metapelitic gneiss. At left, a coarse-grained garnetiferous leucosome transgresses compositional banding and regional foliation. A K-feldspar-rich, pegmatitic vein occurs at the base of the outcrop, containing rootless stringers of matrix gneiss. Hammer shaft is 29 cm.

Plate 9. Unzoned leucosomes occurring parallel to the regional, gneissic banding and foliation in garnet-biotite metapelitic gneiss. Note that many garnet grains intersect matrix-leucosome boundaries, but are always surrounded by, at least a narrow anhydrous halo. Hammer shaft is 29 cm.

Plate 10. Cross-section of a anatectic granite sill root zone in garnet-biotite metapeltic gneiss. Note the nebulitic internal structure of disjointed matrix stringers. Hammer shaft is 29 cm.

Plate 11. Coarse-grained orthopyroxene-K-feldspar leucosome patches in orthopyroxene-cordierite-phlogopite magnesian gneiss. Hammer shaft is 29 cm.

Plate 12. Transgressive, orthopyroxene-bearing quartzofeldspathic leucosome in biotite-orthopyroxene leucoparagneiss. Hammer head is 18 cm.

Plate 13. Vein and patch leucosomes, subparallel to regional foliation in biotite-orthopyroxene leucoparagneiss. The dark patches in both matrix and leucosome assemblages are orthopyroxene-biotite intergrowths. Hammer shaft is 29 cm.

Plate 14. Boudin-like, quartzofeldspathic sill in banded quartzofeldspathic gneiss. It is not clear whether these structures are igneous (i.e. pinch-and-swell) or truely tectonic (i.e. stretching boudins) in origin. Hammer head is 18 cm.

LIST OF APPENDICES

Appendix 3. Mass and Volume Balance Calculations

Assumptions and Constraints

3A. Biotite dehydration in FB48

3B. Biotite dehydration melting in FB1

3C. Biotite dehydration in FB266A

3D. Biotite dehydration melting in DWN673

Appendix 4. Publications

4A. Baars (1988)

Partial melting in granitic and supracrustal gneisses of the central Namaqualand Metamorphic Complex

4B. Waters and Baars (1989)

Melt extraction from granulite facies migmatites

CHAPTER 1 INTRODUCTION

1.1 The Problem - Granulite Facies Migmatization

Understanding of the origin of granulite facies terranes has increased enormously during recent years. It is generally believed that they formed in response to regional metamorphic events at pressures corresponding to depths between 15 and 35 km in continental crust (Bohlen, 1987; Ellis, 1987; Harley, 1989). While the heat sources and thermal evolution paths of these terranes differ widely, granulite facies metamorphism takes place at temperatures above 600°C and at significantly reduced water activity or $P(H_2O)$ (Harley, 1989).

Fluid behaviour is now known to have had a profound effect on the character of granulite terranes. The anhydrous mineral assemblages of many rocks in Precambrian granulite terranes are the products of prograde dehydration reactions at the amphibolite -granulite facies boundary (e.g. Waters and Whales, 1984; Sandiford, 1985a). Under the influence of increasing water activity and changing bulk rock compositions, these reactions become metastable with respect to melting (Grant 1985a, b; Johannes, 1988). The result is that granulite facies assemblages can co-exist with the crystalline products metamorphic partial melting.

A number of models have been proposed to account for the low

water activity indicated by the persistence of granulite facies assemblages to temperatures above granite melt stability (Waters, 1988). In an open system, volumes of melt may be efficiently extracted leaving an anhydrous granulite facies residue (Fyfe, 1973; Powell, 1983). Sufficiently large volumes of extracted melt may cause the destabiliztaion of the rock mass at the site of emplacement (Wickham, 1987).

Alternatively, water activity may be reduced by passing large volumes of carbon dioxide, or some other non-hydrous fluid, through relatively non-porous granite-gneissic crust. The resulting mixed fluid tends to maintain equilibrium with an anhydrous granulite assemblage, which will partially melt at temperatures above the minimum melting temperature for a particular rock composition. This model of open system behaviour has been proposed by many workers for the granulite facies rocks of the Indian Shield (e.g. Janardhan et al. 1979; Newton et al., 1980).

Lamb and Valley (1984, 1985) suggested that the granulite facies rocks of the Adirondacks were produced by entirely vapour-absent processes, because the precursor rocks were already dry at the time of onset of granulite facies conditions. Frost and Frost (1987) indicated that the passage of high temperature and strongly water-undersaturated magmas would cause both the dehydration of and the channelized passing of CO_2-rich fluids

through the country rock.

In a compositionally and texturally banded metamorphic rock pile, water released from dehydrating amphibolite facies minerals can concentrate in particular lithologies. When these melt at relatively low, water-saturated temperatures during prograde metamorphism, the system's excess water dissolves in the resulting silicate liquid. On cooling and recrystallization of the melt, this water may be trapped in fluid inclusions or hydrous minerals, or cause local retrograde rehydration. This closed system mechanism is believed to have formed stromatic, or layered migmatites at, for instance, Nelaug, Norway (Johannes and Gupta, 1982; Johannes, 1988). This model infers closed system behaviour on a large scale (Baars, 1988; Waters, 1988)

In the Garies-Platbakkies supracustal gneiss belt of the Central Namaqualand Metamorphic Complex, the presence of vein and patch migmatites has been interpreted as being evidence for metamorphic partial melting (Baars, 1986, 1988; Waters, 1986, 1988). This project aims to constrain the geologic history of the belt in terms of its intrusive, deformational and metamorphic evolution on the basis of detailed field mapping and petrographic analysis. In this context, it is possible to investigate evidence for partial melting, or migmatisation, and test the applicability of the above models to Namaqua regional metamorphism. Ultimately, this will place valuable constraints on the nature of this metamorphism, and particularly on the role of metamorphic fluids.

The nature of intrusive activity during and after metamorphism will provide evidence for the tectonic setting of the Namaqua event, and on the formation and stabilisation of that continental crust.

1.2 Regional Geology - The Namaqualand Metamorphic Complex

This summary draws on the historical reviews of the Namaqualand Metamorphic Complex by Joubert (1971, 1986), Tankard et al. (1982), Botha (1983), Albat (1984), Hartnady et al. (1985) and Watkeys (1986).

The Complex is an early and mid-Proterozoic province in southwestern Africa that is the western arm of the Namaqua-Natal Province. It flanks the western and southern boundaries of the Kaapvaal Craton (Fig. 1.1, after Stowe, 1984; Stowe et al., 1984; Hartnady et al., 1985). The Namaqua Province has been subdivided into a number of distinct tectonostratigraphic subprovinces and terranes.

In the west, the Richtersveld Subprovince is separated from the Gordonia Subprovince along the WNW-ESE-trending Tantalite Valley Belt near the Pofadder Lineament. The Richtersveld Subprovince contains the 2.0 Ga Orange River Group supracrustal sequence (Clifford et al., 1975; Reid, 1979b; Reid et al., 1987a, b; Betton, 1984) and the Vioolsdrif, Richtersveld and Goodhouse Intrusive Suites (Blignaut, 1977; Reid, 1979; Reid and Barton,

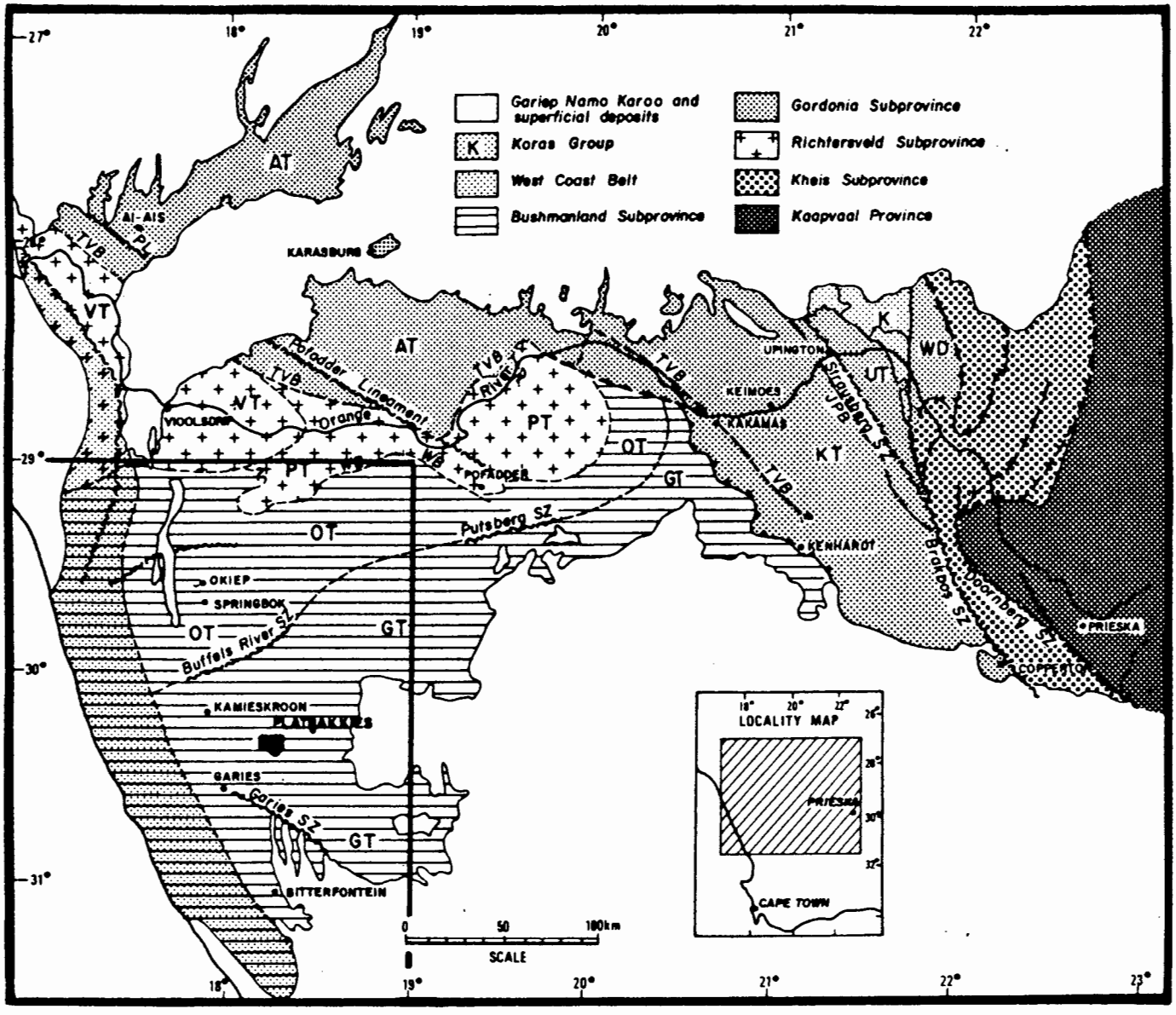

Fig. 1.1 The geology of the Namaqua Province, South Africa, showing the major Suprovinces and tectonostratigraphic terranes after Stowe (1984), Stowe et al. (1984), Hartnady et al. (1985). Locality of Fig. 1.2 shown. OT - Okiep Terrane; GT - Garies Terrane; KT - Kakamas Terrane; UP - Upington Terrane; AT - Ai-Ais Terrane; TVB - Tantalite Valley Belt; PL - Pofadder Lineament.

1983). The Gordonia Subprovince consists of Proterozoic rocks. Bifurcating shear zones with north-west trends, which segment the terrane, are deformed against the complex Kheis Belt (Watkeys, 1986; Stowe, 1986, 1988). The latter structurally overlies the Kaapvaal Craton in the west along a thrust contact. The northern margins of the Gordonia Suprovince are obscured under the cover of the late Precambrian Nama Group (Tankard et al., 1982; Stowe, 1986). The Grunau Sequence at Aus and Luderitz in Namibia is considered to be the western extension of the Gordonia Subprovince (Joubert, 1986).

The Bushmanland Subprovince is structurally overlain in the north by the Richtersveld Subprovince along the Groothoek thrust zone (Stowe, 1984; Strydom, 1985; Strydom and Visser, 1986; Grutter, 1986; Watkeys, 1988; Van Der Merwe and Botha, 1989) and to the east by the Gordonia Subprovince along the Hartbees thrust zone (Harris, 1988). The Proterozoic rocks of the Bushmanland Subprovince have been divided into three terranes. The Okiep and Garies Terranes are separated by the Buffels River and the Putsberg Shear Zones. These terranes are separated on the basis that they contain different supracrustal sequences, in that quartzites are concentrated in the Okiep Terrane (Joubert, 1986). However, many researchers now believe that this distinction merely reflects regional sedimentary facies changes, and that the terrane boundary is a late Proterozoic feature (Moore, 1986; McStay, in prep.; Stowe, pers. comm.). Recently some workers have

considered the Steinkopf Terrane to be a structural enclave against the Richtersveld Subprovince (Tankard et al., 1982; Joubert, 1986; Van Aswegen, 1988). It contains the distinctive Gladkop Intrusive Suite (Joubert, 1974a; Reid and Barton, 1983). The Steinkopf Terrane is separated from the Okiep Terrane along the Ratelpoort Shear Zone (Joubert, 1971, 1974c, 1986; Watkeys, 1986).

The Bushmanland Subprovince comprises largely granitic rocks of Kibaran age (1400 - 1100 Ma: e.g. Joubert, 1974b, 1986; Clifford et al., 1975, 1981; Tankard et al., 1982; Hawkesworth et al., 1984; Harris et al., 1987) (Fig. 1.2). These are intrusive into and infolded with E-W-trending belts of supracrustal rocks (Joubert, 1971, 1974b, 1986). The supracrustal rocks are the key to understanding the metamorphic evolution of the Bushmanland Subprovince (e.g. Waters, 1986a, b). There is as yet no confirmed recognition of a basement to the supracrustal rocks, although certain candidates have been proposed (section 2.6; Watkeys, 1986).

The work of Strauss (1941), Joubert (1971), Moore (1986) and Praekelt and Colliston (1988) has allowed the recognition of regional stratigraphic trends in the Bushmanland Subprovince supracrustal rocks. On the scale of the regional distribution of these successions, and in view of their intense deformation and high grade of metamorphism, variations in the strict stratigraphic sequence are expected and observed (e.g. SACS,

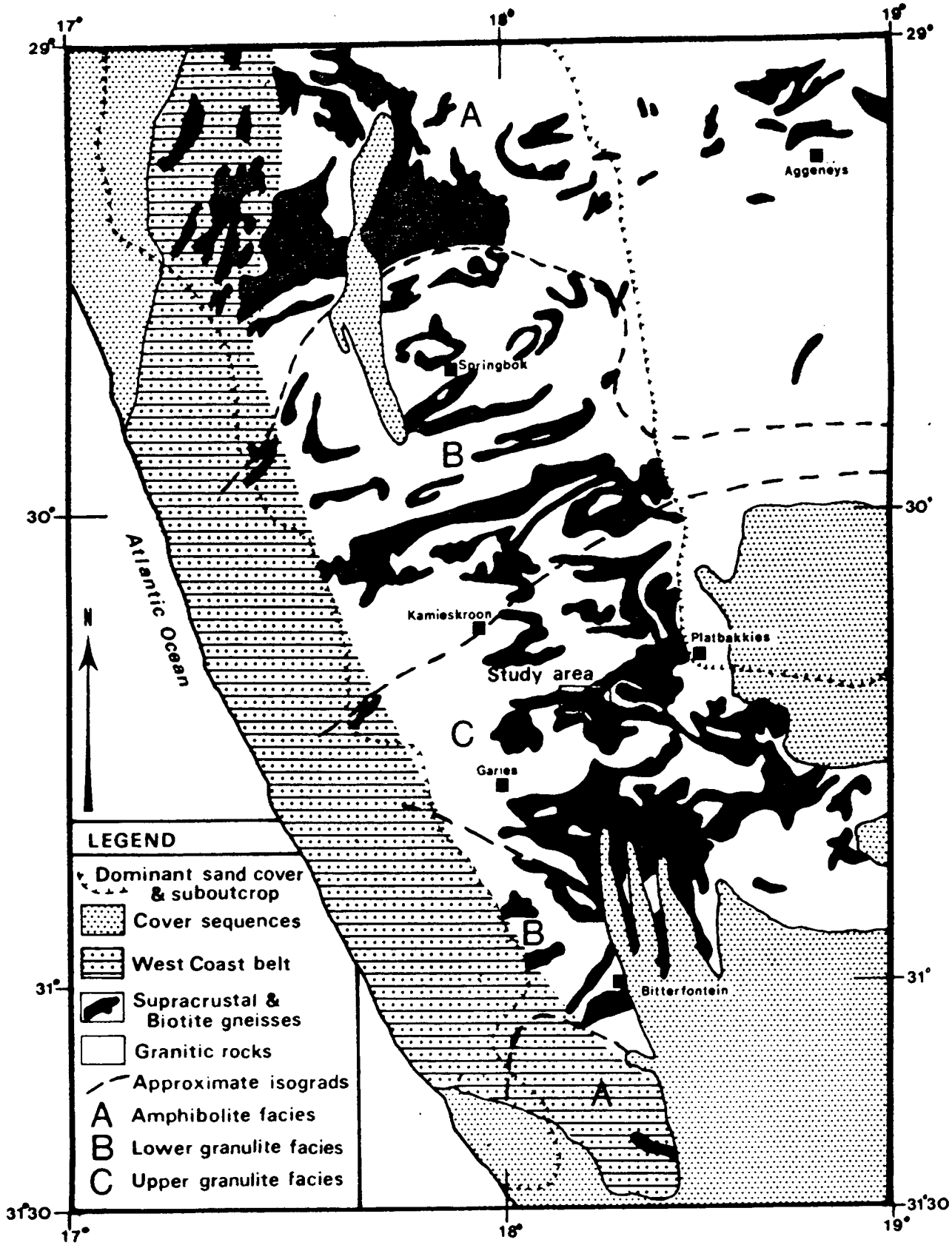

Fig. 1.2 The geology of the western Bushmanland Subprovince showing the distribution of granitic and supracrustal rocks after Joubert (1986). The distribution of metamorphic facies is after Waters (1986b).

1980; Moore, 1986; McStay, in prep.; this study). The mineral assemblages, in particular of the metapelitic and metavolcanic rock types, reveal a pattern of E-W-trending metamorphic zones (Fig. 1.2, after Waters, 1986). The central granulite facies rocks are enclosed to the north and south by rocks metamorphosed in the amphibolite facies. This study focuses on the geologic history of a portion of a supracrustal belt, here named the Garies-Platbakkies Belt, in the gneissic, upper granulite facies zone.

Very little geologic work has been performed in this field area. De Jager and Simpson (1962) described the occurrence of wollastonite in the same belt. Joubert (1971) mapped (1:100 000) the belt as a shear zone in the granite-gneiss complex. He recognised the presence of a number of different granitic varieties in the area, most of them being emplaced syntectonically. Moore (unpubl. data) provided a more detailed map (1:50 000) of a portion of the belt. Moore (1986) analysed bulk samples of some of the supracrustal rocks, and concluded that the metapelitic and related rocks were of sedimentary origin, while the 'pink' homogeneous K-feldspar-quartz gneisses were probably metamorphosed felsic volcanics. Albat (1984) mapped (1:100 000) a large area to the east, and proposed a geologic history for those rocks. Waters (1986) studied the metamorphic evolution of some of the metapelitic and magnesian gneisses from the belt. Baars (1986) mapped (1:10 000) a small area of the

belt, and it is this work that provided the background to the present study.

1.3 Acknowledgements

I thank Dr. Dave Waters for his stimulating instruction in metamorphic petrology, particularly in respect of granulite facies metamorphism. Dr. John Moore originally found the field area, and provided guidance in Dr. Waters's absence. Their constructive critcisms greatly improved the manuscript. Discussions with, critical reviews of work by, and the consistent support of my colleagues Jon McStay, Huw Humphreys, Peter Siegfried, Herman Grutter and Ian Ransome have been invaluable to the progress of this study. Profs. Clive Stowe and Maarten de Wit maintained an avid interest in the project.

My special thanks and warmth go to Messrs. Gerrit Visser, Samuel Saul, Abraham Visser and Gerrit Visser, and their families, whose hospitality provided for many comfortable nights camping on their farms Witwater and Rooiwal. Permission to work on the land was also granted by Messrs. N.J. Dreyer, K. Dreyer (whose general store was a treasure-house of supplies at all times!), G. Visser, G. Schreuder, G. Schreuder, G. Schreuder, A. Schreuder (I kid you not!), J. Kriel and the Paulshoek Community.

I thank Dick Rickard for his guidance on using the CAMECA electron microprobe, and for ensuring the best quality of data

possible. Thanks go to Prof. Andy Duncan and Dave Hill for putting up with my 'hacking' on the HP9000 Computer of the U.C.T. Dept. of Geochemistry.

Sarah Ward, Mandy Uys, Roddy Sauls and Margie Tonin assisted with some of the draughting and colouring. Rose Kovats was always willing to provide advice and draughting resources. Gizella Weich produced the photographic plates, and Charles Basson assisted. Annette Collins typed the tables. This work was made possible by the efficient and generous printing services provided by Patrick Sieas and Joe Apollis. Robert Oliver, Henry Hendriks and David Wilson prepared the petrographic samples. Peter Meyer, Neville Buchanan and Ivan Wilson were always ready to help with field preparation. Shirley Whitmore provided the administrative backing to all the work.

The research towards this thesis was adequately supported by grants from the CSIR's FRD NW Cape research program, and from the University of Cape Town's research funds granted to Dr. Dave Waters. The Council for Mineral Technology (MINTEK, Randburg) gave permission for the my post-graduate studies.

1.4 Publications

Work towards this thesis was presented orally and as a poster at the 7th International Gondwana Symposium, Sao Paulo, Brazil, 18 -

22 July, 1988. An abstract entitled

Partial melting in granitic and supracrustal gneisses of the Central Namaqualand Metamorphic Complex, South Africa.

is enclosed (Appendix 4A). The poster is currently on display in the Dept. of Geology. The financial assistance of MINTEK, through Dr. J.P.R. de Villiers and Mrs. A. Wedepohl, and of the Symposium Organising Committee, through Prof. A.C. Rocha-Campos and Dr. P. Santos (Institute of Geosciences, University of Sao Paulo), is gratefully acknowledged. U.C.T. provided the costs of poster production. I bore all other expenses. While the contents of the presentation have changed slightly, after more fieldwork and research, the essence of the conclusions remains unchanged.

Partial melting data was included in a co-authored presentation by Dr. Dave Waters at the 28th International Geological Congress, Washington D.C., 9-19 July, 1989. An abstract entitled

Melt extraction from granulite facies migmatites.

is enclosed (Appendix 4B).

CHAPTER 2 LITHOLOGIES AND PETROGRAPHY

2.1 Introduction

An area of 47.5 km^2 between $18^{o}10'40"E$ and $18^{o}19'20"E$, and $30^{o}22'30"S$ and $30^{o}27'40"S$ at Witwater, between Garies and Platbakkies, Namaqualand, has been geologically and structurally mapped on a 1:15 000 scale (see enclosure). Reconnaissance mapping (1:50 000), based on aerial photography, sporadic ground control, and previous mapping (Joubert, 1971; Moore, 1986), provided additional information for a total area of ca. 225 km^2. Overlapping photographs and strips were used in the field to minimise image distortion. A total of twenty weeks' field work was completed. Samples of the entire range of exposed and mapped rock types, including some collected by Drs. John Moore and Dave Waters provided material for 273 thin and polished sections, which were examined using a Leitz monocular, petrographic microscope. The localities of all samples referred to in the text, tables and appendices are shown on the 1:15 000 map.

The area contains outcrops of a wide variety of ortho- and paragneisses. The regional reconnaissance work of Joubert (1971) identified the lithologies of the belt as being sheared rocks, many of supracrustal origin. Moore (1986, unpubl. data) identified metapelitic, mafic and felsic metavolcanic, calc-silicate, quartzofeldspathic, magnesian and granitic supracrustal rock compositions from the belt. Their maps served as initial

field guides. SACS (1980) classifies the granitic gneisses of the area with the Little Namaqualand Suite and the supracrustal gneisses as part of the Garies Subgroup. The geology of an area on Rooiwal farm in the east of the field area was studied for an Honours project (Baars, 1986). The field and petrographic relationships of the rocks are described below.

2.2 Granite, Gneiss and Migmatite Nomenclature

At the outset, it is necessary to define the use of the terms 'granite' and 'gneiss', and to explain 'migmatite' terminology.

Streckeisen (1967; 1973) presented recommendations for the classification of plutonic rocks. 'Granites' (sensu stricto) contain between 20% and 60% normative quartz, K-feldspar: plagioclase ratios between 9:1 and 7:13, and mafic mineral contents of <10%. In the field area, the set of criteria used to identify rocks of granitic compositions as having igneous origins (section 2.3) is:

a) intrusive country rock relationships;
b) compositional homogeneity;
c) the absence of compositional banding;
d) the presence of phenocrysts or augen;
e) seriate textures; and
f) the presence of xenoliths.

Granites are additionally named by an appropriate prefixed word, according to their mafic mineralogy. The term 'charnockite' (e.g. De Waard, 1969, 1973; Tobi, 1971; Winkler and Sen, 1973) has been avoided for orthopyroxene-bearing rocks with a granitic bulk composition. It is suggested that this term be restricted in application to the Kliprand Suite-type granitic intrusives (SACS, 1980), for which the igneous origin of orthopyroxene is not in dispute (Joubert, 1971; Albat, 1984; Andreoliet al., 1987).

The term 'gneiss' is used for rocks that are compositionally banded and that are characterised by the alternation of a schistose mineral foliation with bands of granular minerals (De Waard, 1973; Winkler and Sen, 1973). The word is also used, as a suffixed term, for granites with a marked mineral foliation. The recommendations appearing in the review of Paterson et al. (1989b) of criteria for the recognition of igneous and metamorphic textures in gneissose terranes, are followed (sections 2.3, 5.2.2). The term 'granulite' is used only for mafic gneisses containing two pyroxenes, the index mineral assemblage of rocks metamorphosed in the granulite facies (e.g. Winkler, 1971; Miyashiro, 1973; Winkler and Sen, 1973; Turner, 1981; Best, 1982).

Mehnert (1968) defined the term 'migmatite', and developed a nomenclature for 'migmatite' description. This study follows the revised definitions of Ashworth and McLellan (1985) and Johannes (1988):

a) 'Leucosome': the leucocratic lithology of a migmatite

suite having a plutonic appearance, and commonly containing one or more ferromagnesian minerals.

b) 'Mesosome' or 'matrix': the mesocratic lithology of a migmatite suite having a gneissose or schistose appearance.

c) 'Stromatic': a banded or layered disposition of leucosomes and and mesosomes.

The term 'segregation' (Baars, 1986, 1988; Waters, 1988) is not used for leucosomes, because of the genetic implications of mass transfer (e.g. Robin, 1979). The terms 'melanosome', 'neosome', 'paleosome' and 'selvage' (e.g. Olsen, 1987; Johannes and Gupta, 1982; Johannes, 1988) are not readily applicable. The term 'anatectic' refers to granites whose field and chemical characteristics suggest their origin as the crystalline products of partial melting of crustal rock, generated at or near their sites of emplacement. The terms 'metatexite' and 'diatexite' (after Mehnert, 1968) are used by Saywer (1987), and Sawyer and Barnes (1988) to refer to migmatites with a mimetic, gneissic fabric, and to homogeneous migmatites, respectively. This distinction is not practicable in the field area. 'Mobilizate' is used for the products of migmatization that have migrated, even locally, from their site of generation (Waters and Baars, 1989).

2.3 Granitic Gneisses and Granites

2.3.1 Introduction

A wide variety of granites and granitic gneisses crop out in the field area. Their relative ages have been determined on the basis of their field relationships with one another and with the supracrustal succession, the local and regional structures, and the regional metamorphic textures. The order in which they are presented below and on the stratigraphic column of the map, is from the oldest to the youngest rocks, as could best be determined. The sequence of intrusive events must be regarded as tentative, in the absence of any confirmatory radiogenic isotopic ages. Locally, ambiguous relationships are described. Each granite and granitic gneiss is described in terms of its contact relationships, textural character, and range of mineral assemblages. Table 1 summarizes the mineral assemblages and representative mineral abundances of the granites and granite gneisses. Fig. 2.1 shows some normative quartzofeldspathic compositions plotted on a Streckeisen QAP triangular diagram.

2.3.2 Hornblende-Biotite Augen Gneiss - 'Streaky' Gneiss

The hornblende-biotite augen gneiss crops out as a stacked series of relatively homogeneous structural wedges in the west of the field area, in contact with leucocratic, homogeneous quartz-K-feldspar gneiss (section 2.4.2). The augen gneiss is

characterized by an intense preferred linear orientation of recrystallized K-feldspar-quartz augen wrapped by hornblende-biotite clusters, set in a quartzofeldspathic groundmass (Plate 1). Its contact with the homogeneous K-feldspar-quartz gneiss is regionally concordant and commonly sheared, although the similar weathering characteristics of the two rocks make it difficult to locate the contact precisely in places. Locally, however, the contact is discordant with respect to the regional foliation (Plate 1). It is unclear whether or not this truncation represents an intrusive relationship between the gneisses. A large body of augen gneiss that has similar characteristics to this rock (J.M. Moore, pers. comm.), crops out in the east of the 1:50 000 reconnaissance map area. Its contact with the homogeneous K-feldspar-quartz gneiss is sheared.

Locally, and elsewhere in the field area, the dominant foliation gives way to to a unique, convoluted internal structural fabric. This gives the rock its characteristic 'streakiness' (Plate 2), and represents a number of deformational episodes. On the basis of this unique internal structure, and the complete recrystallization of the augen, the hornblende-biotite augen gneiss is deduced to be older than the supracrustal gneisses or any of the other granitic rocks.

The mineral assemblage of hornblende-biotite augen gneiss (as on Table 1) is

Qtz + Kfs + Pl + Bt + Hbl + Chl + Opq + Ap $\pm$ Zrn.

Equal proportions of quartz and K-feldspar (both <4 mm) form granophyric intergrowths that are ovoid augen with a preferred orientation set in a seriate-textured groundmass. Quartz shows evidence of extensive annealment with minor subgrain boundaries and sutured, neoblastic grain boundaries. Quartz is common as rounded inclusions in perthitic microcline. Minor plagioclase is evenly distributed in the rock as fine (<1 mm), subhedral grains.

Biotite forms clusters that define foliation parallel to and surrounding the augen. Individual grains are fine (<2 mm) laths. Hornblende occurs as fine (<1 mm), anhedral grains that are resorbed by biotite. Both biotite and hornblende are intensely altered to chlorite. Opaque phases, apatite and sparse zircon are accessory minerals.

2.3.3 Garnet-Biotite Augen Gneiss

Narrow (<10 m thick), lenticular bodies of garnet-biotite augen gneiss occur on the farm Rooiwal intercalated with the supracrustal gneisses. Biotite wraps large (<2 cm), quartz-rich augen defining a foliation parallel to that of the supracrustal gneisses. Contacts with the supracrustal rocks are concordant and sharp.

The mineral assemblage of biotite-garnet augen gneiss (Table 1) is

Qtz + Kfs + Pl + Bt + Grt + Opx + Opq + Zrn.

Quartz is recrystallized with sutured grain boundaries, and is the main constituent of the augen (<1 cm). Microcline (<3 mm), quartz (<2 mm) and plagioclase (<2 mm) constitute the major proportion of the rock's seriate-textured groundmass. The augen are wrapped by clusters of fine-grained (<1.5 mm) biotite with a preferred orientation. Locally, skeletal biotite and quartz intergrowths pseudomorph orthopyroxene, which is mildly pleochroic enstatite*, altered to bastite, and associated with microcline. (*A recent investigative commission (Morimoto, 1989) recommends the discontinued usage of the word 'hypersthene', and its replacement with 'enstatite' for compositions containing greater than 50 molecular % MgO, as is the case here.)

Garnet occurs as coarse (<5 mm), subhedral porphyroblasts that are filled with rounded biotite inclusions and have euhedral magnetite cores. These grains are partially rimmed by subhedral, skeletal garnet-quartz intergrowths associated with microcline and abut against biotite clusters. Interstitial opaque phases and zircon occur as accessory minerals.

2.3.4 Megacrystic K-feldspar-Biotite Granite Gneiss

The supracrustal succession is structurally overlain to the north along a poorly exposed, negatively weathering, sheared contact by a massive body of megacrystic K-feldspar-biotite granite gneiss. This granite is coarse-grained and contains large (<5 cm) K-

feldspar megacrysts set in a biotite-rich quartzofeldspathic groundmass. The megacrysts are largely randomly oriented, while biotite defines a weak foliation parallel to the contact with the supracrustal succession. However, within 50 m of the contact, the megacrysts progressively exhibit a preferred orientation parallel to the contact. These are only locally wrapped as augen by a biotite foliation, and evidence for their rotation into their present orientation is largely absent. In view of this, it is suggested that the megacryst orientation is largely an igneous, and not a tectonic foliation (cf. Paterson et al., 1989b). The contact is between a narrow (<2.5 m wide), laterally continuous zone of friable, schistose granite-equivalent, and feldspathic quartzite. It is essentially concordant, although it is locally discordant.

Large (ca. 100 m x 500 m), oblate bodies of quartz-rich biotite-hornblende metabasic gneiss crop out parallel to the contact with the supracrustal succession. These bodies are compositionally massive, and biotite and hornblende have a preferred orientation parallel to the bodies' contacts. This concordance makes it unclear whether these bodies are pretectonic intrusives, or large, oriented xenoliths. Close to the contact with the supracrustal gneisses, metre-scale xenoliths of quartzo-feldspathic gneiss are sparsely distributed subparallel to the contact.

The mineral assemblage of megacrystic K-feldspar-biotite granite gneiss (Table 1) is

$$Qtz + Kfs + Pl + Bt \pm Hbl \pm Opx + Chl + Opq + Ap + Zrn.$$

K-feldspar is perthitic microcline that is commonly simply twinned as large (<5 cm) megacrysts that are partially recrystallized with sutured subgrain and grain boundaries. Inclusions of quartz are common. Quartz (<4 mm), K-feldspar (<4 mm) and plagioclase (<3 mm) constitute the seriate-textured groundmass. Both feldspars are intensely sericitized.

Biotite forms medium-grained, decussate clusters (<3 mm) that define a weak foliation. Near the contact with the supracrustal succession, biotite has a preferred orientation parallel to that of the K-feldspar megacrysts, although not around augen. Biotite is intensely altered to chlorite. Hornblende occurs with biotite as medium-grained (<3 mm), subhedral clusters. Orthopyroxene forms medium-grained (<3 mm), granular aggregates associated with biotite, and intensely altered to bastite. Both hornblende and orthopyroxene commonly surround subrounded biotite laths. Interstitial opaque phases, apatite and zircon are accessory minerals.

2.3.5 Biotite-Orthopyroxene Granite Gneiss

Biotite-orthopyroxene granite gneiss is an inhomogeneous granite which crops out as sill-like intrusions in the supracrustal succession. The granite typically grades from being leucocratic and biotite-bearing at its peripheries to being darker-weathering, sparsely porphyritic and orthopyroxene-bearing away from its boundaries. Its relatively dark weathered appearance, led Joubert (1971) to classify it as 'mafic porphyroblastic granite' (unit 'KhM' on his map).

Intrusive contacts commonly truncate supracrustal horizons and their compositional banding (Plate 3). The synformal sheet at Brakfontein southeast of Witberg, however, is concordantly bound by a narrow (<5 m thick) zone of intensely foliated, biotite-rich granite gneiss. Away from the contacts, biotite defines a moderate foliation which is subparallel to the regional foliation of the supracrustal gneisses. Widely spaced, N-S faults truncate the E-W foliation and the exposures.

At Brakfontein, the granite contains large (ca. 50 m x 500 m), elongate xenolithic rafts of quartzofeldspathic gneiss and biotite-orthopyroxene leucoparagneiss, which are oriented parallel to the granite gneiss's foliation. The compositional banding and foliation of the xenoliths is parallel to their elongation, and is truncated by the host granite. At Rooiwal, the granite contains quartz-rich biotite-hornblende metabasic gneiss

pods in an en echelon distribution. These have a foliation that is at an acute angle to that of the granite, suggesting that they are xenoliths. Calc-silicate gneisses also occur locally as xenoliths.

The mineral assemblage of the biotite-orthopyroxene granite gneiss (Table 1) is

Qtz + Kfs + Pl + Bt ± Hbl ± Opx ± Cpx + Opq + Ap + Zrn.

Microperthitic microcline commonly occurs as coarse (<1 cm), sparsely distributed, compositionally zoned porphyritic grains. These are typically filled with rounded quartz, plagioclase and biotite inclusions. Grain boundaries are sutured. The groundmass is seriate-textured and contains varying proportions of quartz, K-feldspar, plagioclase and ferromagnesian minerals. In some cases, the rock is sufficiently plagioclase-rich to be classified as a granodiorite (Fig. 2.1). Quartz is fine-grained (<2 mm) with recrystallized, sutured, neoblastic grain boundaries. Quartz and microcline are commonly granophyrically intergrown. Myrmekitic intergrowths of fine (<2 mm), antiperthitic plagioclase are common, especially near microcline. Plagioclase grains (An_{25-40}) are commonly compositionally zoned to rims with lower anorthite compositions.

Medium- to fine-grained (<3 mm), subhedral biotite laths have a moderately defined preferred orientation. They occur as decussate

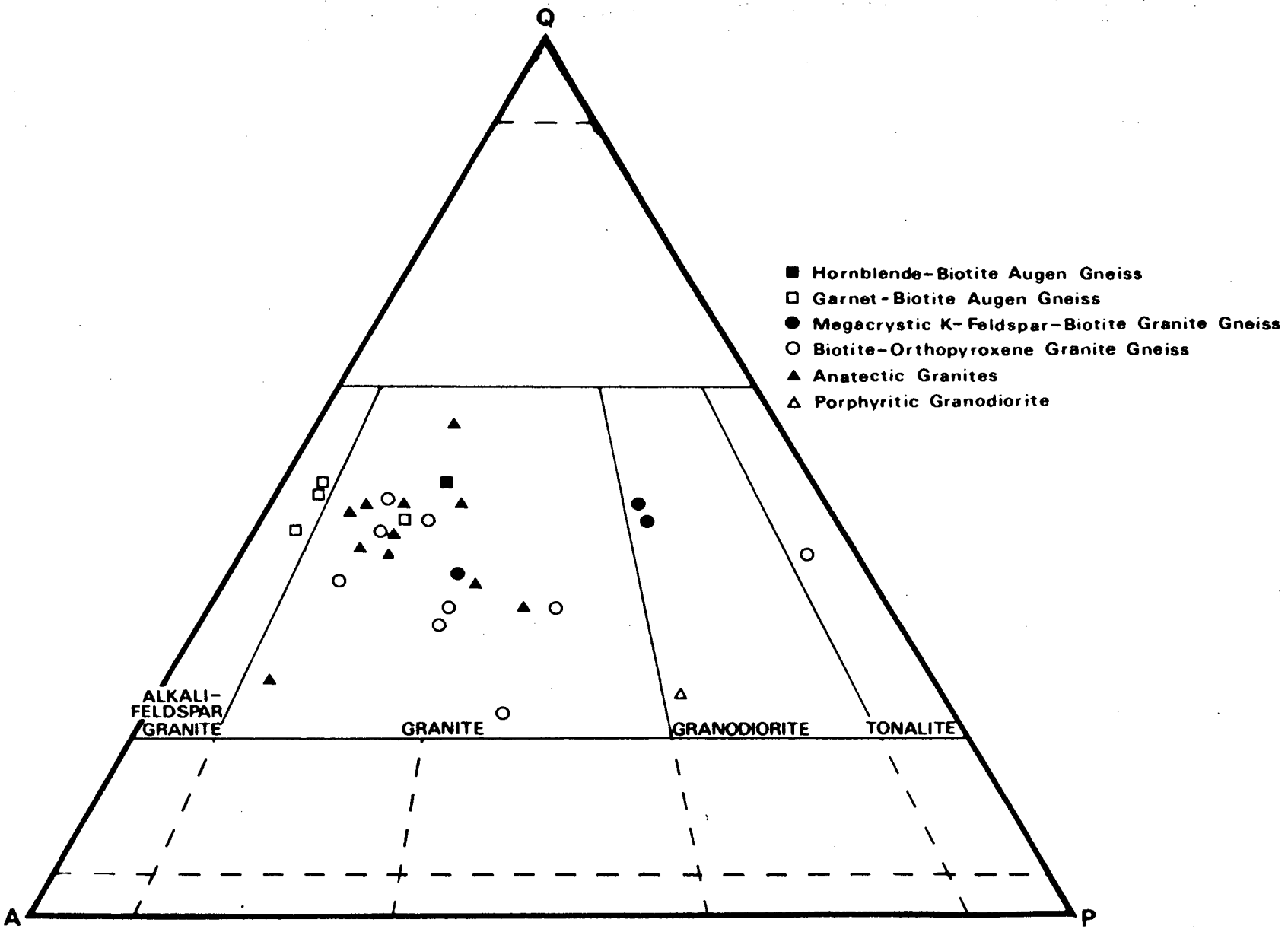

Fig. 2.1 A Streckeisen QAP plot of representative granitic rocks from the study area.

clusters, which are locally altered to chlorite. Fine-grained (<2 mm), granular, equant orthopyroxene, which is weakly pleo-chroic enstatite, is commonly, but not exclusively associated with biotite and microcline. Locally, skeletal biotite-quartz intergrowths replace orthopyroxene. Orthopyroxene is commonly altered to fine-grained bastite aggregates. Fine-grained (<2 mm), subhedral, granular clinopyroxene, which is weakly pleochroic diopside, occurs in the vicinity of orthopyroxene. Subhedral and rounded inclusions and embayments of hornblende are associated with clinopyroxene. Fine-grained (<1.5 mm) opaque grains, probably magnetite and ilmenite, are evenly distributed throughout the rock. Apatite occurs as fine (<0.5 mm), euhedral grains associated with biotite and opaque phases. Zircon occurs as fine (<0.5 mm), metamict grains evenly distributed in the groundmass.

The biotite-orthopyroxene granite gneiss foliation is locally truncated by coarse grained (<1 cm), centimetre-scale leucosomes that commonly contain orthopyroxene and locally clinopyroxene. The matrix-leucosome contact is gradational in most cases. Orthopyroxene is associated with perthitic microcline and skeletal biotite-quartz intergrowths, and is partially altered to bastite. Clinopyroxene commonly contains rounded hornblende inclusions, and is not altered. In a few cases, especially near the contact between the granite gneiss and the supracrustal gneisses, leucosomes contain abundant, zoned, antiperthitic plagioclase with rounded hornblende inclusions. Coarse (<8 mm)

biotite laths with quartz inclusions occur locally in the leucosomes, and are usually associated with opaque minerals.

2.3.6 Anatectic Granites

A wide variety of granite dykes, sills and pods of diverse mineralogy are emplaced in the supracrustal succession. Their field and textural relationships suggest that most of them are genetically coeval with the migmatitic textures described in this chapter, and that they are thus anatectic in origin.

On the basis of their field relationships, the anatectic granites may be classified as follows:

a) Sills of medium- to coarse-grained (<8 mm) granite intercalated with the supracrustal banding, have root zones in stromatic, or banded, migmatites (Plate 4). At the north of Witwater, near the contact with the megacrystic K-feldspar-biotite granite gneiss, a lensoid body of quartzofeldspathic granite swells to a thickness of ca. 300 m. These sills are emplaced in horizons of aluminous- and quartzofeldspathic gneiss, and metapelitic gneiss and biotite-orthopyroxene leucoparagneiss.

b) Lensoid pods of medium-grained (<5 mm) granite up to 5 m thick locally truncate the host supracrustal compositional banding. They have sharp contacts with the country rock. Locally, biotite defines a weak fabric that is parallel to the pods' contacts.

c) Laterally continuous and discontinuous sills of sparsely porphyritic biotite-rich granite are emplaced in quartzofeldspathic gneiss. Biotite defines a weak foliation. However, north of Brakfontein in host rocks that are intensely sheared, biotite defines an intense foliation parallel to the sills' contacts and the foliation of the host rock. Some extensive bodies of anatectic granite have characteristics of both types b) and c).

d) Irregularly shaped dykes of medium-grained (<5 mm) and mineralogically variable granite are emplaced transgressively with respect to all supracrustal horizons in the large scale structures at and east of Witberg. Their contacts with the country rock are locally pegmatitic (grain size <2 cm). Biotite defines a weak foliation that is at an acute angle to the dyke walls and the foliation of the country rocks which the dyke intrudes.

The mineral assemblage of anatectic granites (Table 1) is

Qtz + Kfs + Pl ± Bt ± Grt ± Opx ± Crd + Opq + Zrn ± Ap ± Rt.

While a few granites are entirely quartzofeldspathic, most contain ferromagnesian minerals in the following compositional varieties:

Bt; Bt ± Grt ± Opx ; Bt + Crd ± Grt.

The granites are seriate-textured with abundant microcline, which is sporadically perthitic. Type (c) anatectic granites contain

sparsely porphyritic K-feldspar. Medium- and fine-grained granophyric intergrowths with quartz are common, and locally these are graphic, having a preferred orientation parallel to the weak biotite foliation. Quartz shows evidence of partial recrystallization with subgrain boundaries and neoblastic rims. Pegmatitic contacts of type (d) dykes are largely quartz and K-feldspar. Plagioclase (An_{20-30}) commonly forms myrmekitic intergrowths with quartz. Locally, cores of medium-grained (<3 mm), antiperthitic plagioclase are partially resorbed and rimmed by plagioclase showing finely repeated multiple twinning.

Most commonly, the anatectic granites contain <10% medium- to fine-grained (<3 mm), subhedral biotite laths, which, in most cases, display a weak preferred orientation. Type (c) sills in sheared rock north of Brakfontein contain up to 20% biotite that is partially altered to rutilated chlorite, although these granites do not contain any other ferromagnesian minerals.

Garnet occurs as medium- to coarse-grained (<8 mm) poikiloblasts that are almost exclusively intergrown with and surrounded by neoblastic quartz (Fig. 2.2a, in aluminous quartzofeldspathic gneiss). These intergrowths are commonly surrounded by anhydrous quartzofeldspathic haloes (Plate 5). In a type (d) granitic dyke east of Witberg, these haloes are elongate parallel to the biotite foliation and constitute 50% of the rock volume . Orthopyroxene occurs as medium- to fine-grained (<4 mm), equant

Legend fo Figs. 2.2, 2.3, 2.4, 2.5:
Coarse stipple - garnet; close stipple - hercynite-magnetite; fine stipple - cordierite; edge stipple - feldspar; dashed - biotite; small euhedra - sillimanite; clear - quartz.

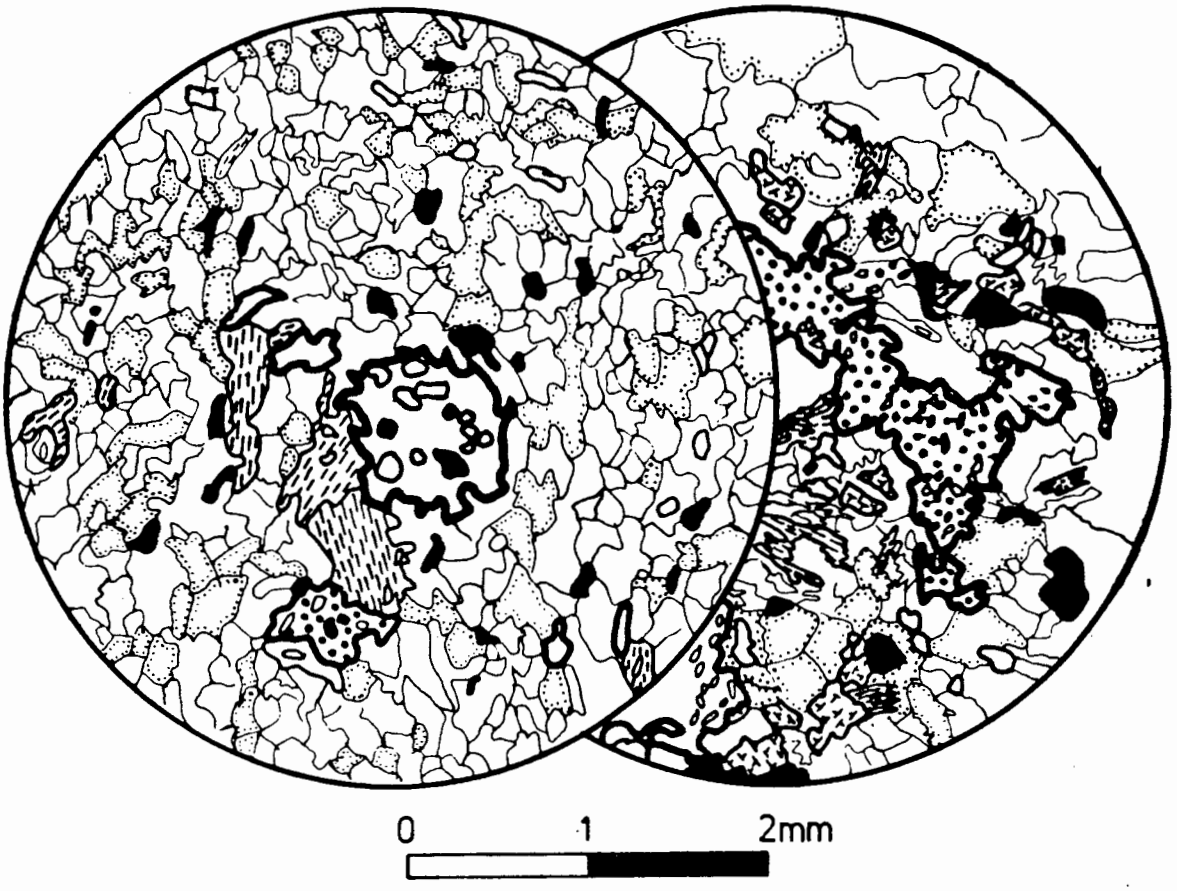

Fig. 2.2a Poikiloblastic garnet in aluminous quartzofeldspathic gneiss FB266C.
2.2b Poikiloblastic garnet, overgrown by radiating skeletal garnet-quartz and biotite-quartz intergrowths; surrounded by orthopyroxene in garnet-biotite-orthopyroxene anatectic granite FB71.

grains associated with microcline. Cordierite forms medium-grained (<4 mm), anhedral, elongate grains that are intensely pinitized. Locally garnet, orthopyroxene and cordierite are overgrown by coarse (<8 mm), skeletal biotite-quartz intergrowths.

At Rooiwal, a granitic sill emplaced in pelitic gneiss contains corona of poikiloblastic garnet, partially overgrown by radiating skeletal garnet-quartz and biotite-quartz intergrowths. These intergrowths are surrounded by orthopyroxene associated with microcline (Fig 2.2b). This corona texture is separated from the biotite granite matrix by a quartzofeldspathic halo, which is significantly more K-feldspar-rich than the matrix granite .

Interstitial opaque phases (<2 mm), apatite and zircon are accessory phases. It is important to note that zircon occurs in all the anatectic granites, and grains with a 1 mm diameter are common.

2.3.7 Porphyritic Granodiorite

At Rooiwal, a sill of coarse to medium-grained porphyritic granodiorite intrudes the supracrustal succession. It contains phenocrysts of K-feldspar (<1 cm) set in a seriate-textured, plagioclase-rich groundmass. The plagioclase (<6 mm) is strongly antiperthitic, and commonly forms myrmekitic intergrowths with quartz. Biotite occurs as medium-grained (<4 mm), anhedral,

randomly oriented laths. Hornblende occurs locally as fine-grained, discrete, subhedral grains in the groundmass. The rock displays no evidence of recrystallization.

2.3.8 Biotite Microgranite

A few metre-scale, elongate bodies of fine-grained (<2 mm), biotite-rich granite are emplaced along portions of the N - S faults that displace portions of the supracrustal succession. The biotite defines a foliation parallel to the fault orientation. K-feldspar is microperthitic microcline.

2.3.9 Quartzofeldspathic Pegmatite

Irregularly shaped bodies of quartz-rich pegmatite are locally emplaced truncating the supracrustal gneisses. They contain minor graphic intergrowths of K-feldspar and quartz, and muscovite occurs locally as subhedral books.

2.4 Supracrustal Gneisses

2.4.1 Introduction

The supracrustal rocks are described as being of supracrustal origin because they crop out as an E - W trending stratiform succession of metasedimentary and metavolcanic bulk compositions. Primary depositional structures and textures have been completely overprinted. The supracrustal gneisses are enveloped to the north and south, and intruded by granitic gneisses of varying ages. The order in which the lithologies are presented below corresponds to the stratigraphic column of the map, However, it must be pointed out that there is no direct age control on the supracrustal gneisses. In addition, many of the rock types are intercalated, so that the sequence is not strict. The general sequence is based on the premise that the homogeneous K-feldspar-quartz gneisses are in contact with the mulitiply deformed 'streaky' hornblende-biotite augen gneiss (section 2.3.2). This relationship corresponds with Moore's (1986) suggestion that the homogeneous K-feldspar-quartz gneiss is the oldest of the supracrustal gneisses in western Namaqualand (also Joubert, 1971). Table 2 summarizes the mineral assemblages and representative modal abundances of the supracrustal gneisses.

2.4.2 Homogeneous K-feldspar-Quartz Gneiss - 'Pink' Gneiss

The homogeneous K-feldspar-quartz gneiss shows little evidence of deformation. Its contacts with the hornblende-biotite augen gneiss are typically sharp, although they are commonly obscured by their similar weathering characteristics. Plate 1 shows an apparently intrusive relationship between them. However, it is not possible to distinguish the relative ages of the two rocks on the basis of their contact relationships. Layering and compositional banding are essentially absent. Locally, interstitial biotite defines a foliation, especially along some of the contact zones with the hornblende-biotite augen gneiss.

The gneiss is composed of microcline and quartz in approximately equal proportions (Table 2) and in granoblastic equilibrium with one another. The microcline (<2.5 mm) contains randomly oriented blebs of perthite. Quartz grains (<2 mm) display evidence of complete annealment with neoblastic grain boundaries.

Anhedral biotite laths (<0.5 mm), partly altered to chlorite containing rutile needles, subhedral opaque phases (probably magnetite rimmed by ilmenite), and trace amounts of zircon constitute the minor accessory mineral component of the gneiss.

The most common inhomogeneity of this massive rock is the presence, locally, of medium to coarse-grained (5 mm) K-feldspar and quartz leucosomes as patches and stringers that are <10 cm

wide. In places, laterally discontinuous pegmatitic veins are emplaced discordantly with respect to the weak biotite foliation.

2.4.3 Metabasic Gneisses

2.4.3.1 Pyroxene Granulite Gneiss

Mafic gneisses occur as narrow (<3 m thick) continuous and discontinuous bands and lenses in the supracrustal succession in association with intermediate mafic (section 2.4.3.2) and pelitic (2.4.4) horizons. They are also common as xenoliths in metamorphosed granites. Their outcrops are dark and massive, and are usually very prominent on aerial photographs. Many outcrops are compositionally banded with respect to their mafic mineralogy, while mineral foliations and lineations are weakly developed. Individual compositional bands are generally equigranular, although mafic mineral grain sizes vary together from 5 mm to less than 1 mm.

The mafic rock mineral assemblage (Table 2) is

$$Pl \pm Qtz \pm Bt \pm Hbl + Opx \pm Cpx + Opq \pm Hc + Ap + Zrn.$$

The plagioclase is fine-grained (average 1 mm) and constitutes between 40% and 70% of the rock volume. Measurement of the extinction angles of multiple twins (Deer et al., 1966, p.333), suggests a variation in plagioclase composition from An_{45}, in a

rock containing about 5% quartz, to An_{75}, in an anhydrous and silica-free rock . This observation is confirmed by electron microprobe analysis (Appendix 1L). Plagioclase grains are subhedral, and have a granoblastic texture. They commonly have annealed neoblastic subgrain and grain boundaries. They seldom show evidence of internal strain. The process of annealing may be accompanied by the formation of multiple twins. Euhedral antiperthitic rhombic and spindle-like inclusions of K-feldspar are commonly aligned along the plagioclase cleavage planes. This is particularly true for grains coarser than 2 mm, and for quartz-bearing assemblages.

In rocks containing hydrous minerals, hornblende (5 mm - 0.5 mm) is significantly more abundant than biotite (2 mm -0.2 mm). Mineral elongation has a preferred linear, and a subordinate planar fabric. Hornblende is pleochroic beige to pale brown to green. There is no optical evidence for compositional zoning. Hornblende grains are commonly partially resorbed by granular pyroxene, and occur with plagioclase as subhedral or rounded anhedral inclusions in pyroxene aggregates. Pleochroic colourless to honey brown biotite flakes have a similar habit. Both these minerals display minor alteration to chlorite.

Of the two pyroxenes present in most samples of pyroxene granulite gneiss, orthopyroxene is the more abundant, coarser phase. Despite the presence of numerous fine-grained inclusions, the pyroxene grains are generally finer-grained than the

accompanying hornblende grains. The orthopyroxene is faintly pleochroic pale pink to pale green to light brown enstatite. It may be altered to chlorite along grain boundaries. The clinopyroxene is mildly pleochroic colourless to pale green diopside. Both pyroxenes are generally subhedral granular and poikiloblastic aggregates that invade and embay hornblende grains. Individual aggregates may be aligned parallel to the preferred linear and planar hydrous mineral fabric. Where compositional banding is present, on a scale from 1 cm to 1 m, it is defined by variations in the relative pyroxene proportions, and/or by the alternation of hydrous, locally silica-saturated, and anhydrous assemblages.

Hercynite occurs locally in association with magnetite in plagioclase-orthopyroxene-quartz assemblages. Opaque phases, probably magnetite and ilmenite, are common as interstitial minerals. Apatite commonly forms subhedral and euhedral embayments on opaque phases. Zircon occurs as discrete, interstitial grains.

The internal fabric and compositional banding of the pyroxene granulite gneisses is disrupted by sparsely distributed, coarse-grained (>5 mm) patches and/or veins that are up to 20 cm wide (Plate 6). These are dominated by plagioclase (Table 2), which is often zoned and strongly antiperthitic; very coarse, dark brown weathering enstatite; and coarse, dark green diopside. These patches are almost exclusively anhydrous, although minor euhedral

hornblende locally replaces the pyroxenes. In patches that contain hornblende, quartz is not present, and vice versa. The mineral proportions of mafic leucosomes vary widely. Transgressive veins and patches are commonly dominated by pale blue plagioclase, with one of the pyroxenes concentrated at the core. Some veins which are parallel to compositional banding and very narrow (<1 cm thick), are composed entirely of pyroxene. Fluid inclusions are abundant in plagioclase, and in quartz where it is present. Zircon occurs as fine (<0.05 mm), unzoned, subhedral grains at opaque mineral grain boundaries.

2.4.3.2 Quartz-rich Metabasic Gneiss/Schist

Mineralogic and textural differences distinguish the quartz-rich metabasic gneisses from the pyroxene granulite gneisses described above. The most important criterion for distinction is the presence of >10% quartz in the quartz-rich, intermediate metabasic gneisses.

These quartz-rich metabasic gneisses crop out as compositionally banded and generally well-foliated horizons (<4 m thick) that are both laterally continuous and lenticular. Locally, the gneisses have developed a schistose fabric. They occur in association with pyroxene granulite gneisses, biotite-ortho-pyroxene leucoparagneisses and quartzofeldspathic gneisses. They are also very common with hornblende-rich metabasic gneisses as en echelon, or oriented xenoliths in metamorphosed and deformed

granites. Outcrop weathering is typically more intense than in the associated pyroxene granulite gneisses.

The quartz-rich metabasic gneiss mineral assemblage (Table 2) is

$$Qtz + Pl \pm Bt \pm Hbl + Opx \pm Cpx + Opq + Ap \pm Hc \pm Zrn.$$

Compositional banding is variously defined by differing quartz, biotite and orthopyroxene abundances. For all mineral species, grain sizes vary together between 3 mm and 0.5 mm. Rock texture generally approaches granoblastic equilibrium.

Plagioclase (An_{30-50}) is commonly antiperthitic near grain boundaries with quartz. In selected samples, partially deformed twin lamellae provide evidence of strain. Furthermore, subgrain boundaries and undulose extinction in quartz suggest the incomplete annealment of strain. Granular, neoblastic quartz is only locally developed.

Anhedral and subhedral biotite laths are pleochroic tan brown to colourless. They have a distinct preferred orientation that is parallel to compositional banding. Biotite and minor hornblende are partially replaced by granular and poikiloblastic pyroxene aggregates. Pleochroic enstatite is locally associated with minor diopside. Intergrown magnetite and ilmenite commonly occur as embayments, or in the cleavages and fractures of biotite and pyroxene. Quartz and biotite often occur as rounded inclusions in

enstatite. In addition, skeletal biotite and homogeneous, unstrained quartz intergrowths commonly replace enstatite. Very fine accessory apatite crystals are evenly distributed in the rock as inclusions in biotite, plagioclase and quartz. Green spinel, hercynite, is locally associated with magnetite as blocky grains.

Small, nebulitic, enstatite-bearing migmatitic leucosomes are very sparsely distributed in this rock.

2.4.4 Metapelitic and Magnesian Gneiss

A wide mineralogic variety of rocks with broadly similar, pelitic bulk compositions (Turner, 1981, p.6) crop out in the supracrustal package. They are divided into the aluminous quartzofeldspathic gneisses, containing >75% total quartz and feldspar, the metapelitic gneisses, with >10% quartz, and the magnesian gneisses, which are characteristically cordierite-bearing and quartz-undersaturated. Each type comprises a number of different ferromagnesian mineral assemblages, that are summarized on Table 2.

2.4.4.1 Aluminous Quartzofeldspathic Gneiss

The banded and massive aluminous quartzofeldspathic gneisses crop out as laterally continuous horizons, intimately intercalated with the metapelitic gneisses (section 2.4.4.2). Individual

massive units are up to 100 m thick, although the effect of tectonic thickening by early folding is hard to determine because of the rocks' homogeneous character. They are, however, less crenulated than the metapelitic gneisses. Compositional banding is from 5 mm to 10 cm thick, and consist of ferromagnesian minerals in a dominant quartzofeldspathic host.

The aluminous quartzofeldspathic gneiss mineral assemblage is

$$Qtz + Kfs \pm Pl \pm Bt \pm Sil \pm Grt \pm Crd \pm Hc + Opq.$$

The compositional varieties are

$$Grt \pm Sil \pm Bt \pm Hc;\ Grt + Crd \pm Sil \pm Bt + Hc;$$
$$Crd + Hc \pm Sil \pm Bt.$$

The ferromagnesian mineral and sillimanite textures are very similar to those of the metapelitic gneisses, and are treated in section 2.4.4.2. Only the quartzofeldspathic minerals demand are described here.

Quartz and K-feldspar have a granoblastic texture, and are equigranular (<2 mm). Quartz grains are partially or competely recrystallized, with a transition from subgrain boundary to neoblast development. K-feldspar is microperthitic microcline. Plagioclase commonly occurs as discrete clusters in quartzo-feldspathic compositional bands. Regional foliation is defined by the preferential planar orientation of fine, interstitial biotite

flakes, or the entrainment of coarse garnet and/or cordierite grains where present. In sheared rocks, usually containing sillimanite, quartz and feldspar are finely recrystallized.

Where present, biotite foliation and compositional banding are disrupted by anhydrous quartzofeldspathic patches containing garnet and/or cordierite. In many cases, entire compositional bands are anhydrous. In these, poikilobastic garnet may form as selvages, or may be concentrated at the cores of anhydrous bands or patches. Unlike other migmatites in the area, many leucosomes in the aluminous quartzofeldspathic gneisses are equigranular with respect to the matrix. However, coarse-grained, and even pegmatitic veins do occur.

2.4.4.2 Metapelitic Gneiss

These rocks are predominantly associated with the aluminous quartzofeldspathic gneisses as intercalated 1 m - 50 m thick compositional units, each displaying internal 1 cm - 2 m thick compositional banding of different mineral assemblages. On the scale of the map, two laterally continuous and distinctive metapelitic units are recognised in the supracrustal succession. Individual horizons are generally laterally continuous, while some pinch out as lenses. It is difficult to estimate the thickness of units accurately, because of folding and consequent thickening, and because of shearing and consequent attenuation.

The metapelitic mineral assemblage (Table 2) is

Qtz + Kfs ± Pl ± Bt ± Sil ± Grt ± Crd ± Hc ± Opx + Opq.

The compositional varieties are

Grt ± Sil; Grt + Crd + Hc ± Sil; Crd + Hc ± Opx ± Sil.

K-feldspar displays a wide range of exsolution textures, from blebby microperthite to lamellar mesoperthite. K-feldspar is more abundant than plagioclase, and its relative proportion to plagioclase increases significantly in leucosomes. Quartz displays varying degrees of recrystallization. Subgrain boundaries are pervasively developed, while neoblastic annealment is limited to sheared rocks and fold closures.

It is significant that most of the sillimanite-bearing gneisses occur as intensely foliated rocks in shear zones subparallel to the compositional banding of the supracrustal package. Sheared rocks occur as laterally continuous and discontinuous bands between 5 mm and 10 cm wide. Quartz and feldspar are completely annealed, with fine-grained, neoblastic textures. This is in contrast to the leucocratic mineral textures of regionally foliated and massive metapelites. Microcline or microperthite is stained red and plagioclase is sericitized.

Sillimanite occurs in a number of distinct textural associations. Fine- and coarse-grained euhedral, acicular overgrowths on cordierite, hercynite and, locally, on garnet define shear

foliations (Fig. 2.3c). Fine-grained sillimanite commonly displays a preferred linear orientation, while coarse, up to 2 cm long euhedral aggregates have a random, planar orientation. Coarse euhedra are embayments in opaque magnetite-hercynite intergrowths. In unsheared rocks narrow (<0.2 mm), euhedral and subhedral sillimanite rims around magnetite-hercynite-quartz associations occur in cordierite-bearing metapelites (Fig. 2.3b). In a few rocks, fine-grained sillimanite spindle clusters are oriented inclusions in cordierite and garnet cores.

Biotite occurs in relatively minor amounts as anhedral and subhedral flakes (<3 mm) defining the refolded regional foliation (Fig. 2.3a). Locally, laths are oriented parallel to the fold hinges of low amplitude and low wavelength crenulations. Biotite is usually pleochroic colourless to tan brown. In compositions with relatively low leucocratic mineral abundance, basal sections are pleochroic colourless to red-brown phlogopite. In compositional bands dominated by garnet and/or cordierite, biotite occurs with quartz and plagioclase as rounded inclusions in these phases (Fig. 2.3a).

Isotropic, pale brown garnet is typically coarse-grained (<10 mm) and easily distingushed in hand specimen. It is almost exclusively poikiloblastic with quartz, and has subhedral, rhombododecahedral grain boundaries (Fig. 2.3a). Other inclusions are rounded biotite, cordierite, hercynite, plagioclase, opaques and sillimanite needles. Garnet is most common in coarse-grained

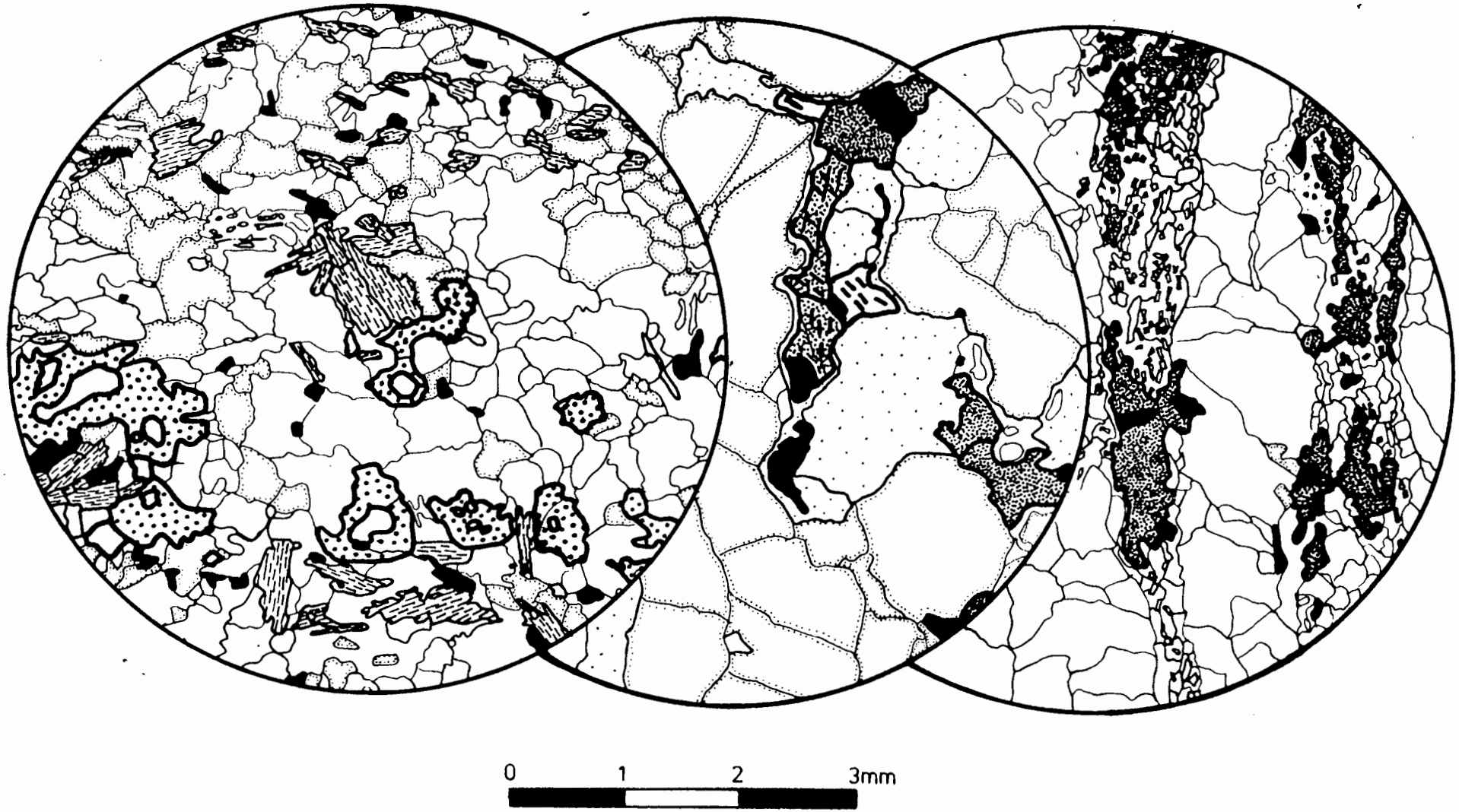

Fig. 2.3a Coarse garnet poikiloblasts with refoliated biotite flakes in garnet-biotite metapelitic gneiss DWN 673.
2.3b Sillimanite rims around magnetite-hercynite-quartz associations in cordierite-bearing metapelitic gneiss FB109.
2.3c Acicular sillimanite overgrowths on cordierite and hercynite in shear foliations metapelitic gneiss DWN679.

leucosome assemblages with quartz and K-feldspar, where skeletal biotite and quartz intergrowths pseudomorph coarse poikilobastic garnet. In some rocks, garnet forms rims with euhedral sillimanite around hercynite-magnetite intergrowths.

Cordierite occurs as coarse (<6 mm), subhedral and rounded, anhedral grains that are commonly altered to pinite, particularly along their fractures. They form elongate, inclusion-filled grains, along compositional bands (Fig. 2.3b). Inclusions are biotite, quartz, plagioclase, opaques, plagioclase and sillimanite needles. Cordierite is associated with garnet and decussate biotite clusters and is widespread as narrow rims around hercynite-magnetite intergrowths. Locally, coarse biotite flakes embay or replace cordierite.

Hercynite is associated with magnetite in two intergrowth styles. In more aluminous bulk compositions, often containing sillimanite, hercynite and magnetite form blebby and vermicular intergrowths that invade cordierite or completely replace it (Fig. 2.3b). In other pelitic rocks, the two phases form a blocky association. Hercynite-quartz contacts are rarely preserved, the two phases usually being separated by narrow cordierite or garnet and sillimanite rims (Fig. 2.3b).

Orthopyroxene, although usually restricted to the quartz-undersaturated magnesian gneisses, dominates the dark compositional bands of one sample, DWN554, which is sillimanite-

free. It is a pleochroic enstatite that is associated with phlogopite and mesoperthite. Skeletal biotite-quartz intergrowths occur in embayments.

Minor corundum crystals locally embay hercynite. At two localities, randomly oriented, ~5 cm hexagonal corundum barrels occur in plagioclase-rich compositional bands. Zircon occurs as fine, metamict inclusions in biotite, or as discrete interstitial grains. Rutile needles occur in rounded biotite inclusions, and in cordierite and quartz.

The regional fabric of the metapelitic gneisses is disrupted by coarse-grained leucosomes. Four varieties are recognised on the basis of scale, internal structure and host rock relationship. These are:

a) Transgressive, oblate, centimetre-scale, leucocratic patches with garnetiferous cores (Plate 7);

b) Compositional bands that contain poikiloblastic garnet and/or less commonly cordierite, and may appear as intensely crenulated lithologies (Plate 8);

c) Completely disruptive, centimetre- and metre-scale veins and patches with no particular mineral distribution, and with some garnet poikiloblasts straddling leucosome-matrix boundaries (Plate 9); and

d) very leucocratic sills, up to 3 m thick, with poorly defined, nebulitic leucosome-matrix contacts (Plate 10).

Gradational varieties between each type exist. In some cases, coarser-scale leucosomes transgress older, finer ones (Plate 10). Locally, veins and patches are crudely aligned parallel to crenulation fold hinges, and more rarely, along their axial planes. In these cases, garnet poikiloblasts are often entrained along these structural elements.

The mineralogy of the leucosomes is dominated by K-feldspar, quartz and garnet, with relatively minor plagioclase (Table 2). Cordierite occurs at sparsely distributed localities, and always in association with garnet. Biotite commonly occurs with quartz as coarse, skeletal and poikiloblastic partial pseudomorphs after garnet, and in association with blocky magnetite. Zircon is a common accessory phase. H_2O and CO_2 fluid inclusions are abundant, especially in quartz.

2.4.4.3 Magnesian Gneiss

The magnesian gneisses occur as lenticular horizons up to 10 m thick and are associated with metapelitic gneisses. Outcrops are weathered dark brown and display a weak compositional banding between feldspathic and ferromagnesian layers. Table 2 shows that most magnesian gneisses are entirely quartz-free and contain cordierite.

The magnesian gneiss mineral assemblage is

$$Kfs \pm Pl + Crd + phl \pm Hc + mag \pm Grt \pm Opx \pm Qtz + Zrn.$$

Four distinct compositional varieties exist, all containing feldspar, cordierite, phlogopite and magnetite. They are

$$Hc \pm Opx;\ Qtz + Opx \pm Hc;\ Hc + Opx + Grt.$$

The magnesian gneisses are texturally complex, and are characterized by a variety of different mineral intergrowths. Cordierite occurs both as coarse, anhedral grains (<6 mm) that are filled with inclusions of feldspar and minor phlogopite, and as fine, subhedral grains (<2 mm) associated with feldspar-rich portions of the rock (Fig. 2.4b). Cordierite usually displays evidence of alteration to pinite along fractures and grain boundaries. In one case, FB22, high relief cordierite is symplectically intergrown with the rims of coarse, relatively low relief cordierite grains. This relief difference may reflect the presence of hydrous cordierite rims around anhydrous cordierite cores (Deer et al., 1968; p.84). Cordierite and orthopyroxene are associated as coarse, granular intergrowths in compositional bands dominated by either mineral. Orthopyroxene is moderately pleochroic pale brown to green to pale pink enstatite. It is typically coarse-grained (<6 mm) and anhedral. It contains rounded inclusions of phlogopite, quartz and rare plagioclase. Both cordierite and orthopyroxene grains are often elongate, parallel to a preferred orientation of coarse phlogopite (Fig.2.4b).

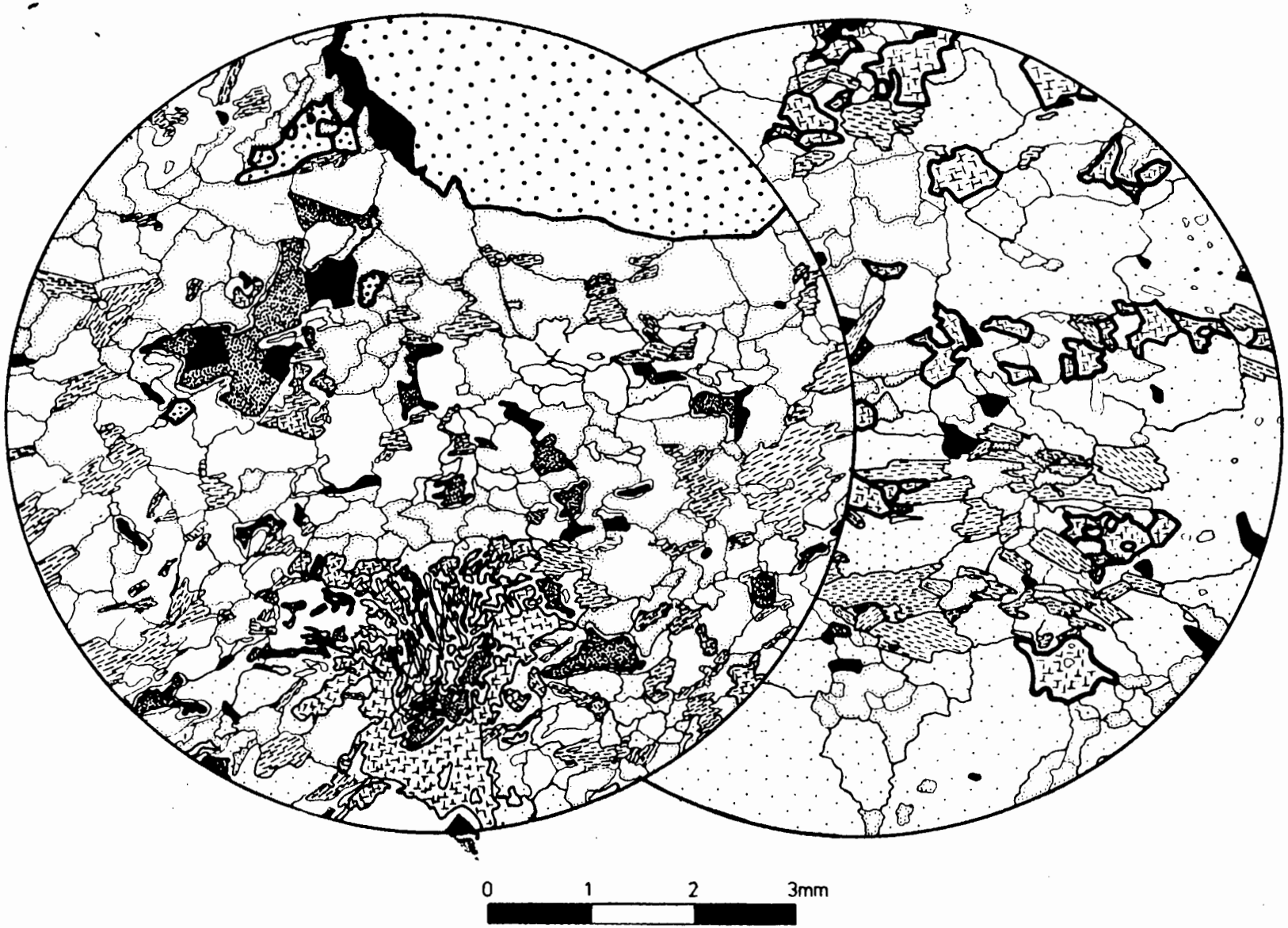

Fig. 2.4a Vermicular hercynite-magnetite intergrowths with orthopyroxene and cordierite near garnet porphyroblast and blocky hercynite-magnteite association with cordierite rim in magnesian gneiss FB26.
2.4b Cordierite-orthopyroxene association with phlogopite in magnesian gneiss FB10.

Phlogopite is strongly pleochroic colourless to red brown. It occurs as a number of different grain sizes, from rounded inclusions (<1 mm) to medium-and coarse-grained (<15 mm) decussate clusters. Locally, these clusters surround orthopyroxene, especially in association with K-feldspar (Fig. 2.4b). Phlogopite and quartz in skeletal intergrowths sometimes pseudomorph orthopyroxene. Phlogopite is locally altered to rutilated chlorite and prehnite along its cleavages.

Feldspar is coarsely (<5 mm) intergrown with cordierite and orthopyroxene. However, feldspar and orthopyroxene seldom occur in mutual contact. They are separated by narrow (<0.5 mm) cordierite rims or by coarse phlogopite haloes. Feldspar occurs in a wide variety of unmixing textures, from homogeneous ternary feldspar to lamellar mesoperthite and blebby microperthite, which coexists with strongly antiperthitic plagioclase. Mesoperthite is sometimes zoned to albitic rims against anhydrous ferromagnesian minerals. Feldspar alteration to sericite is limited, but commonly mimics zonation patterns.

Hercynite and magnetite are intimately associated as medium-grained (<3 mm) lobate and vermicular intergrowths with orthopyroxene and rarely with cordierite (Fig.2.4a). Alternatively, they form blocky associations with mesoperthite. Anhedral, elongate, inclusion-filled, poikilobastic intergrowths may define regional foliation. Hercynite and magnetite form a vermicular intergrowth with quartz in only one magnesian gneiss sample,

FB29. In other samples these phases are mutually exclusive. Fine-grained, narrow (<0.1 mm) cordierite rims around hercynite-magnetite are common against all phases, except cordierite itself. Hercynite is locally altered to diaspore, and magnetite to hematite.

Two generations of garnet occur in garnet-bearing magnesian gneisses (Fig. 2.4a). Early, coarse-grained (<8 mm), subhedral garnet is inclusion-free. Much of the second generation occurs as fine- grained (<3 mm), euhedral and subhedral poikiloblastic and skeletal rims and embayments on the coarse grained garnet. It also embays orthopyroxene, phlogopite and hercynite, which is the most common inclusion type. Garnet and cordierite do not occur in contact with one another.

Sapphirine occurs in one sample, FB276, as a fine, symplectic intergrowth with cordierite. The intergrowths are surrounded by cordierite and have suhedral, tabular boundaries (<1.5 mm). The sapphirine is colourless and non-pleochroic, with a high, negative $2V_a$, suggesting that its composition may be near that of the pure end Mg-member (Christophe-Michel-Levy, 1962; Zotov, 1966; in Deer et al., 1978, p. 614-639). In the same rock, corundum forms fine (<1 mm), sub-hedral grains associated with cordierite, and in contact with elongate, poikiloblastic hercynite porphyroblasts. The rock contains no quartz.

Zircon is an accessory mineral in most magnesian gneisses. It occurs as fine-grained (<0.5 mm), anhedral, metamict intergranular grains, or as inclusions in biotite, feldspar, cordierite or orthopyroxene.

At a few outcrops, spectacular transgressive leucosome patches occur in cordierite-phlogopite-orthopyroxene magnesian gneiss (Plate 11). Orthopyroxene in these leucosomes is coarse grained, even pegmatitic (subhedral, orthorhombic crystals, up to 15 cm diameter). It is associated with coarsely mesoperthitic microcline, minor interstitial quartz and plagioclase, and anhedral phlogopite inclusions. Zircon occurs along quartzofeldspathic grain boundaries.

2.4.5 Quartzite and Quartz Magnetitite

Quartzite and quartz magnetitite occur as narrow (<4 m thick), lenticular horizons associated with the metapelitic gneisses. A laterally continuous horizon of sheared feldspathic quartzite separates the quartzofeldspathic gneisses from the structurally overlying megacrystic augen gneiss at the northern boundary of the supracrustal succession.

Quartzite occurs as white or grey weathering outcrops. Compositional banding is generally poorly exposed, and may be only microscopically evident. Medium- to fine-grained (<4 mm) granoblastic, quartz-dominated layers that are partly

recrystallized, alternate with layers containing a variety of ferromagnesian minerals. Commonly granular magnetite (<3 mm) with minor exsolved blocky hercynite, is the major component of these layers. Ilmenite exsolution lamellae exploit the octahedral magnetite cleavage planes. In cases where hercynite is intensely altered to diaspore, magnetite is altered to hematite. Fine-grained (<0.5 mm), subhedral to euhedral apatite occurs as an important accessory phase associated with magnetite. Locally andradite garnet occurs as granoblastic concentrations with magnetite. Garnet, orthopyroxene and biotite are present as narrow (<0.2 mm) rims around magnetite-hercynite associations. Fine-grained (<0.5 mm) zircon occurs with magnetite.

The feldspathic component of quartzite is entirely andesine plagioclase (An_{30-40}), which is distributed evenly in a granoblastic texture in the quartz-dominated layers. The sheared quartzite is significantly more feldspathic. Both quartz and feldspar are entirely recrystallized into a planar fabric.

Transgressive pods and veins of milky quartz are commonly associated with quartzite. These contain no compositional banding or zonation, and contain H_2O and CO_2 fluid inclusions.

At one locality, FB229, magnetitite occurs as a lenticular body (ca. 40 m X 4 m) between quartzite and K-feldspar-cordierite-biotite metapelite. The body has gradational hanging-wall and

footwall contacts. It contains minor amounts of subhedral to euhedral pyrrhotite.

The term quartz magnetitite has been reserved for lithologies displaying a discrete centimetre-scale banding between quartz- and magnetite-rich layers, resembling that of classic iron formations (e.g. Kimberley, 1978; Guilbert and Park, 1986; Zhai and Windley, 1989). Quartz is coarse-grained (<1 cm) with serrated grain boundaries and shows internal subgrain boundary development and undulose extinction. In bands dominated by magentite, however, quartz is fine-grained (<2 mm) and less strained. Suhedral magnetite and subhedral andradite garnet (both <2 mm) are granoblastically intergrown in the magnetite-dominated bands. Sillimanite occurs as fibrolitic overgrowths on quartz. Grunerite occurs as minor rounded inclusions in quartz. Apatite and zircon are present as accessory minerals throughout the rock.

2.4.6 Biotite-Orthopyroxene Leucoparagneiss

Biotite-orthopyroxene leucoparagneisses constitute a major proportion of the supracrustal succession. They are distinct from the granite gneisses with similar mineralogies on the basis of their well-developed gneissic layering which is defined in 1 mm to 10 m thick compositional banding. Massive bands are up to 100 m thick. Outcrops are exfoliated domes, broad, low relief pavements, lenticular, stratiform ridges, or massive boulder tors. Biotite-rich varieties weather grey, earning the rocks

their common name, the 'grey gneisses' (e.g. Joubert, 1971, 1986; Jack, 1980; Moore, 1986). Orthopyroxene-bearing outcrops are stained light brown. These characteristics contribute to the name used here for the light coloured gneisses which are considered to be of volcano-sedimentary origin.

Regional foliation is defined by the consistent biotite planar fabric. At a few localities, intrafolial folds of narrow, centimetre-scale compositional bands show an axial planar orientation of the biotite flakes. Contacts with most other rock types are sharp. In places, contacts with quartzofeldspathic gneiss and intermediate mafic gneiss are gradational.

The mineral assemblage of the biotite-orthopyroxene leucoparagneiss is

$$Qtz + Kfs + Pl + Bt \pm Opx + Opq.$$

Compositional bands are simply defined by the alternation of layers containing ferromagnesian minerals with more quartzofeldspathic layers. The massive variations are defined by a range of plagioclase to K-feldspar ratios from 1:10 to 8:1. The composition of plagioclase (<2 mm), which is locally antiperthitic, varies correspondingly in the range An_{25-45}. K-feldspar is microperthitic microcline or orthoclase (<4 mm), and locally shows evidence of neoblastic recrystallization. Quartz (<2 mm) shows evidence of subgrain development and recrystallization.

Subhedral, fine-grained biotite flakes (<2 mm) are interstitial and their preferred orientation defines the regional foliation. They are truncated, in compositional bands, by granular, equant orthopyroxene grains (<3 mm) (Fig. 2.5a). The orthopyroxene is mildly pleochroic enstatite. Locally, skeletal biotite-quartz intergrowths surround and embay orthopyroxene (Fig. 2.5b). Locally, chlorite and pinite replace biotite and orthopyroxene respectively.

Coarse-grained leucosomes that transgress the regional foliation are a widespread feature of the biotite-orthopyroxene gneiss. They occur as four distinct varieties.

a) Unzoned, medium- to coarse-grained quartzofeldspathic patches with poorly defined boundaries and randomly distributed biotite and orthopyroxene. These trangress foliation completely.

b) Variously pegmatitic to aplitic lenticular pods with concentrations of biotite and orthopyroxene separated from the host rock by anhydrous quartzofeldspathic haloes (Plate 12).

c) Similarly zoned ovoid patches with macroscopically well-defined boundaries. They truncate foliation, but are broadly parallel to it (Plate 13).

d) Pegmatitic quartz and K-feldspar-rich transgressive veinlets that truncate compositional banding.

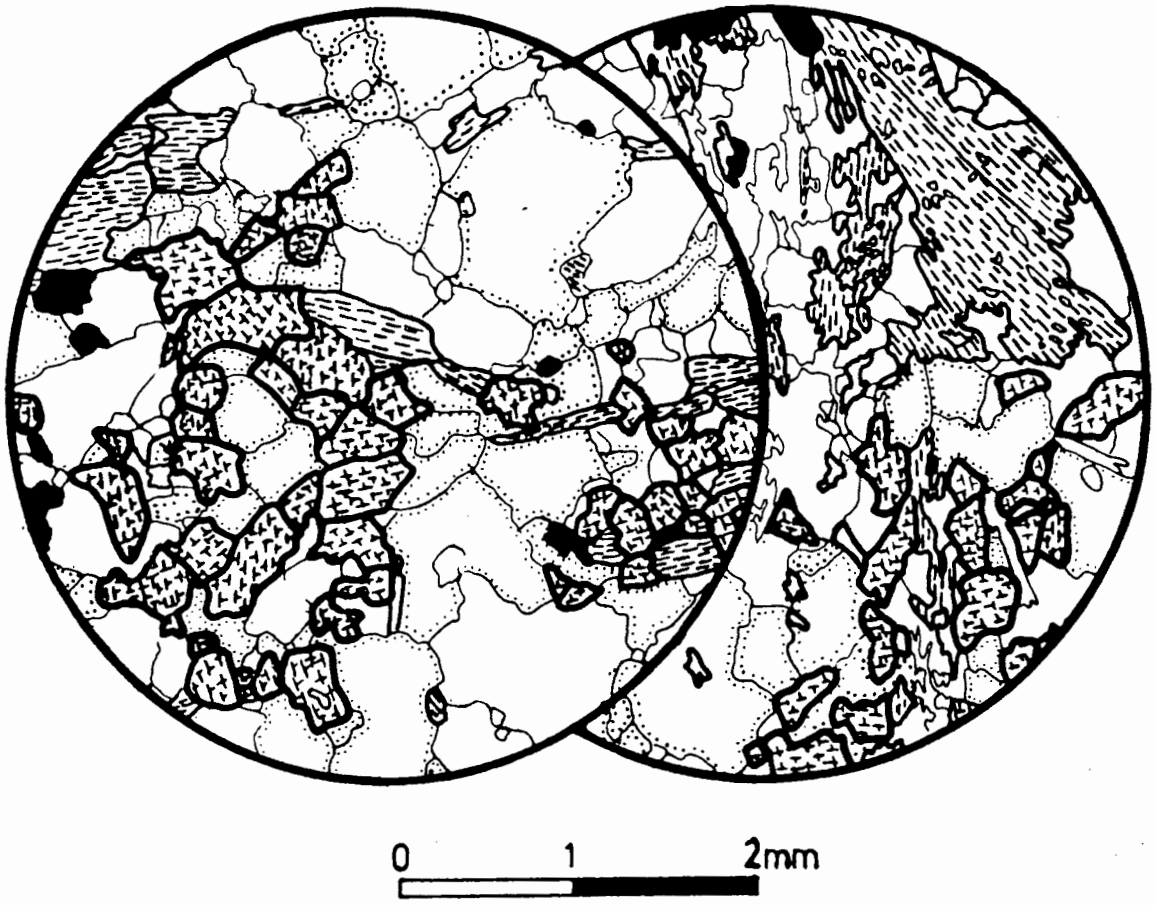

Fig. 2.5a Equant orthopyroxene grains truncating biotite foliation biotite-orthopyroxene leucoparagneiss FB170.
2.5b Skeletal biotite-quartz intergrowths surrounding orthopyroxene in biotite-orthopyroxene leucoparagneiss FB256.

The leucosomes have seriate textures, with grain size varying up to 5 mm. The grain size contrast between matrix and leucosome is both gradational and sharp. In general, sharply defined leucosomes, types (b) and (c) above, are suitable for modal analysis. Quartz and K-feldspar are locally intergrown in granophyric textures, and quartz and plagioclase are commonly myrmekitic. Perthitic and antiperthitic exsolution textures are widespread in the respective feldspar hosts. CO_2 and H_2O fluid inclusions are common in quartz and K-feldspar.

Orthopyroxene in the leucosomes is relatively coarse (<5 mm), subhedral and equant. It is commonly, but not exclusively, associated with K-feldspar. Alternatively, grains are surrounded or embayed by coarse, anhedral, randomly oriented biotite flakes that locally form skeletal intergrowths with quartz parallel to biotite cleavage. The biotite is locally rutilated. Rounded inclusions of biotite and quartz are common in the orthopyroxene.

A comprehensive analysis of the methods and results of detailed modal analysis is presented in section 5.5. In general, leucosomes show an increase in abundance of K-feldspar and orthopyroxene relative to the host matrix, with a concommitant decrease in biotite and plagioclase abundance. While matrix rock may contain up to 3% orthopyroxene, some leucosomes contain 10% orthopyroxene.

2.4.7 Calc-silicate Gneiss

The calc-silicate gneisses occur as laterally discontinuous horizons associated with the biotite-orthopyroxene leucoparagneiss and pyroxene granulite gneiss. A number of distinct compositional varieties crop out in the area. These are:

a) Pl + Di ± Qtz ± Cal ± Bt + Opq;

b) Di ± Pl + Czo + Scp ± Grs ± Ep ± Qtz;

c) Di ± Pl + Cal + Wo + Grs ± Scp.

Type (a) is the most common and crops out as narrow (<2 m thick), grey weathering horizons within the biotite-orthopyroxene leucoparagneisses. It is compositionally banded with plagioclase- and diopside-rich layers. Subhedral diopside and plagioclase (<2 mm) form a granoblastic texture. Quartz is recrystallized and calcite occurs as minor interstitial grains near diopside. Biotite occurs as minor anhedral remnant laths associated with diopside. The opaque minerals have a granular texture.

Only type (a) calc-silicate gneiss contains sparse, coarse-grained (<8 mm) leucosomes. These have antiperthitic, quartz-filled, poikiloblastic plagioclase cores. Diopside and plagioclase occur as granoblastic associations, with minor associated scapolite and epidote, in the haloes that transgress matrix compositional banding. Locally, grossular garnet rims calcite.

Type (b) crops out alternately as dark green and white weathering compositional bands that persist laterally for up to 200 m. In the dark bands, coarse- to medium-grained (<6 mm) subhedral diopside and aggregates of fine-grained (<0.5 mm), euhedral clinozoisite are granoblastically intergrown. Epidote occurs as subrounded embayments in diopside. Scapolite (<3 mm) is subhedral marialite (Deer et al., 1968). Grossular garnet (<2 mm) is a minor granoblastic phase. In the light bands, plagioclase (<4 mm) is pseudomorphed by clinozoisite aggregates, or is weathered to coarse-grained (<4 mm) muscovite laths.

Type (c) crops out at two localities within the 1:50 000 map area, and the same rock type that is described by De Jager and Simpson (1962) at Modderfontein ca. 15 km west of the field area. The latter locality is currently being exploited for fibrous wollastonite for use as an industrial refractory mineral. The outcrops are very rugged, and display a centimetre-scale compositional banding between diopside-rich and wollastonite-rich layers. The rock textures are complex, and are not discussed here.

2.4.8 Quartzofeldspathic Gneiss

The quartzofeldspathic gneisses constitute a major proportion of the supracrustal succession. They are intimately associated with the biotite-orthopyroxene leucoparagneiss, and in places grade into aluminous equivalents (section 2.4.4.1). They occur as

laterally continuous, stratiform horizons up to 500 m thick. The rock is largely homogeneous, with little evidence of either compositional banding or deformation.

Quartz is medium- to fine-grained, with neoblastic rims. The feldspar content varies from 20% to 60%, and is dominated by microperthitic microcline. In outcrops where this K-feldspar is weathered to sericite, the gneiss resembles the homogeneous K-feldspar-quartz gneiss (section 2.4.2). Plagioclase is andesine (An_{20-40}) and has the same granoblastic texture as the rest of the rock. Biotite and magnetite are minor mafic constituents.

Locally, coarse grained (<8 mm) K-feldspar-quartz segregations form ovoid lenses parallel and subparallel to stratification. These are up to 3 m thick, and commonly form boudin-like structures with pegmatitic necks (Plate 14). Narrow (<1 cm), biotite-rich selvages occur locally at the leucosome-matrix contact.

2.5 Fault Zone Cataclasite

The N-S trending fault zones commonly contain mylonitized country rock. It is pink weathering sericitized K-feldspar- and quartz-rich rock that has a strong recrystallized mineral fabric parallal to the orientation of the fault zone. Locally, nebulitic epidote-rich veins permeate the rock. Brecciation of country rock occurs in lenticular pods. It is interesting to note that the farming community use these rocks as ground water source.

2.6 Discussion: Basement to the Supracrustal Succession

Some researchers have proposed, inconclusively, candidates for basement to the supracrustal gneisses of the Bushmanland Subprovince. This work is notably hampered by the paucity of well-distributed radiogenic isotopic data across the terrane. The problem is compounded by geochemical sampling performed without adequate field control.

Watkeys (1986) recently confirmed Moore's (1977, 1986) suggestion that the Achab Gneiss forms part of the basement to the supracrustal succession. A whole rock Pb-Pb isochron age of 2020 ± 150 Ma (Welke and Smith, 1984), and a zircon Pb-Pb age of between 1800 Ma and 2000 Ma (Armstrong et al., 1988) have been derived for this gneiss. Reid et al. (1987a) measured a maximum age for sedimentation, using apparently detrital zircons, of about 1700 Ma for the Bushmanland supracrustal rocks. However, further south, near the field area, there has been no conclusive recognition of a basement to the Garies Subgroup (SACS, 1980) supracrustal rocks.

Augen gneisses of the type described in section 2.3.2 above have traditionally been classified as syntectonic intrusive granites on the basis of their porphyroblastic character (Joubert, 1971; SACS, 1980). Little emphasis has been placed on the distinction between these and the Nababeep-type gneiss, which is intrusive into the supracrustals (e.g. Jack, 1980; Albat, 1984; Moore,

1986). The 'streaky' gneiss, as the hornblende-biotite augen gneiss of the field area have been called, displays regionally concordant contacts with the supracrustal gneisses. Locally, discordant contacts against homogeneous K-feldspar-quartz gneiss are documented. It is possible that this type of contact may be the result of the supracrustal deposition of felsic volcanic lavas (Moore, 1986). The complex internal structure of 'streaky' hornblende-biotite gneiss suggests that it experienced at least on phase of deformation prior to the deposition of the supracrustal rocks. It is thus concluded that the hornblende-biotite augen gneiss, which is exposed over large areas in the southern Bushmanland Subprovince (e.g. Jack, 1980; Albat, 1984), is the most likely candidate for basement to the deposition of the supracrustal succession.

CHAPTER 3 STRUCTURE

3.1 Introduction

The structural relationships within the gneisses and granites of the mapped area have been determined by regional reconnaissance, mineral fabric measurement, and outcrop mapping at selected, critical localities. The results of this structural investigation are outlined in a chronological sequence of deformation events from the earliest, D1, to the most recent, D5. The structural data have been compiled onto an equal area (Schmidt) stereonet, Fig. 3.1. A possible earlier deformation recorded in the biotite-hornblende augen gneiss, for which no data could be systematically collected, is discussed in section 2.5.1. All planar structural measurements are given in terms of dip and dip direction. Linear measurements are given in terms if direction and plunge.

3.2 D1 - Regional Fabric Development

The earliest, unequivocal deformation recognized in granitic and supracrustal gneisses is preserved as locally developed, tight, refolded closures defined by the axial planar orientation S_1 of chloritized biotite in hornblende-biotite augen gneiss, and as centimetre-scale intrafolial folds of S_0 compositional banding in biotite-orthopyroxene leucoparagneiss. In most of the exposures in the area, the regional fabric S_1 is parallel to compositional

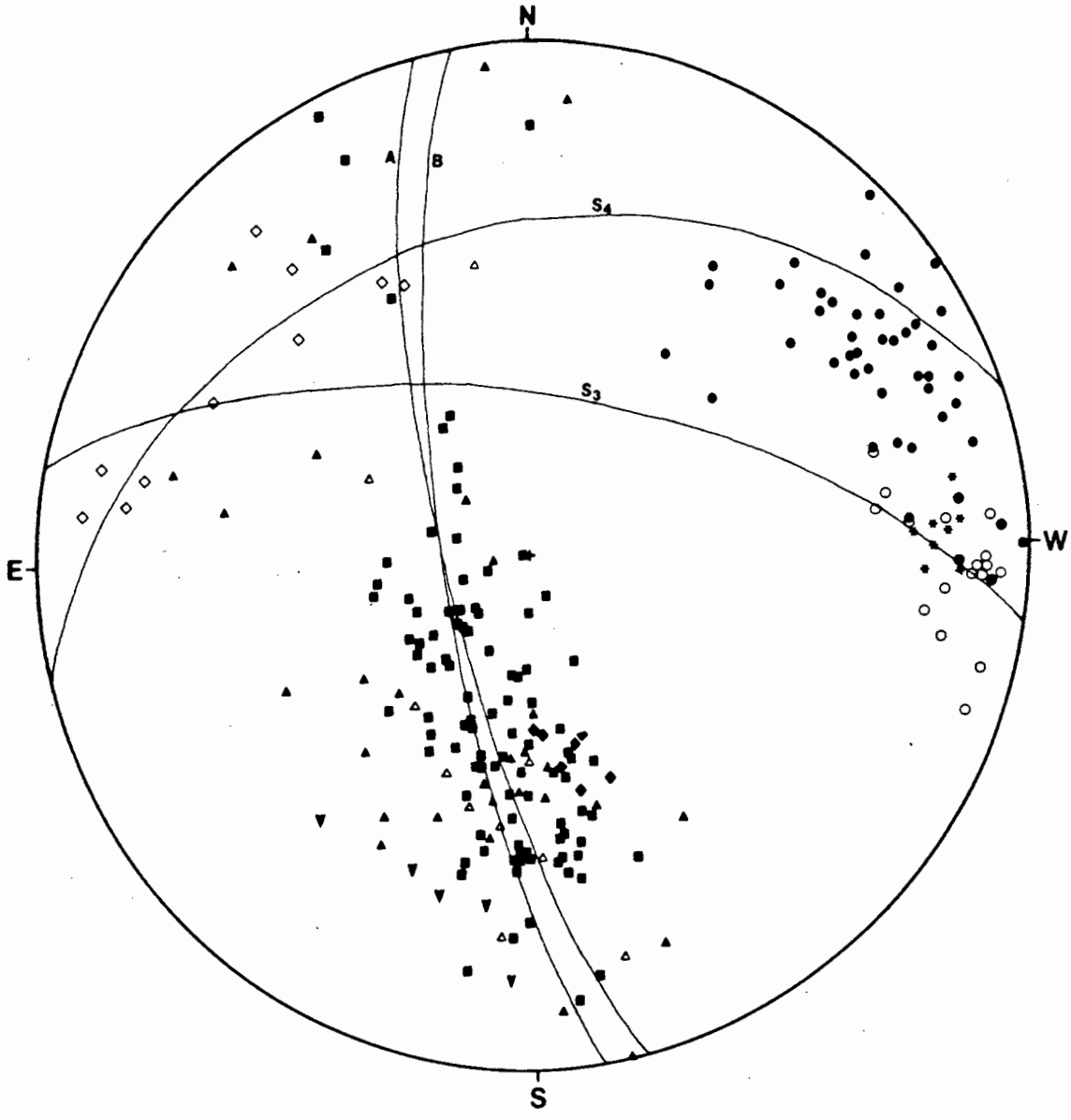

Legend	n
■ Poles to $S_{0/1}$ Compositional Banding, Regional Foliation	98
△ Poles to S_2 Axial Planes	11
▲ Poles to S_2 Mineral Foliations	27
▼ Poles to S_3 Axial Planar Fracture	5
◆ Poles to S_4 Shear Fabric	7
○ L_2 Fold Axes	17
● L_2 Mineral Lineations	48
* L_3 Fold Axes (Observed & Calculated)	8
◇ L_4 Sillimanite Lineation	10
A Great Circle to ■	
B Great Circle to △,▲	
S_3 Mean S_3 Axial Plane	
S_4 Mean S_4 Shear Plane	

Fig. 3.1 Composite plot on a Schmid steroenet of structural elements measured in the study area. See text for discussion.

banding S_0. S_1 and S_0 are regionally N-dipping at between 30^0 and 60^0 in rocks apparently unaffected by later deformation. The poles to S_0 and S_1 fabrics (n = 98) define a trend on the great circle 257/75.

3.3 D2 - N-vergent, Overturned Folding

The compositional banding S_0 and the penetrative regional foliation S_1 are refolded in tight, centimetre- and metre-scale crenulation folds that are near-isoclinal. These folds are best preserved in finely banded metapelitic gneisses (Plate 8), but are also exposed in aluminous quartzofeldspathic and metabasic gneisses, and in biotite-orthopyroxene leucoparagneisses.

The fold axes of class IC (Ramsay, 1967) s- and z-parasitic folds plunge consistently in the range 078/30 to 110/08, with the main cluster of values (n = 17) plunging around 093/10. The poles to the axial planar orientations of sufficiently 3-dimensionally exposed crenulation folds dip in a range of values (n = 11) between 348/42 and 166/48. These describe a trend on the great circle 262/75, on which the main cluster of values dip at about 015/40 in N- and NE-dipping compositional bands.

Locally, four types of mineral lineation are aligned parallel to the crenulation fold hinges. These are:

a) Quartz-rodding in finely banded aluminous- and -quartzo-feldspathic gneisses;

b) Preferred orientations of biotite laths in quartz-rich metabasic, aluminous quartzofeldspathic and metapelitic gneisses, and biotite-orthopyroxene leucoparagneiss;

c) Oriented aggregates of sillimanite surrounded and mimicked by hercynite and opaque phases in quartz-rich metapelitic gneiss at Witberg; and

d) Entrainments of garnet- and/or cordierite-bearing leucosome assemblages in aluminous quartzofeldspathic and metapelitic gneiss.

These textures are not observed at an angle to crenulation fold hinges, but they do occur in horizons apparently unaffected by D2 deformation. Two other mineral lineations also occur away from crenulation folds. These are:

e) Sparsely distributed, linear entrainments of orthopyroxene-bearing leucosome assemblages in biotite-orthopyroxene leuco-paragneiss;

f) Centimetre-scale, poikiloblastic intergrowths of ortho- and clinopyroxene, and hornblende prisms in pyroxene granulite and quartz-rich metabasic gneiss; and

g) Clusters of biotite and hornblende that define the prominent lineation of hornblende-biotite augen gneiss (section 2.3.2).

The mineral lineations plunge consistently in the range 045/38 and 095/09, with the main cluster of values (n = 48) at 064/20.

Although D2 deformation is not associated with a penetrative S_2-

fabric in the supracrustal gneisses, mineral foliations are developed that are locally parallel to the axial planes of crenulation folds. These textures include:

a) Lenticular, garnet- and/or cordierite-bearing leucosome assemblages, which also transgress crenulation folds, in massive aluminous quartzofeldspathic and metapeltic gneiss; and

b) Narrow, poikiloblastic ortho- and clinopyroxene aggregates surrounding hornblende prisms in plagioclase-rich pyroxene granulite gneiss (FB 324) intercalated with metapelitic gneiss.

These foliations intersect S_0 compositional banding and S_1 regional foliation, thereby defining some of the intersection mineral lineations described above. Fig. 3.1 shows that the poles to the S_2 mineral foliations (n = 27) consistently define a trend on the great circle 270/70, on which the main cluster of values is around 184/50 in N- and NE-dipping compositional horizons.

Biotite-orthopyroxene granite gneiss is characterised by a weak biotite foliation which is broadly parallel to the regional foliation of the supracrustal gneisses. Since the granite truncates S_1, its own foliation represents fabric development after D1. The poles to the granite gneissic foliation trend on the same great circle as that described by the D2 mineral

foliations, and, therefore, probably represents an S_2-fabric. Similarly, the foliation of biotite and of the garnet-bearing leucosome assemblage in an anatectic granite dyke east of Witberg (section 2.3.6) is an S_2-fabric.

The minimum metamorphic conditions prevailing at the time of the onset of D2 deformation are indicated by mineral lineation textures (b) and (c) above, and the preferred orientation of fine, acicular sillimanite inclusions in garnet and cordierite in metapelitic and aluminous quartzofeldspathic gneiss (section 2.4.5.1), parallel to the elongation of its prograde products, garnet and cordierite. The prograde growth of sillimanite under at least amphibolite facies conditions ($T>550^{o}C$; Turner, 1981) coincided with its orientation during D2 deformation. Similarly, the orientation of early, prograde sillimanite, surrounded by hercynite and opaques, parallel to crenulation fold hinges (mineral lineation texture (c) above) attests to this coincidence. Biotite is stable under at least upper greenschist facies conditions (Turner, 1981). Quartz-rodding (mineral lineation texture (a) above) can take place under a wide range of P-T conditions (Hobbs et al., 1976, p. 280-283), and thus cannot be used as a reliable tectonothermal indicator.

It is important to note here that, while the mineral lineations and foliations have been used to characterize the orientation of D2 deformation, the metamorphic conditions responsible for producing many of these mineral assemblages and textures were not

necessarily coeval with D2 deformation. Evidence is given in sections 5 and 6 for the importance of pre-existing compositional control on, in particular, the site and orientation of the products of upper amphibolite and granulite facies partial melting. In this way, for example, the apparently axial planar orientation of garnet-bearing leucosomes in metapelitic gneisses reflects a pre-existing orientation of a biotite-sillimanite-quartz assemblage. The presence of leucosomes that completely transgress D2 crenulation folds, suggests that prograde metamorphism outlasted the D2 deformation event. The absence of textures indicating that leucosomes or their constituents were rotated into their present orientation during D2 crenulation folding, confirms this suggestion.

There are no recognisable exposures of major D2 fold closures in the field area. Furthermore, there is no clear systematic spatial distribution of s- and z-parasitic crenulation folds that might give clues as to the location of these closures, if indeed they exist. The repetition of certain supracrustal horizons is also ambiguous, in that it has its origin in synsedimentary intercalation and late shearing (section 3.5, below).

3.4 D3 - Upright, Asymmetric, Open Folding

The map shows exposures of large, kilometre-scale, approximately east-plunging antiformal and synformal fold closures of S_0 compositional banding and S_1 regional foliation. The closures typically have steep or moderately dipping northern limbs that

gradually dip shallower in a southward traverse. The southern limbs are typically steeply N-dipping, commonly consisting of relatively narrow bands (<100 m wide) of intensely foliated or sheared rock that are negatively weathering. The fold closures themselves are consequently relatively poorly exposed and it is difficult to maeasure their orientations. Although the folds cannot be accurately classified, they are probably class III folds (Ramsay, 1967).

A composite plot of all S_0 and S_1 values from the area (n = 98, Fig. 3.1) shows a consistent regional relationship with D3, and indicates an average plunge of 087/15 for D3 folds. Similarly, S_2 mineral foliations are folded around D3 fold closures. An average plunge of 090/20 is calculated from their great circle trend (Fig. 3.1). D2 crenulation folds are typically open, even monoclinal on the broad northern fold limbs, and tight on the steeply-dipping southern limbs of D3 folds.

Locally, centimetre- and metre-scale, E-plunging, cuspate folds are developed in the hinge zones of D3 fold closures. Measurement of their plunge (n = 5) confirms the calculated plunge of D3 folds at 090/20.

D3 folds are not associated with any penetrative cleavage or mineral fabric development. Locally, in quartzofeldspathic gneiss, regular fractures spaced between 5 m and 10 m apart occur

in the hinge zones of D3 folds. Their orientation appears to be axial planar with respect to fold limbs. Fig. 3.1 shows the poles to their dip values (n = 5) varying between 184/18 and 220/32. The calculated and observed values of L_3, fold plunge, plot within this range, defining an average axial plane dipping at 010/65.

It is difficult to constrain precisely the metamorphic conditions prevailing during D3 deformation. The deformation of S_2 and L_2 mineral and crenulation fold fabrics around D3 fold closures, and the absence of any mineral fabrics associated with D3 structural elements, confirm that granulite facies migmatite generation was complete at the onset of D3 deformation.

3.5 D4 - Shearing

The overturned and near-vertical southern limbs of D3 asymmetric folds are typically composed of intensely refoliated rock in E-W-trending and steeply N-dipping bands, continuous over a few km and <50 m wide. Elsewhere, similar bands of sheared rock occur within the regionally foliated, N-dipping gneisses that are apparently not folded by D2 and D3 deformation. Locally, the bands occur as discrete horizons, as between the homogeneous K-feldspar-quartz gneiss and the hornblende-biotite augen gneiss. However, commonly they form stacks of three or more recognisable sheared horizons within <500 m thickness. Where S_0 compositional banding and S_1 regional foliation in rocks immediately adjacent

granitic gneisses, quartz and feldspar display evidence of fine-grained, neoblastic recrystallization in narrow, mm- and cm-scale bands that overprint earlier metamorphic textures. In biotite-bearing assemblages, retrograde biotite grains form planar oriented clusters, which locally resorb peak ferromagnesian phases. In aluminous quartzofeldpathic and metapelitic gneisses, sillimanite associated with recrystallized quartz and feldspar forms in compositional planes. In biotite-orthopyroxene granite gneiss, K-feldspar-rich leucosomes are stretched into an orientation parallel to the biotite-defined c-surfaces of the sheared rock. Fig. 3.1 shows the poles to the S_4 refoliation fabric (n = 7) plunging consistently around 168/58, thus defining an average shear plane that dips at 348/32. The two shallow easterly-dipping values represent the curvature of schistosity around the western contact of biotite-orthopyroxene granite gneiss with quartzofeldspathic gneiss.

Coarse-grained sillimanite in shear planes of aluminous quartzo-feldspathic and metapelitic gneiss is randomly oriented within the shear plane. However, fine-grained sillimanite crystals commonly have a preferred linear orientation. Fig. 3.1 shows the L_4, mineral lineations plunging consistently in the range from 277/09 to 335/41. They define a trend on the great circle 345/36, a calculated shear plane orientation that is consistent with the above observed average. However, it is important to note that no consistent transport direction in this shear plane has been determined for D4 shearing.

3.6 D5 - N-S Faulting

The rocks of the field area are truncated along a series of NW-SE to N-S trending near-vertical and vertical faults and fault zones (as defined by Hobbs et al., 1976, p.300). The faults give rise to sharp lithological discontinuities, although regional litho-stratigraphic trends are continuous across the boundaries. The fault zones are <500 m wide between the bounding faults, and lithologies commonly show incremental displacements across shorter faults within the fault zones. However, some fault zones contain cataclastic fault breccia, which locally contains a mylonitic fabric, parallel to the fault zone boundaries. Locally, narrow, discontinuous dyke-like pods of microgranite are emplaced along fault planes. These contain biotite with a preferred orientation parallel to the fault plane.

The sense and amount of displacement across the fault zones has not been determined accurately. A combination of dextral, vertical, and rotational displacements of the order 10 and 100 m is inferred for many of the faults and fault zones, with obvious exceptions (see map).

3.7 Discussion

It is generally agreed that the regional foliation of many of the

supracrustal and early granitic augen gneisses was formed at relatively high metamorphic grades in response to isoclinal deformation, evident in the local occurrence of intrafolial folds of S_0 compositional banding with axial planar orientations of biotite S_1.

Hartnady et al. (1985), Strydom (1985), Joubert (1986), Strydom and Visser (1986) and Watkeys (1986) consider D2 deformation to represent a phase of approximately south-directed thrusting and south-vergent overfolding related to the accretion of the Namaqua Province. Evidence for this occurs at the boundary between the Bushmanland and Richtersveld Subprovinces along the Groothoek Thrust zone. D2 crenulation folding in the field area is correlated in style and geometry with the folding associated with thrusting. However, D2-age thrusting is not evident in the field area. Mineral textures suggest that prograde mineral growth and metamorphic partial melting coincided with the onset of D2 deformation in a compressional tectonic regime, and continued for a significant period of time after its relaxation.

D3 deformation is not associated with any textures of prograde mineral growth and metamorphic partial melting. The onset of D3 deformation post-dated peak metamorphic conditions. The metamorphic conditions prevailing during D3 deformation can be loosely bracketed by the occurrence of biotite and sillimanite associated with D4 shearing, viz. post-peak granulite facies. Most accounts of other areas in the western Bushmanland

Subprovince point to the near-coeval temporal relationship between shearing and open, east-plunging, asymmetric folding (e.g. Joubert, 1971, 1986; Jack, 1980; McStay, in prep.).

There is a marked spatial association between D4 shear zones and the overturned and steeply-dipping southern limbs of asymmetric D3 folds, where refolded D2 crenulation folds are apparently shortened. Horizons in D3 fold closures are commonly truncated or attenuated at D4 shear zones, suggesting that shearing occurred as consequence of D3 deformation. D4 shear zones are also developed as discrete horizons between rock types with marked differences in competency, e.g. between biotite-orthopyroxene granite gneiss and supracrustal quartzofeldpathic gneiss.

Popular models of simple flexural shear suggest that the fold axes are oriented perpendicular to the direction of shearing on fold limbs (Donath and Parker, 1964; Hobbs et al., 1976). In the field area the calculated plunge of D3 asymetric folds, L_3, occurs at oblique angles of between 95^0 and 150^0 to the L_4 shear lineation. Earlier models have been modified to account for the origin of this oblique relationship (Ramsay, 1967; Hobbs et al. 1976), suggesting that a significant component of shear folding accompanied D3 deformation, in order to produce D4 simple (rotational) shearing.

No unambiguous tectonic model can be applied to the formation of

D3 and D4 deformation entirely on the basis of the structural relationships described, without accounting for the thermal evolution during that interval. Classical models of crustal thickening, and subsequent uplift and erosion infer conditions of compressional tectonics for the entire history of regional metamorphism (e.g. England and Richardson, 1977). In such a model, thrusting and simple shear necessarily predates the metamorphic peak. Researchers are increasingly recognizing that uplift occurs with gravitational collapse and the consequent extension of previously thickened crust (England and Thompson, 1984; Chamberlain and England, 1985; Chamberlain and Karabinos, 1987; Ellis, 1987). As shown in this study significant amounts of simple shear postdated the metamorphic peak, and retrograde re-equilibration of peak assemblages is common along these shear zones.

Much attention has recently been given to the possible significance of extensional tectonics in producing at least some of features of regionally metamorphosed and deformed terranes (e.g. Sandiford, 1985a, b, 1989; Wickham and Oxburgh, 1985; Sandiford and Powell, 1986; Ruppel et al., 1988; Robinson, 1987; Robinson and Bevins, 1989). Reston (1988) showed that extension in the lower crust offshore Britain "may be accomodated by the relative movement of low-strain lozenges along intervening zones of simple shear" by seismic reflection studies. In such a model, extension along narrow, anastomosing shear zones (low-angle, normal faults) necessarily accompanies retrograde metamorphism.

These observations are consistent with the relationships between metamorphism and deformation in the study area. It is significant to note that all the deformation episodes, D1 to D4, reflect ductile behaviour.

The only brittle deformation recorded in the field area is reflected in the vertical and near-vertical N-S faulting, which is a characteristic feature of the western Bushmanland Sub-province (Joubert, 1974c). These faults are believed to have formed in response to Pan African deformation of southwestern Africa. The faults are parallel to the coastal margin of low-grade metamorphism, generally ascribed to the Pan African orogeny (Waters et al., 1983; Waters, 1986; see Fig. 1.2).

CHAPTER 4 GEOTHERMOBAROMETRY

4.1 Introduction

The peak mineral assemblages developed in Garies-Platbakkies supracrustal gneiss belt during the Namaqua tectonothermal event belong to the granulite facies. Temperatures and pressures which may approximate peak metamorphic conditions and part of the retrograde P-T path have been calculated using experimentally and thermochemically calibrated equilibria applied to selected assemblages from the study area.

Bohlen et al. (1983b) and Bohlen and Lindsley (1987) reviewed the thermobarometers that are most useful for igneous and metamorphic rocks. Those involving cordierite are investigated by Bhattacharya (1986). This chapter generally follows their recommendations. The equilibria used in this study are usefully classified into multivariant thermobarometers, cation exchange thermometers and solvus thermometers.

Representative mineral analyses of rocks used for thermobarometry are listed in Appendices 1B, K-M. Some of these data were collected for an Honours project (Baars, 1986).

4.2 Multivariant Thermobarometers

4.2.1 Introduction

Equilibria in which one or more of the phases has appreciable solid solution are multivariant in P-T-X space. The compositions of co-existing minerals in assemblages related by these equilibria can provide quantitative estimates of pressure and/or temperature, if the equilibrium and mineral solution parameters are adequately calibrated (Bohlen and Lindsley, 1987). Assemblages, whose textures suggest equilibration at the metamorphic peak and for which accurate mineral composition data are known, include:

a) Grt + Pl + Sil + Qtz;

b) Grt + Hc + Sil + Qtz;

c) Grt + Opx + Pl + Qtz;

d) Grt + Crd + Sil + Qtz;

e) Grt + Crd + Sil + Hc;

f) Crd + Hc + Qtz.

4.2.2 Garnet-Plagioclase-Sillimanite-Quartz Thermobarometry

The equilibrium [An = Grs + Sil + Qtz] is a barometer that has

recieved popular application in granulite facies terranes (e.g. Grew, 1981; Ghent et al. 1982; Brown and Earle, 1983; Albat, 1984; Sandiford, 1985; Grutter, 1986; Schreurs and Westra, 1986; Edwards and Essene, 1988) based on experimental calibrations by inter alia Ghent (1976), Ghent et al. (1979), Newton and Haselton (1981), and Koziol and Newton (1988). The thermochemical calibration of Powell and Holland (1988) provides an independent estimate. Bohlen and Lindsley (1987) discredit this barometer because of an error in precision of at least ±2 kbar, and the extrapolation of the equilibrium from high pressures and temperatures. This is in contrast to the contention of Hodges and Spear (1982) and Baker and Droop (1983) that the P-estimates are reasonably accurate.

In the field area, the assemblage occurs in a sheared metapelitic gneiss FB210. Sillimanite forms prismatic overgrowths on garnet and cordierite, and narrow rims around hercynite. Sillimanite is associated with finely recrystallized bands of quartz. At 700°C, 750°C and 800°C, the following estimates of pressure are respectively derived (all ±2 kbar) (Fig. 4.1):

a) Powell and Holland (1985): 4.8, 4.1 and 3.5 kbar.
b) Newton and Haselton (1981): 5.1, 4.5 and 3.9 kbar; and
c) Ghent (1976): 4.7, 4.2 and 3.8 kbar;

In view of the eight-phase assemblage and the retrograde texture of the rock, the P-T conditions of any one calibration cannot be

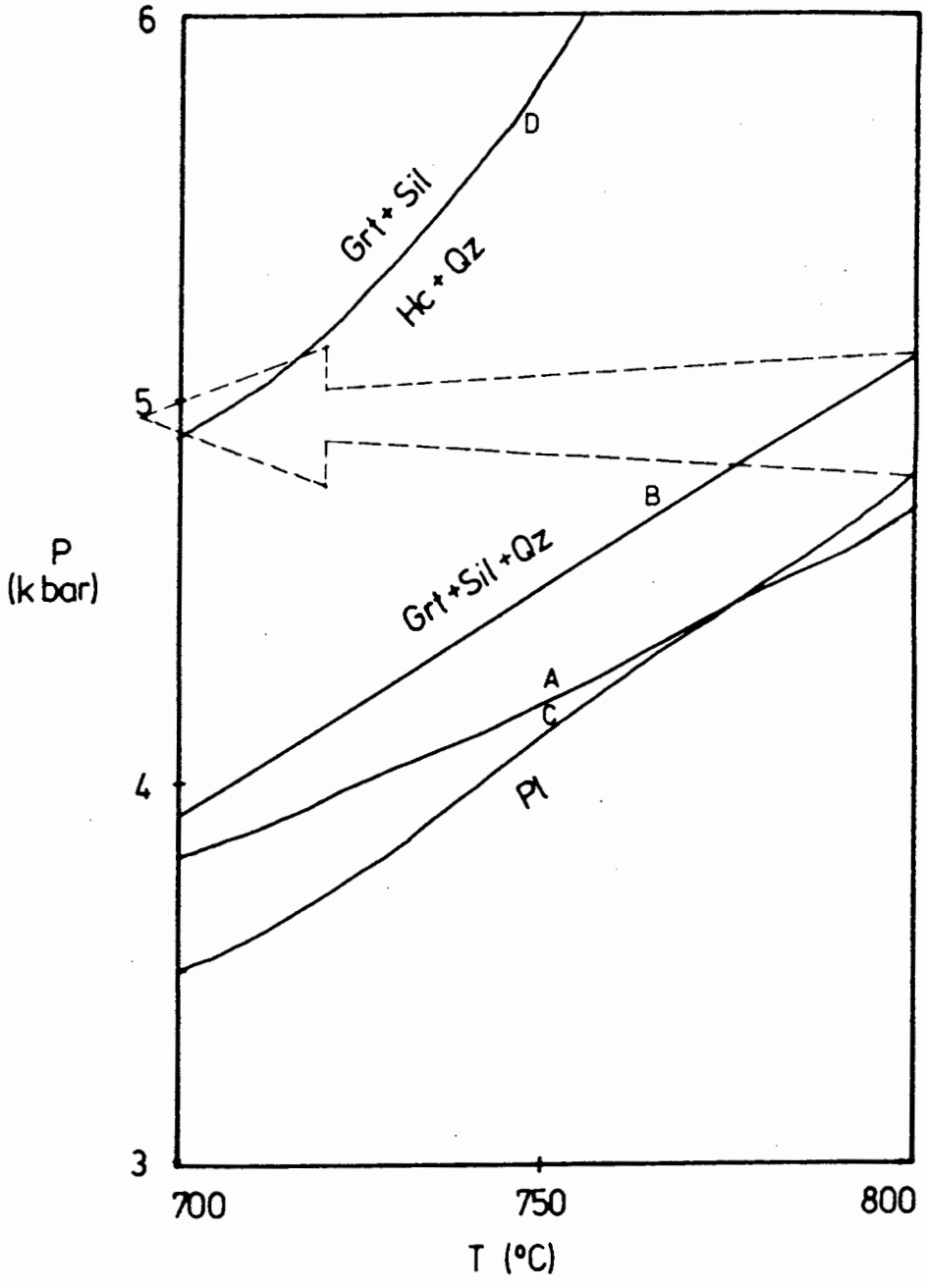

Fig. 4.1 P-T conditions of stability of the assemblage Grt-Pl-Sil-Qtz in FB210
using the geothermobarometer calibrations of
A - Ghent (1976)
B - Newton and Haselton (1981)
C - Powell and Holland (1988);
and of the assemblage Grt-Hc-Sil-Qtz in FB210
using the calibration of Perkins and Chipera (1985).
Dashed arrow indicates possible retrograde P-T path.

taken to approximate peak metamorphic conditions. Rather, they define a curve (locus of points) across which the retrograde cooling path passed passed at some point (Fig. 4.1).

4.2.3 Garnet-Hercynite-Sillimanite-Quartz Thermobarometry

Bohlen et al. (1986) present an experimental calibration of the equilibrium [Hc + Qtz = Alm + Sil]. In FB210, hercynite is separated from quartz by narrow garnet and/or sillimanite rims. The equilibrium constant is given by the expression

$$K = [(a_{Alm})(a_{Sil})^3]/[(a_{Hc})^3(a_{Qtz})^5].$$

The activities of almandine and hercynite are calculated from the expressions of Perkins and Chipera (1985) (after Fuji and Scarfe, 1982) that include terms accounting for the spessartine component of garnet. The ferric:ferrous iron ratio of hercynite is computed stoichiometrically using the expression of Droop (1987). At 700°C, 750°C and 800°C the pressures (±1 kbar) are estimated at 4.9 kbar, 5.8 kbar and 7.5 kbar, respectively (Fig. 4.1). These P-T values describe a curve across which the retrograde cooling path of the rock passed at some point.

4.2.4 Garnet-Orthopyroxene-Plagioclase-Quartz Thermobarometry

Thermobarometers using the generalized equilibrium

$$[Opx + An = Grt + Qtz],$$

existing with garnet, $[Opx_{Fs-En} + Opx_{Ts} = Grt_{Alm-Py}]$, have been

calibrated by a number of authors (Wood and Banno, 1973; Wood, 1974; Danckworth and Newton, 1978; O'Hara and Howells, 1978; Perkins and Newton, 1980; Harley and Green, 1982; Newton and Perkins, 1982; Bohlen et al., 1983d; Harley, 1984b; Perkins and Chipera, 1985; Powell and Holland, 1988), on the basis of thermodynamic calibrations and/or experimental reaction reversals. The stability of aluminous orthopyroxene is expressed as a hypothetical, divariant solvus equilibrium (section 4.4). It is convenient to treat both reactions together for the purposes of comparison. The earliest five (of the above) calibrations are useful for application in mantle-derived rocks (Bohlen and Lindsley, 1987), and are not used here.

In leucosomes of sample FB71, an anatectic garnet-biotite granite (Fig.2.2b), a central core assemblage of massive garnet subhedra that are embayed and partially rimmed by poikilitic garnet euhedra, are surrounded by a discontinous mantle of granular orthopyroxene and microperthitic microcline. Coarse-grained garnet cores are partially pseudomorphed by skeletal biotite-quartz intergrowths forming radiating clusters with plagioclase. Despite this retrogression, a remnant textural equlibrium in the assemblage [Grt-Pl-An-Opx] of a crystallised, early anatectic peraluminous granite has been preserved.

In the range 730°C to 830°C, the pressure estimates are in the range (Fig.4.2):

Harley and Green (1982), CFMAS: 2.4 to 5.8 ± 1 kbar;

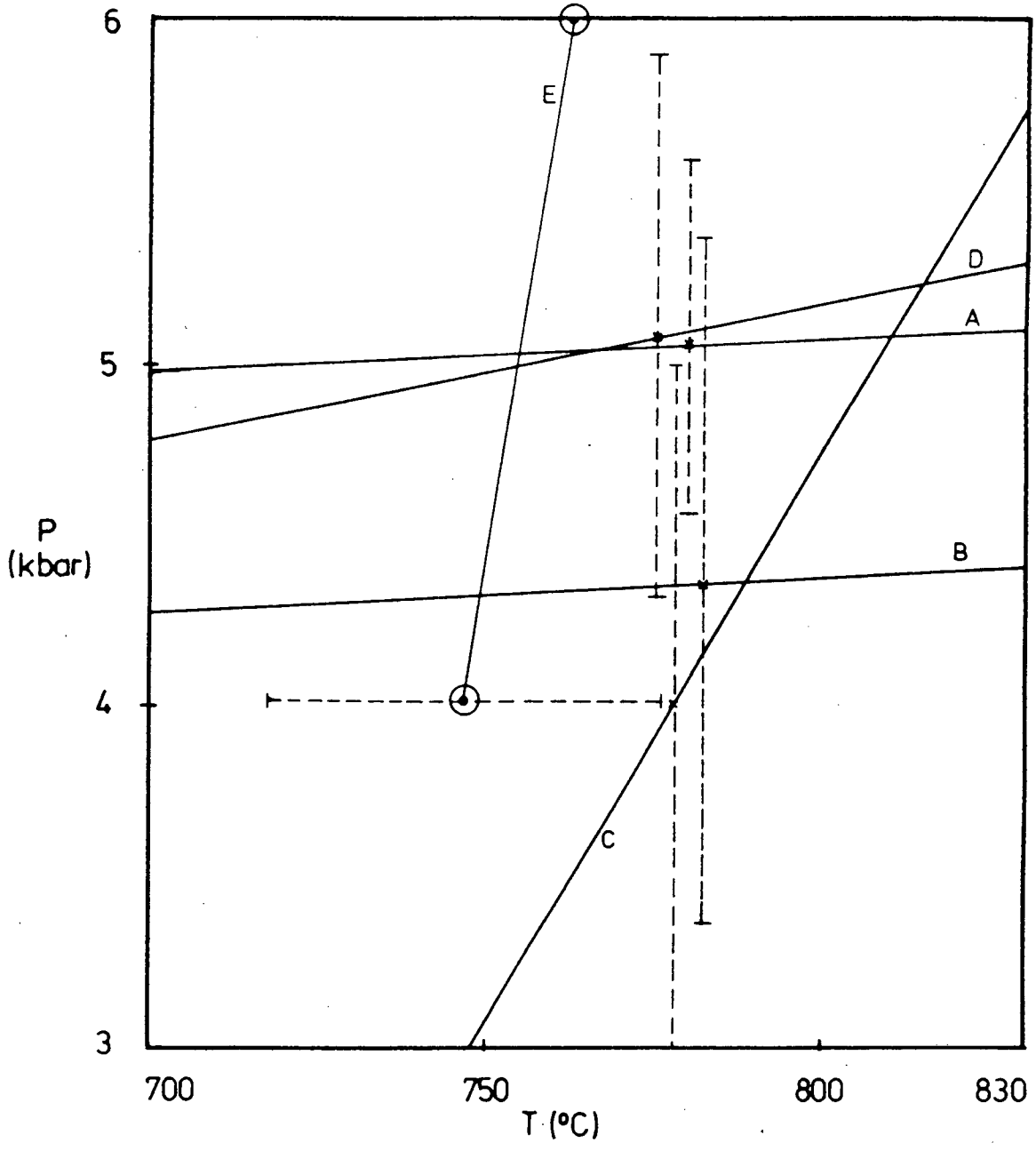

Fig. 4.2 P-T conditions with errors of stability of the assemblage
Grt-Opx-Pl-Qtz in FB71
using the geothermobarometer calibrations of
A - Newton and Perkins (1982)
B - Powell and Holland (1988)
C - Harley and Green (1982)
D - Harley (1984b);
and using the Fe-Mg exchange thermometer of
E - Sen and Bhattacharya (1985).

Newton and Perkins (1982), CMAS: 5.0 to 5.1 ± 0.5 kbar;

Harley (1984b), CFMAS: 4.9 to 5.3 ± 0.8 kbar; and

Powell and Holland (1985), CMAS: 4.3 to 4.4 ± 1 kbar.

Harley (1984b) proposed a barometer based on experimental calibration of the pressure-dependence of the solubility of alumina in orthopyroxene co-existing with garnet. The assignment of Al to the tetrahedral and M1 sites is critical in Al-rich species (>3 wt% Al_2O_3). His method of assigning equal quantities of Al to each site is an improvement on the stoichiometric method of Deer et al. (1968), because the latter is too critically dependent on the accuracy of silica analysis. This method applied to co-existing garnet and orthopyroxene in sample DWN554, a magnesian gneiss, yields a pressure estimate of 5.5 ± 1.5 kbar at 750°C.

Perkins and Chipera (1985) present a model of temperature-dependent end-member activities in plagioclase and spessartine-bearing garnet (cf. Ganguly and Saxena, 1984). At 750°C, application of their barometer to sample FB71 yields pressue-estimates of 7.5 ± 0.5 kbar in CMAS and 6.7 ± 1 kbar in CFAS. The discrepancy between the two end-member results sheds doubt on the internal consistency of their thermobarometers.

4.2.5 Garnet-Cordierite-Sillimanite-Quartz/Hercynite Thermobarometry

In view of the retrograde nature of the textures in the eight-phase assemblage of FB210, and the possibility of both textural and chemical disequilibrium (sections 4.2.2 and 4.2.3), it is inappropriate to apply the barometric expressions of Hensen and Green (1973), Lonker (1981), Martignole and Sisi (1981), Bhattacharya (1986) to this rock.

4.2.6 Cordierite-Hercynite-Quartz Thermobarometry

Bhattacharya (1986) calibrated the reaction [Crd = Hc + Qtz] in the system FAS. In sillimanite-free compositional bands of metapelitic gneiss FB210, lobate hercynite-magnetite intergrowths pseudomorph cordierite grains. These intergrowths have narrow rims of cordierite against quartz, suggesting that a limited amount of retrogression occurred.

The equilibrium [Crd <-> 2Hc + 5Qtz] is sensitive to Fe-Mg partitioning between cordierite and hercynite (section 4.3.6), and local or regional metamorphic fluid activity gradients at a given temperature and pressure (Newton, 1972; Kars et al., 1980; Johannes and Schreyer, 1981; Vielzeuf, 1983; Bhattacharya, 1986; Waters, 1986b). Fig. 4.3 shows how calculated pressures for a cordierite-hercynite pair co-existing with quartz in sample FB210 depend on water activity. The P-T curves of the reaction boundary are logarithmically scaled plots in terms of temperature and $X(H_2O)^{Crd}$. It is important to note that the barometric

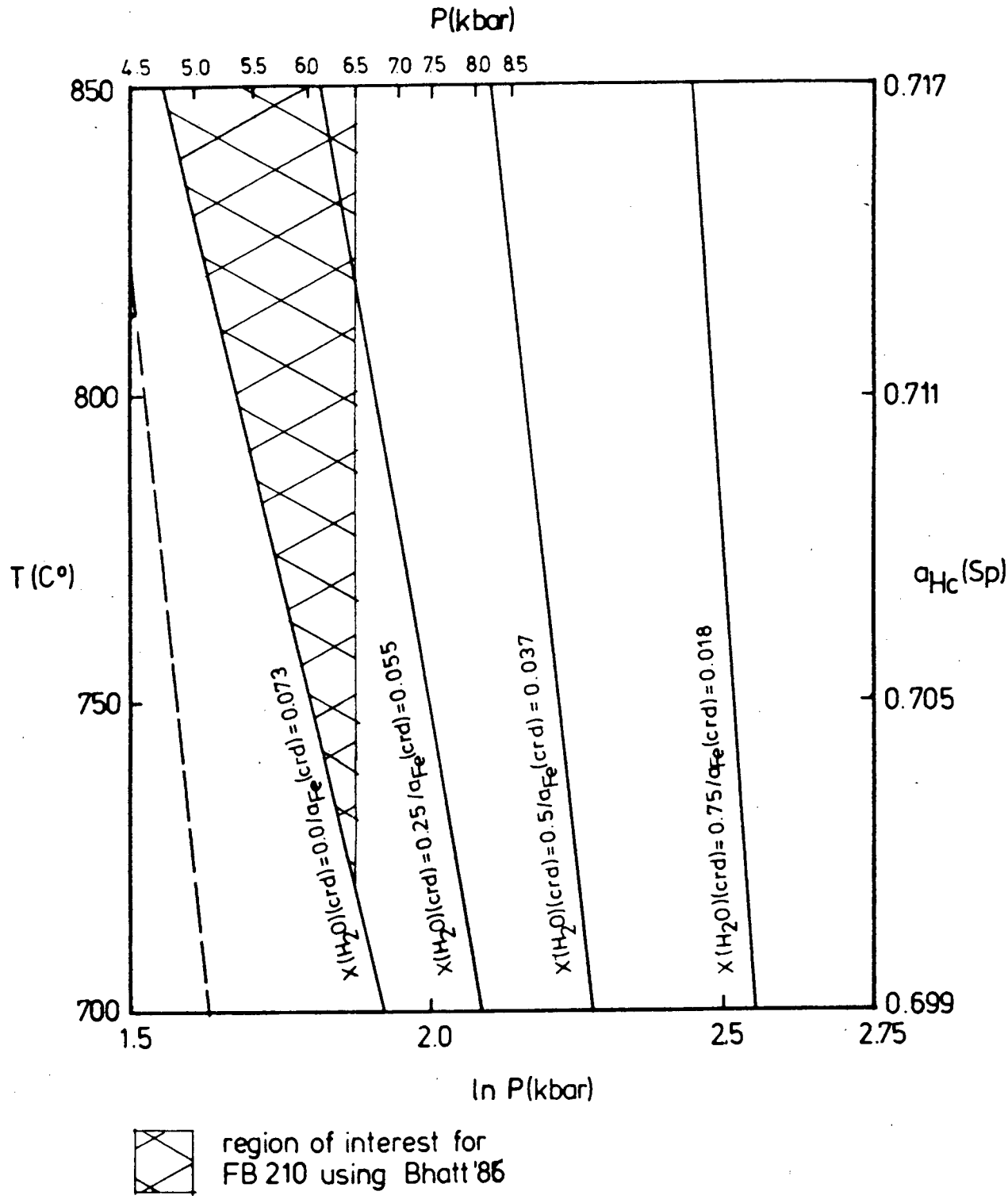

Fig. 4.3 Pressures calculated for a cordierite-hercynite pair co-existing with quartz in FB210, using the calibration of Bhattacharya (1986). This calibration is sensitive to $X(H_2O)$(Crd).The dashed line at relatively low P shows the P-T conditions of stability of Fe-Mg exchange of the same pair using the calibration of Vielzeuf (1983).

formulation indicated on the diagram incorporates the effect of ambient $a(H_2O)$ on the activity composition of cordierite, as in Bhattacharya and Sen (1985). Similarly, the acitvity composition of hercynite is temperature-dependent, as in Bhattacharya (1986) (similar to O'Neil and Navrotsky, 1984), respectively.

Bhattacharya's (1986) model does not systematically account for analytical error. He suggests, by comparison with other barometers that the error is $\pm$1.2 kbar. On Fig. 4.3 the pressure contours intersect the P-T range of interest indicated by multivariant garnet-orthopyroxene thermo-barometry in the shaded area. This suggests that dry cordierite equilibrated with hercynite in FB210 P-T range between 6.5 $\pm$ 1.2 kbar at 750°C and 4.7 $\pm$ 1.2 kbar at 850°C. Alternatively, cordierite with $X(H_2O)$ = 0.25 may have equilibrated with hercynite in the P-T range between 6.5 $\pm$ 1.2 kbar at 815°C and 6.0 $\pm$ 1.2 kbar at 850°C. These results are difficult to interpret without an independent estimate of the local metamorphic fluid $a(H_2O)$ or $X(H_2O)^{Crd}$. In addition, it is noted that FB210 contains shear lamina, so that the constrained P-T conditions define a region through which the retrograde cooling path of the rock passed after peak metamorphism.

Trial runs in MAS with data from Holland and Powell (1985, 1988) and Powell and Holland (1988) indicate the same compositional trends as in FAS, with reaction boundaries displaced to higher pressures. This is predicted by inter alia Thompson (1976), Grant

(1985a) and Vielzeuf and Boivin (1984). The precise determination of the vapour-content of cordierite is a priority for further investigation of the hercynite-cordierite transition. The strong Fe-Mg partitioning between hercynite and cordierite (Vielzeuf, 1983) is discussed in section 4.3.6.

4.3 Cation Exchange Thermobarometry

4.3.1 Introduction

The exchange of a cation pair between two phases or between two sites of the same phase is a useful measure of the metamorphic stability conditions. The criterion for exchange equilibrium is that the chemical potential for each component is the same in both phases (Bohlen and Lindsley, 1987). The equilibrium constant is

$$K_{A-B}(x-y) = [a_A(x).a_B(y)]/[a_A(y).a_A(x)]$$

and

$$a_A(x) = X_A(x).\&_A(x), \text{ etc.,}$$

so that

$$K_{A-B}(x-y) = K_D.K_\&$$

where $a_A(x)$ is the activity of component A in phase x,

$X_A(x)$ is the mole fraction of A in phase x,

$\&_A(x)$ is the activity coefficient,

K_D is the ratio of mole fractions, and

$K_\&$ is the ratio of activity coefficients.

For ideal solutions, $K_\&$ is unity, and the ratio of mole fractions can be expressed as a function of temperature and pressure (Wood

and Fraser, 19??). Since the pressure-variance of exchange reactions depends on the volume change of the reaction which is commonly low, K_D is temperature-dependent. In this way, cation exchange equilibria are useful as thermometers if accurate composition data for ferro-magnesian mineral pairs.
The distribution of Fe^{2+} and Mg^{2+} between the following mineral pairs has been independently calibrated and their usefulness is considered below.

Grt-Opx; Grt-Bt; Opx-Bt; Grt-Crd; Crd-Hc.

4.3.2 Garnet-Orthopyroxene Thermometry

Harley (1984a) and Sen and Bhattacharya (1984) propose experimental and thermochemical calibrations of Fe-Mg partitioning between garnet and orthopyroxene, respectively.

The textures of FB71 and DWN552 (sections 2.3.6 and 2.4.4.3, respectively) suggest that garnet and orthopyroxene co-existed at the metamorphic peak. Garnet-orthopyroxene pairs of FB71 have an average K_{Fe-Mg}(Grt-Opx) of 0.346. Between 4 and 6 kbar the temperature estimates are:

Harley (1984a): 689 to 701 $\pm$ 70°C; and

Sen and Bhattacharya (1984): 760 to 775 $\pm$ 30°C (Fig. 4.2).

In DWN552 garnet-orthopyroxene pairs have a K_{Fe-Mg}(Grt-Opx) of 0.356. Between 4 and 6 kbar the temperature estimates are:

Harley (1984a): 690 to 701 $\pm$ 70°C; and

Sen and Bhattacharya (1984): 747 to 762 $\pm$ 30°C.

The thermometers are reasonably consistent in terms of the error brackets, with the Sen and Bhattacharya (1984) estimate being 60 to 70°C greater than that of Harley (1984a). As in the case of most exchange thermometers, retrograde re-equilibration may occur without obvious textural evidence (Bohlen and Lindsley, 1987). Neither model accounts for the effects of Mn and Fe^{3+} on the equilibration temperature. Temperature estimates are raised significantly by incorporating these components (Harley, 1984a).

4.3.3 Garnet-Biotite Thermometry

The distribution of Fe and Mg between garnet and biotite has been calibrated as a geothermometer by Ferry and Spear (1976, 1978), Thompson (1976), Holdaway and Lee (1977), Perchuk and Lavrent'eva (1983) and Indares and Martignole (1985). Each revision of the popularly applied thermometer is based on improved thermodynamic data for the exchange reaction. Most recently, Indares and Martignole (1985) present a thermometer that may account for the effect of Al^{IV} and Ti^{IV} in biotite on the garnet-biotite equilibration temperature.

In samples FB71, DWN552, DWN554 and DWN673, have garnet co-existing with flaky, matrix biotite grains. This texture may have formed at the metamorphic peak. Samples DWN673, FB202, FB210 and

FB266A, amongst others contain retrograde, skeletal biotite-quartz inter-growths after garnet. The results of the various thermometers at 5 kbar are given on Table 3. The effect of pressure on the calculated estimates are similar to that on the garnet-orthopyroxene exchange thermometer (section 4.3.2) and are not shown on the tabulation.

Matrix biotite-garnet pairs have K_{Fe-Mg}(Grt-Bt) in the range 3.66 to 4.62 corresponding to a decrease of X_{Mg}(Grt,Bt). Retrograde garnet-biotite pairs have K_{Fe-Mg}(Grt-Bt) $\geq$ 5.52, corresponding relatively low X_{Mg}(Grt,Bt). The Ferry and Speer (1978) thermometer yields temperature estimates for matrix biotite-garnet pairs in the range 647 to 751 $\pm$ 6°C (op. cit., analytical error), representing a maximum temperature of Fe-Mg garnet-biotite equilibration in DWN554 and DWN552. Coarse, retrograde biotite after garnet in DWN673 records a temperature of 474°C. Essene (1982), Bohlen and Lindsley (1987), Frost and Chacko (1989) and Harley (1989) recognise that garnet-biotite thermometry commonly records the closure temperature of garnet (550 - 700°C; after Elphick et al., 1985, and Bohlen, 1987). Bhattacharya and Sen (1985) show that these temperature estimates are meaningless without an independent estimate of the metamorphic fluid activity at the time of garnet-biotite equilibration. Alternatively, independent temperature determinations (e.g. Goldman and Albee, 1977) can constrain a(H_2O).

The temperature estimates from the different calibrations con-

verge on 710 ± 40°C at 5 kbar for metapelitic gneiss, DWN552. This does not represent the peak metamorphic temperature. The variation of the different temperature estimates reflects the sensitivity of the calibrations to small variations in mineral compositions (Bohlen and Lindsley, 1987). They suggest that the thermometers of Perchuk and Lavrent'eva (1983) and Indares and Martignole (1985) are the most successful.

4.3.4 Biotite-Orthopyroxene Thermometry

Fonarev and Konilov (1986) present an experimental calibration of the distribution of Fe and Mg between biotite and orthopyroxene at 490 MPa in the system CFMASH. X_{Mg}(Bt,Opx) compositions are plotted on a part of their graphical calibration. The range of matrix biotite-orthopyroxene pairs suggest Fe-Mg equilibration of pairs at between 750 and 850°C. Unfortunately, the polynomial expression proposed, is inconsistent with the experimental results! More accurate estimates can therefore not be made. In addition, their calibration does not account for, *inter alia*, Al substitution in biotite or orthopyroxene, which may affect the pressure-dependence of the exchange reaction. The temperature estimates are not accurate. The Fe-Mg exchange reaction between biotite and orthopyroxene thermometer requires rigorous thermochemical modelling in order for it to be useful as a new thermometer.

4.3.5 Garnet-Cordierite Thermometry

The Fe-Mg distribution between garnet and cordierite has been calibrated empirically by Thompson (1976), Holdaway and Lee (1977) and experimantally by Perchuk and Lavrent'eva (1983). The results of application of the proposed thermometers at 5 kbar are displayed on Table 4 to a variety of garnet-cordierite-bearing rock assemblages occurring in the metapelitic and magnesian gneiss horizons in the area of the 1:50 000 map.

It is apparent that the results for each calibration are consistent with one another in terms of an error of $\pm 50^{o}C$ (Holdaway and Lee, 1977). The Thompson (1976) calibration yields estimates 30 to $40^{o}C$ higher than those of Holdaway and Lee (1977) and Perchuk and Lavrent'eva (1983). Mineral core pairs from unsheared without rehydration textures suggest Fe-Mg equilibration at peak metamorphic conditions in the range 800 - 819 $\pm$ $50^{o}C$. This is a maximum temperature estimation for garnet-cordierite pairs that were equilibrated at the peak metamorphic conditions, including $P(H_2O) << P(total)$. The K_D(Grt-Crd) is lower for core pairs (5.32 - 5.59) than for higher X_{Fe}(Grt) and X_{Mg}(Crd) rim and retrogade pairs ($\geq$6.41). Temperature estimates are up to $115^{o}C$ lower for these rocks. Retrograde processes that may have reset the thermometer include garnet-cordierite re-equilibration with coarse-grained sillimanite (e.g. FB210) and/or with skeletal biotite (e.g. PH1 and WW3). These temperatures may represent the blocking temperature of garnet (Harley, 1989) at 5

kbar for retrogressive Fe-Mg exchange.

4.3.6 Hercynite-Cordierite Thermometry

Vielfzeuf (1983) proposed an Fe-Mg exchange thermometer for co-existing hercynite and cordierite. In addition, he proposed a barometer using cordierite and hercynite compositions in quartz-bearing assemblages (the multivariant reaction of section 4.2.6). His model does not account for the hydration state of cordierite, which has a significant effect on the activity of cordierite (section 4.2.6, Fig. 4.3). Fe^{3+}(Hc) was estimated using the technique of Droop (1987). In FB210, cordierite-hercynite pairs have K_D(Crd-Hc) = 0.129, corresponding to a temperature estimate of 783 $\pm$ 40°C. Fig. 4.3 shows the P-T calibration of the reaction [Crd = 2Hc + 5Qtz]. The barometer estimates a pressure of 4.7 $\pm$ 0.4 kbar at the time of hercynite-cordierite-quartz equilibration. These conditions represent minimum values for the P-T conditions of the metamorphic peak.

RW4 is a quartz-free magnesian gneiss containing hercynite and cordierite in a near peak metamorphis association. Application of the exchange thermometer suggests a temperature of equilibration of 844 $\pm$ 40°C.

4.4 Solvus Thermobarometry

4.4.1 Introduction

The temperature-dependence of the miscibility gap between two end members of a partial solid solution series is potentially more useful as a thermometer than exchange equilibria (Bohlen and Lindsley, 1987). The miscibility gaps in quarternary pyroxene and ternary feldspar systems are multivariant equilibria in P-T-X space, because of non-ideal solid solution in participating phases. Recent calibrations in both systems are applied to assemblages in metabasic and metapelitic gneisses, respectively, from the study area.

4.4.2 Quadrilateral Pyroxene Thermobarometry

Early calibrations of the P-T stability relations between Ca-Mg-Fe-pyroxenes (e.g. Wood and Banno, 1973) were improved by the graphical solution of Lindsley (1983), which accounts for Ca, as well as Fe-Mg distribution between co-existing pyroxenes. Recent thermodynamic calibrations (Davidson and Lindsley, 1985; Carlson and Lindsley, 1988) give promise for a mathematical solution in the near future.

In metabasic gneiss DWN545, fine-grained, granular orthopyroxene, $Wo_1En_{58}Fs_{41}$, forms a granoblastic texture with clinopyroxene, $Wo_{45}En_{38}Fs_{17}$. These compositions plot in the pyroxene quadrilateral on the 700°C isotherm determined by Lindsley (1983).

Because of the possibility of retrograde resetting among co-existing, fine-grained pyroxenes, especially at $P \leq 10$ kbar (e.g. Bohlen and Essene, 1978, 1979; Nickel and Brey, 1984; Schreurs and Westra, 1986), this temperature represents a lower limit for the peak of metamorphism.

4.4.3 Ternary Feldspar Thermobarometry

The stability ternary feldspars has been studied by inter alia Seck (1971), Lofgren and Gooley (1977), Johannes (1979), Haselton et al. (1983), and (Ghiorso, 1984), Green and Usdansky (1986), and Fuhrman and Lindsley (1988). Calibration of a thermometer is complicated by the variable structural state of feldspar solid solution (Morse and Lofgren, 1978; Petersen and Lofgren, 1986; Bohlen and Lindsley, 1987). Additional experimentation is required.

Coarsely perthitic microcline co-existing with antiperthitic plagioclase is intergrown with the assemblage [Grt-Opx-Hc] in magnesian gneiss DWN552. In magnesian gneiss RW4 a single ternary feldspar has exsolved to mesoperthite co-existing with the assemblage [Crd-Opx-Hc]. The compositions of these feldspars are shown on Fig. 4.4. The compositions of lamellar textures were resolved, with partial success, by focussing the microprobe beam to a 5um diameter. They fall on a trend between $Ab_{10}Or_{90}$ and $Ab_{75}An_{25}$. Single feldspar compositions were measured in RW4 in the range $Ab_{52}Or_{33}An_{15}$ to $Ab_{37}Or_{54}An_{9}$, which may approximate bulk

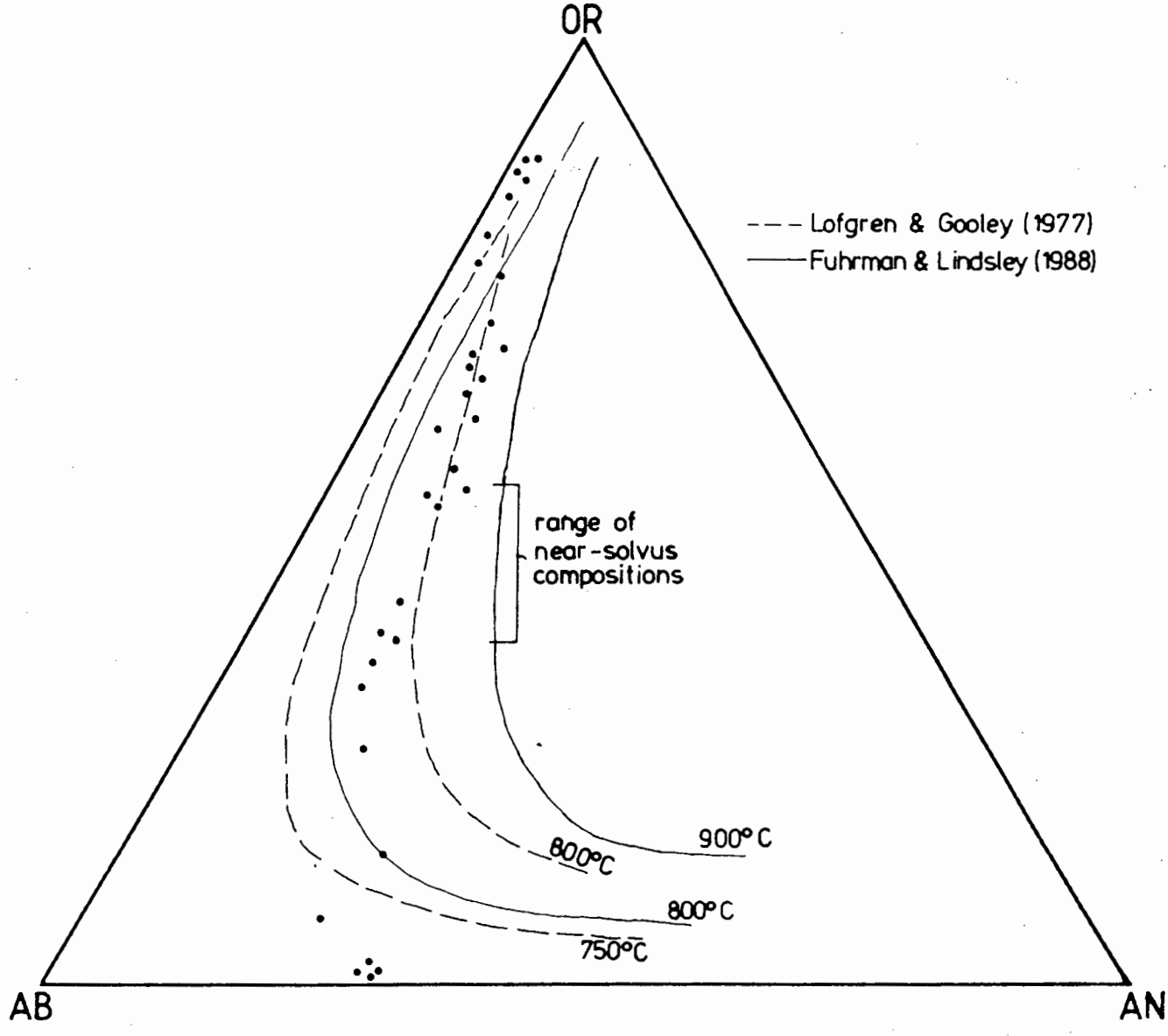

Fig. 4.4 Ternary feldspar and mesoperthite compositions from magnesian gneisses DWN552 and RW4. Solid curves are the isotherms of Lofgren and Gooley (1977). Dashed curves are the approximate isotherms of Fuhrman and Lindsley (1988).

feldspar composition. This composition and the unmixing trend corresponds of compositions shown on Fig. 4.4 corresponds closely to that of the cooled initial composition F-8 of Lofgren and Gooley (1977), $Ab_{45}Or_{44}An_{11}$, at 5 kbar. A temerature of at least 780°C is required to stabilize a single ternary feldspar in RW4.

The improved numerical model of Fuhrman and Lindsley (1988) involves the programmed iteration of temperature estimates derived for each of the three calculated activity compositions. The FORTRAN program is not yet available to me. Fig.4.4 shows the estimated position of the isotherm of Fuhrman and Lindsley (1988) at 5 kbar. The trend of feldspar compositions approximately intersects their 820°C solvus at 5 kbar. In the absence of an accurate mathematical analysis, the results of the two calibrations are considered to be in reasonable agreement.

4.5 **Discussion**

4.5.1 Garies-Platbakkies Belt Metamorphic Peak

Fig. 4.5 is a summary of the estimates of the pressure and temperature conditions of the Namaqua metamorphic peak in the field area. Calculated estimates of mineral equilibria that are interpreted as being retrograde, and of thermobarometers that are internally inconsistent are not included. The merits of calibrations not quoted for particular equilibria are discussed in

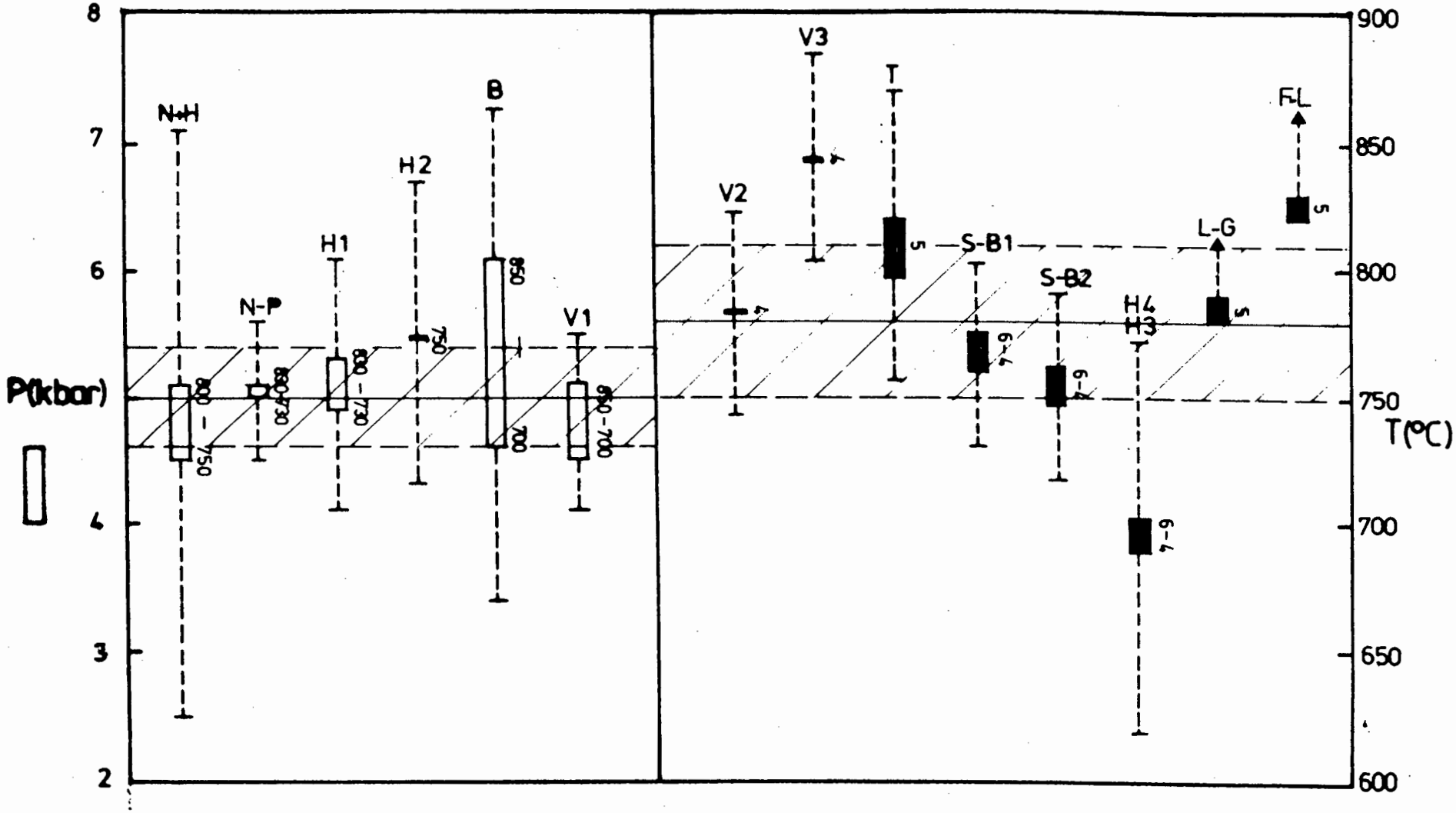

Fig. 4.5 Summary of the P and T estimates of the peak of Namaqua metamorphism in the study area. Numbers indicated alongside each bar refer to the T or P bracket in which each barometer and thermometer was calibrated, respectively. The shaded regions are the estimated peak conditions using all these results. See overleaf for list of author abbreviations.

References used on Figure 4.5

N-H	Newton and Haselton (1981)	Grt-Pl-Sil-Qtz in FB210
N-P	Newton and Perkins (1982)	Grt-Opx-Pl-Qtz in FB71
H1	Harley (1984b)	Al(Opx)-Grt in FB71
H2	Harley (1984b)	Al(Opx)-Grt in DWN554
B	Bhattacharya (1985)	Crd-Hc-Qtz in FB210
V1	Vielzeuf (1983)	Crd-Hc-Qtz in FB210
V2	Vielzeuf (1983)	Crd-Hc in FB210
V3	Vielzeuf (1983)	Crd-Hc in RW4
T	Thompson (1976)	Grt-Crd in DWN554, WW13, RW3, WW8
S-B1	Sen and Bhattacharya (1985)	Grt-Opx in FB71
S-B2	Sen and Bhattacharya (1985)	Grt-Opx in DWN552
H3,H4	Harley (1984a)	Grt-Opx in FB71, DWN552
L-G	Lofgren and Gooley (1977)	Ternary feldspar in RW4,DWN552
F-L	Fuhrman and Lindsley (1988)	Ternary feldspar in RW4,DWN552

the text.

The estimates, with their respective errors, shown on Fig. 4.5 converge on a region in P-T-space described by the brackets 780 ± 30°C and 5.0 ± 0.4 kbar. This temperature is a minimum estimate of the granulite facies metamorphic peak.

A major problem in the estimation of peak metamorphic conditions is the difficulty of estimating $a(H_2O)$, which may vary independently of P and T (e.g. Waters and Whales, 1984; Bhattacharya and Sen, 1985). Water activity significantly affects the stability of cordierite and biotite (e.g. Martignole and Sisi, 1981; Indares and Martignole, 1985). Thermodynamic and experimental evidence suggests that temperature and pressure estimates of many multivariant dehydration equilibria may be artificially low as a result of over-estimates of $X(H_2O)$(Crd,Bt) (Thompson, 1982; Grant 1985a,b). In section 5.5, $a(H_2O)$ conditions in biotite-bearing assemblages from the field area are estimated using known P-T-$X(H_2O)$ stability conditions of dehydration reaction equilibria. Independent determinations of the volatile contents of hydrous phases are required for more accurate estimations.

Frost and Chacko (1989) introduce the 'granulite uncertainty principle', which suggests that the temperatures derived from the conventional exchange thermometers may represent the closure temperatures for cation diffusion in the minerals concerned.

These closure temperatures may be calculated if the diffusion coefficients and cooling rates are known (e.g. Lasaga, 1983). The closure temperatures of thermobarometers involving net-transfer reactions, in which phases grow and are consumed, have not been calculated, because the reactions involve more than just lattice diffusion. In view of these uncertainties, the T-estimates of the peak metamorphism must be regarded must be regarded as minima.

Petrogenetic grids may be used as an independent check on calculated P-T conditions, using assemblages with restricted stability in P-T-space. (e.g. Lal et al., 1978; Grew 1980, 1982; Waters, 1986). The quartz-free assemblage

[Spr + Sil + Crd + Hc + Phl]

containing resorbed corundum, occurs in sample FB276. The P-T bracket calculated by thermobarometry in the field area, is consistent with the stability conditions inferred for this assemblage (Waters, 1986: after Hensen and Green, 1973; Ellis et al., 1980).

4.5.2 Regional Thermobarometric Variation in Western Bushmanland

Thermobarometry has been performed by many researchers in the western Bushmanland Subprovince (Zelt, 1978, 1980; Jack, 1980; Whales, 1983; Albat, 1984; Waters and Whales, 1984; Baars, 1986, this study; Grutter, 1986; Moore, 1986; Nowicki, 1986; Waters, 1986a, b, 1988, 1989; Van Aswegen, 1988; Mcstay, in prep.).

Approximate isograds shown on Fig. 1.2 from Waters (1986b, 1989) are based on the following reactions, relevant to common metapelitic assemblages:

$$Bt + Sil + Qtz = Grt + Crd + kfs + H_2O;$$

$$Grt + Sil = Hc + Qtz; \text{ and}$$

$$Crd = Hc + Qtz.$$

Waters (1989) summarized the peak metamorphic conditions recorded by the rocks in the zones A, B and C on Fig. 1.2. He established a database of thermobarometric estimates for samples from a large number of localities in western Bushmanland (Jack, 1980; Albat, 1984; Waters and Whales, 1984; Moore, 1986; Waters, 1985, 1986; McStay, in prep.; this study; unpubl. data 1977 - 1989). Using part of this database, Fig. 4.6 shows the variation of pressure and temperature along an approximately N-S traverse between 29°00'S and 31°30'S through the field area of this study. Temperatures are estimated using the garnet-biotite and garnet-cordierite thermometers of Perchuk and Lavrent'eva (1983). Pressures are estimated using the calibrated garnet-cordierite equilibria of:

a) Perchuk and Lavrent'eva (1983), (KFASH-experiments);

b) Thompson (1976), (Fe-Mg exchange); and

c) Powell and Holland (1988), (KMASH-thermodynamics).

Error brackets shown are the standard deviations of individual sample groups. The P-T conditions of the metamorphic peak of the rocks from the field area (section 4.5.1) are shown. P-T

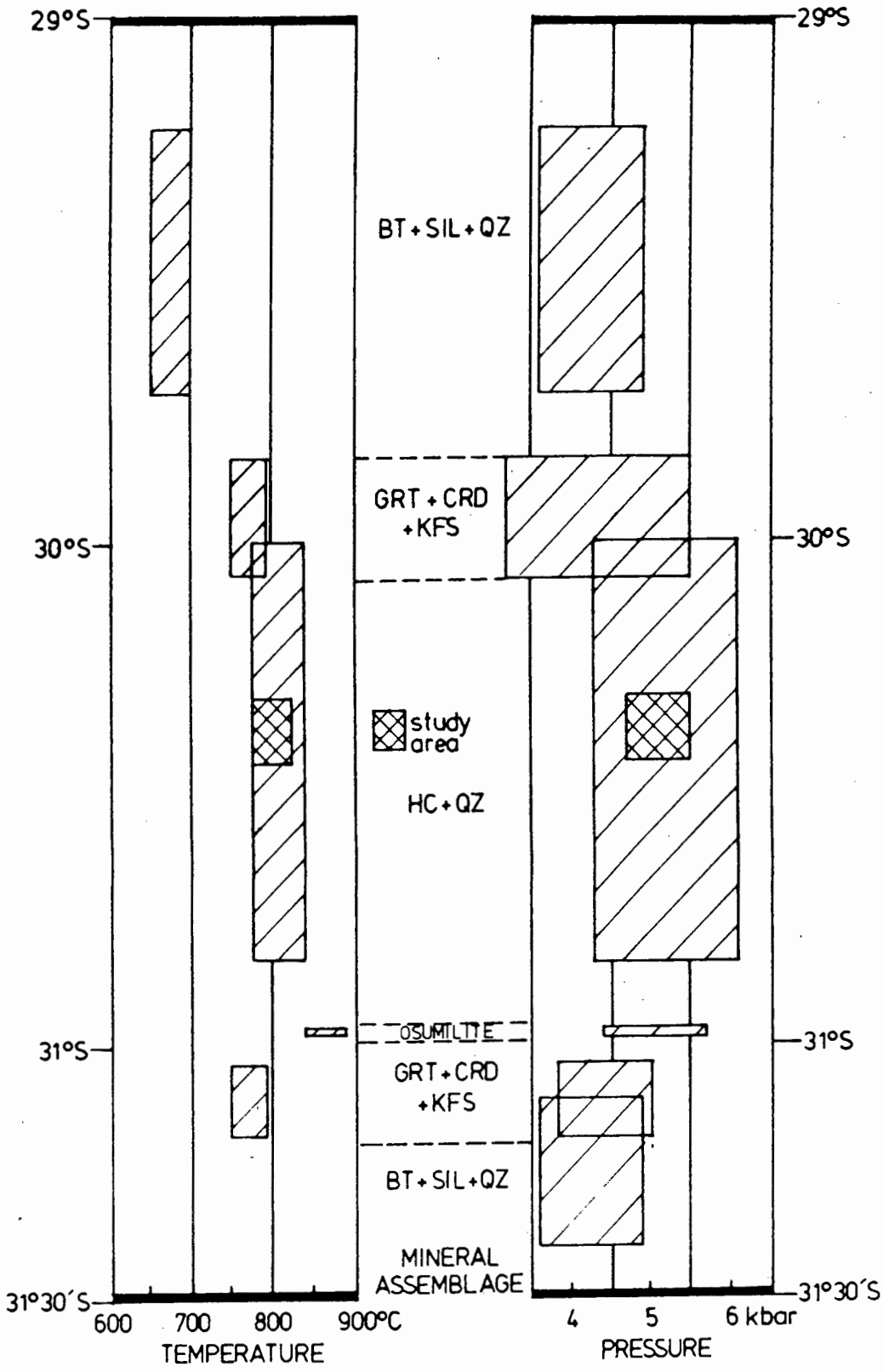

Fig. 4.6 The variation of pressure and temperature estimates of the peak of metamorphism along an approximately N-S traverse across the western Bushmanland Subprovince (c.f. text and Fig. 1.2)

estimates from a single locality on the farm Brandewynskraal near Bitterfontein where osumilite occurs, are from Nowicki (1986).

P-T estimates range from 675 ± 25°C at 4.3 ± 0.7 kbar in the amphibolite facies to 810 ± 30°C at 5.1 ± 0.9 kbar in the upper granulite facies. The temperature estimates vary significantly between groups, while the pressure-section across the terrane is nearly isobaric, in terms sample variance. The consistency between these results and stabilities of natural assemblages (Waters, 1989) suggests that the observed P-T distribution reflects near-peak conditions reality, and is not entirely an artifact of slow cooling and exchange re-equilibration above mineral closure temperatures.

Granulite facies peak conditions correspond to an average geothermal gradient of 50 ± 10°Ckm^{-1}, which is identical to that indicated by the amphibolite facies peak. Similar thermal gradients are estimated for other regionally metamorphosed granulite terranes including the English River, Ontario (Perkins and Chipera, 1985), Napier Complex, Enderby Land (Ellis, 1980; Sandiford, 1985a, b), Rogaland, Norway (Kars et al., 1980), and West Uusimaa, Finland (Schreurs and Westra, 1986). Only the anorthosite aureole-related granulites of the Nain Complex record a higher geothermal gradient. Any geotectonic model for granulite facies metamorphism in Namaqualand must account for a heat source for the high geothermal gradient.

CHAPTER 5 PETROLOGY OF GRANITIC AND ALUMINOUS MIGMATITES

5.1 Introduction

Rocks of granitic bulk composition, comprising para- and ortho-gneisses, and granites, are volumetrically the most important both in the field area and in the western Bushmanland Subprovince as a whole (many quoted studies, including this one). In addition, rocks with peraluminous bulk compositions are commonly found in association with the abundant quartzofeldspathic para-gneisses. Many of these rocks, including some of the granites, are migmatitic in the field area. The style of migmatization provides important constraints, regarding metamorphic fluid activity, on the tectonothermal evolution of the granulite facies terrane.

The migmatite leucosomes contain granulite facies minerals such as orthopyroxene, garnet and cordierite, depending on bulk composition. The textures, mineral composition and modal abundances, as shown below, indicate that an important process in migmatite development here is prograde dehydration melting in biotite-bearing assemblages (e.g. Thompson, 1976; Grant 1985a, b, Waters, 1988). Similar processes have been inferred elsewhere (Sen and Bhattacharya, 1985; Warren and Stewart, 1988), though certain analogous textures in transitional charnockite trranes have been ascribed to the infiltration of CO_2-rich fluids (e.g. Newton et al., 1980; Janardhan et al., 1982).

In the following sections, only relatively simple assemblages are considered in detail. These are:

a) Qtz + Kfs + Pl + Bt + Opx ± Opq in granitic bulk compositions;

b) Qtz + Kfs + Pl + Bt + Sil + Grt ± Opq in peraluminous bulk compositions.

Lower variance assemblages can now also be modelled, owing to recent important advances in petrogenetic modelling (Holland and Powell, 1985; Powell and Holland, 1985, 1988; Spear and Cheney, 1987).

5.2 Migmatite Petrography

5.2.1 Mesosomes

In granitic rocks, orthopyroxene occurs in the gneissic matrix as equant grains associated with K-feldspar. These grains truncate biotite foliation, and are locally embayed by skeletal biotite-quartz intergrowths. Biotite, quartz and plagioclase occur as rounded inclusions in orthopyroxene. In paragneisses clusters of orthopyroxene are commonly entrained in compositional bands of paragneiss, alternating with biotite-rich bands. In biotite-orthopyroxene granite gneiss, orthopyroxene is commonly associated with minor amounts of subhedral, granular clino-pyroxene embaying hornblende.

In aluminous quartzofeldspathic gneiss and garnet-biotite metapelitic gneiss, medium- and coarse-grained garnet poikiloblasts truncate biotite foliation in compositional bands. Garnet grains occur in certain layers of a pre-existing compositional banding. Garnet is subhedral to anhedral and contains abundant, round quartz inclusions, as well as biotite, plagioclase and hercynite. Fine-grained sillimanite occurs locally as oriented inclusions in garnet, although this texture is most common in cordierite-bearing rocks. Locally, garnet cores contain concentrations of opaque mineral inclusions. There is a gradation from garnets in contact with matrix biotite, to garnet-quartz intergrowths surrounded by quartzofeldspathic haloes, free of biotite. This is true in both aluminous quartzofeldspathic gneisses and in some anatectic garnet-biotite granites.

5.2.2 Leucosomes

The field relationships of the various migmatitic assemblages occurring in rocks with granitic bulk compositions are described in sections 2.3.5 and 2.4.5, and those in rocks with peraluminous bulk compositions in sections 2.3.6, 2.4.4.1 and 2.4.4.2.

Criteria for recognizing igneous textures in leocosomes in deformed, gneissic terranes are extensively reviewed by Paterson et al. (1989a, b). Unequivocal recognition of the textures of reaction products is hampered by sluggish experimental reaction rates, especially at high metamorphic grades (Murrel and Ismail,

1976; Brodie and Rutter, 1985; Rutter and Brodie, 1988). The mechanisms of pore fluid redistribution from different textural analyses are in dispute (Hibbard, 1987 vs. Paterson et al., 1989b). No single criterion can be used to identify igneous textures in migmatites. Paterson et al. (1989b) suggest that a set of textural criteria be used as evidence for melt generation, crystallization and extraction, and associated fluid re-distribution.

The following set of textural criteria is used to indicate that significant proportions of quartzofeldspathic phases in leucosomes are the products of crystallization from melt in both granitic and per-aluminous rock types. They are based on the guidelines of Johannes and Gupta (1982), Johannes (1983), Ashworth and McLellan (1985) and Vernon and Collins (1988).

a) The coarse grain size of quartzofeldspathic phases in many leucosomes with respect to matrix, epecially at the pegmatitic contacts of many anatectic biotite granites;

b) the complete transgression of regional foliation by most leucosome types;

c) the local, intrusive truncation of compositional banding by leucosome assemblages;

d) the local occurrence of K-feldspar as subhedral and euhedral phenocrysts (c.f. Vernon, 1978);

e) the local presence of graphic and granophyric K-feldspar-quartz intergrowths;

f) the common occurrence of myrmekitic plagioclase-quartz intergrowths near K-feldspar grains, (cf. Paterson et al., 1989b; Vernon et al., 1983; Simpson, 1985); and

g) the absence of an tectonic foliation in leucosome assemblages unaffected by D4 shearing.

Ashworth and McLellan (1985) recognize the importance of a number of possible alternative mechanisms to anatexis, involving subsolidus processes, for the production of the migmatitic textures (c.f. also Lindh and Wahlgren, 1985; Sawyer and Barnes, 1988; McLellan, 1989). Long and Luth (1986) show that K-feldspar phenocrysts can feasibly be grown by metasomatic processes involving H_2O-rich fluids, in contrast to the argument for an igneous origin (e.g. Vernon, 1978). Hibbard (1987) relates the origin of myrmekite and granophyre to subsolidus H_2O-rich fluid replacement. These processes require rock permeability and porosity at the time of formation of the textures to have been greater than those inferred to be representative of mid-crustal granulites (Walther and Orville, 1982; Brady, 1988).

Orthopyroxene grains are commonly coarser in leucosome assemblages of granitic rocks than in the matrix, and are surrounded by quartzofeldspathic haloes containing no matrix biotite. However, coarse-grained skeletal biotite-quartz intergrowths locally occur as partial or complete pseudomorphs after orthopyroxene. Garnet in leucosomes of peraluminous rocks, is texturally similar to inclusion-filled matrix garnet.

Inclusions of sillimanite are absent leucosome garnet. The association of garnet and quartz is ubiquitous. Partial pseudomorphs of skeletal biotite-quartz intergrowths after poikiloblastic garnet are common.

5.3 Mineral Compositions

5.3.1 Introduction

Certain mineral textures described above suggest that in rocks with granitic bulk compositions, orthopyroxene is the product of biotite breakdown reactions. Similarly, garnet in peraluminous rock compositions is the product of biotite breakdown, perhaps in the presence of sillimanite. In both cases it is inferred that silicate melt is also the product of orthopyroxene- and garnet-forming reactions. It is important to describe the mineral compositions in these assemblages, because the partition of chemical components between, in particular, the ferromagnesian phases is a measure of reaction divariance.

5.3.2 Biotite-Orthopyroxene

Representative mineral analyses from rocks with the assemblage

Qtz + Kfs + Pl + Bt + Opx + Opq

are listed in Appendices 1A, E-J. The important variables are summarized on Table 5.

Samples FB48, FB279 and DWN544 (Appendices 1C, 1D, 1J) are biotite-orthopyroxene leucoparagneisses without leucosomes, and are respectively K-feldspar-rich through to plagioclase-rich. They contain plagioclase compositions in the range $Ab_{65}Or_2An_{33}$ to $Ab_{45}Or_{1.5}An_{53.5}$, respectively. X_{Mg}(Opx) correspondingly increases from 0.54 to 0.64.

Figs. 5.1a-c show the chemical relationships between biotite and orthopyroxene in these rocks in terms of molecular proportions of $K_2Al_2O_4$, (FeO + MnO) and MgO projected from plagioclase, quartz and H_2O in the model system $CaO-Na_2O-K_2O-FeO-MgO-Al_2O_3-SiO_2-H_2O$ (CNKFMASH). In FB48 and FB279, orthopyroxene co-exists with relatively coarse-grained and skeletal biotite with an average X_{Mg}(Bt) of 0.62 and 0.71, respectively. These mineral pairs have $K_D(Opx-Bt)_{Fe-Mg}$ in the ranges 1.64 to 1.35 and 1.30 to 1.24, respectively. In each case, biotite flakes not in contact with orthopyroxene have lower average X_{Mg}(Bt) of 0.52 and 0.64, respectively, than biotite in contact with orthopyroxene.

In contrast, all biotites in the plagioclase-rich rock DWN544 have similar morphologies. Flaky biotites in contact with orthopyroxene have slightly lower X_{Mg}(Bt) than those occurring in com positional bands free of orthopyroxene compositional bands (0.73 and 0.76, respectively). Co-existing pairs have a relatively constant $K_D(Opx-Bt)_{Fe-Mg}$ of 1.12.

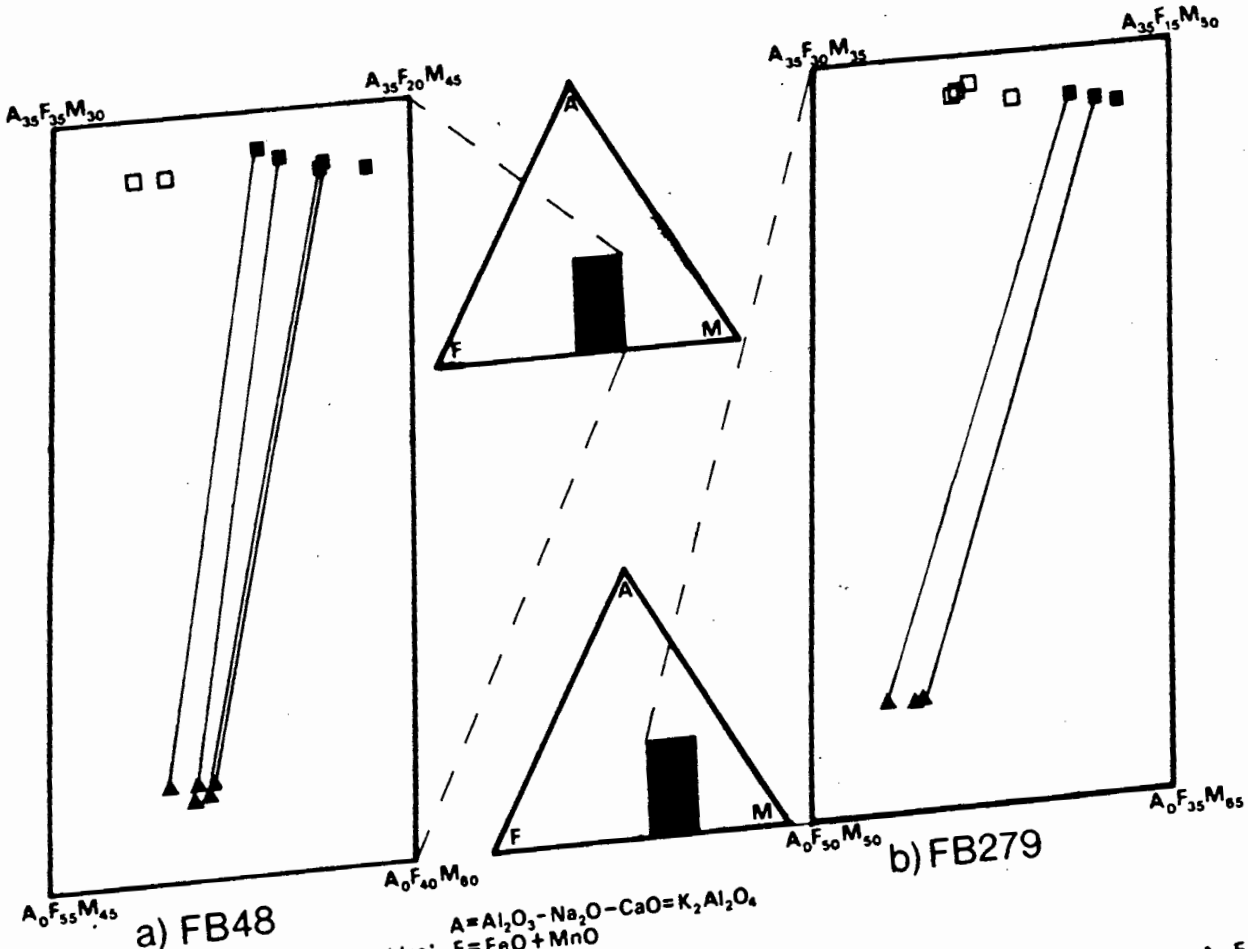

Molecular proportions of oxides: $A = Al_2O_3 - Na_2O - CaO = K_2Al_2O_4$
$F = FeO + MnO$
$M = MgO$

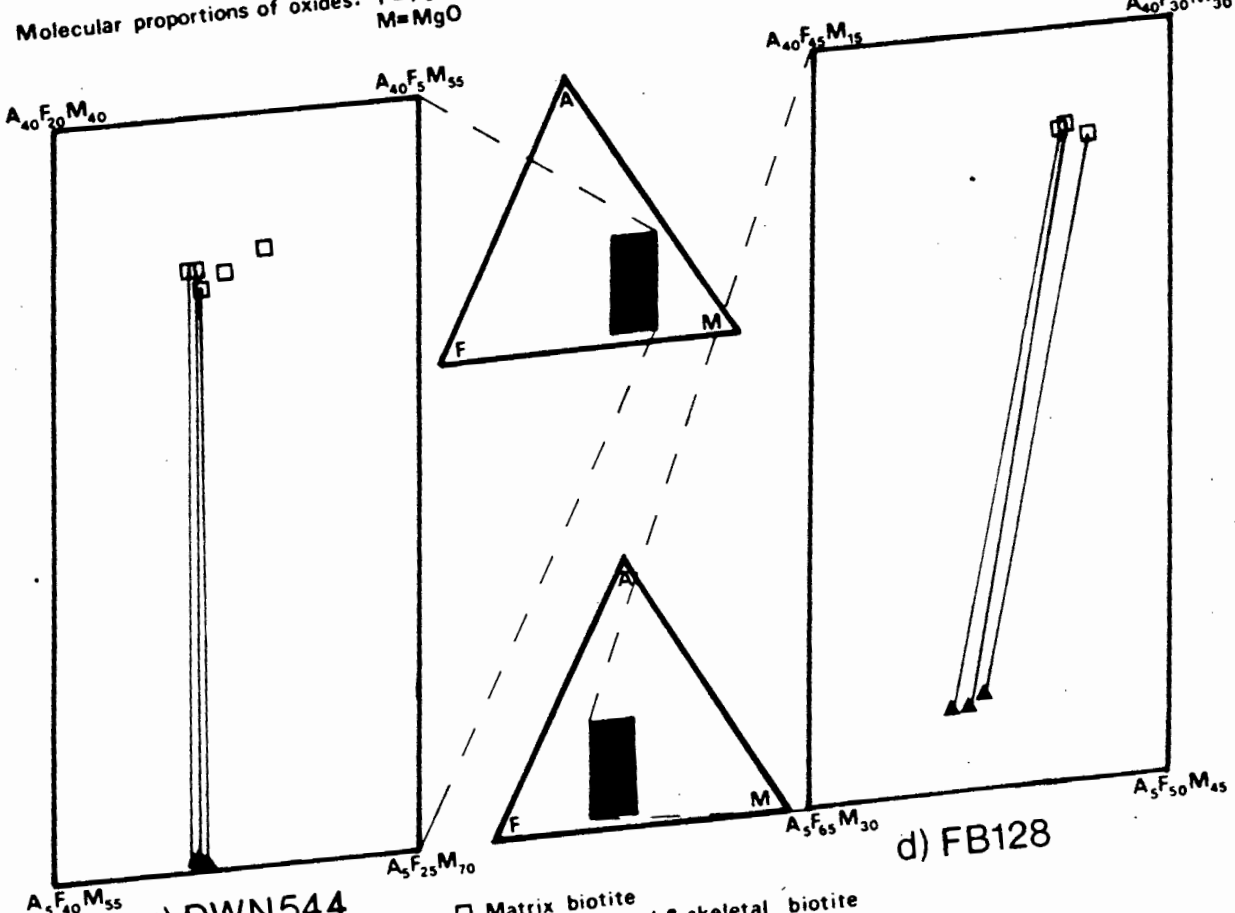

□ Matrix biotite
■ Coarse-grained & skeletal biotite
▲ Orthopyroxene

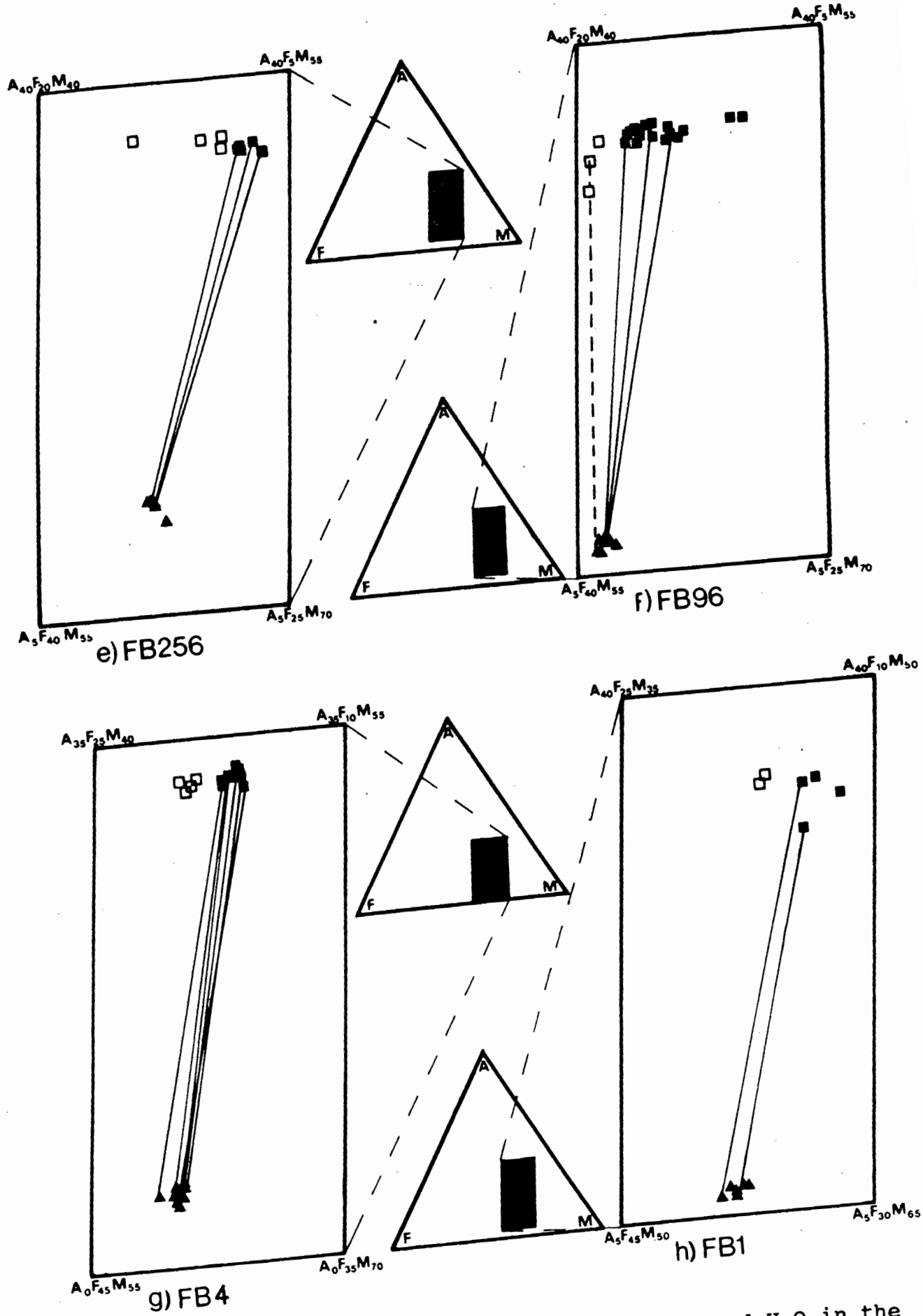

Fig. 5.1 Projection from quartz, plagioclase and H_2O in the system CNKFMASH of the compositions of biotite and orthopyroxene in rocks with granitic bulk compositions.

In biotite-orthopyroxene leucoparagneisses with leucosomes, samples FB256, FB96, FB4 and FB1, orthopyroxene generally occurs in the leucosomes, co-existing with relatively coarse-grained, skeletal biotite. It is separated from flaky, matrix biotite grains. Figs. 5.1e-h show the relationships between biotite and orthopyroxene on the same CNKFMASH projection as above. In each case, biotites that co-exist with orthopyroxene have higher average X_{Mg}(Bt) than matrix biotites (e.g. 0.64 vs. 0.58 for FB256). $K_D(Opx\text{-}Bt)_{Fe\text{-}Mg}$ varies in the range 1.48 to 1.77, corresponding to a decrease in X_{Mg} of co-existing pairs. A rounded biotite inclusion in orthopyroxene in FB96 has a composition like that of the rock's matrix biotite.

Sample FB128 is a biotite-orthopyroxene granite gneiss in which all biotite co-exists with orthopyroxene in granite matrix. Tie-lines joining co-existing pairs are shown on Fig. 5.1d. $K_D(Opx\text{-}Bt)_{Fe\text{-}Mg}$ is relatively constant around 1.24.

Fig. 5.2 shows plots of X_{Mg}(Bt) against molecular proportions of F and Ti, for each of the rocks a-h described above. In all rocks except FB1, the F-content of biotite increases significantly with increasing X_{Mg}, while the Ti-content decreases correspondingly with X_{Mg}. In biotite-orthopyroxene granite gneiss, FB128, the Cl-content of biotite decreases with increasing X_{Mg}(Bt). No significant amounts of Cl were detected in the biotites of the supracrustal gneisses, even with extended counting times.

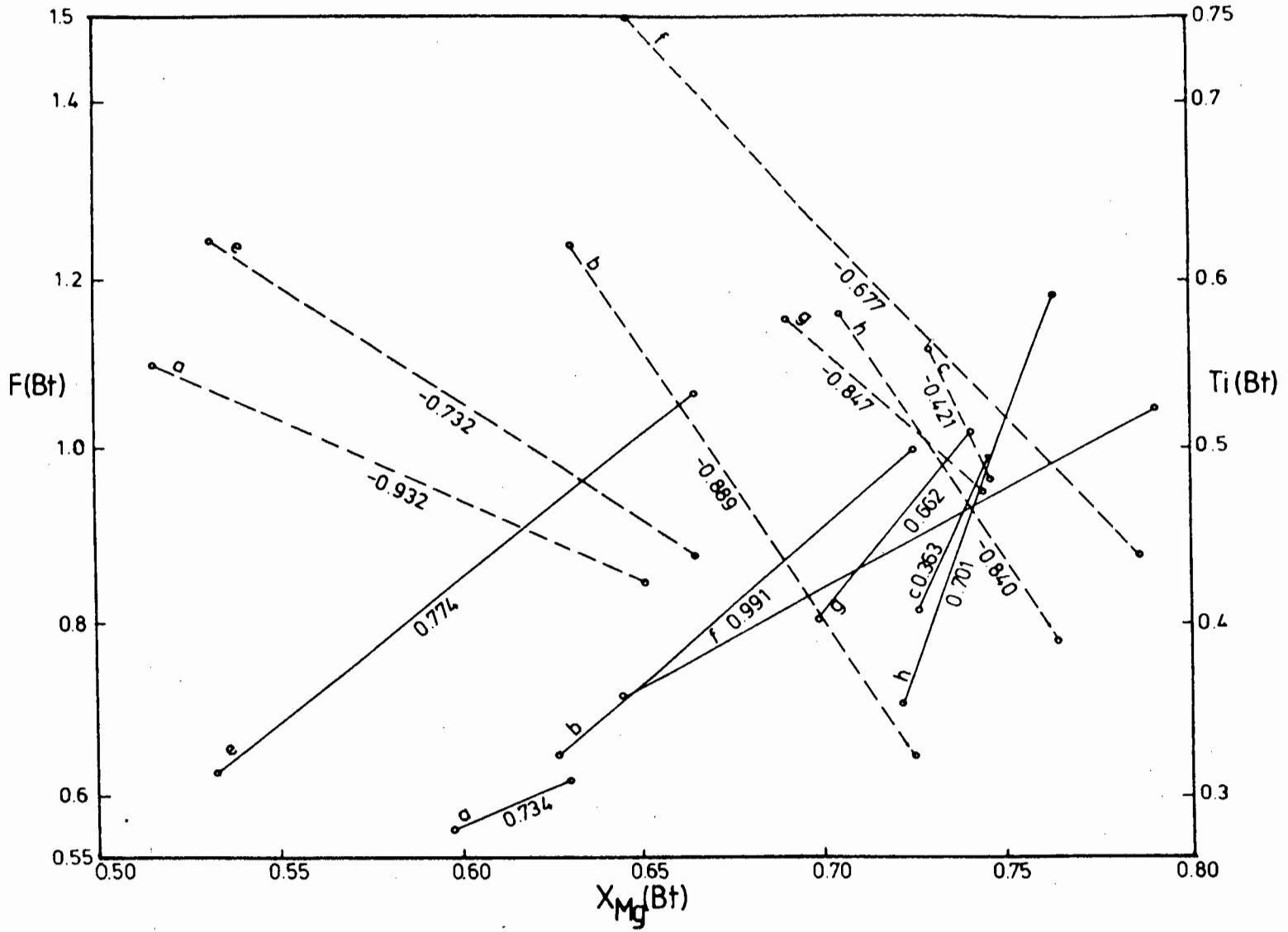

Fig. 5.2 The variation of F(Bt) and Ti(Bt) with X_{Mg}(Bt) in rocks with granitic bulk compositions. The annotations refer to the rocks of Fig.5.1. Best-fit straight lines of the data are given with correlation coefficients.

Mineral analyses for the following samples of different rock types indicate the same trends as the data described above:

a) FB59, FB113, FB239, FB278, biotite-orthopyroxene leuco-paragneisses without leucosomes;

b) FB2, FB5, FB170 and DWN543, biotite-orthopyroxene leuco-paragneisses with leucosomes; and

c) FB59 and FB195, biotite-orthopyroxene granite gneiss.

5.3.3 Biotite-Garnet

Representative mineral analyses from rocks with the assemblage

Qtz + Kfs + Pl + Bt + Grt + Opq

are listed in Appendices 1L, 1M . The important variables are summarized on Table 6.

Fig. 5.3 shows the compositions of garnet and biotite in DWN673 and FB266A in terms of Al_2O_3, (FeO+MnO) and MgO molecular proportions in the system FMAS. In garnet-biotite metapelitic gneiss DWN673, garnet in leucosomes has cores with $X_{Mg} \geq 0.21$ and rims with $X_{Mg} = 0.19$. Retrograde biotite blades have X_{Mg} range 0.59 to 0.70, while compositions of matrix biotites are restricted to 0.56 ± 0.01. $K_D(Grt\text{-}Bt)_{Fe\text{-}Mg}$ varies from 4.6 to 7.9, for matrix and leucosome pairs, respectively. F-content is higher, and Ti-content lower in retrograde biotite (Fig. 5.4). The quartzo-feldspathic gneiss FB266A is finer-grained and contains less matrix biotite than DWN673, but shows the same textural generations of garnet and biotite. Their compositions are the

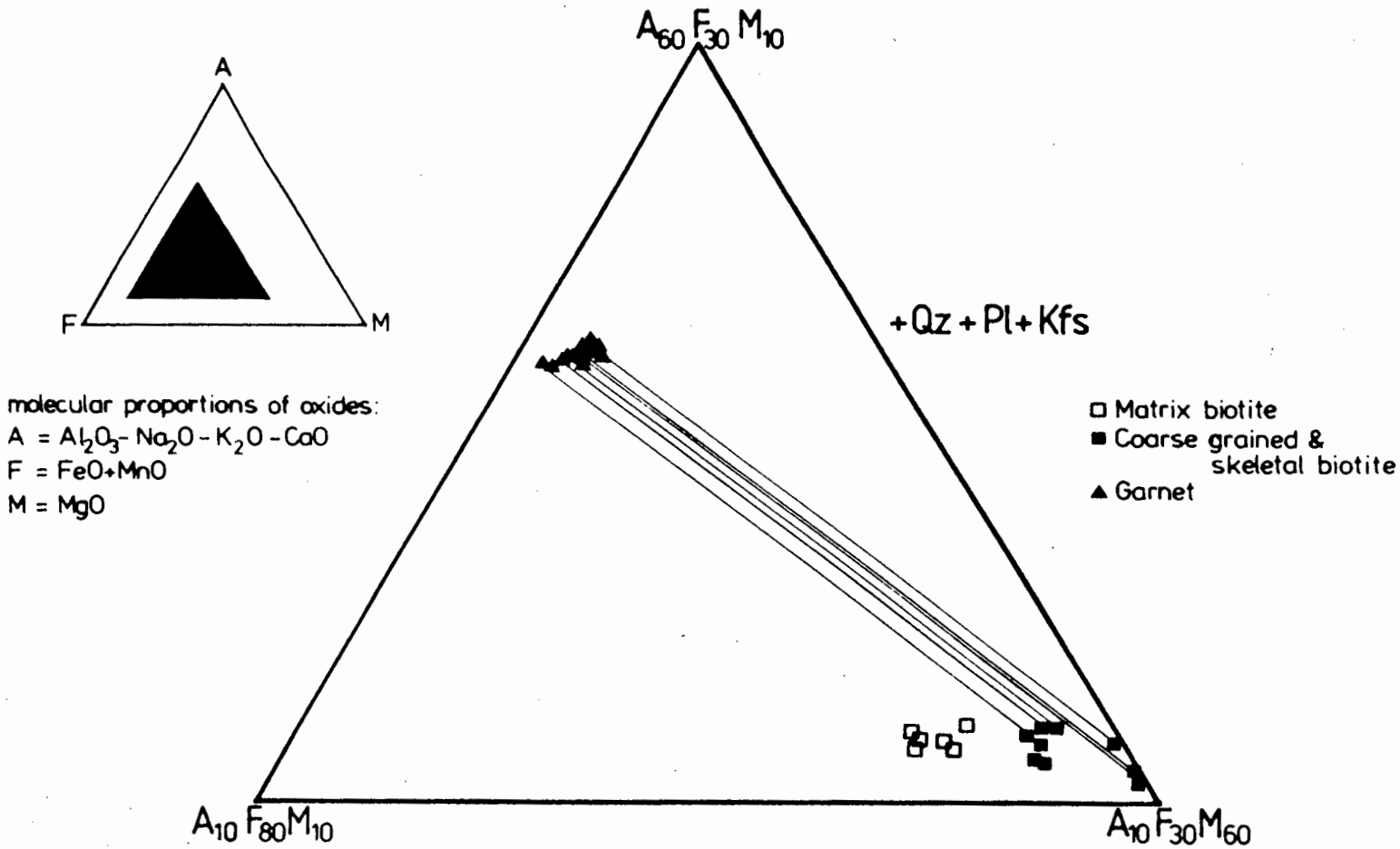

Fig. 5.3 Projection from quartz, plagioclase, K-feldspar and H_2O in the system CNKFMASH of the compositions of biotite and garnet in FB266A and DWN673, rocks with peraluminous bulk compositions.

same as those of the equivalent generation in DWN673.

5.3.4. Reaction Variance

Biotite breakdown reactions responsible for the growth of orthopyroxene and garnet in granitic and peraluminous rocks are sensitive to partition of Fe and Mg, F and OH, and Ti^{IV} and Al^{VI}. Fe and Mg are exchanged between biotite and orthopyroxene or garnet such that

$$X_{Mg}(Opx/Grt) < X_{Mg}(matrix\ Bt) < X_{Mg}(retrograde\ Bt).$$

$K_D(Opx/Grt\text{-}Bt)_{Fe\text{-}Mg}$ increases corresponding to an increase of the X_{Mg} of the mineral pair in any one rock. This trend is a result of the relatively wide range of Fe:Mg ratios of biotite in one rock. Figs. 5.2 and 5.4 shows that $X_{Mg}(Bt)$ correlates positively with both the F- and Ti-contents of biotites in most rocks. Biotite break-down and regrowth reactions are therefore divariant with respect to F- and Ti-exchange. Munoz and Ludington (1974, 1977) showed that F-OH partition between fluid and/or silicate melt produces a higher concentration of F in biotite at higher temperatures. In an a system with low $a(H_2O)$, fluid and/or melt composition is therefore very sensitive to biotite composition, being the only hydrous phase present in many granulite facies rocks. Dymek (1983) showed that intracrystalline exchange of Ti^{IV} with Al^{VI} during prograde reaction produces higher Ti biotite. These observations suggest that coarse-grained, skeletal biotites

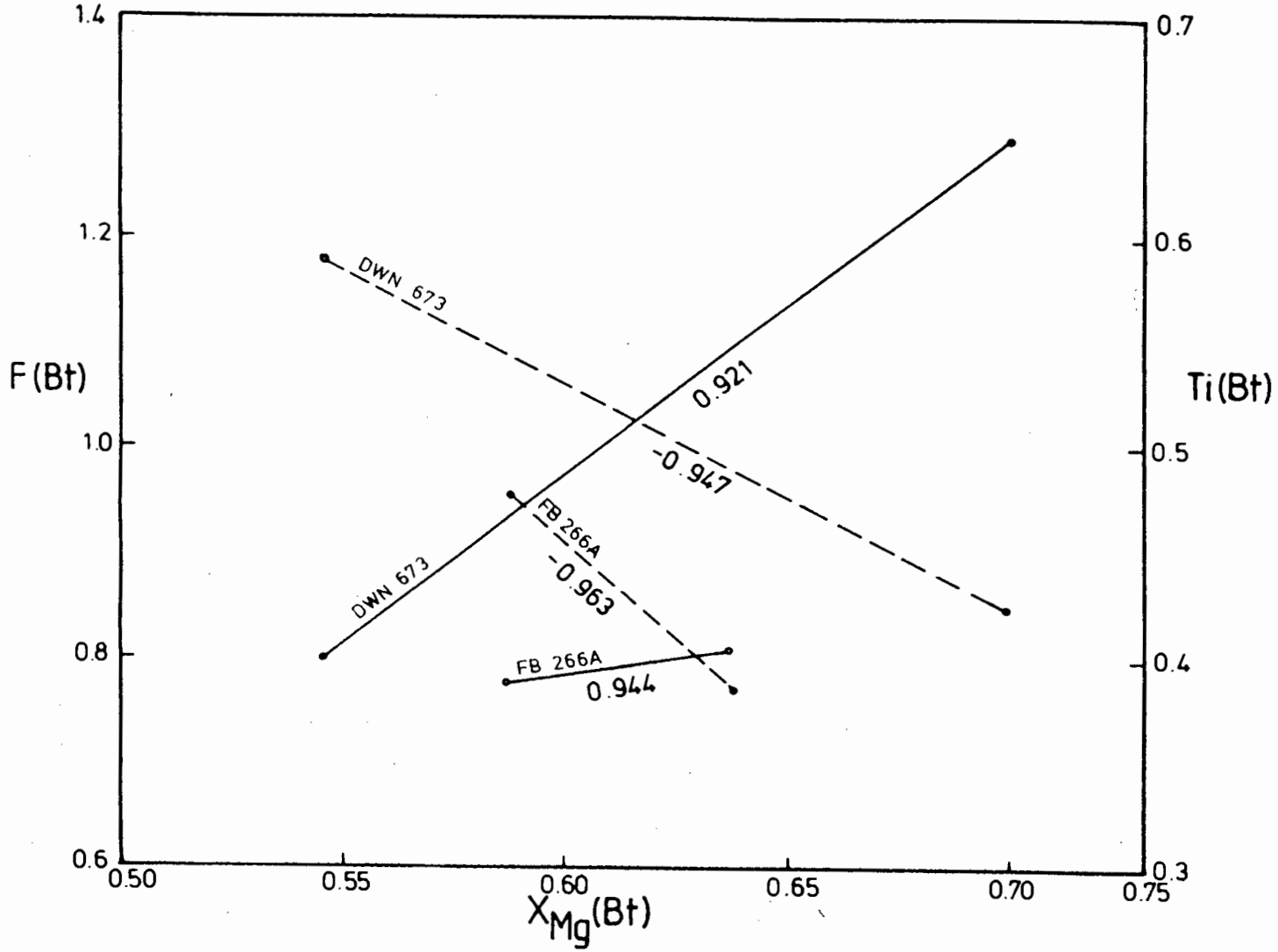

Fig. 5.4 The variation of F(Bt) and Ti(Bt) with X_{Mg}(Bt) in rocks with peraluminous bulk compositions FB266A and DWN673. Best-fit straight lines of the data are given with correlation coefficients.

are the products of retrograde growth after orthopyroxene and/or garnet at higher temperatures than their original breakdown.

5.4 Models of Migmatization

5.4.1 Introduction

The following two sections examine the phase relations near the onset of melting in rocks with granitic and peraluminous bulk compositions. An attempt is made to determine and balance the reactions responsible for generating anhydrous assemblages and melt. In this way, some constraints are placed on the temperature and water activity during migmatization.

5.4.2 Granitic Bulk Compositions

This consideration of the theoretical phase relations around melting temperatures in granitic bulk compositions is drawn and revised from Baars (1986, section 5.1) and Waters (1988).

The schematic geometry of the reactions involving the phases quartz, plagioclase, K-feldspar, phlogopite, enstatite, aqueous vapour and silicate melt in the model system CNKMASH are shown on Fig. 5.5 after Luth (1967), Bohlen et al. (1983a) and Grant (1985a, 1986b). The components Na_2O and CaO are accomodated in plagioclase and melt (e.g. Clemens and Wall, 1981; Naney, 1983).

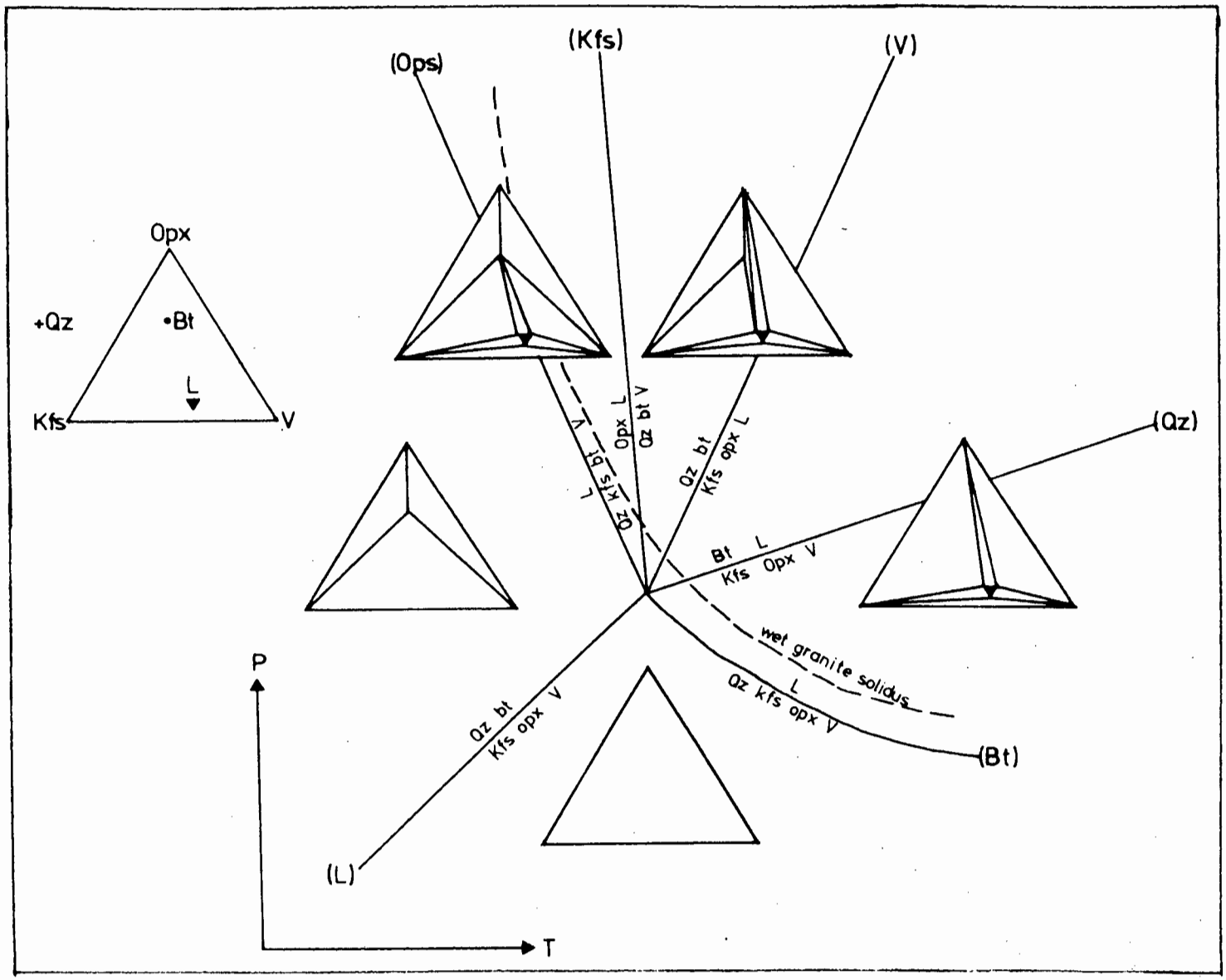

Fig. 5.5 The phase relationships involving the assemblage Bt-Opx-Qtz-Kfs-Pl-H_2O-L shown schematically in P-T space after Luth (1967), Bohlen et al. (1983a), Grant (1986a, b).

The experiments of Hoffer and Grant (1980), and the calculations of Holdaway and Lee (1977) suggest that the introduction of albite into the KMASH-system reduces the temperature of the invariant point by only 10°C, in accordance with the predictions of Grant (1973, 1985a, b).

The important features of Fig. 5.5 are:

a) The biotite dehydration reaction (L) terminates in melting reactions (Phl) and (En) at temperatures corresponding to the wet granite solidus of Tuttle and Bowen, 1958). At $P(H_2O)$ = P(total) reaction (L) is metastable with respect to melting at pressures and temperatures greater than those of the invariant point;

b) Incongruent melting can occur in granitic rocks at the appropriate metamorphic conditions in the case of the exhaustion of one or more of the components Kfs, Qtz, Pl or H_2O by the reactions (Kfs), (Qtz), (Pl) and (V), respectively; and

c) In the absence of a H_2O-rich vapour during metamorphism, enstatite and K-feldspar co-exist with a water-undersaturated melt as the products of reaction (V), known as dehydration melting (Thompson, 1982, 1988).

At pressures below 5 kbar, reaction (V) changes

from Bt + Qtz + Pl = Opx + Kfs + L [5.1]

to Bt + Qtz + Pl + Kfs = Opx + L [5.2]

owing to a thermal divide that results from changes in the H_2O-content of the melt in response to pressure variation (Grant, 1986b).

The reactions shown on Fig. 5.5 are divariant in the CNKFMASH-system, owing to Fe-Mg exchange among biotite and orthopyroxene (Fonarev and Konilov, 1986) and silicate melt. Other cationic and anionic exchanges (e.g. Ti^{IV}-Al^{IV}: Dymek, 1983; Indares and Martignole, 1985; Abrecht and Hewitt, 1988; and OH-F: Munoz and Ludington, 1974, 1977; Abercrombie et al., 1987)) also cause reaction divariance. The reversed experiments of Hoffer and Grant (1980) constrain the conditions of the invariant point to 720 $\pm$ 30°C and 2 $\pm$ 0.8 kbar for $X_{Mg}(Bt)$ = 0.5. Their experiments were performed with natural mineral compositions, similar to those described in section 5.3.

The calculated conditions of metamorphism for the Garies-Platbakkies supracrustal gneiss belt are in the range 750 - 810°C and 4.6 - 5.4 kbar. Furthermore, orthopyroxene-bearing assemblages in rocks with granitic bulk compositions equilibrated in other granulite facies terranes in continental crust at pressures in the range 3 - 11 kbar (e.g. Bohlen et al., 1983c; Harley, 1984c, 1989; Perkins and Chipera, 1985). The discrepancy between the observed conditions and the experimental results of Hoffer and

Grant (1980) suggests that it is important to consider the above phase equilibria at conditions of $P(H_2O) < P(total)$ (c.f. Wendlandt, 1981; Boettcher et al., 1987; Peterson and Newton, 1989).

Fig. 5.6 shows the experimental results in KMASH and KFASH that can be used to calibrate an isobaric T-$a(H_2O)$ section through Fig. 5.5. For clarity, only data for the reaction (V) of the form [5.1] above are included. For experiments performed with H_2O-CO_2 mixtures, $a(H_2O)$ is calculated as a function of the temperature and fugacity of the mixture using the regular solution model of Holland and Powell (1985). Using their dataset, the T-$X(H_2O)$ location Fe- and Mg-end member dehydration reactions (L) are calculated. The intersection of these reactions (L) with the solidus gives a calculated position of end member dehydration reactions (V). The thermochemical datasets of Perkins et al. (1986) or Berman et al. (1987) might also be used to calculate the position of reactions (L).

The position of reaction (Kfs) in KMASH at unit water activity is in dispute. The reversals of Peterson and Newton (1989b) suggest that Bohlen et al. (1983b) underestimated the temperature of this reaction by about 50°C at 5 kbar. Peterson and Newton (1989b) also hold that Bohlen et al. (1983b) overestimated the temperature of reaction (V) by 40°C, owing to their inability to reverse the reaction. In both cases, the recent reversals are preferred.

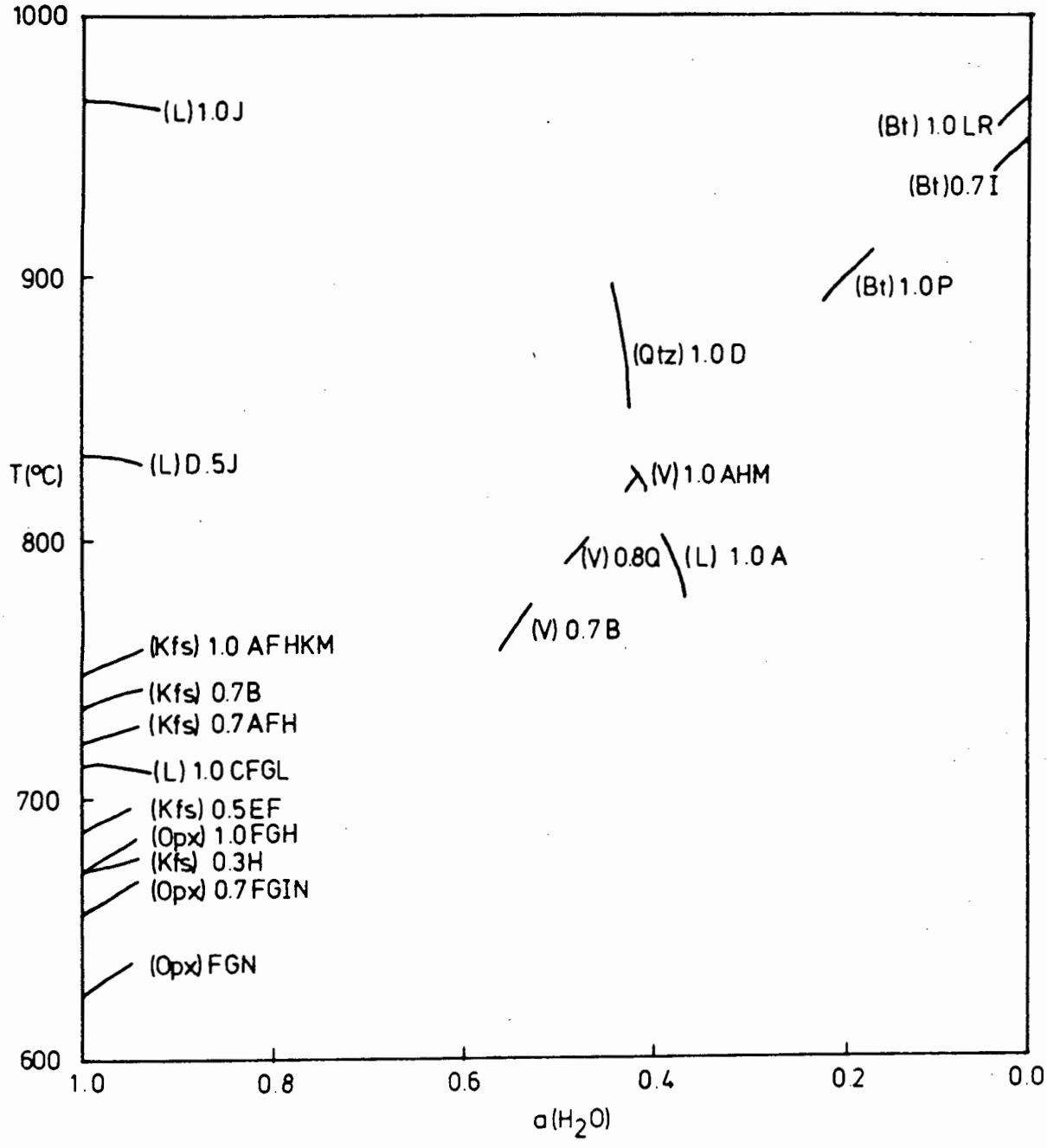

Fig. 5.6 Experimental and thermodynamic constraints on the phase relationships in an isobaric T-a(H_2O) section at 5 kbar through Fig.5.5. See overleaf for a list of the references used and an explanation of reaction names. The numeric prefix to each reference is the X_{Mg}(Bt) used.

References used on Fig. 5.6

A Bohlen et al. (1983b)

B Clemens and Wall (1981)

C Eugster and Wones (1962)

D Grant (1985a, b)

E Hoffer and Grant (1980)

F Hoschek (1976)

G Johannes (1978, 1980, 1985)

H Luth (1967), Hewitt and Wones (1984)

I Naney (1983)

J Percival (1983)

K Peterson and Newton (1989a, b)

L Rutherford (1969)

M Wendlandt (1981)

N Winkler (1976)

P Wones and Dodge (1976)

Q Wones and Eugster

R Wyllie (1977a, b)

REACTIONS

(L) bt + qz + pl → opx + kfs + V

(opx) bt + qz + kfs + pl + V → L

(bt) opx + qz + kfs + pl + V → L

(kfs) bt + qz + pl + V → opx + L

(qz) bt + L → opx + kfs + pl + V

(pl) bt + qz + L → opx + kfs + V

(V) bt + qz + pl → opx + kfs + L

Orthopyroxene with $X_{Mg}(Opx) \leq 0.15$, corresponding to biotite with $X_{Mg}(Bt) \leq 0.14$ in the temperature range of 600°C to 800°C (Fonarev and Konilov, 1986), is metastable with respect to fayalite + quartz (Eugster and Wones, 1962; Modreski and Boettcher, 1972; Brearsly and Montana, 1989).

Fig. 5.7 is visual, best-fit calibration of these results in CNKFMASH at P = 5 kbar. Preference was given to data from reversed experiments. A correction of approximately 30°C was applied to experimental results in the KFMASH-system to account for the effect of plagioclase (Peterson and Newton, 1989b vs. Keppler, 1989).

A number of important predictions about the prograde metamorphic behaviour of rocks with granitic bulk compositions, with the assemblage Qtz + Kfs + Pl + Bt + V, arise from considering the phase equilibria shown on Fig. 5.7 (c.f. Waters, 1988). The temperatures quoted apply to $X_{Mg}(Bt) = 0.6$ which is a typical value for the rocks in the study area.

a) In the presence of a pure H_2O vapour, the assemblage melts congruently at about 650°C by reaction (Opx), producing a water-saturated melt into which all the vapour dissolves. If other components are present in the vapour, H_2O is partitioned into the melt. With further temperature increase and continued melting, the residual vapour composition is buffered to lower $a(H_2O)$ along the reaction

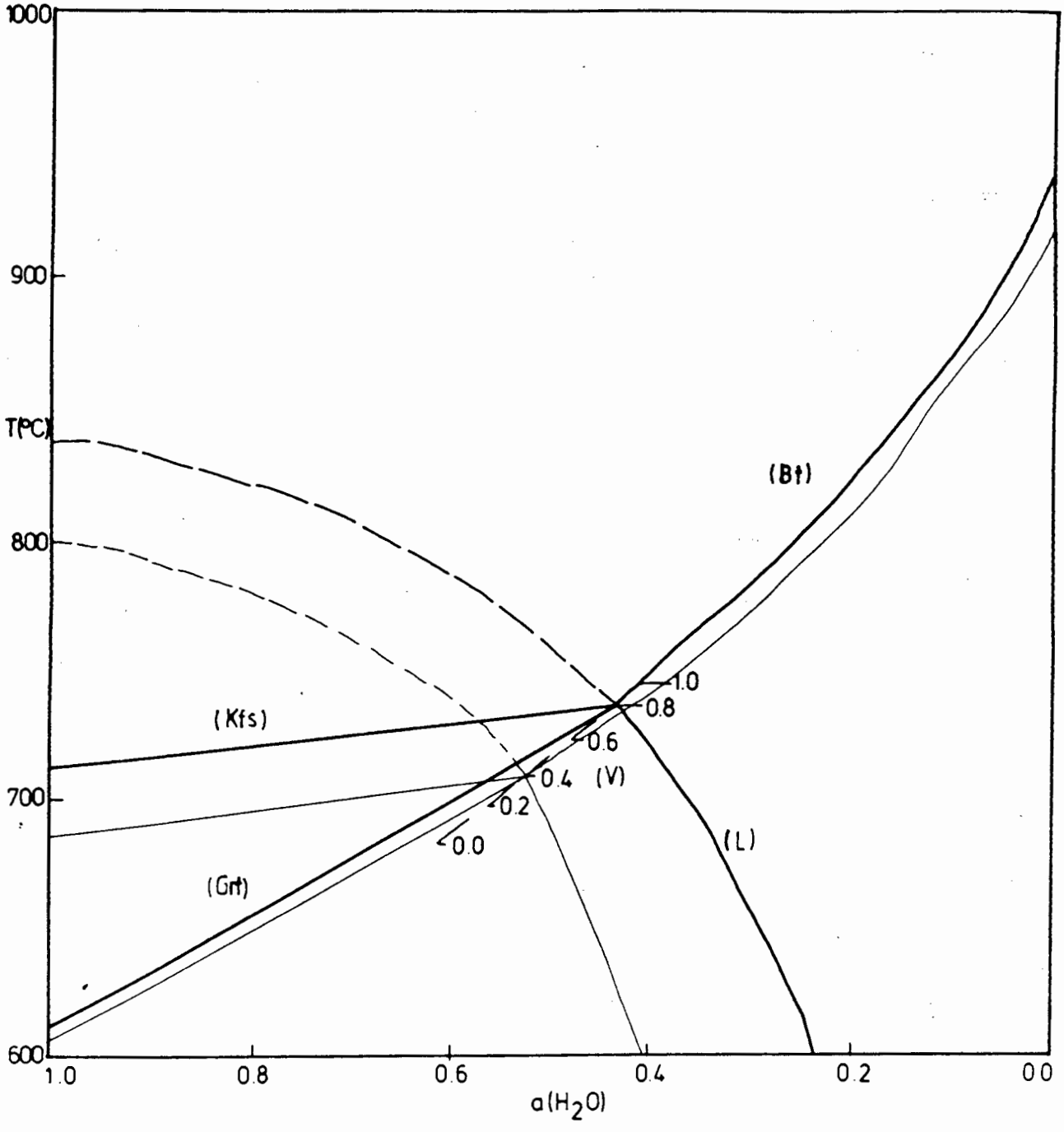

Fig. 5.7 A best-fit calibration of the data shown on Fig. 5.7, in terms of Fe- (light lines) and Mg- (heavy lines) end-member reactions in T-a(H_2O) space. Dashed lines of reaction (L) indicate that it is metastable with respect to melting. Reaction (V) is calibrated in terms of X_{Mg}(Bt). See text for discussion.

curve towards reaction (V).

b) In the presence of a vapour with low $a(H_2O)$, (either by reason of vapour-undersaturation in the low porosity and/or low permeability rock volume, or by dilution by another vapour species, say CO_2, or both), the assemblage dehydrates at $T \leq 760^oC$, producing an anhydrous assemblage. In a closed system, the prograde liberation of H_2O from biotite buffers the vapour to higher $a(H_2O)$ along the reaction curve towards reaction (V).

c) In a vapour-absent assemblage whose $a(H_2O)$ is a function of the chemical potential of water bound in biotite, dehydration melting of the assemblage occurs at about 760^oC, producing a water-undersaturated melt co-existing with orthopyroxene and K-feldspar. The volume of melt produced is directly proportional to the amount of biotite available in the reactant assemblage. Reaction (V) takes place over a small temperature interval, say 20^oC, corresponding to the degree of reaction divariance.

This model predicts that a rock with granitic bulk composition and containing a small volume of vapour encounters dehydration melting, unless one of the reactants is exhausted, or the fluid composition is controlled by an external reservoir. In granulite terranes, the latter is commonly supposed to be CO_2-rich derived from depth (e.g. Janardhan et al., 1979, 1982; Newton et al., 1980; Wendlandt, 1981; Grant, 1986b; Harris, 1989).

5.4.3 Peraluminous Bulk Compositions

The phase relations of rocks with peraluminous bulk compositions (Zen, 1988) at melting temperatures are discussed with reference to the observed mineral assemblages and estimated bulk compositions of garnet-biotite metapelitic and quartzofeldspathic gneisses.

It is relevant to consider sillimanite as a precursor mineral in these for two principal reasons:

a) Textures, such as sillimanite needle inclusions in garnet and/or cordierite, and shear-related sillimanite regrowth with biotite, suggest that sillimanite was stable in many metapelitic bulk compositions at conditions before and after the metamorphic peak. It is possible that the common, poikiloblastic garnet habit is the result of selective garnet nucleation near grain boundaries between quartz, biotite and sillimanite.

b) Similar rock types have been collected from areas closer to the amphibolite-granulite facies boundaries in western Bushmanland (e.g. Joubert, 1971; Jack, 1980; Albat, 1984; Waters and Whales, 1984; Moore, 1986; Waters, 1986b, 1988; McStay, 1988; in prep.). These contain biotite and sillimanite co-existing with garnet porphyroblasts in matrix and leucosome assemblages of quartzofeldspathic metapelitic schists and gneisses, suggesting that the dehydration reaction

$$Bt + Sil + 2Qtz \pm Pl = Grt + Kfs + H_2O \quad [5.3]$$

was responsible for garnet growth in these rocks.

At relatively high temperatures the dehydration of Al-rich phlogopite, the eastonite component (Guidotti, 1984), co-existing with quartz can be responsible for the production of garnet by the KMASH-reaction

$$3East + Phl + 12Qtz = 3Py + 4Kfs + 4H_2O$$

Fig. 5.8 shows the phase equilibria in P-T space among

$$[Qtz + Kfs + Pl + Bt + Sil + Grt + H_2O + L]$$

in the system CNKFMASH after Grant (1973, 1985a, b), Thompson (1976, 1982), Vielzeuf and Boivin (1984) and Spear and Cheney (1988). The scheme is estimated at $P(H_2O) = 0.6P(total)$ because reaction [5.3] is metastable with respect to melting at $P(H_2O) = P(total)$ (Holdaway and Lee, 1976; Grant 1985a, b). The reactions are strongly divariant with respect to Fe-Mg exchange. Only the reactions arising from the termination of subsolidus reaction [5.3] in melting are shown.

The important features of Fig. 5.8 are:

a) The biotite dehydration reaction (L) terminates in melting reactions (Bt), (Grt) and (Sil) temperatures below the wet granite solidus of Tuttle and Bowen (1958). The stability of peraluminous granitic magmas is reviewed by Zen (1988), after important studies by inter alia White and Chappell (1977), Abbott and Clarke (1979), Clemens and Wall

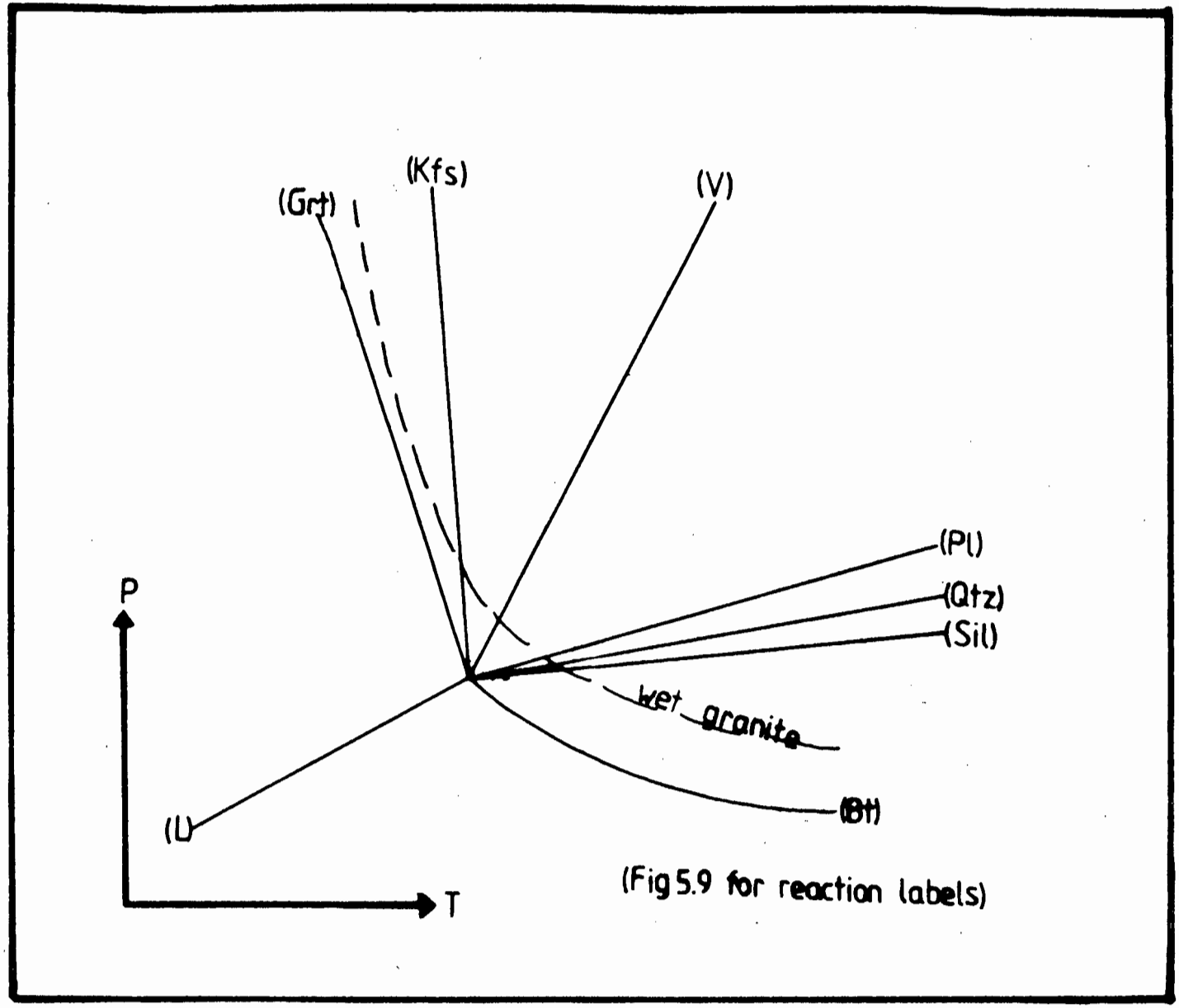

Fig. 5.8 Phase relationships involving the assemblage Bt-Grt-Sil-Qtz-Kfs-Pl-L-H_2O shown schematically in P-T space after Grant (1973, 1985a, b), Thompson (1976, 1982), Vielzeuf and Boivin (1984) and Speer and Cheney (1988).

(1981, 1988), and Clemens and Vielzeuf (1987);

b) Incongruent melting can take place in peraluminous rock compositions at the apprpriate metamorphic conditions in the case of exhaustion of one, or more of the principal phases Kfs, Sil or H_2O by the reactions (Kfs), (Sil) or (V), respectively; and

c) In the absence of a H_2O-rich vapour during metamorphism, garnet and K-feldspar can co-exist with a water-undersaturated melt as the products of reaction (V), the dehydration melting reaction.

Abbott and Clarke (1979) estimate the position of the invariant point at 4 kbar and 670°C for the Fe end member reaction at $P(H_2O) = 0.6\ P(total)$. The equivalent reaction for intermediate Fe-Mg compositions of biotite and garnet observed in DWN673 and FB266A is metastable with respect to the wet peraluminous granite solidus (Grant 1985a, Vielzeuf and Holloway, 1988). It is useful, therefore, to represent the equilibria on an isobaric T-$a(H_2O)$ diagram.

Fig. 5.9 shows the of experimental and calculated results that can be used to calibrate the $a(H_2O)$-dependent phase equilibria in cordierite-free metapelitic gneisses. For experiments conducted with H_2O-CO_2 fluid mixtures, $a(H_2O)$ was calculated using Holland and Powell (1985) as for Fig. 5.6.

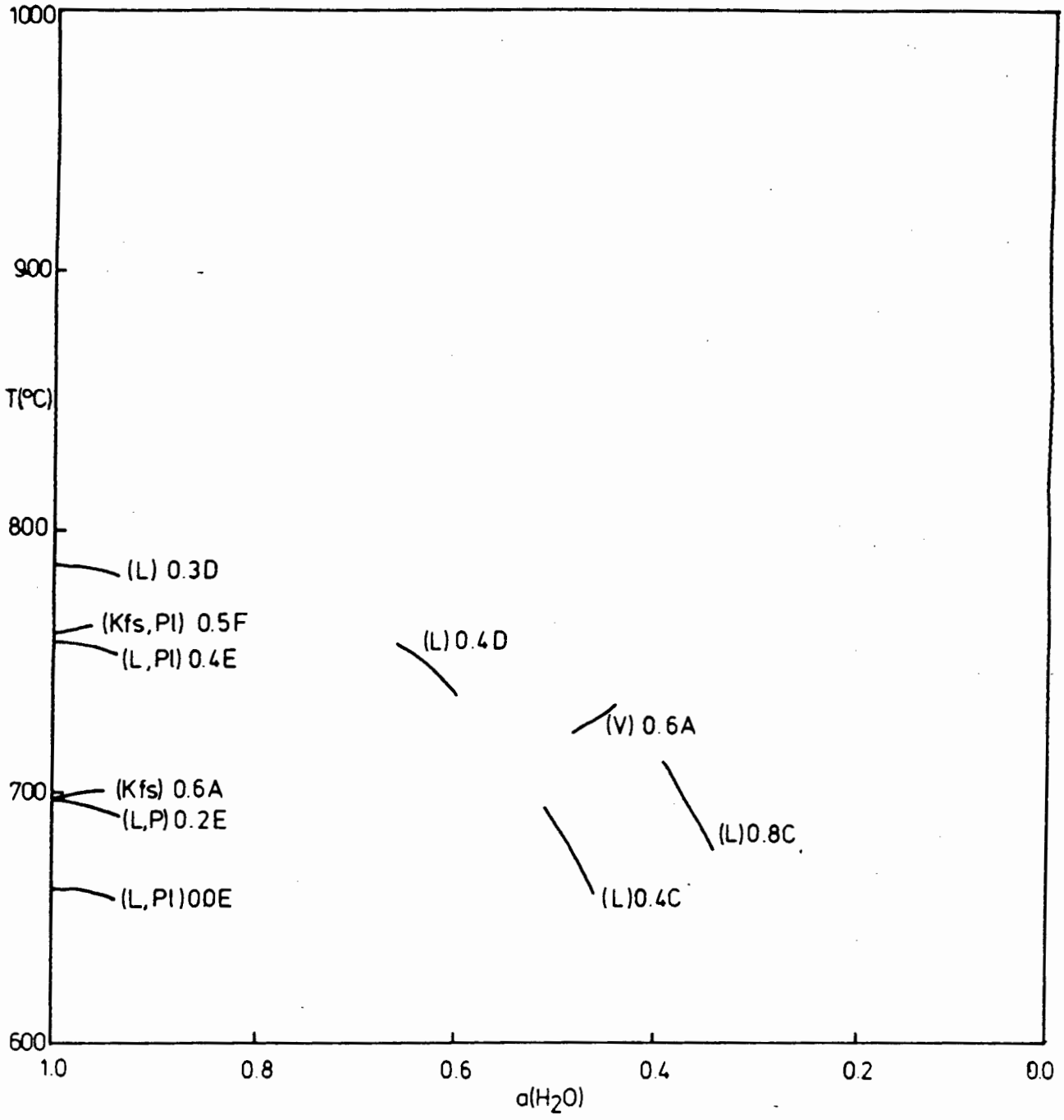

Fig. 5.9 Experimental and thermodynamic constraints on the phase relationships of an isobaric T-a(H_2O) section at 5 kbar through Fig. 5.8. See overleaf for a list of the references used and an explanation of the reaction labels. The prefix number to each reference refers to the X_{Mg}(Bt) used.

References used on Fig. 5.9

A Clemens and Wall (1981)

B Holdaway and Lee (1977)

C Holland and Powell (1988)

D Lee and Holdaway (1978)

E Thompson (1976)

F Vielzeuf (1980)

REACTIONS

(L) bt + sil + qz → grt + kfs + V

(grt) bt + sil + qz + kfs + pl + V → L

(bt) grt + sil + qz + kfs + pl + V → L

(kfs) bt + sil + qz + pl + V → grt + L

(sil) grt + qz + kfs + pl + V → bt + L

(qz) bt + sil + L → grt + kfs + pl + V

(pl) bt + sil + qz + L → grt + kfs + V

(V) bt + sil + qz + pl → grt + kfs + L

Fig. 5.10 is a visual best-fit of these constraints, for $X_{Mg}(Bt)$ in the range 0.4 to 0.8. The following predictions arise from considering of the phase equilibria shown on Fig. 5.10 (Waters, 1988). Temperatures are quoted for $X_{Mg}(Bt) = 0.5$, a typical value for the peraluminous rocks in the study area.

a) In the presence of a pure H_2O vapour, the assemblage melts congruently at reaction (Grt) at about 650°C, producing a water-saturated melt into which the H_2O-vapour dissolves. In the presence of a mixed fluid, the partition of H_2O into the melt buffers the vapour composition to lower $a(H_2O)$ along the reaction curve towards reaction (V).

b) In the presence of a vapour with low $a(H_2O)$ the assemblage dehydrates at $T \leq 650°C$, producing an anhydrous assemblage. The prograde liberation of H_2O from biotite buffers the vapour to higher $a(H_2O)$ along the reaction curve towards reaction (V).

c) In a vapour-absent assemblage whose $a(H_2O)$ is a function of water-content of biotite, dehydration melting of the assemblage occurs at 720°C. This produces an incongruent, water-undersaturated melt co-existing with garnet and K-feldspar. The amount of melt produced is a function of the amount of sillimanite and biotite in the reactant assemblage. In the case of sillimanite exhaustion, the remaining phases are related by reaction (Sil). Increasing temperature will continue to buffer the vapour composition to lower $a(H_2O)$ (c.f. Waters, 1988, p.395). Reaction (V) takes place over a small temperature interval, say 15°C,

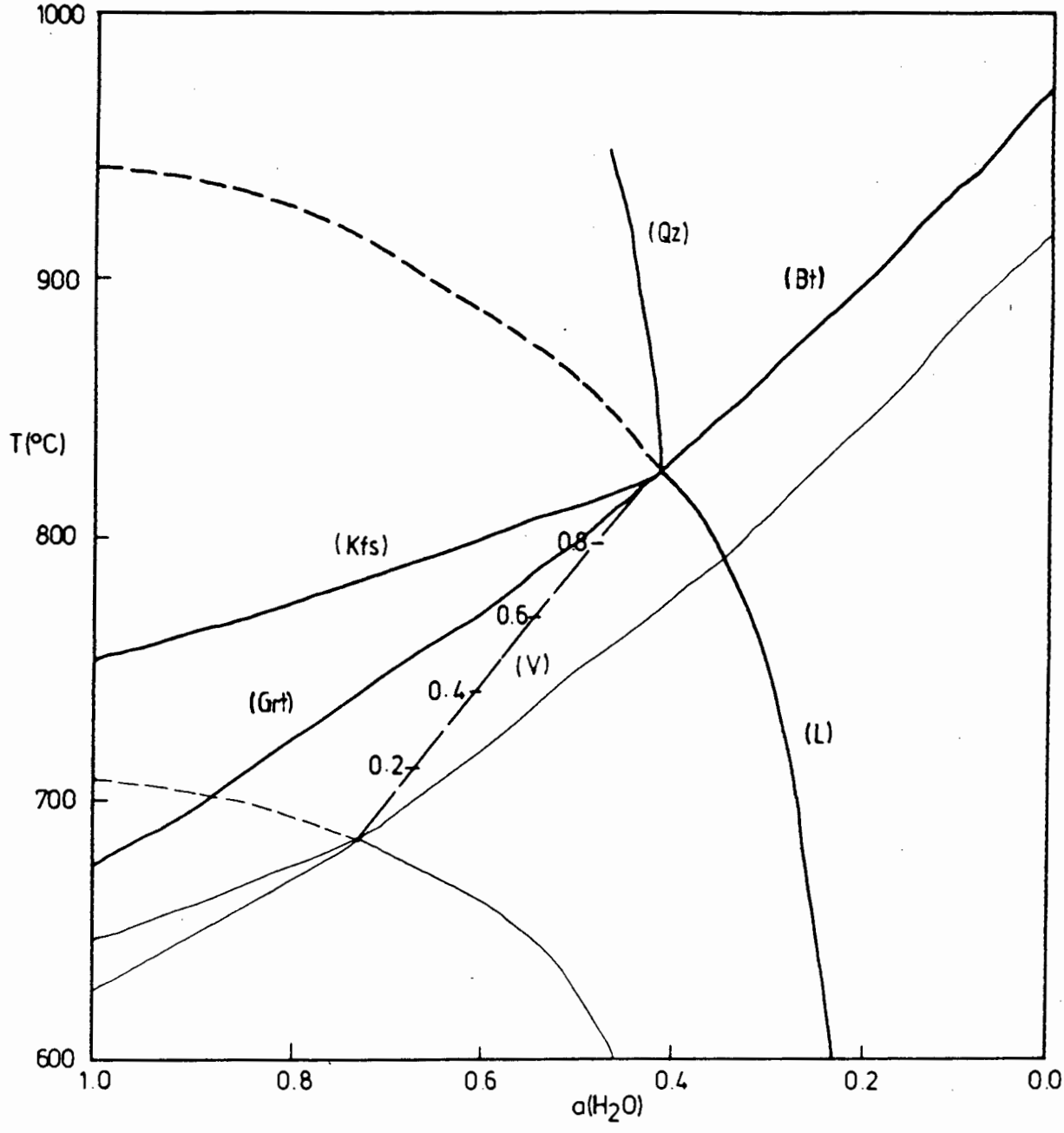

Fig. 5.10 A best-fit calibration of the reaction constraints shown on Fig. 5.9 in terms X_{Mg}(Bt) = 0.4 (light lines) and X_{Mg}(Bt) = 0.8 (heavy lines). Dashed curves of reaction (L) indicate that it is metastable with respect to melting. Reaction (V) is calibrated in terms of X_{Mg}(Bt).

corresponding to the degree of reaction divariance.

This model predicts that a sillimanite-garnet-biotite metapelitic gneiss encounters dehydration melting, unless one of the reactants is exhausted, or the fluid composition is controlled by an externally derived fluid species.

5.5 Biotite Dehydration and Dehydration Melting

The observed mineral assemblages and modal abundances in selected granitic and peraluminous bulk compositions are compared with those predicted by the phase relations of Figs. 5.7 and 5.10. Mineral compositions and modal abundances are used to test the applicability of the reactions

$$Bt + Qtz + Pl = Opx + Kfs + V \quad [5.4]$$

$$Bt + Qtz + Pl = Opx + Kfs + L \quad [5.5], \text{ and}$$

to assemblages in biotite-orthopyroxene leucoparagneisses FB48 and FB2, respectively; and the reactions

$$Bt + Sil + Qtz + Pl = Grt + Kfs + V \quad [5.6], \text{ and}$$

$$Bt + Sil + Qtz + Pl = Grt + Kfs + L \quad [5.7]$$

to assemblages in garnet-biotite aluminous quartzofeldspathic gneiss FB266A and garnet-biotite metapelitic gneiss DWN 673, respectively.

The modal abundances of these four rocks are shown on Table 7. The methods used to estimate the modal abundances of matrix and leucosome in these and other rocks are described in Appendix 2.

Reactions [5.4 - 5.7] are respectively balanced using the natural mineral compositions of FB48, FB2, FB266A and DWN 673, and estimated melt compositions. This is shown in Appendix 3. These mass balance calculations were each solved as a series of simultaneous equations for the major oxide concentrations of the phases involved. The respective reactions can be balanced for each rock by the calculated mass balance coefficients, suggesting that the reactions are valid as written.

By converting the coefficients to volume proportions, the predicted modal abundances are be compared with those observed in the product assemblages of the rocks, as shown in Appendix 3. These results are conveniently represented on 'isochon' diagrams for FB2 and (Figs. 5.13a, b). This simple method was adapted by Grant (1986a) after Gresens (1967), and compares the observed modal abundances of migmatite assemblages with those predicted by mass balance.

The results suggest that K-feldspar is under-represented in the leucosomes of both FB256 and DWN673, as is commonly the case in other migmatized rocks of the area (e.g. Baars, 1986, 1988; Waters, 1988). In DWN673, plagioclase is also strongly under-represented in the leucosome. The high observed concentration of garnet in the DWN673 leucosome may be the result of garnet growth by dehydration melting occurring after an initial period of garnet growth by dehydration.

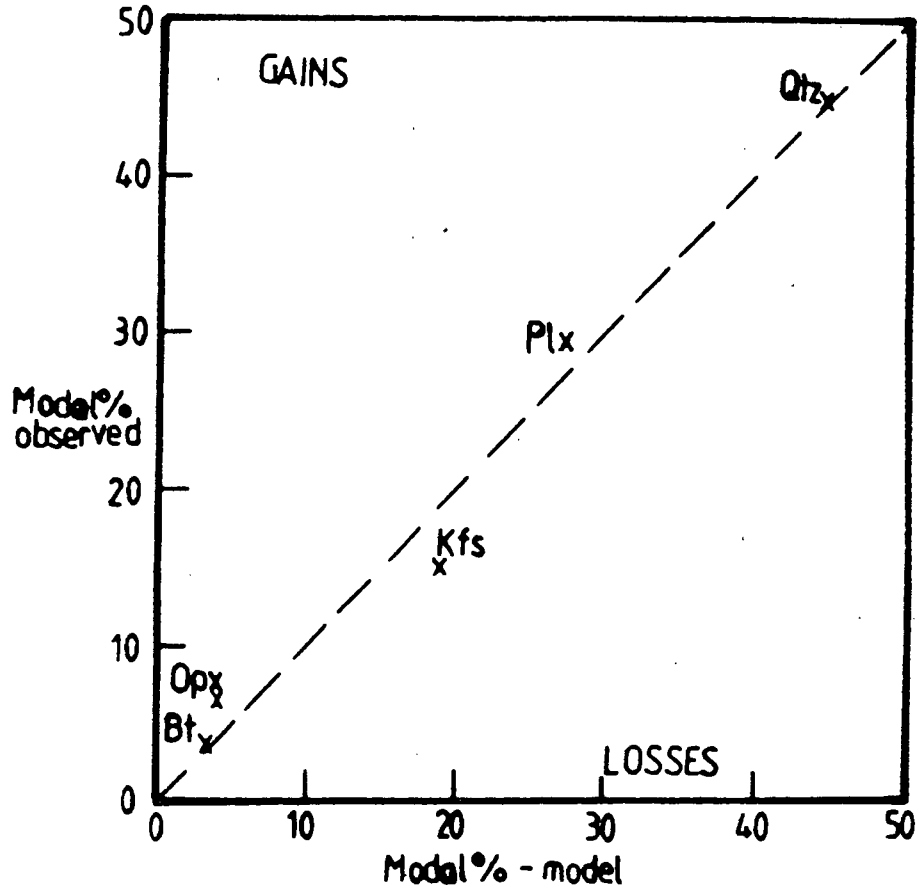

Fig. 5.13a An 'isochon' diagram (Grant, 1986a) comparing the observed modal proportions of a leucosome in Bt-Opx leucoparagneiss FB256 against those predicted by mass balance calculations on the biotite-rich matrix (Appendix 3B). Gains and losses refer to those of the leucosome relative to the matrix.

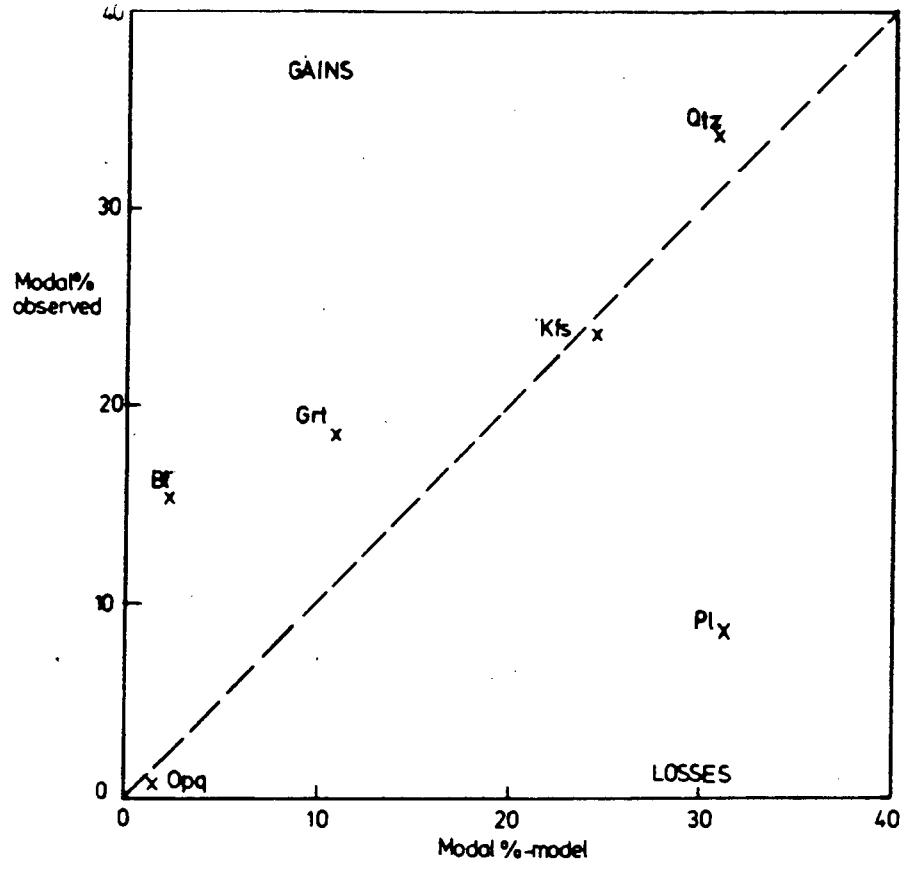

Fig. 5.13b An 'isochon' diagram (Grant, 1986a) comparing the observed modal proportions of a leucosome in Grt-Bt metapelitic gneiss DWN673 against those predicted by mass balance calculations on the biotite-rich (Appendix 3D). Gains and losses refer to those of the leucosome relative to the matrix.

Fig. 5.11 is a 1:1 scale representation of the distribution of matrix, garnet and quartzofeldspathic leucosome of part of a metre-scale migmatite in garnet-biotite metapelitic gneiss, FBM2. Matrix- and leucosome-dominated zones within the outcrop are marked.

Fig. 5.12a is a plot of the ratios of quartzo-feldspathic leucosome and garnet to matrix, respectively. The points fall on a straight line passing through the origin, suggesting that garnet and leucosome are generated in a uniform ratio (slope = garnet:leucosome = 0.14) at the expense of matrix. This trend is also reflected on the inset to Fig. 5.12b, a logarithmically scaled plot of the same ratios which emphasises the differences between low ratio, matrix-dominated and intermediate zones, M1-3 and C1-3, respectively. The compositions of phases in DWN673, sampled in a petrographically similar horizon, are used to predict a garnet:quartzofeldspathic leucosome ratio of between 0.11 and 0.15 (biotite consumed between 15 and 20 volume%) generated by vapour-absent dehydration melting. This corresponds closely to the observed value of 0.14 (Fig. 5.12a).

5.6 Fluid Infiltration

Some authors have preferred to account for the low values of $a(H_2O)$ characteristic of granulite facies terranes by the infiltration of large quantities of CO_2 into the lower continental crust (e.g. Janardhan et al. 1979; Newton et al. 1980; Frost and

Fig. 5.11 A simplified outcrop map of migmatitic garnet-biotite metapelitic gneiss FBM2. The marked off areas indicate matrix- and leucosome-dominated, and intermediate geometric portions of the outcrop. See Appendix 2 for an explanation of the method of estimation of the modal proportions of this rock.

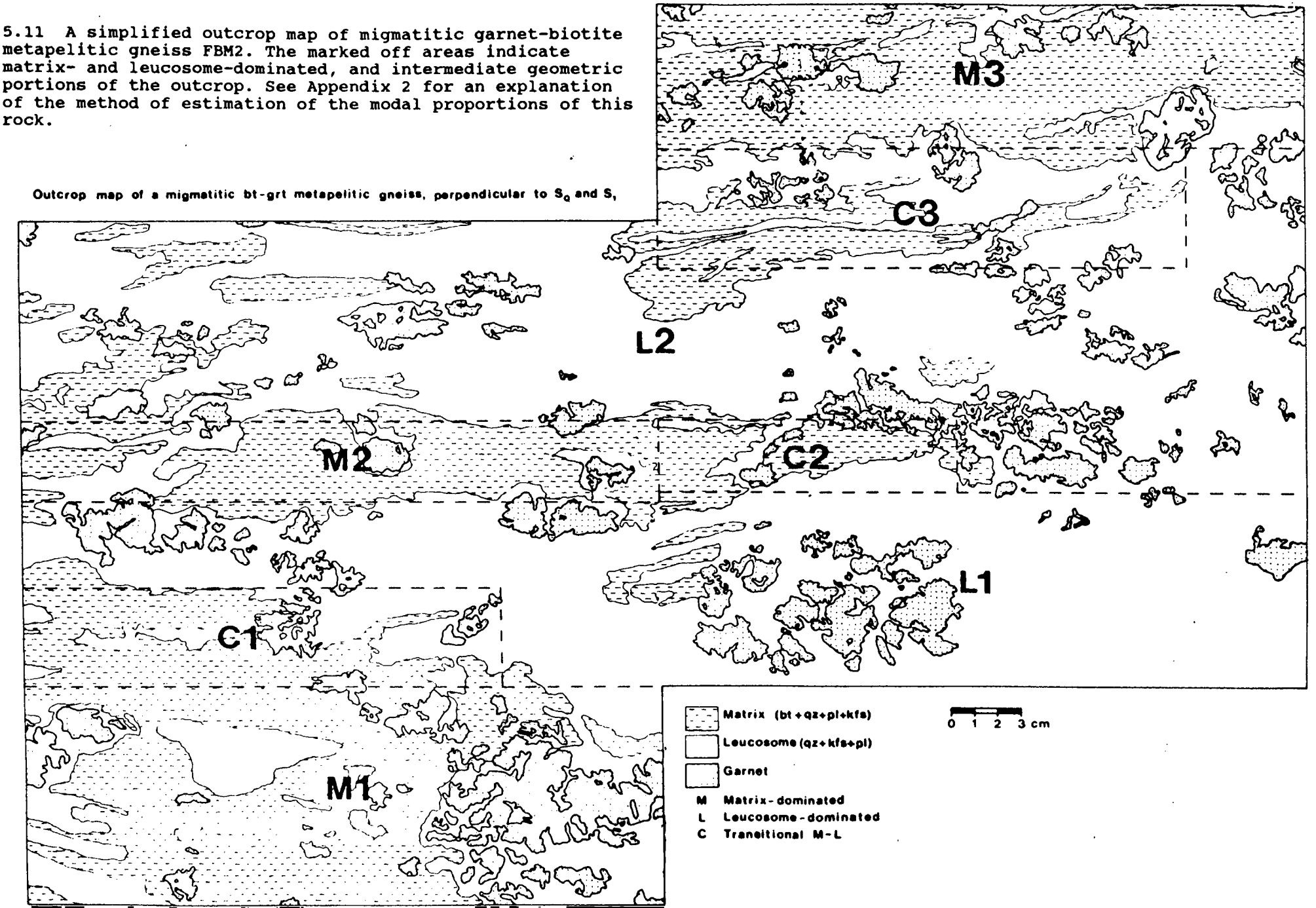

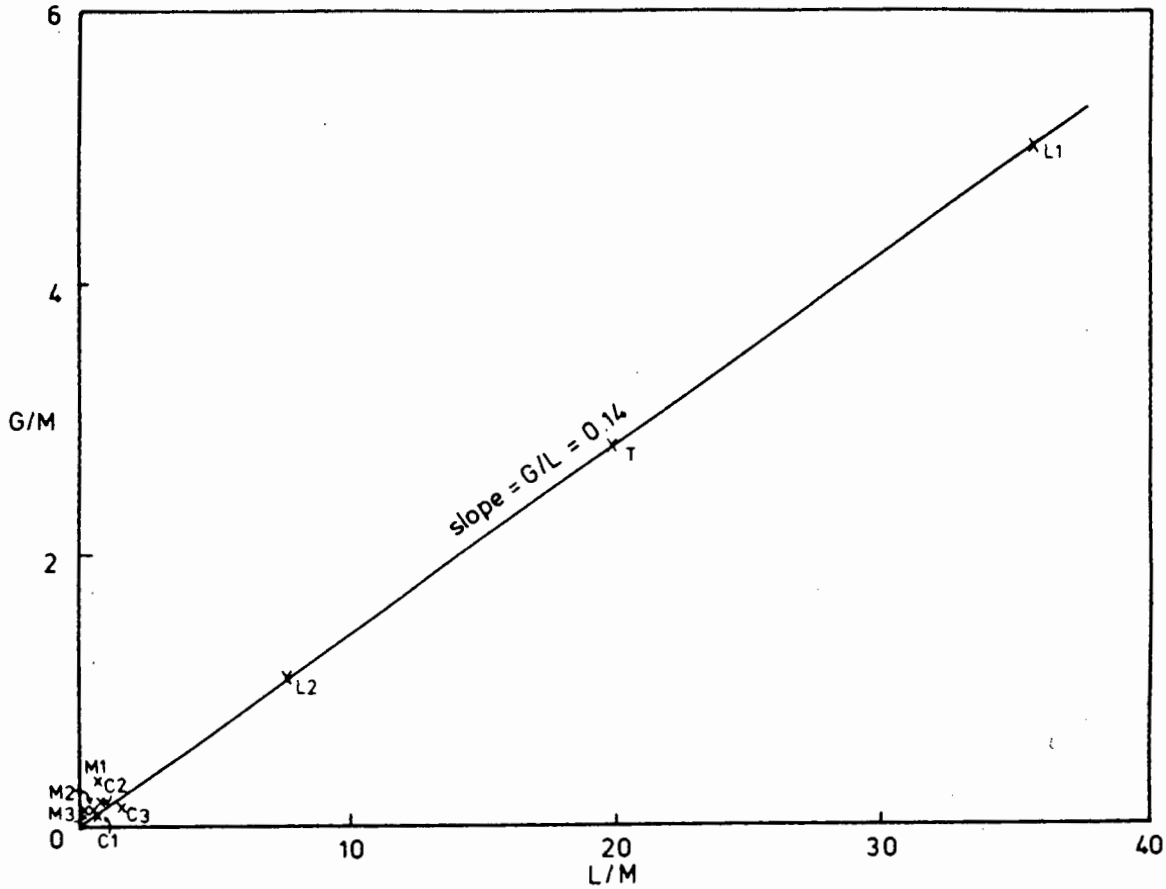

Fig. 5.12a Plot of the ratios of modal proportions G/M against L/M in the different zones of FBM2 on Fig. 5.11. The points define a straight line with slope G/L = 0.14. Point T, the total modal proportions of the sample, is shown for reference.

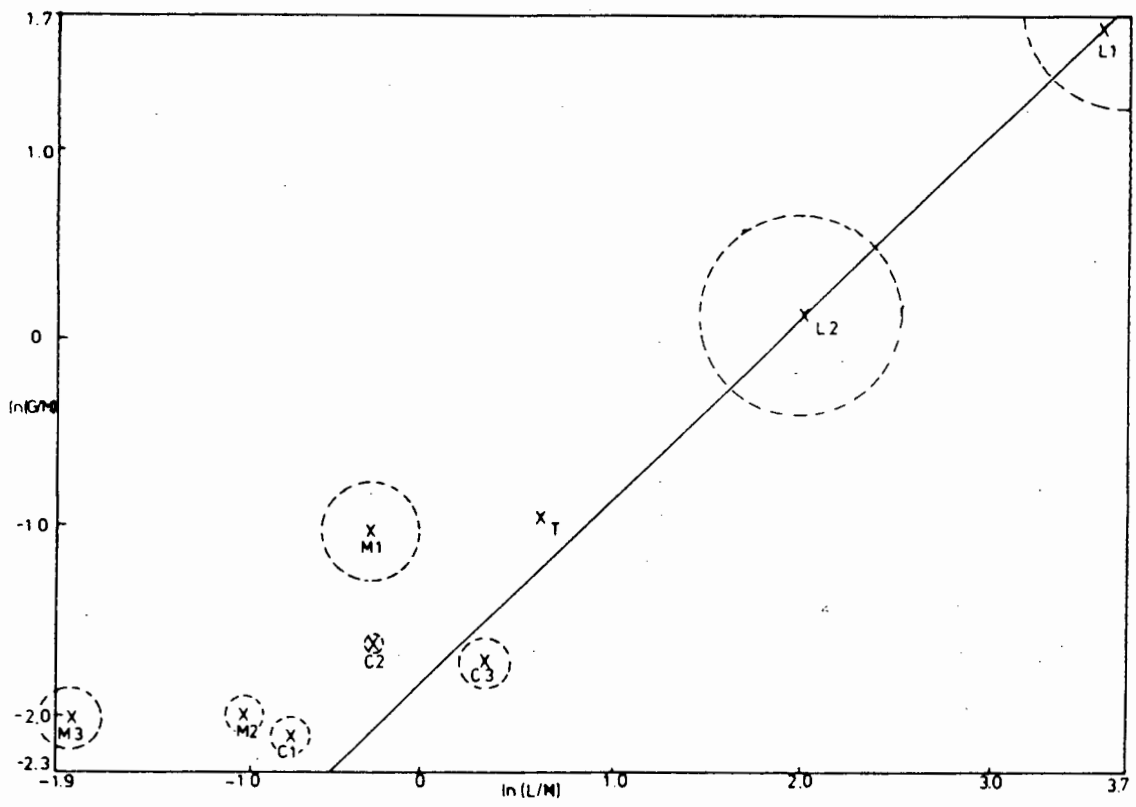

Fig. 5.12b Logarithmically scaled plot of the ratios of modal proportions G/M against L/M in the different zones of FBM2 shown on Fig. 5.11. The circle radii of each data point is propotional to the sample size in each zone. The best-fit straight line through these points is strongly weighted to larger sample sizes, and has a slope of +1.0. This confirms the constant G/L ratio indicated on Fig. 5.12a.

Frost, 1987; Hollister, 1988; Peterson and Newton, 1989a). In each case this conclusion is supported by abundant evidence from CO_2-rich fluid inclusions (e.g. Touret, 1971; Hansen et al. 1985) and stable isotopes (e.g. Jackson et al. 1988). Newton et al. (1980) regard the interconnectedness of charnockitic leucosomes as evience for large-scale fluid infiltration. However, this evidence is commonly diputed (e.g. Chacko et al., 1988 vs. Klatt et al., 1988 and Raith et al., 1988 for the granulites of southern Kerala, India).

Some experiments on the formation of migmatites suggest that crustal rocks can melt in the presence of a CO_2-bearing fluid at temperatures as low as those in the pure H_2O system (Wendlandt, 1981; Peterson and Newton, 1989a).

Baars (1986) showed a plot of volume% orthopyroxene production and biotite consumption in FB48 by prograde, internally buffered dehydration against $X(H_2O)$ of a fluid mixture. Temperatures for $X_{Mg}(Bt)$ were taken a similar diagram to Fig. 5.7. Between 700 and 840^{o}C, orthopyroxene production in excess of 2.5 volume% is limited to rocks having a porosity greater than 3%. Orthopyroxene abundance in matrix (or mesosome) portions of biotite-orthopyroxene gneisses does not exceed 2.5%. It was concluded that orthopyroxene in matrix granitic compositions was produced almost entirely by the dehydration of biotite in the presence of $\leq$ 3% pore space. The same amount of orthopyroxene

could only be produced by the infiltration of up to 6.5 volume% CO_2. A similar situation can be modelled for the partial melting reactions in biotite-orthopyroxene and biotite-garnet quartzo-feldspathic assemblages (Waters, 1988).

5.7 Discussion

The results of modal analysis in this study are consistent with the production anhydrous granulite and migmatitic assemblages in granitic and peraluminous rock types by biotite dehydration and dehydration melting. This mechanism of progressive migmatization acted as an efficient reducer of $a(H_2O)$ to between 0.25 and 0.5 at the peak metamorphic temperature. Water from the dehydration of biotite (and/or hornblende) was dissolved into melts that formed in a system closed to measurable external fluid control.

This and other studies (Waters, 1988; McStay, in prep.) have consistently observed small, locally variable discrepancies between the modal abundances of leucosomes and those predicted by the dehydration melting reactions. In part this is the result of the sampling methods of inhomogeneous leucosome assemblages. However, Waters and Baars (1989) argue that this may be accounted for by the extraction of small, but significant quantities of metamorphic partial melt. In the Garies-Platbakkies Supracrustal gneiss belt, migmatitic root zones in granitic and peraluminous rock types are continuous into zones (commonly D4 shear zones) extensively intruded by sills and dykes of anatectic granites.

These are commonly K-feldspar-rich granites, suggesting that they may be locally extracted partial melts. Silicate melt mobility is limted by its high viscosity and the amount of melt extracted.

CHAPTER 6 CONCLUSIONS

6.1 Partial Melting

In the Garies-Platbakkies supracrustal gneiss belt, approximately 10% of the mapped area is comprised of the crystalline products of migmatization. These products occur as *in situ* leucosomes and locally derived dykes and sills that were emplaced during and soon after the upper granulite facies peak of Namaqua metamorphism in the western Bushmanland Subprovince (Waters, 1988, 1989; Waters and Baars, 1989; this study).

The mechanism of migmatization was controlled by the mineral assemblages of the host rocks. The amount of partial melting was strongly limited by the amount of water available from the dehydration of biotite and hornblende during prograde metamorphism. There is no chemical evidence that points to the control of fluid composition and partial melting by an external fluid reservoir.

Migmatization had a significant effect on the tectonic behaviour of the terrane. The spatial coincidence of at least three coaxial phases of deformation with the generation, extraction, emplacement and crystallization of viscous silicate partial melt has produced an attenuated, E-W trending belt of paragneisses. Ductile behaviour and limited mass transfer has been localized along structural discontinuities (S_{1-4} foliations planes) and in

particular rock types (aluminous quartzo-feldspathic, metapelitic and some biotite gneisses) within the supracrustal gneiss belt.

The effect of partial melting on the thermal evolution of the crust under study is difficult to constrain precisely. Many models of regional metamorphism attribute the transfer of significant quantities of heat by advection in large fluid fluxes (Etheridge et al., 1983; Wickham and Taylor, 1985; Ferry, 1986a, b; Lamb et al., 1987; Brady, 1988; Whitney, 1988; Harris and Bickle, 1989; Peacock, 1989). There is overwhelming evidence in the study area for low fluid:rock ratios for the period of metamorphism between the amphibolite-granulite transition and the granulite facies peak. This fluid-undersaturation and local fluid activity gradients are the direct results of low rock porosity, dehydration partial melting approaching and at the peak of metamorphism, and the extraction of small quantities ($\leq$ 10%) of partial melt.

Towards the peak of metamorphism ($\geq$ 780 $\pm$ 30^{o}C), fluids were dissolved into water-undersaturated partial melts. Some refractory, phlogopite-bearing horizons retained $\geq$ 90% of their hydrous mineral component. Water-undersaturated partial melts acted as "thermal sinks", retarding the advance of metamorphic isotherms in adjacent, relatively anhydrous lithologies. Similar effects have been recorded in the Adinrondacks (Lamb and Valley, 1984) and in Eastern Scotland (McLellan, 1989).

6.2 Tectonothermal Evolution

Fig. 6.1 is a schematic P-T-t path for the ca. 1150 Ma granulite facies imprint on the Garies-Paltbakkies supracrustal gneiss belt (after Waters, 1988, 1989) based, in part, on petrologic evidence from the study area. Radiometric age estimates of the various portions of the path have been omitted, because these are not adequately constrained in southern Namaqualand. The annotations refer to the following sequence of geologic and petrologic responses to tectonothermal events since the early Proterozoic.

1) The supracrustal gneiss sequence, deposited on an unconfirmed basement and intruded by sills of porphyritic granite, was isoclinally folded and a regional foliation was developed (D1 deformation). The metamorphic grade of this event is not known.

2) Pretectonic, K-feldspar megacrystic granite was emplaced, structurally overlying the supracrustal sequence. The paraconformable relationship may be the result of south-directed thrusting during D2 or sill-like igneous intrusion.

3) D2 deformation, accompanied by amphibolite facies metamorphic conditions ($\geq 550^{o}C$, 3.5 kbar), produced crenulation folds in incompetent lithologies on the limbs of south-vergent, overturned folds.

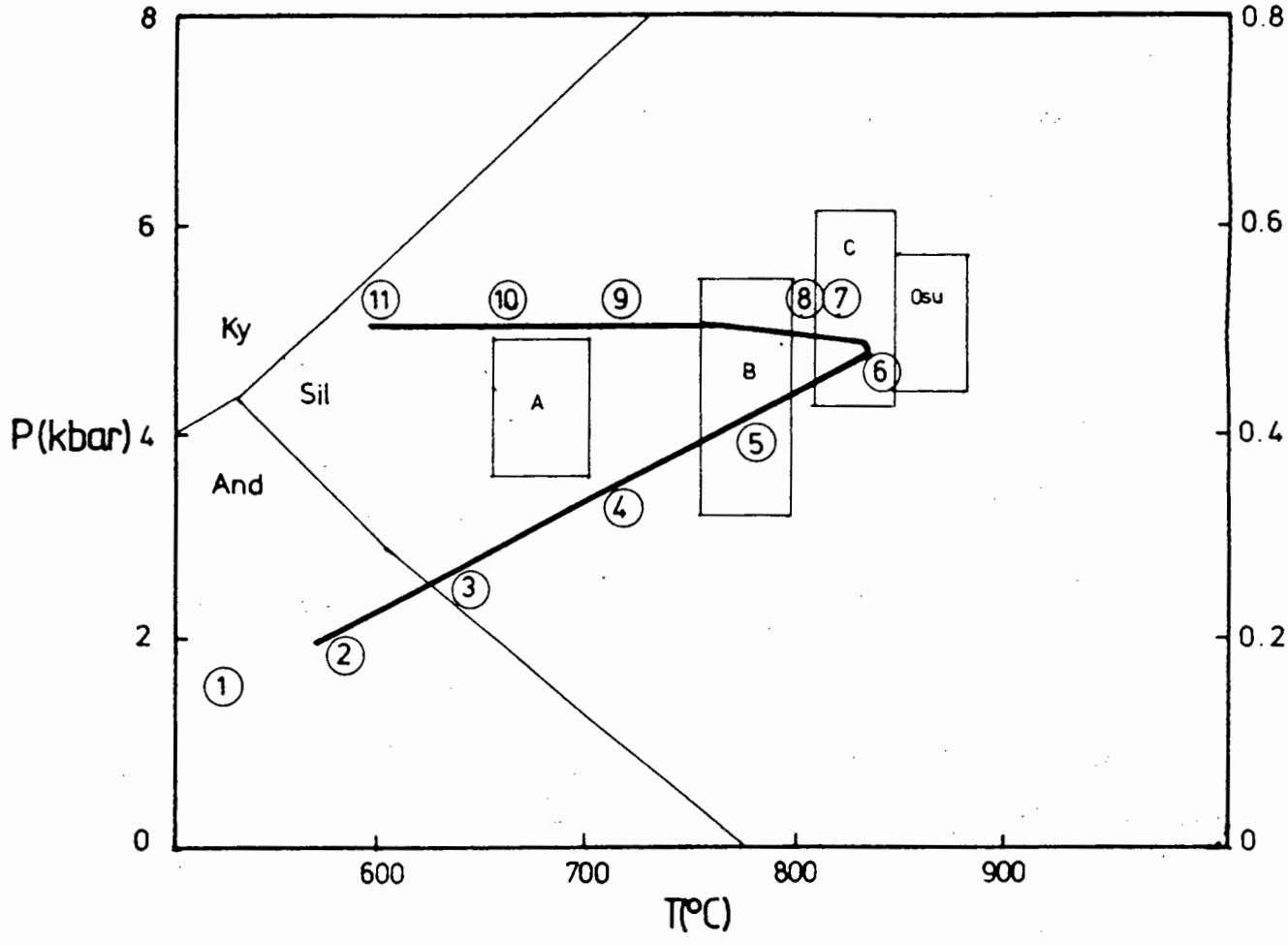

Fig. 6.1 A semi-quantitative P-T-time path for the granulites of the field area, adapted after Waters (1989). The numbers refer to events summarized in section 6.2. Thgeir order indicates the direction of the path The letters in the P-T boxes are the different metamorpohic facies of western Bushmanland (Fig. 1.2, from Waters, 1986).

4) The late stages of D2 deformation were accompanied by the intrusion of sills and dykes of crust-derived per- and metaluminous granite, which inherited a moderate biotite foliation on crystallization.

5) The advance of the granulite facies metamorphic isotherm, was marked by the dehydration of hydrous assemblages (including the formation pyroxene granulites), the onset of partial melting and the consequent buffering of $a(H_2O)$ to lower values. The earliest migmatites were formed in biotite-rich metapelitic and quartzofeldspathic gneisses and then in granitic bulk composition rocks. Dehydration melting also occurred in metabasic gneiss.

6) The granulite facies peak is characterised by the stability of the following mineral assemblages at $780 \pm 30^{o}C$, 5.0 ± 0.4 kbar and $a(H_2O)$ in the range 0.2 to 0.5:

a) Hc + Qtz (in metapelitic gneisses);

b) Spr + Crd + Phl $\pm$ Crn + Hc, and

c) Opx + Crd + Hc + Kfs $\pm$ Qtz (in magnesian gneisses);

d) Grt $\pm$ Crd + Kfs $\pm$ L (in aluminous quartzofeldspathic and metapelitic gneisses);

e) Opx + Kfs $\pm$ L (in biotite and granite gneisses);

f) Opx + Cpx + Pl $\pm$ L (in metabasic gneisses);

g) Grt + Opx + Qtz (in banded iron formation); and

h) Wol + Cal + Cpx + Pl + Grt (in calc-silcate gneiss).

The amount of partial melt present at the metamorphic peak was largely controlled by the amount of water available from dehydrating amphibolite facies assemblages, i.e. the amount of biotite and/or hornblende in the precursor rock types. Partial melting never exceeded 15-20% and some its products were emplaced as a variety of anatectic granite dykes and sills. These had largely crystallized before the onset of D3 deformation.

7) D3 deformation produced asymmetric, south-vergent overturned folds. These are characterized by the duplication and thickening of horizons in moderately north-dipping northern limbs, and the omission and attenuation of horizons in the steeply north- and south-dipping southern limbs of antiforms.

8) During isobaric metamorphic cooling, significant quantities of water were extracted with uncrystallized partial melt and were emplaced in the overturned, southern limbs of developing D3 folds at and above the present-day erosion level. This caused a marked depletion of H_2O and K_2O from granitic bulk compositions, as well as Na_2O from peraluminous bulk compositions.

9) Post-tectonic relaxation was accompanied by retrograde metamorphism along developing D4 pure and simple shear zones, located on the southern limbs of open D3 folds and along the synformal contact between biotite-orthopyroxene granite gneiss and quartzofeldspathic gneiss. Retrograde mineral assemblages include:

a) Bt $\pm$ Grt + Sil + Qtz (after Hc + Qtz $\pm$ Crd);

b) Crd (after Hc + Qtz); and

c) Bt ± Hbl + Qtz (after Opx ± Cpx + Pl ± L).

10) The crystallization of anatectic melts of all scales was accompanied by the partial rehydration of anhydrous, ferromagnesian phases (e.g. orthopyroxene, garnet) to form common, skeletal biotite-quartz intergrowths. Complete retrogression was retarded by: a) the armouring of anhydrous phases by other solid, incongruent melting reaction products (K-feldspar) and partially crystallized melt; and

b) the extraction of relatively low viscosity, H_2O-bearing melts from their sites of generation.

11) During the late stages of D3 deformation, shear zones developed on the steeply dipping southern limbs of asymmetric D3 folds, and at the contact between relatively homogeneous biotite-orthopyroxene granite gneiss and foliated quartzofeldspathic gneiss. Both pure and simple shearing, the latter involving small amounts of displacement, were responsible for the attenuation of horizons. Shear zones served as the loci for some anatectic melt emplacement and the partial retrogression of peak metamorphic assemblages.

12) Approximately N-S faults, involving rotational and vertical displacement, segmented the gneiss belt into juxtaposed fault blocks, commonly separated by narrow zones of cataclasite. Small bodies of microgranite were emplaced in the fault zones. Faulting

may have developed in response to Pan-African sinistral shearing approximately 100 km west of the field area.

6.3 Recommendations

A number of important recommendations for future work arise from recent studies in the western Bushmanland Subprovince, including this one.

1) Radiometric ages are extremely scarce for this part of the Namaqua Province. Since recent studies (inter alia Albat, 1984; Waters and Whales, 1984; Waters, 1986a, b, 1988, 1989; McStay, 1988, in prep.; this study) have added considerably to our knowledge of the field and petrographic relationships of metamorphic and granitic rocks in a number of supracrustal gneiss belts, this may now be adressed. It is necessary to constrain the relationship between D2 and D3 deformation, and the Namaqua metamorphic event by determining the ages of peak metamorphic assemblages and fabric-producing mineral growth events. In particular, Sm/Nd fractionation in garnets and U/Pb fractionation in zircons from leucosomes, granites and gneisses will provide valuable constraints on the P-T-t path proposed by Waters (1989). This work is imperative for further metamorphic studies to advance the understanding of the tectonothermal evolution of the Proterozoic Province.

2) Fluid inclusion and stable isotope studies (e.g. McStay, 1988) should be extended to localities containing rocks metamorphosed in the upper granulite facies. This will help constrain the composition of the metamorphic fluid at and after the peak of metamorphism. To this end, accurate volatile contents of cordierite, biotite and hornblende are also required. An oxygen isotope study of quartz-magnetite pairs in metamorphosed iron formations will provide an independent estimate of the conditions of the metamorphic peak.

3) A detailed understanding of the kinematic character of D4 (or late D3) shear zones is necessary to test the hypothesis that regional metamorphism during the Namaqua event occurred in a post-collisional, extensional tectonic regime (Ellis, 1987; Harley, 1989; Sandiford, 1989). In this regard, a N-S deep seismic profile from north of the Groothoek Thrust to south of Bitterfontein will provide evidence for the existence of a basaltic underplate and the persistence at depth of major, exposed structural features (thrusts and shear zones).

4) A careful correlation of the metasedimentary stratigraphies of the supracrustal gneiss and schist belts in the western Bushmanland will add to the understanding of the early Proterozoic depositories of these rocks. This is possible against the background of recent mapping (Whales, 1983; Albat, 1984; Baars, 1986; Moore, 1986, unpubl. data; Nowicki, 1986; McStay, in prep.; this study).

REFERENCES

This list of references cited in the aforegoing text and the appendices follows the format and abbreviations used in Contributions to Mineralogy and Petrology, Springer-Verlag, New York.

Abbot RN Jr., Clarke DB (1979)

Hypothetical liquidus relationships in the subsystem Al_2O_3-FeO-MgO projected from quartz, alkali feldspar and plagioclase for $a(H_2O) \leq 1$. Can. Miner. 17:549-560.

Abercrombie HJ, Skippen GB, Marshall DD (1987)

F-OH substitution in natural tremolite, talc and phlogopite. Contrib. Min. Petrol. 97:305-312.

Abrecht J, Hewitt DA (1988)

Experimental evidence on the substitution of Ti in biotite. Am. Miner. 73:1275-1284.

Albat H-M (1984)

The Proterozoic granulite facies terrane around Kliprand, Namaqualand Metamorphic Complex. Bull. Precambr. Res. Unit, Univ. Cape Town, 33, 386pp.

Andreoli MAG, Andersen NJB, Levin M, Niemand N (1987)

Geology of the Vaalputs radioactive waste disposal site in the Republic of South Africa: Explanatory notes for the geological map of the site on the scale 1:25 000. Atomic En. Corp. S.A. PER-151. 40pp.

Armstrong RA, Reid DL, Watkeys MK, Welke HJ, Lipson RD, Compston W (1988)

Zircon U-Pb ages from the Aggeneys area, central Bushmanland. Ext. Abs. 22nd Earth Sc. Congr. Geol. Soc. S.A. p.493-496. Univ. Natal Durban.

Ashworth JR, McLellan EL (1985)

Textures. In: Migmatites. p.180-203, Ashworth JR (ed.) Blackie, Glasgow.

Baars FJ (1986)

Granulite facies orthopyroxene production in a belt of supracrustal and orthogneisses SW of Platbakkies, Namaqualand Metamorphic Complex, South Africa. Unpubl. B.Sc.(Hons.) Proj., Univ. Cape Town, 49pp.

Baars FJ (1988)

Partial melting in granitic and supracrustal gneisses of the central Namaqualand Metamorphic Complex, South Africa. Abs. 7th Gondwana Symp., Sao Paulo, Brazil. p.122 (add.). Inst. Geosc., Univ. Sao Paulo.

Baker AJ, Droop GTR (1983)

Grampian metamorphic conditions deduced from mafic granulites and sillimanite-K-feldspar gneisses in the Dalradian of Glen Muick, Scotland. J. Geol. Soc. London. 140:489-497.

Bence AE, Albee AL (1968)

Empirical correction factors for the electron microanalysis of silicates and oxides. J. Geol. 76: 382-403.

Berg JH (1977)

Regional geobarometry in the contact aureoles of the anorthositic Nain Complex, Labrador. J. Petrol. 18:399-430.

Berman RG, Brown TH, Perkins EH (1987)

GEO-CALC: Software for calculation and display of PTX phase diagrams. Am. Miner. 72:861-862.

Best MG (1982)

Igneous and Metamorphic Petrology. Freeman, New York. 630pp.

Betton PJ (1984)

Nd and Sr isotopic evidence for the evolution of the Namaqualand mobile belt, southern Africa. Abs. Int. Conf. Mid-late Protero. Evol., p.1. Precambr. Res. Unit, Univ. Cape Town.

Bhattacharya A (1986)

Some geobarometers involving cordierite in the $FeO-Al_2O_3-SiO_2$ ($\pm H_2O$) system: refinements, thermodynamic calibration, applicability in granulite facies rocks. Contrib. Miner. Petrol. 94:387-394.

Bhattacharya A, Sen SK (1985)

Energetics of hydration of cordierite and water barometry in cordierite granulites. Contrib. Miner. Petrol. 89:370-378.

Blignaut HJ (1977)

Structural-metamorphic imprint on part of the Namaqua mobile belt in South West Africa. Bull. Pecambr. Res. Unit, Univ. Cape Town 23, 197pp.

Boettcher AL, Luth RW, White BS (1987)

Carbon in silicate liquids: the systems $NaAlSi_3O_8$-CO_2, $CaAl_2Si_2O_8$-CO_2, and $KAlSi_3O_8$-CO_2. Contrib. Min. Petrol. 97: 297-304.

Bohlen SR (1987)

Pressure-temperature-time paths and a tectonic model for the evolution of granulites. J. Geol. 95:617-632.

Bohlen SR, Essene EJ (1978)

Igneous pyroxenes from metamorphic anorthisite massifs. Contrib. Miner. Petrol. 65:153-169.

Bohlen SR, Essene EJ (1979)

A critical evaluation of two-pyroxene thermometry in Adirondack granulites. Lithos 12:335-345.

Bohlen SR, Lindsley DH (1987)

Thermometry and barometry of igneous and metamorphic rocks. Ann. Rev. Earth Planet. Sc. 15:397-420.

Bohlen SR, Boettcher AL, Wall VJ, Clemens D (1983a)

Stability of phlogopite-quartz and sanidine-quartz: a model for melting in the lower crust. Contrib. Min. Petrol. 83:270-277.

Bohlen SR, Wall VJ, Boettcher AL (1983b)

Geobarometry in granulites. In: Kinetics and Equilibrium in Mineral Reactions. Adv. Phys. Geochem. 3:141-171, SK Saxena (ed.) Springer-Verlag, New York.

Bohlen SR, Wall VJ, Boettcher AL (1983c)

Experimental investigations and geological applications of equilibria in the system $FeO-TiO_2-Al_2O_3-SiO_2-H_2O$. Am. Miner. 68:1049-1058.

Bohlen SR, Wall VJ, Boettcher AL (1983d)

Experimental investigation and application of garnet granulite equilibria. Contrib. Miner. Petrol. 83:52-61.

Bohlen SR, Dollase WA, Wall VJ (1986)

Calibration and applications of spinel equilibria in the system $FeO-Al_2O_3-SiO_2$. J. Petrol. 27:1143-1156.

Botha BJV (ed.) (1983)

Namaqualand Metamorphic Complex. Geol. Soc. S.A. Spec. Publ. 10. 198pp.

Brady JB (1988)

The role of volatiles in the thermal history of metamorphic terranes. J. Petrol. 29:1187-1213.

Brodie KH, Rutter EH (1985)

On the relationship between deformation and metamorphism, with special reference to the behaviour of basic rocks. In: Metamorphic Reactions: Kinetics, Textures and Deformation. Adv. Phys. Geochem. 4:138-179, Thompson AB and Rubie DC (eds.) Springer-Verlag, New York.

Brown GC, Fyfe WS (1970)

The production of granitic melts during ultrametamorphism. Contrib. Min. Petrol. 28:310-318.

Brown M, Earle MM (1983)

Cordierite-bearing schists and gneisses from Timor, eastern Indonesia: P-T conditions of metamorphism and tectonic implications. J. Met. Geol. 1:183-203

Carlson WD, Lindsley DH (1988)

Thermochemistry of pyroxenes on the join $Mg_2Si_2O_6$-$CaMgSi_2O_6$. Am. Miner. 73:242-252.

Chamberlain CP, England PC (1985)

The Acadian thermal history of the Merrimack synclinorium in New Hampshire. J. Geol. 93:593-602.

Chamberlain CP, Karabinos P (1987)

Influence of deformation on pressure-temperature paths of metamorphism. Geol. 15:42-44.

Cheeney RF (1981)

Statistical Methods in Geology. Allen and Unwin, London. 169pp.

Christophe-Michel-Levy M (1962)

Quelques remarques sur la saphirine. C.R. 86th Congr. Nat. Soc. Savantes Montpellier 1961, Sect. Sc. p.383-385.

Clemens JD, Vielzeuf D (1987)

Constraints on melting and magma production in the crust. Earth Planet. Sc. Lett. 86:287-306.

Clemens JD, Wall VJ (1981)

Origin and crystallization of some peraluminous (S-type) granitic magmas. Can. Miner. 19:111-131.

Clemens JD, Wall VJ (1988)

Controls on the mineralogy of S-type volcanic and plutonic rocks. Lithos 21:53-66.

Clifford TN, Gronow J, Rex DC, Burger AJ (1975)

Geochronological and petrogenetic studies of high-grade metamorphic rocks and intrusives in Namaqualand, South Africa. J. Petrol. 16:154-188.

Clifford TN, Stumpfl EF, Burger AJ, McCarthy TS, Rex DC (1981)

Mineral-chemical and isotopic studies of Namaqualand granulites, South Africa. Contrib. Min. Petrol. 77:225-250.

Danckworth PA, Newton RC (1978)

Experimental determination of the spinel peridotite to garnet peridotite reaction in the system $MgO-Al_2O_3-SiO_2$ in the range 900^{o}-$1100^{o}C$ and Al_2O_3 isopleths of enstatite in the spinel field. Contrib. Miner. Petrol. 66:189-201.

Davidson PM, Lindsley DH (1985)

Thermodynamic analysis of quadrilateral pyroxenes. Part II. Model calibration from experiments and applications to geothermometry. Contrib. Miner. Petrol. 91:390-404.

Deer WA, Howie RA, Zussman J (1968)

An Introduction to the Rock Forming Minerals. Longman, London. 528pp.

Deer WA, Howie RA, Zussman J (1978)

Rock-Forming Minerals. Vol. 2A: Single-Chain Silicates. 2nd edn. Longman, London. 668pp.

De Jager DH, Simpson W

Wollastonite near Garies, Namaqualand. Ann. Geol. Surv. S.Afr. 1:127-135.

De Waard D (1969)

The occurrence of charnockite in the Adirondacks: a note on the origin and definition of charnockite. Am. J. Sc. 267: 983-987.

De Waard D (1973)

Classification and nomenclature of felsic and mafic rocks of high-grade regional-metamorphic terrains. Neues Jb. Min. Monatsh. 9:381-392.

Dixon WJ, Massey FJ (1969)

Introduction to Statistical Analysis. McGraw-Hill-Kogakusha, Tokyo. 638pp.

Donath FA, Parker RB (1964)

Folds and folding. Geol. Soc. Am. Bull. 75:45-62.

Droop GTR (1987)

A general equation for estimating Fe^{3+} concentrations in ferromagnesian silicates and oxides from microprobe analyses. Min. Mag. 51:431-435.

Dymek RF (1983)

Titanium, aluminium and interlayer cation sustitutions in biotite from high-grade gneisses, West Greenland. Am. Miner. 68:880-899.

Edwards RL, Essene EJ (1981)

Zoning patterns and their effect on biotite-garnet K_D thermometry. Trans. Am. Geophys. Union 62:411

Ellis DJ (1980)

Osumilite-sapphirine-quartz granulites from Enderby Land, Antarctica: P-T conditions of metamorphism, implications for garnet-cordierite equilibria and the evolution of the deep crust. Contrib. Min. Petrol. 74:201-210.

Ellis DJ (1987)

Origin and evolution granulites in normal and thickened crusts. Geol. 15:167-170.

Ellis DJ, Sheraton JW, England RN, Dallwitz WB (1980)

Osumilite-sapphirine-quartz granulites from Enderby Land, Anatarctica - mineral assemblages and reactions. Contrib. Min. Petrol. 72:123-143.

Elphick SC, Ganguly J, Loomis TP (1985)

Experimental determination of cation diffusivities in aluminosilicate garnets. I. Experimental methods and interdiffusion data. Contrib. Miner. Petrol. 90:36-44.

England PC, Richardson SW (1977)

The influence of erosion upon the mineral facies of rocks from different metamorphic terrains. J. Geol. Soc. London 134:201-213.

England PC, Thompson AB (1984)

Pressure-temperature-time paths of regional metamorphism. I: Heat transfer during the evolution of regions of thickened crust. J. Petrol. 25:894-928.

Essene EJ (1982)

Geologic thermometry and barometry. Rev. Miner. 10:153-206.

Etheridge MA, Wall VJ, Vernon RH (1983)

The role of the fluid phase during regional metamorphism and deformation. J. Met. Geol. 1:205-226.

Eugster HP, Wones DR (1962)

Stability relations of ferrugenous biotite, annite. J. Petrol. 3:82-125.

Ferry JM (1986a)

Reaction progress: A monitor of fluid-rock interactions during metramorphic and hydrothermal events. In: Fluid-Rock Interactions During Metamorphism. p.60-88, Walther JV and Wood BJ (eds.) Springer-Verlag, New York.

Ferry JM (1986b)

Infiltration of aqueous fluid and high flui-rock ratios during greenschist facies metamorphism: A reply. J. Petrol. 27: 695-714.

Ferry JM, Spear FS (1978)

Experimental calibration of the partitioning of Fe and Mg between biotite and garnet. Contrib. Miner. Petrol. 66:113-117.

Fonarev VI, Konilov AN (1986)

Experimental study of Fe-Mg distribution between biotite and orthopyroxene at P = 490 MPa. Contrib. Miner. Petrol. 93: 227-235.

Frost BR, Chacko T (1989)

The granulite uncertainty principle: Limitations on thermobarometry in granulites. J. Geol. 97:435-450.

Frost BR, Frost CD (1982)

CO_2, melts and granulite metamorphism.

Nature 327:503-505.

Fuji T, Scarfe CM (1982)

Equilibrium experimnents on natural peridotites and basalt: a recalibration of the olivine-spinel geothermometer. EOS. 63:471.

Fuhrman ML, Lindsley DH (1986)

Ternary feldspar modelling and thermometry.

Am. Miner. 73:201-215.

Fyfe WS (1973)

The granulite facies, partial melting and the Archaean crust. Phil. Trans. Roy. Soc. London A273:457-462.

Ganguly J, Saxena SK (1984)

Mixing properties of alumino-silicate garnets: constraints from natural and experimental data and its applications to geothermobarometry. Am Miner. 61:88-97.

Ghent ED (1976)

Plagioclase-garnet-Al_2SiO_5-quartz: a potential geothermometer-geobarometer. Am. Miner. 61:710-714.

Ghent ED, Knitter CC, Raeside RP, Stout MZ (1982)

Geothermometry and geobarometry of pelitic rocks, upper kyanite and sillimanite zones, Mica Creek area, British Columbia. Can. Miner. 20:295-305.

Ghent ED, Robbins DB, Stout MZ (1979)

Geothermometry, geobarometry, and fluid composition of metamorphosed calc-silicates and pelites, Mica Creek, British Columbia. Am. Miner. 64:874-885.

Ghiorso MS (1984)

Activity/composition relations in the ternary feldspars. Contrib. Miner. Petrol. 87:282-296.

Goldman DS, Albee AL (1977)

Correlation of Mg/Fe partitioning between garnet and biotite with $^{18}O/^{16}O$ partitioning between quartz and magnetite. Am. J. Sc. 277:750-767.

Goldsmith JR, Newton RC (1977)

Scapolite-plagioclase stability relations at high pressure and temperatures in the system $NaAlSi_3O_8$-$CaAl_2Si_3O_8$-$CaCO_3$-$CaSO_4$. Am. Miner. 62:1063-1081.

Grant JA (1973)

Phase equilibria in high-grade metamorphism and partial melting of pelitic rocks. Am. J. Sc. 281:1127-1143.

Grant JA (1985a)

Phase equlibria in low-pressure partial melting of pelitic rocks. Am. J. Sc. 285:409-435

Grant JA (1985b)

Phase equilibria in partial melting of pelitic rocks. In: Migmatites. p.86-144, Ashworth JR (ed.). Blackie, Glasgow.

Grant JA (1986a)

The isochon diagram - A simple solution to Gresens' equation for metasomatic alteration. Econ. Geol. 81:1976-1982.

Grant JA (1986b)

Quartz-phlogopite-liquid equilibria and origins of charnockites. Am. Miner. 71:1071-1075.

Green NL, Usdansky SI (1986)

Ternary-feldspar mixing relations and thermobarometry. Am. Miner. 71:1100-1108.

Gresens RL (1967)

Composition-volume relationships of metasomatism. Chem. Geol. 2:47-55.

Grew ES (1980)

Sapphirine and quartz associations from Archean rocks in Enderby Land, Antarctica. Am. Miner. 65:821-836.

Grew ES (1981)

Granulite facies metamorphism at Molodezhnaya Station, East Antarctica. J. Petrol. 22:297-336.

Grew ES (1982)

Osumilite in sapphirine-quartz terrane of Enderby Land, Antarctica: implications for osumilite petrogenesis in the granulite facies. Am. Miner. 67:762-767.

Grutter HS (1986)

The petrography and petrology of polymetamorphic cordierite-quartz gneisses near Geselskapbank, northeast of Springbok. Unpubl. B.Sc.(Hons.) Proj., Univ. Cape Town, 62pp.

Guidotti CV (1984)

Micas in metamorphic rocks. In: Micas. Rev. Min. 13:438-448, Bailey SW (ed.) Min. Soc. Am.

Guilbert JM, Park CF Jr. (1986)

The Geology of Ore Deposits. Freeman, New York. 985pp.

Gupta LN, Johannes W

Petrogenesis of a stromatic migmatite (Nelaug, Southern Norway). J. Petrol. 23:548-567.

Harley SL (1984a)

An experimental study of the partitioning of Fe and Mg between garnet and orthopyroxene. Contrib. Miner. Petrol. 86:359-373.

Harley SL (1984b)

The solubility of alumina in orthopyroxene coexistng with garnet in $FeO-MgO-Al_2O_3-SiO_2$ and $CaO-FeO-MgO-Al_2O_3-SiO_2$. J. Petrol. 25:665-696.

Harley SL (1984c)

Comparison of the garnet-orthopyroxene geobarometer with recent experimental studies, and applications to natural assemblages. J. Petrol. 25:697-712.

Harley SL (1989)

The origins of granulites: a metamorphic perspective. Geol. Mag. 126:215-247.

Harley SL, Green DH (1982)

Garnet-orthopyroxene barometry for granulites and garnet peridotites. Nature 300:697-700.

Harris NBW (1989)

Carbon dioxide in the deep crust. Nature 340:347-348.

Harris NBW, Bickle MJ (1989)

Advective fluid transport during charnockite formation; an example from southern India. Earth Planet. Sc. Lett. 93:151-156.

Harris NBW, Hawkesworth CJ, Van Calsteren PCW, McDermott F (1987)

Evolution of continental crust in southern Africa. Earth Planet. Sc. Lett. 83:85-93.

Harris RW (1988)

Examination of dextral transpression as a model for the development of thrusts and late folds in eastern Namaqualand. S. Afr. J. Geol. 91:329-336.

Hartnady CJH, Joubert P, Stowe CW (1985)

Proterozoic crustal evolution in southwestern Africa. Episodes 8:236-244.

Haselton HT Jr., Hovis GL, Hemingway BS, Robie RA (1983)

Calorimetric investigation of the excess entropy of mixing in analbite-sanidine solid solutions: Lack of evidence for Na,K short-range order and implications for two-feldspar thermometry. Am. Miner. 68:398-413.

Hawkesworth CJ, Van Calsteren PWC, Menzies MA, Rogers NW (1984)

Evolution of the lithosphere beneath southern Africa: evidence from Nd-isotope studies. Abs. Int. Conf. Mid-late Protero. Evol. p.1-2. Precambr. Res. Unit, Univ. Cape Town.

Hensen BJ, Green DH (1973)

Experimental study of the stability of cordierite and garnet in pelitic compositions. III. Synthesis of experimental data and geological applications. Contrib. Min. Petrol. 38:151-166.

Hewitt DA, Wones DR (1984)

Experimental phase relationships of the micas. In: Micas. Rev. Min. 13:201-256, Bailey SW (ed.) Min. Soc. Am.

Hibbard MJ (1987)

Deformation of incompletely crystallised magma systems: granitic gneisses and their tectonic implications. J. Geol. 95:543-561.

Hobbs BE, Means WD, Williams PF (1976)

An Outline of Structural Geology. Wiley, Toronto. 571pp.

Hodges HV, Spear FS (1982)

Geothermometry, geobarometry and the Al_2SiO_5 triple point at Mt. Moosilauke, New Hampshire. Am Miner. 67:1118-1134.

Hoffer E (1976)

The reaction sillimanite + biotite + quartz = cordierite + K-feldspar + H_2O and partial melting in the system K_2O-FeO-MgO-Al_2O_3-SiO_2-H_2O. Contrib. Min. Petrol. 55:127-130.

Hoffer E, Grant JA (1980)

Experimental investigation of the formation of cordierite-orthopyroxene parageneses in pelitic rocks. Contrib. Min. Petrol. 73:15-22.

Holdaway MJ, Lee SM (1977)

Fe-Mg cordierite stability in high-grade pelitic rocks based on experimental, theoretical and natural observations. Contrib. Miner. Petrol. 63:175-198.

Holland TJB, Powell R (1985)

An internally consistent thermodynamic dataset with uncertainties and correlations: 2. Data and results. J. Met. Geol. 3:343-370.

Hoschek G (1976)

Melting relations of biotite + plagioclase + quartz. Neues Jarb. Min. Monatsh. 1976:79-83.

Indares A, Martignole J (1985)

Biotite-garnet geothermometry in the granulite facies: the influence of Ti and Al in biotite. Am. Miner. 70:272-278.

Jack AM (1980)

The geology of western Namaqualand. Bull. Pecambr. Res. Unit, Univ. Cape Town, 173pp.

Janardhan AS, Newton RC, Smith JV (1979)

Ancient crustal metamorphism at low $P(H_2O)$: Charnockite formation at Kabbaldurga, south India. Nature 278:511-514.

Janardhan AS, Newton RC, Hansen EC (1982)

The transformation of amphibolite facies gneiss to charnockite in southern Kanartaka and northern Tamil Nadu, India: Contrib. Min. Petrol. 79:130-149.

Johannes W (1978)

Melting of plagioclase in the systems Ab-An-H_2O and Qz-Ab-An-H_2O at P(H_2O) = 5 kbar, an equilibrium problem. Contrib. Miner. Petrol. 66:295-303.

Johannes W (1979)

Ternary feldspars: Kinetics and possible equilibria at 800°C. Contrib. Miner. Petrol. 68:221-230.

Johannes W (1980)

Metastable melting in the granite system Qz-Or-Ab-An-H_2O. Contrib. Min. Petrol. 72:73-80.

Johannes W (1983)

On the origin of layered migmatites. In: Migmatites, Melting and Metamorphism. p.234-249, Atherton MP and Gribble CD (eds.) Shiva, Nantwich.

Johannes W (1985)

The significance of experimental studies for the formation of migmatites. In: Migmatites. p.36-85, Ashworth JR (ed.) Blackie, Glasgow.

Johannes W (1988)

What controls partial melting in migmatites? J. Met. Geol. 6:451-465.

Johannes W, Gupta LN (1982)

Origin and evolution of a migmatite. Contrib. Min. Petrol. 79:114-123.

Johannes W, Schreyer W (1981)

Experimental introduction of H_2O and CO_2 into Mg-cordierite. Am. J. Sc. 281:299-317.

Joubert P (1971)

The regional tectonism of part of Namqualand. Bull. Precambr. Res. Unit, Univ. Cape Town 10, 220pp.

Joubert P (1974a)

Geological survey of Namaqualand and Bushmanland. Ann. Rep. Precambr. Res. Unit, Univ. Cape Town 10-11:24-30.

Joubert P (1974b)

The gneisses of Namaqualand and their deformation. Trans. Geol. Soc. S. Afr. 77:339-345.

Joubert P (1974c)

Wrench-fault tectonics in the Namaqualand Metamorphic Complex. Bull. Precambr. Res. Unit, Univ. Cape Town 15:17-23.

Joubert P (1986)

Namaqualand - a model of Proterozoic accretion? Trans. Geol. Soc. S. Afr. 89:79-96.

Kars H, Jansen JBH, Tobi AC, Poorter RPE (1980)

The metapelitic rocks of the polymetamorphic precambrian of Rogaland, SW Norway. Part II: Mineral relations between cordierite hercynite and magnetite within the osumilite-in isograd. Contrib. Miner. Petrol. 74:235-244.

Keppler H (1989)

The influence of the fluid phase composition on the solidus temperatures in the haplogranite system $NaAlSi_3O_8$-$KAlSi_3O_8$-SiO_2-H_2O-CO_2. Contrib. Min. Petrol. 102:321-327.

Kimberley MM (1978)

Paleoenvironmental classification of iron formations. Econ. Geol. 73:215-229.

Koziol AM, Newton RC (1988)

Redetermination of the anorthite breakdown reaction and improvement of the plagioclase-Al_2SiO_5-quartz geobarometer. Am. Miner. 73:216-223.

Kretz R (1983)

Symbols for rock-forming minerals. Am. Miner. 68:277-279.

Lal RK, Ackermand D, Seifert F, Haldar SK (1978)

Chemographic relationships in sapphirine-bearing rocks from Sonaphar, Assam, India. Contrib. Min. Petrol. 67:196-187.

Lamb WM, Valley JW (1984)

Metamorphism of reduced granulites in low-CO_2 vapour-free environments. Nature 312:56-58.

Lamb WM, Valley JW (1985)

C-O-H fluid calculations and granulite genesis. In: The Deep Proterozoic Crust of the North Atlantic Provinces. p.119-131, Tobi AC, Touret JLR (eds.) Reidel, Dordrecht.

Lamb WM, Valley JW, Brown PE (1987)

Post-metamorphic CO_2-rich fluid inclusions in granulites. Contrib. Min. Petrol. 96:485-495.

Lasaga AC (1983)

Geospeedometry: An extension of geothermometry. In Kinetics and Equilibrium in Mineral Reactions. Adv. Phys. Geochem. 3: 81-114, Saxena SK (ed.). Springer-Verlag, New York.

Lee SM, Holdaway MJ (1978)

Significance of Fe-Mg cordierite stability relations on temperature, pressure, and water pressure in cordierite granulites. In: The Earth's Crust: Its Nature and Physical Properties. p.79-94, Heacock JG (ed.) Am. Geophys. Union Monthly.

Le Roex AP, Reid DL (1978)

Geochemistry of Karoo dolerite sills in the Calvinia District, Western Cape Province, South Africa. Contrib. Min. Petrol. 66:351-360.

Lindh A, Wahlgren C-H (1985)

Migmatite formation at subsolidus conditions - an alternative to anatexis. J. Met. Geol. 3:1-12.

Lindsley DH (1983)

Pyroxene thermometry. Am. Miner. 68:477-493.

Lofgren GE, Gooley R (1977)

Simultaneous crystallization of feldspar intergrowths from the melt. Am. Miner. 62:217-228.

Long PE, Luth WC (1986)

Origin of K-feldspar megacrysts in granitic rocks: Implications of a partitioning model for barium. Am. Miner. 71:367-375.

Luth WC (1967)

Studies in the system $KAlSiO_4$-Mg_2SiO_4-SiO_2-H_2O: I. Inferred phase relations and petrologic applications. J. Petrol. 8:372-416.

Martignole J, Sisi J-C (1981)

Cordierite-garnet-H_2O equilibrium: a geological thermometer, barometer and water fugacity indicator.

Contrib. Min. Petrol. 77:38-46.

McLellan EL (1983)

Contrasting textures in metamorphic and anatectic migmatites: an example from the Scottish Caledonides. J. Met. Geol. 1:241-262.

McLellan EL (1989)

Sequential formation of subsolidus and anatectic migmatites in response to thermal evolution, Eastern Scotland. J. Geol. 97:165-182.

McStay JH (1988)

Fluid evolution and uplift path of Namaqualand granulites - evidence from fluid inclusions. Extd. Abs., Geocongr. 88, Geol. Soc. of SA, Durban, 411-414.

Mehnert KR (1968)

Migmatites and the Origin of Granitic Rocks. Elsevier, Amsterdam. 405pp.

Miyashiro A (1973)

Metamorphism and Metamorphic Belts. Wiley, New York. 479pp.

Modreski PJ, Boettcher AL (1972)

The stability of phlogopite + enstatite at high pressures: A model for micas in the interior of the Earth. Am. J. Sc. 272:852-869.

Montana A, Brearly M (1989)

An appraisal of the stability of phlogopite in the crust and the mantle. Am. Miner. 74:1-4.

Moore JM (1977)

The geology of Namiesberg, northern Cape. Precambr. Res. Unit, Univ. Cape Town Bull. 20. 69pp.

Moore JM (1986)

A comparitive study of supracrustal rocks from the western Namaqualand Metamorphic Complex. Unpubl. Ph.D. thesis, Univ. Cape Town, 346pp.

Morimoto N (1989)

Nomenclature of pyroxenes. Can. Miner. 27:143-156.

Morse SA, Lofgren GE (1978)

Simultaneous crystallization of feldspar intergrowths from the melt: A discussion. Am. Miner. 63:419-421.

Munoz JL, Ludington S (1974)

Fluoride-hydroxyl exchange in biotite. Am. J. Sc. 274:396-413.

Munoz JL, Ludington S (1977)

Fluorine-hydroxyl exchange in synthetic muscovite and its application to muscovite-biotite assemblages. Am. Miner. 62: 304-308.

Murrel SAF, Ismail IAH (1976)

The effect of decomposition of hydrous minerals on the mechanical properties of rocks. Tectonophys. 31:207-258.

Naney MT (1983)

Phase equilibria of rock-forming ferromagnesian silicates in granitic systems. Am. J. Sc. 283:993-1033.

Newton RC (1972)

An experimental determination of high pressure stability limits of magnesian cordierite under wet and dry conditions. J. Geol. 80:398-420.

Newton RC, Haselton HT (1981)

Thermodynamics of the garnet-plagioclase-Al_2SiO_5-quartz geobarometer. In: Thermodynamics of Minerals and Melts. Adv. Phys. Geochem. 1:129-145, RC Newton, A Navrotsky, BJ Wood (eds.) Springer-Verlag, New York.

Newton RC, Perkins D III (1982)

Thermodynamic calibration of geobarometers for charnockites and basic granulites based on the assemblages garnet-plagioclase-orthopyroxene (clinopyroxene)-quartz with applications to high grade metamorphism. Am. Miner. 67:203-222.

Newton RC, Smith JV, Windley BF (1980)

Carbonic metamorphism, granulites and crustal growth. Nature 288:45-50.

Nickel KG, Brey G (1984)

Subsolidus orthopyroxene-clinopyroxene systematics in the system CaO-MgO-SiO_2 to 60 kb: a re-evaluation of the regular solution model. Contrib. Miner. Petrol. 87:35-42.

Nowicki TE (1986)

The petrology of osumilite-bearing and related metapelitic gneisses from the Bitterfontein area, Namaqualand. Unpubl. B.Sc. (Hons.) Proj., Univ. Capa Town, 90pp.

O'Hara MJ, Howells S (1978)

The enstatite-pyrope geobarometer. In: Progress in Experimental Petrology D-4:175-179, WS MacKenzie (ed.), Nat. Env. Res. Counc. Publ.

O'Neil HSC, Navrotsky A (1984)

Cation distributions and thermodynamic properties of binary spinel solid solutions. Am. Miner. 69:733-753.

Olsen SN (1987)

The composition and role of the fluid in migmatites: a fluid inclusion study of the Front Range rocks. Contrib. Min. Petrol. 96:104-120.

Paterson SR, Tobisch OT, Vernon RH (1989a)

Criteria for establishing the relative timing of pluton emplacement and regional deformation. Geology 17:475-476.

Paterson SR, Vernon RH, Tobisch OT (1989b)

A review of criteria for the identification of magmatic and tectonic foliations in granitoids. J. Struct. Geol. 11:349-363.

Pattison DRM, Harte B (1988)

Evolution of structurally contrasting anatectic migmatites in the 3-kbar Ballachulish aureole, Scotland. J. Met. Geol. 6:475-494.

Peacock SM (1989)

Numerical constraints on the rate of metamorphism, fluid production, and fluid flux during regional metamorphism. Geol. Soc. Am. Bull. 101:476-485.

Perchuk LL, Lavrent'eva IV (1983)

Experimental investigation of exchange equilibria in the system cordierite-garnet-biotite. In: Kinetics and Equilibrium in Mineral Reactions. Adv. Phys. Geochem. 3:199-239, SK Saxena (ed.) Springer-Verlag, New York.

Percival JA (1983)

High-grade metamorphism in the Chapleau-Foleyet Area, Ontario. Am. Miner. 68:667-686.

Perkins D, Chipera SJ (1985)

Garnet-orthopyroxene-plagioclase-quartz barometry: refinement and application to the English River subprovince and the Minnesota River Valley. Contrib. Miner. Petrol. 89:69-80.

Perkins D, Newton RC (1980)

The compositions of coexisting pyroxenes and garnet in the system $CaO-MgO-Al_2O_3-SiO_2$ at 900^{o}-$1100^{o}C$ and high pressures. Contrib. Miner. Petrol.75:291-300.

Perkins D, Essene EJ, Wall VJ

THERMO: a computer program for calculation of mixed volatile equilibria. Am. Miner. 72:446-447.

Petersen JS, Lofgren GE (1986)

Lamellar and patchy intergrowths in feldspars: Experimental crystallization of eutectic silicates. Am. Miner. 71:343-355.

Peterson JW, Newton RC (1989a)

CO_2-enhanced melting of biotite-bearing rocks at deep-crustal pressure-temperature conditions. Nature 340:378-380.

Peterson JW, Newton RC (1989b)

Reversed experiments on biotite-quartz-feldspar melting in the system KMASH: implications for crustal anatexis. J. Geol. 97:465-485.

Pitcher WS (1983)

Granite: Typology, geological environment and melting relationships. In: Migmatites, Melting and Metamorphism. p.277-285, Atherton MP, Gribble CD (eds.) Shiva, Nantwich.

Powell R (1983)

Processes in granulite-facies metamorphism. In: Migmatites, Melting and Metamorphism. p.127-139, Atherton MP, Gribble CD (eds.) Shiva, Nantwich.

Powell R, Holland TJB (1985)

An internally consistent thermodynamic dataset with uncertainties and correlations: 1. Methods and a worked example. J. Met. Geol. 3:327-342.

Powell R, Holland TJB (1988)

An internally consistent dataset with uncertainties and correlations: 3. Applications to geobarometry, worked examples and a computer program. J. Met. Geol. 6:173-204.

Praekelt HE, Colliston WP (1988)

The flaw in the floor rocks of Bushmanland. Ext. Abs. 22nd Earth Sc. Congr. Geol. Soc. S.A. p.469-472. Univ. Natal Durban.

Ramsay JG (1967)

Folding and Fracturing of Rocks. McGraw-Hill, New York. 568pp.

Reid DL (1979a)

Age relationships within the Mid-Proterozoic Vioolsdrif batholith, lower Orange River region. Trans. Geol. Soc. S.Afr. 82:305-311.

Reid DL (1979b)

Total rock Rb-Sr and U-Th-Pb isotopic study of Precambrian metavolcanic rocks in the lower Orange River region, southern Africa.

Reid DL (1982)

Age relationships within the Vioolsdrif batholith, lower Orange River region. II: A two stage emplacement history and the extent of Kibaran overprinting. Trans. Geol. Soc. S.A. 85: 105-110.

Reid DL, Barton ES (1983)

Geochemical Characterization of granitoids in the Namaqualand geotraverse. In: Namaqualand Metamorphic Complex. Botha BJV (ed.) Geol. Soc. S.A. Spec. Publ. 10:67-82

Reid DL, Welke HJ, Erlank AJ, Betton PJ (1987a)

Composition, age and tectonic setting of amphibolites in the central Bushmanland Group, western Namaqua Province, southern Africa. Precambr. Res. 36:99-126.

Reid DL, Welke HJ, Erlank AJ, Moyes A (1987b)

The Orange River Group: a major Proterozoic calcalakaline volcanic belt in the western Namaqua Province, southern Africa. In: Geochemistry and Mineralization of Proterozoic Volcanic Suites. Pharaoh TC, Beckinsdale RD and Rickard D (eds.) Geol. Soc. Spec. Publ. 33:327-346.

Reston TJ (1988)

Evidence for shear zones in the lower crust offshore Britain. Tectonics 7:929-945.

Richardson SW (1968)

Staurolite stability in a part of the system Fe-Al-Si-O-H. J. Petrol. 9:467-488.

Robie RA, Hemingway BS, Fisher JR (1978)

Thermodynamic Properties of Minerals and Related Substances at 298.15K and 1 Bar (10^5 Pascals) Pressure and at Higher Temperatures. US Geol. Surv. Bull. 1452, Wasington. 456pp.

Robin P-YF (1979)

Theory of metamorphic segregation and related processes. Geochim. Cosmochim. 43:1587-1600.

Robinson D (1987)

Transition from diagenesis to metamorphism in extensional and collisional settings. Geol. 15:866-869.

Robinson D, Bevins RE (1989)

Diastathermal (extensional) metamorphism at very low grades and possible high grade analogues. Earth Planet. Sc. Lett. 92:81-88.

Ruppel C, Royden L, Hodges KV (1988)

Thermal modelling of extensional tectonics: application to pressure-temperature-time histories of metamorphic rocks. Tectonics 7:945-957.

Rutherford MJ (1969)

An experimental determinations of iron biotite-alkali feldspar equilibria. J. Petrol. 10:381-408.

Rutter EH, Brodie KH (1988)

Experimental approaches to the study of deformation/metamorphism relationships. Min. Mag. 52:35-42.

Sandiford MA (1985a)

The metamorphic evolution of granulites at Fyfe Hills: implications for Archaean crustal thickness in Enderby Land, Antarctica. J. Met. Geol. 3:155-178.

Sandiford MA (1985b)

The origin of retrograde shear zones in the Napier Complex: implications for the tectonic evolution of Enderby Land, Antarctica. J. Struct. Geol. 7:477-488.

Sandiford MA (1989)

Horizontal structures in granulite terrains: A record of mountain building or mountain collapse? Geol. 17:449-452.

Sandiford MA, Powell R (1986)

Deep crustal metamorphism during continental extension: Modern and ancient examples. Earth Planet. Sc. Lett. 79:151-158.

Sawyer EW (1987)

The role of partial melting and fractional crystallization in determining discordant migmatite leucosome compositions. J. Petrol. 28:443-473.

Sawyer EW, Barnes S-J (1988)

Temporal and compositional differences between subsolidus and anatectic migmatite leucosomes from the Quetico metasedimentary belt, Canada. J. Met. Geol. 6:437-450.

Schreurs J, Westra L (1986)

The thermotectonic evolution of a Proterozoic, low pressure, granulite dome, West Uusimaa, SW Finland. Contrib. Miner. Petrol. 93:235-250.

Seck HA (1971)

Koexistierende Alkalifeldspate un Plagioklase im System $NaAlSi_3O_8$-$KAlSi_3O_8$-$CaAl_2Si_2O_8$-H_2O bei Temperaturen von 650°C bis 900°C. Neues Jahrb. Miner. Abh. 115:315-345.

Sen SK, Bhattacharya A (1984)

An orthopyroxene-garnet thermometer and its application to the Madras charnockites. Contrib. Miner. Petrol. 88:64-71.

Simpson C, Schmid SM (1983)

An evaluation of the criteria to deduce the sense of movement in sheared rocks. Geol. Soc. Am. Bull. 94:1281-1288.

Simpson C (1985)

Deformation of granitic rocks across the brottle-ductile transition. J. Struct. Geol. 7:503-511.

South African Committee for Stratigraphy (SACS) (1980)

Stratigraphy of South Africa, Part 1. Handb. 8 Geol. Surv. S. Afr., Pretoria. 690pp.

Spear FS (1988)

Thermodynamic projection and extrapolation of high-variance mineral assemblages. Contrib. Min. Petrol. 98:346-351.

Spear FS, Cheney JT (1989)

A petrogenetic grid for pelitic schists in the system SiO_2-Al_2O_3-FeO-MgO-K_2O-H_2O. Contrib. Miner. Petrol. 101:149-164.

Stowe CW (1983)

The Upington Geotraverse and its implications for craton margin tectonics. Spec. Publ. Geol. Soc. S.A. 10:147-171.

Stowe CW (1984)

The Lower-Middle Proterozoic tectonic framework of Southern Africa. Abs. Int. Conf. Mid-Late Protero. Evol. p.30-32, Precambr. Res. Unit, Univ. Cape Town.

Stowe CW (1986)

Synthesis and interpretation of structures along the north-eastern boundary of the Namaqua Tectonic Province, South Africa. Trans. Geol. Soc. S.A. 89:185-198.

Stowe CW, Hartnady CJH, Joubert P (1984)

Proterozoic tectonic terranes of Southern Africa. Precambr. Res. 25:229-231.

Strauss CA (1941)

The geology, copper-ore deposits and groundwater hydrology of the area around Springbok and O'okiep, Namaqualand. Unpubl. D.Sc. thesis, Univ. Stellenbosch.

Streckeisen A (1967)

Classification and nomenclature of igneous rocks. Neues Jb. Min. Abh. 107:144-240.

Streckeisen A (for IUGS) (1973)

Classification and nomenclature of plutonic rocks: Recommendations. Neues Jb. Min. Monatsh. 4:149-164.

Strydom D (1985)

'n Struktureel-stratigrafiese studie van die metasedimente van noordwesterlike Boesmanland. Unpubl. Ph.D. Thesis, Univ. Orange Free State, Bloemfontein. 172pp.

Strydom D, Visser JNJ (1986)

Nappe structures in the highly deformed Proterozoic sedimentary Aggeneys-type sequence of western Bushmanland, South Africa. Precambr. Res. 33:171-187.

Tankard AJ, Jackson MPA, Eriksson KA, Hobday DK, Hunter DR, Minter WEL (1982)

Crustal Evolution of Southern Africa. 3.8 Billion Years of History. Springer-Verlag, New York. 523 pp.

Thompson AB (1976)

Mineral reactions in pelitic rocks. II. Calculation of some P-T-X(Fe-Mg) phase relations. Am. J. Sc. 276:425-454.

Thompson AB (1982)

Dehydration melting of pelitic rocks and the generation of H_2O-undersaturated granitic liquids. Am. J. Sc. 282:1567-1595.

Thompson AB (1988)

Dehydration melting of crustal rocks. Rendi. Soc. Ital. Min. Petrol. 43:41-60.

Tobi AC (1971)

The nomenclature of the charnockitic rock suite. Neues Jb. Min. Monatsh. 7:193-206.

Turner FJ (1981)

Metamorphic Petrology: Mineralogical, Field and Tectonic Aspects. 2nd edn. McGraw-Hill, Washington. 524pp.

Tuttle OF, Bowen NL (1958)

Origin of granite in the light of experimental studies in the system $NaAlSi_3O_8$-$KAlSi_3O_8$-H_2O. Geol. Soc. Am. Mem. 74.

Van Aswegen G (1988)

The evolution of the Proterozoic gneisses and other metamorphites between Springbok and Vioolsdrif, South Africa. Unpubl. Ph.D. Thesis, Univ. Orange Free State.

Van Der Merwe SW, Botha BJV (1989)

The Groothoek Thrust Belt in western Namaqualand; an example of a mid-crustal structure. S. Afr. J. Geol. 92:155-166.

Vernon RH (1978)

Porphyroblast-matrix microstructural relationships in deformed metamorphic rocks. Geol. Rundschau 67:288-305.

Vernon RH, Collins WJ (1988)

Igneous microstructures in migmatites. Geology 16:1126-1129.

Vernon RH, Williams VA, D'Arcy WF (1983)

Grainsize reduction and foliation development in a deformed granitoid batholith. Tectonophys. 92:123-145.

Vielzeuf D (1980)

Petrologie des ecailles granulitiques de la region de Lherz (Ariege-Zone Nord Pyreneennee). Introduction a l'etude experimentale de l'association grenat (Alm-Pyr)-feldspath potassique. These 3eme cycle, Clermont-Ferrand, 219pp. (In: Vielzeuf and Holloway (1988)).

Vielzeuf D (1983)

The spinel and quartz associations in high grade xenoliths from Tallante (S.E. Spain) and their potential use in geothermometry and barometry. Contrib. Miner. Petrol. 82:301-311.

Vielzeuf D, Boivin P (1984)

An algorithm for the construction of petrogenetic grids: application to some equilibria in granulitic paragneisses. Am. J. Sc. 284:760-791

Vielzeuf D, Holloway (1988)

Experimental determination of the fluid-absent melting relations in the pelitic system. Consequences for crustal differentiation. Contrib. Min. Petrol. 98:257-276.

Walther JV, Orville PM (1982)

Volatile production and transport in regional metamorphism. Contrib. Min. Petrol. 79:252-257.

Warren RG, Stewart AJ (1988)

Isobaric cooling of Proterozoic high-temparature metamorphites in the Northern Arunta Block, central Australia: implications for tectonic evolution. Precambr. Res. 40-41: 175-198.

Waters DJ (1986a)

Metamorphic history of sapphirine-bearing and related magnesian gneisses from Namaqualand, South Africa. J. Petrol. 27:541-565.

Waters DJ (1986b)

Metamorphic zonation and thermal history of pelitic gneisses from western Namaqualand, South Africa. Trans. Geol. Soc. S.A. 89:97-102.

Waters DJ (1988)

Partial melting and the formation of granulite facies assemblages in Namaqualand, South Africa. J. Met. Geol. 6:387-404.

Waters DJ (1989)

Metamorphic evidence for the heating and cooling path of Namaqualand granulites. In: Evolution of Metamorphic Belts. Geol. Soc. London Sp. Publ. 42:357-363. Daly JS, Cliff RA, Yardley BWD (eds.).

Waters DJ, Baars FJ (1989)

Melt extraction from granulite migmatites. Abs. 28th Int. Geol. Congr. Geol. Soc. Am. 3:335. Washington D.C.

Waters DJ, Whales CJ (1984)

Dehydration melting and the granulite transition in metapelites from southern Namaqualand, S. Africa. Contrib. Min. Petrol. 88:269-275.

Waters DJ, Joubert P, Moore JM (1983)

A suggested re-interpretation of Namaqua basement and cover rocks south and west of Bitterfontein. Trans. Geol. Soc. S.A. 86:293-299.

Watkeys MK (1986)

The Achab Gneiss: a "floor" in Bushmanland or a flaw in Namaqualand? Trans. Geol. Soc S.A. 89:103-116.

Watkeys MK (1988)

A spectrum of thrust related structures in Bushmanland. Ext. Abs. 22nd Earth Sc. Congr. Geol. Soc. S.A. p.729-732. Univ. Natal Durban.

Watkeys MK, Moore JM, Duncan AR (1988)

The pink gneiss of Bushmanland: Mid-Proterozoic felsic pyroclastics. Ext. Abs. 22nd Earth Sc. Congr. Geol. Soc. S.A. p.717-720. Univ. Natal Durban.

Weisbrod A (1973)

Refinements of the equilibrium conditions of the reaction Fe-cordierite = almandine + quartz + sillimanite (+ H_2O). Carnegie Inst. Wash. Yb. 72:518-521.

Welke HJ, Smith CB (1984)

Lead isotope characterization of the Aggeneys-Gamsberg ore bodies in relation to possible source rocks, with implications for Bushmanland metallogenesis. Int. Conf. Mid-late Protero. Evol. p.8-9. Pecambr. Res. Unit, Univ. Cape Town.

Wendlandt RF (1981)

Influence of CO_2 on melting of model granulite facies assemblages: a model for the genesis of charnockites. Am. Miner. 66:1164-1174.

Whales CJ (1983)

The amphibolite/granulite facies transition in the metapelitic rocks of the Zout River paragneiss belt near Bitterfontein. Unpubl. B.Sc.(Hons.) Proj., Univ. Cape Town, 113pp.

White AJR, Chappell BW (1977)

Ultrametamorphism and granitoid genesis. Tectonophys. 43:7-22.

Whitney JA (1988)

The origin of granite: The role and source of water in the evolution of granitic magmas. Geol. Soc. Am. Bull. 100:1886-1897.

Wickham SM (1987)

The segregation and emplacement of granitic magmas. J. Geol. Soc. London 144:281-297.

Wickham SM, Oxburgh ER (1985)

Continental rifts as a setting for regional metamorphism. Nature 318:330-333.

Wickham SM, Taylor HP Jr. (1985)

Stable isotopic evidence for large-scale seawater infiltration in aregional metamorphic terrane: The Trois Seigneurs Massif, Pyrenees, France. Contrib. Min. Petrol. 91: 122-137.

Winkler HGF (1976)

Petrogenesis of Metamorphic Rocks. 4th edn. Springer-Verlag, Berlin, 334pp.

Winkler HGF, Sen SK (1973)

Nomenclature of granulites and other high grade metamorphic rocks. Neues Jb. Min. Monatsh. 9:393-402.

Wones DR, Dodge FCW (1976)

The stability of phlogopite in the presence of quartz and diopside. In: Thermodynamics in Geology. p.229-248, Fraser DG (ed.) Reidel, Dordrecht.

Wones DR, Eugster HP (1965)

Stability of biotite: experiment, theory and application. Am. Miner. 50:1228-1272.

Wood BJ (1974)

The solubility of alumina in orthopyroxene coexisting with garnet. Contrib. Miner. Petrol. 46:1-15.

Wood BJ, Banno S (1973)

Garnet-orthopyroxene and orthopyroxene-clinopyroxene relationships in simple and complex systems. Contrib. Miner. Petrol. 42:109-124.

Wood BJ, Fraser DG (1976)

Elementary Thermodynamics for Geologists. Oxford Univ. Press, Oxford. 303pp.

Wyllie PJ (1977a)

Crustal anatexis: An experimental review. Tectonophys. 43: 41-71.

Wyllie PJ (1977b)

Effects of H_2O and CO_2 on magma generation in the crust and mantle. J. Geol. Soc. London 134:215-234.

Zelt GAD (1978)

Mafic populations and high-grade metamorphic zoning in western Namaqualand. Ann. Rep. Precambr. Res. Unit, Univ. Cape Town 14-15:103-113.

Zelt GAD (1980)

Granulite-facies metamorphism in Namaqualand, South Africa. Precambr. Res. 13: 253-274.

Zen E-an (1966)

Construction of pressure-temperature diagrams for multicomponent systems after the method of Schreinemakers. U.S. Geol. Surv. Bull. 1225.

Zen E-an (1988)

Phase relations of peraluminous granitic rocks and their petrogenetic implications. Ann. Rev. Earth Planet. Sc. 16: 21-51.

Zhai M-G, Windley BF (1989)

Banded iron formation in high-grade gneisses in northern China and implications for early crustal growth. Trans. Inst. Mining Metall. (Sect. B: Appl. Earth Sc.) 98:32-34.

APPENDIX OF TABLES

Rock Type	Sample	Qtz	Kfs	Pl	Bt	Hbl	Grt	Opx	Cpx	Crd	Opq	Ap	Zrn	Alteration
Hbl-Bt	(n=5)	+	+	+	+	+					+	+	+	Chl, Ms
Augen	FB155	40	38	3	10	5					3	1	tr	Chl, Ms
Gneiss														
Grt-Bt	(n=1)	+	+	+	+		+	+			+	+	+	Chl, Ms
Augen	FB88	40	28	13	10		5	2			2		tr	Chl, Ms
Gneiss														
Megacrystic	(n=3)	+	+	+	+	±		±			+	+	+	Chl, Ms, ±Srp
Kfs-Bt	FB158	30	50	3	8	5					4	tr	tr	Chl, Ms, Srp
Granite														
Gneiss														
Bt-Opx	(n=12)	+	+	+	+	±		±	±		+	+	+	±(Chl, Ms, Srp)
Granit	FB43	27	3	36	12	tr		12	4		6	tr	tr	Chl, Ms, Srp
Gneiss	FB143	30	37	20	10						3	1	tr	Chl, Ms
Anatectic	(n=1)	+	+	+	±						+	+	+	±(Chl, Ms)
Granites	FB151[a]	30	33	10	20						5	1	1	Chl, Ms
	(n=10)	+	+	+			±	±			+	1	1	±(Chl, Ms, Srp)
	FB129	35	36	10	2		15				2	tr	tr	Chl, Ms
	(n=2)	+	+	+	+		±			+	+	+	+	±(Chl, Ms, Srp)
	FB255	39	38	5	2					12	4	tr	tr	Chl, Ms, Srp
Porphyritic	(n=1)	+	+	+	+	±					+	+	+	±(Chl, Ms)
Granodiorite	FB94	20	20	40	10	2					7	1	tr	MS

Table 1 : Mineral assemblages and representative modal abundances of granitic rocks.
a: Sample FB151 is a sheared anatectic granite.

Rock Type	Sample	Qtz	Kfs	Pl	Bt	Hbl	Sil	Opx	Cpx	Grt	Crd	Hc	Opq	Ap	Zrn	Alteration
Homogeneous	(n=1)	+	+		+								+		+	Ms, ±Hem
Kfs-Qtz	FB110	47	50		2								1		tr	Ms
Pyroxene	(n=18)	±		+	±	±		+	+			±	+	+	±	±(Chl, Ms, Srp)
Granulite	DWN545	10		63	2	4		14	4				3			
Gneiss	FB116M			59	tr			30	5				5	1		
Qtz-rich	(n=10)	+		+	+	±		+	±				+	+	±	±(Chl, Ms, Srp)
Metabasic	FB65	20		40	5			30					5	tr		
Gneiss																
Aluminous	(n=22)	+	+	±	±		±			+		±	+		±	±(Chl, Ms, Dsp)
Quartzo-	FB60	27	50		6					15		1	1		tr	Ms
feldspathic	(n=4)	+	+	±	±		±			+	+	+	+		±	±(Chl,Ms,Srp,Dsp)
Gneiss	FB53	75	2	5	1					4	8	2	3			Ms, Srp, Dsp
	(n=27)	+	+	±	±		±				+	+	+		±	±(Chl,Ms,Srp,Dsp)
	FB127	34	33	10	tr		6				20	4	2		tr	Ms, Srp, Dsp
Metapelitic	(n=7)	+	+	±	±		±			+			+		±	±(Ms, Chl)
Gneiss	DWN673	34	16	28	17					4			1			
	(n=16)	+	+	±	±		±			+	+	+	+		±	±(Ms,Chl,Srp,Dsp)
	FB72	49		5	1					15	25	3	2			Ms, Srp, Dsp
	(n=16)	+	+	±	±		±	±			+	+	+		±	±(Ms,Chl,Srp,Dsp)
	FB119	20	24	12	7						20	4	6		tr	Ms, Srp, Dsp
Magnesian	(n=18)		+	±	+			±			+	+	+		tr	±(Srp, Dsp)
Gneiss	DWN553		25	15	5						40	10	5		tr	Srp, Dsp
	(n=3)		+	±	+			+		+	+	+	+		+	±(Srp, Dsp)
	DWN552		12	5	12			13		8	42	4	4		tr	Dsp
	(n=6)	+	+	±	+			+			+	±	+		+	±(Srp, Dsp)
	FB10	5	8		12			24			50		1		tr	Srp

Table 2 : Mineral assemblages and representative modal abundances of common supracrustal rocks.

Sample	Mineral Pair	X_{Mg}(Grt)	X_{Mg}(Bt)	K_D(Grt-Bt)	T(T76)	T(HL77)	T(FS78)	T(PL83)
DWN554	Grt-core - Bt	0.373	0.685	3.655	727	691	751	672
DWN552	Grt-core - Bt	0.362	0.677	3.694	724	688	746	670
FB71	Grt - matrix Bt	0.283	0.616	4.064	691	661	702	648
DWN673	Grt core - matrix Bt	0.207	0.547	6.626	651	627	647	621
DWN673	Fe-Grt - retro Bt	0.213	0.599	5.519	601	583	582	587
DWN673	Mg-Grt - retro Bt	0.227	0.699	7.908	515	507	474	524
FB210	Grt - retro Bt	0.257	0.661	5.637	596	579	575	583
FB202	Grt - retro Bt	0.268	0.694	6.195	571	557	544	566
FB266A	Grt - retro Bt	0.219	0.637	6.258	569	555	541	564

Table 3 : The results of garnet-biotite thermometry on mineral pairs in different aluminous quartzofeldspathic, metapelitic and magnesian gneisses.
T76 : Thompson (1976); HL77 : Holdaway and Lee (1977); FS78 : Ferry and Spear (1978); PL83 : Perchuk and Lavrent'eva (1983). See text for discussion.

Sample	Mineral Pair	X_{Mg}(Grt)	X_{Mg}(Crd)	K_D(Grt-Crd)	T(T76)	T(HL77)	T(PL83)
RW3	Grt-Crd cores	0.303	0.698	5.317	819	775	778
WW8	Grt-Crd cores	0.336	0.731	5.370	815	772	775
DWN554	Grt-Crd cores	0.373	0.769	5.596	797	758	761
WW13	Grt-Crd cores	0.328	0.731	5.568	800	760	762
PH1	Retro Grt-Crd	0.302	0.735	6.410	745	714	716
DWN552	Retro Grt-Crd	0.362	0.793	6.752	726	699	700
WW3	Retro Grt-Crd	0.248	0.702	7.143	706	682	683
WW8	Grt rim - Crd	0.297	0.763	7.620	685	664	664
FB210	Retro Grt-Crd	0.265	0.734	7.653	683	663	663

Table 4 : The results of garnet-cordierite thermometry on mineral pairs in different metapelitic and magnesian gneisses in the study area
T76 : Thompson (1976); HL77 : Holdaway and Lee (1977); PL83 : Perchuk and Lavrent'eva (1983). See text for discussion.

Rock Type	Sample	X_{Mg}(BtA)	X_{Mg}(BtB)	X_{Mg}(Opx)	K_D(Bt-Opx)	An(Pl)	X_F(BtA)	X_F(BtB)	Ti(BtA)	Ti(BtB)
Bt-Opx	F848	0.52(5)	0.62(5)	0.62(3)	1.35-1.64(4)	33(2)	0.39	0.46	0.51	0.47
leucoparagneiss	F8279	0.64(4)	0.71(3)	0.54(5)	1.24-1.30(3)	46(1)	0.57	0.68	0.58	0.39
without leucosomes	DWN544	0.76(2)	0.72(3)	0.64(7)	1.12(3)	54(4)	0.67	0.63	0.50	0.54
Bt-Opx	F8256	0.58(4)	0.65(6)	0.51(5)	1.61-1.73(3)	34(1)	0.53	0.66	0.58	0.47
lecuoparagneiss	F896	0.66(3)	0.75(17)	0.59(7)	1.48-1.67(3)	35(3)	0.60	0.70	0.65	0.51
with	F84	0.70(4)	0.73(9)	0.61(12)	1.51-1.72(9)	36(3)	0.61	0.64	0.59	0.52
leucosomes	F81	0.71(2)	0.75(4)	0.60(6)	1.56-1.57(2)	37(3)	0.63	0.70	0.57	0.45
Bt-Opx granite gniess	F8128	-	0.44(3)	0.39(3)	1.22-1.26(3)	38(1)	-	0.14-0.40	-	0.52

Table 5 : Summary of important mineral chemical parameters of biotite and orthopyroxene in different rock types with peraluminous bulk compositions.
BtA: matrix biotite; BtB: retrograde biotite

Rock Type	Sample	X_{Mg}(BtA)	X_{Mg}(BtB)	X_{Mg}(Opx)	K_D(Bt-Opx)	An(Pl)	X_F(BtA)	X_F(BtB)	Ti(BtA)	Ti(BtB)
Grt-Bt aluminous quartzo-feldspathic gneiss	F8266A	0.56(1)	0.64(1)	0.23(7)	6.26(1)	33(1)	0.61	0.64	0.62	0.39
Grt-Bt metapelitic gneiss	DWN673	0.56(5)	0.65(12)	0.22(8)	4.63-7.91(5)	33(2)	0.62	0.69	0.62	0.42

Table 6 : Summary of important mineral chemical parameters of garnet and biotite in two rocks with peraluminous bulk compositions.
BtA: matrix biotite; BtB: retrograde biotite

	FB48	FB1	FB256[a]	FB256[b]	FB266A	FB266B	DWN673[a]	DWN673[b]
Bt[c]	6.5	5.7	9.8	3.1	15.0	0.0	19.0	2.1
Bt[d]	-	-	-	-	-	-	-	13.3
Opx	tr	0.7	0.4	6.2	-	-	-	-
Grt	-	-	-	-	0.0	9.4	0.0	18.5
Qtz	27.1	31.2	47.2	44.8	40.0	35.4	34.5	33.2
Pl	37.9	33.0	27.4	29.0	17.0	17.1	33.0	8.7
Kfs	25.9	28.3	13.0	14.8	28.0	38.1	12.2	23.5
Mag	2.6	1.1	2.2	2.1	0.0	0.0	1.3	0.7
n[e]	800[f]	600[f]	800[f]	3000[g]	400[f]	2000[g]	500[f]	1500[f]

Table 7: Modal abundances of FB48, FB1, FB256, FB266A, FB266B and DWN673.
a: matrix gneiss
b: leocosome
c: matrix biotite
d: skeletal biotite
e: total counts on a grid spacing of 1 mm
f: thin section, SWIFT ponit counter
g: polished slab, transparent overlay grid

APPENDIX OF PLATES

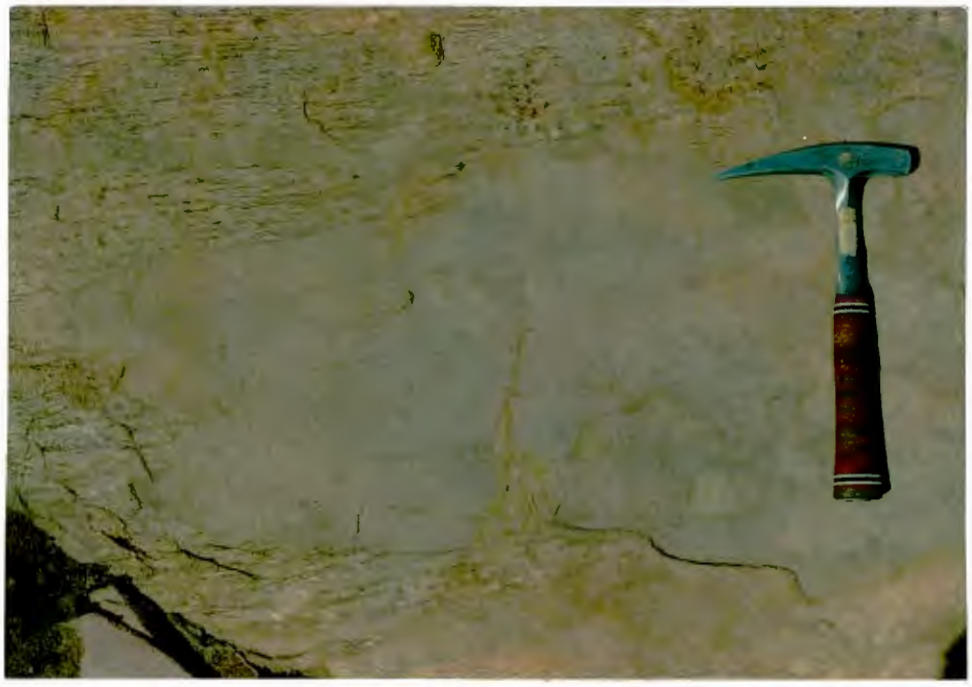

Plate 1. Discordant contact of hornblende-biotite augen gneiss against homogeneous K-feldspar-quartz gneiss. Note the presence of recrystallized augen wrapped by the strong ferromagnesian mineral foliation. Hammer shaft is 29 cm.

Plate 2. The typical green, 'streaky' character of hornblende-biotite augen gneiss with refolded internal structure. The contact with homogeneous K-feldspar-quartz gneiss is commonly concordant. Hammer shaft is 26 cm.

Plate 3. Well-foliated, biotite-rich biotite-orthopyroxene granite gneiss at a concordant contact against biotite leucoparagneiss. Hammer shaft (27 cm) is perpendicular to S_2 mineral foliation (s-surface), and pencil is parallel to the trace of the c-surface. Note the presence of a sheared, recrystallized leucosome parallel to the S_2 mineral foliation.

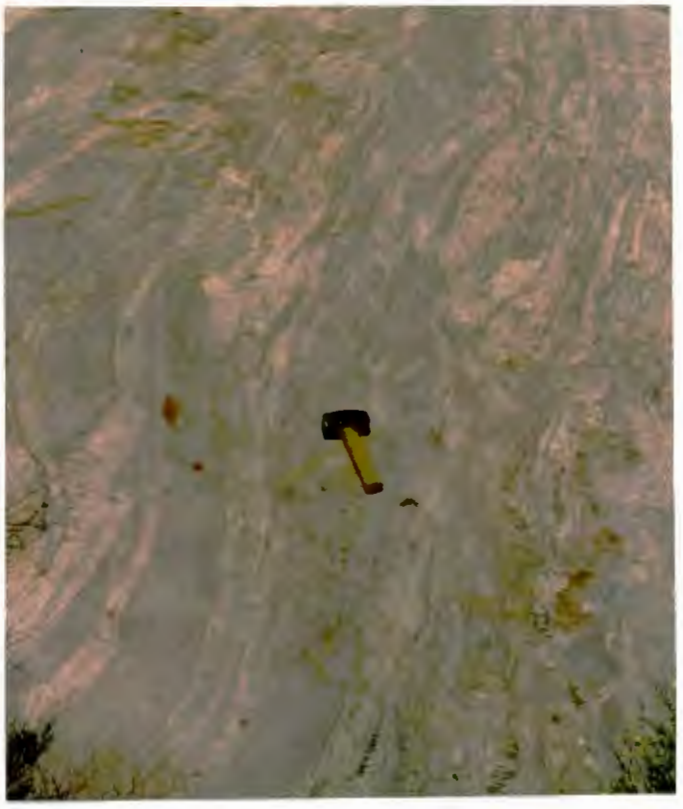

Plate 4. A stromatic migmatite root zone to a lenticular body of quartzofeldspathic anatectic granite (ca. 3 X 0.5 km) in biotite-orthopyroxene leucoparagneiss. Many of the dark spots in the leucosome assemblages are orthopyroxene. Hammer shaft is 26 cm.

Plate 5. Leucosome assemblages, containing garnet-quartz patches surrounded by anhydrous, quartzofeldspathic haloes, in a dyke of anatectic biotite granite that is intrusive into garnet-biotite quartzofeldspathic gneiss. The leucosomes comprise 50% of the rock volume. Hammer shaft is 26 cm.

Plate 6. Discordant leucosome, containing orthopyroxene (light green-brown), clinopyroxene (dark green-black) and plagioclase (white to pale blue), in hornblende-pyroxene granulite gneiss. Hammer shaft is 83 cm.

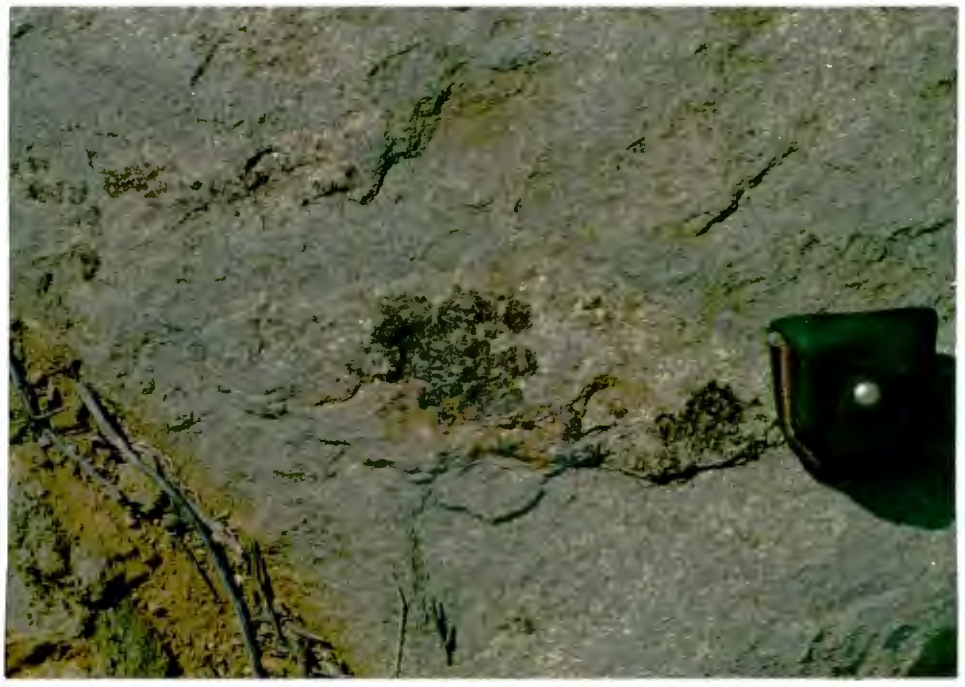

Plate 7. An ovoid leucosome patch, containing rhombododecahedra of garnet intergrown with quartz, and surrounded by an anhydrous, quartzofeldspathic halo, in garnet-biotite quartzofeldspathic gneiss. Compass pouch is 8 cm wide.

Plate 8. Garnetiferous and entirely quartzofeldspathic leucosomes occurring as crenulated compositional bands in garnet-biotite metapelitic gneiss. At left, a coarse-grained garnetiferous leucosome transgresses compositional banding and regional foliation. A K-feldspar-rich, pegmatitic vein occurs at the base of the outcrop, containing rootless stringers of matrix gneiss. Hammer shaft is 29 cm.

Plate 9. Unzoned leucosomes occurring parallel to the regional, gneissic banding and foliation in garnet-biotite metapelitic gneiss. Note that many garnet grains intersect matrix-leucosome boundaries, but are always surrounded by, at least a narrow anhydrous halo. Hammer shaft is 29 cm.

Plate 10. Cross-section of a anatectic granite sill root zone in garnet-biotite metapeltic gneiss. Note the nebulitic internal structure of disjointed matrix stringers. Hammer shaft is 29 cm.

Plate 11. Coarse-grained orthopyroxene-K-feldspar leucosome patches in orthopyroxene-cordierite-phlogopite mag-nesian gneiss. Hammer shaft is 29 cm.

Plate 12. Transgressive, orthopyroxene-bearing quartzofeldspathic leucosome in biotite-orthopyroxene leucoparagneiss. Hammer head is 18 cm.

Plate 13. Vein and patch leucosomes, subparallel to regional foliation in biotite-orthopyroxene leucoparagneiss. The dark patches in both matrix and leucosome assemblages are orthopyroxene-biotite intergrowths. Hammer shaft is 29 cm.

Plate 14. Boudin-like, quartzofeldspathic sill in banded quartzofeldspathic gneiss. It is not clear whether these structures are igneous (i.e. pinch-and-swell) or truely tectonic (i.e. stretching boudins) in origin. Hammer head is 18 cm.

APPENDIX 1 MINERAL ANALYSES

Appendices 1A - 1S list representative mineral analyses from various rock types in the study area. The results were used for geothermoarometry (chapter 4) and mass balance calculations (section 5.5, appendix 3).

Samples were analysed for major element chemistries (and in some cases, Cr_2O_3, MnO, F and Cl) using the CAMECA electron microprobe of the Department of Geochemistry, University of Cape Town. Accelerating voltage was 15kV, and the electron beam was focussed to a 1μm diameter for most species. A 10 second counting time was used for all elements except Cl (see note f below). Natural mineral standards used are detailed Le Roex and Reid (1978). A ZAF correction procedure was employed for most analyses, except where indicated that a Bence and Albee (1968) procedure was used. The total number of mineral analyses made for each rock is indicated in parentheses at the heading of each Appendix. The additional results are available on request.

The cation amounts for each phase are based on x oxygens per formula unit as follows: Ilm(3), Hc(4), Mgt(4), Crd(6), Cpx(6), Opx(6), Kfs(8), Pl(8), Grt(12), Bt(22), Hbl(23). Superscript notes referred to in appendices are explained overleaf.

EXPLANATION OF APPENDIX 1 NOTES

a: Bence-Albee correction procedure.

b: Opaques: Total weight % FeO = FeO + Fe_2O_3 by stoichiometry.

$F_{x.y}$ = Fe_2O_3/FeO weight percents.

c: Massive garnet.

d: Skeletal garnet.

e: Matrix biotite.

f: 60 second counting time used for Cl.

g: RW3 and RW4 collected by Dr. J.M. Moore (1986).

RW3 analysed by Dr. D.J. Waters (unpubl. data).

h: Cordierite analysis calculated on the basis of 18 oxygens.

i: Mesoperthites: Fsp7 is the mean of 4 spots;

Fsp2 is the mean of 7 spots.

j: X_{Mg}(Bt) is variable between 0.58 and 0.75.

k: Garnet core analysis.

m: Garnet rim analysis.

n: Hercynite: Fe^{3+} calculated using the method of Droop (1987).

$F_{x.y}$ = Fe_2O_3/FeO weight percents.

1A: Representative mineral analyses for biotite-orthopyroxene granite gneiss FB128 (n=13)

	Opx3	Bt1	Kfs3	Pl 1	Ilm3
SiO_2	47.56	36.22	65.27	59.47	nd
TiO_2	0.13	4.51	-	-	50.58
Al_2O_3	4.23	15.10	18.71	25.91	nd
FeO	35.81	22.12	nd	nd	48.84[b]
MnO	0.24	nd	-	-	0.47
MgO	12.37	9.44	nd	0.28	7.76
CaO	0.18	nd	0.28	7.76	-
Na_2O	nd	0.10	1.43	6.78	-
K_2O	-	9.41	14.42	0.30	-
F	-	0.32	-	-	-
Cl	-	0.67	-	-	-
Total	100.52	97.89	100.11	100.22	99.89
Si	1.882	5.510	2.991	2.645	-
Ti	0.004	0.517	-	-	0.973
Al	0.197	2.708	1.011	1.358	-
Fe	1.185	2.815	-	-	1.037
Mn	0.008	-	-	-	0.010
Mg	0.729	2.140	-	-	-
Ca	0.008	-	0.014	0.370	-
Na	-	0.028	0.127	0.585	-
K	-	1.826	0.843	0.017	-
F	-	0.155	-	-	-
Cl	-	0.173	-	-	-
Total	4.013	15.872	4.986	4.975	2.025
MF	38.09	43.19	$Ab_{12.9}$ $Or_{85.7}$ $An_{1.4}$	$Ab_{60.2}$ $Or_{1.8}$ $An_{38.0}$	$F_{0.088}$[b]

18: Representative mineral analyses for garnet-biotite-orthopyroxene anatetic granite gneiss FB71 (n=25)

	Opx3[a]	Bt4	Grt9[ac]	Pl 2	Kfs1	Grt5[d]	Bt1[e]	Ilm2
SiO_2	48.88	38.70	37.46	60.74	65.29	36.98	37.11	nd
TiO_2	0.11	2.80	nd	-	-	0.07	4.69	50.82
Al_2O_3	3.72	14.50	21.43	24.43	18.44	21.42	14.88	nd
FeO	27.55	12.84	27.29	nd	nd	29.24	15.50	44.96[b]
MnO	1.52	0.13	5.27	-	-	6.06	0.26	3.96
MgO	17.65	17.63	6.04	nd	nd	4.43	13.96	nd
CaO	0.18	nd	1.94	6.81	0.05	1.79	nd	nd
Na_2O	nd	0.13	nd	7.46	1.90	nd	0.11	-
K_2O	nd	9.53	-	0.25	13.42	-	9.89	-
F	-	1.94	-	-	-	-	1.33	-
Total	99.61	98.20	99.43	99.69	99.55	99.99	97.73	99.72
Si	1.888	5.654	2.971	2.709	2.999	2.957	5.516	-
Ti	0.003	0.308	-	-	-	0.004	0.525	1.957
Al	0.169	2.496	2.004	1.284	0.999	2.019	2.607	-
Fe	0.890	1.569	1.811	-	-	1.951	-	
Mn	0.050	0.016	0.354	-	-	0.410	0.032	1.911
Mg	1.016	3.839	0.715	-	-	0.528	3.094	0.172
Ca	0.007	-	0.165	0.326	0.025	0.153	-	-
Na	-	0.037	-	0.645	0.169	-	0.031	-
K	-	1.776	-	0.014	0.787	-	1.875	-
F	-	0.898	-	-	-	-	0.624	-
Total	4.023	16.593	8.020	4.978	4.979	8.027	16.230	4.040
MF	53.39	71.09	28.3 Or_1 An_{33}	Ab_{66} Or_{80} An_3	Ab_{17}	21.2	61.6	$F_{0.078}$[b]

1C: Representative mineral analyses from biotite-orthopyroxene leucoparagneiss FB48 (n=22)

	Opx1[a]	Bt1	Opx6[a]	Bt4	Bt5[e]	Bt6	Pl2	Kfs2	Mgt2	Ilm2
SiO_2	49.99	38.25	49.92	38.41	36.93	37.79	63.10	65.8	nd	nd
TiO_2	0.10	4.19	0.13	4.48	4.93	4.21	-	-	0.05	52.29
Al_2O_3	2.04	14.29	2.15	14.85	14.35	14.25	24.39	18.43	nd	nd
Cr_2O_3	nd	nd	nd	nd	nd	nd	-	0.06	nd	
FeO	28.38	15.48	28.77	16.92	20.00	19.36	nd	nd	98.84[b]	38.12[b]
MnO	1.54	0.31	1.58	0.19	0.37	0.18	-	-	nd	7.34
MgO	17.46	14.68	17.14	13.56	11.92	12.28	nd	nd	nd	0.03
CaO	0.24	nd	0.24	nd	nd	nd	5.93	0.09	nd	nd
Na_2O	nd	0.10	nd	0.12	0.07	nd	6.68	0.95	-	-
K_2O	nd	9.72	nd	9.50	8.95	9.55	0.33	14.25	-	-
F	-	1.32	-	1.21	0.95	1.05	-	-	-	-
Total	99.75	98.34	99.93	99.24	98.47	98.67	100.43	99.70	98.95	97.78
Si	1.934	5.629	1.931	5.614	5.518	5.621	2.768	3.022	-	-
Ti	0.003	0.464	0.004	0.492	0.554	0.471	-	-	0.002	1.009
Al	0.093	2.478	0.098	2.588	2.527	2.498	1.261	0.995	-	-
Cr	-	-	-	-	-	-	-	-	0.002	-
Fe	0.918	1.905	0.931	2.068	2.449	2.409	-	-	3.984	0.818
Mn	0.050	0.039	0.052	0.023	0.047	0.023	-	-	-	0.159
Mg	1.007	3.221	0.988	2.955	2.654	2.723	-	-	-	0.001
Ca	0.010	-	0.010	-	-	-	0.279	-	-	
Na	-	0.030	-	0.003	0.020	-	0.568	0.084	-	-
K	-	1.824	-	1.771	1.707	1.812	0.019	0.883	-	-
F	-	0.613	-	0.560	0.450	0.495	-	-	-	-
Total	4.015	16.203	4.014	16.074	15.976	16.052	4.895	4.939	3.988	1.987
MF	52.39	62.89	51.5	58.86	51.5	53.1	Ab^{66} Or_2 An_{32}	Ab_9 Or_{90} An_1	$F_{2.23}$[b]	F_0[b]

1D: Representative mineral analyses from biotite-orthopyroxene leucoparagneiss F8279 (n=12)

	Opx1	Bt1	Bt6	Pl 1
SiO_2	50.72	37.89	37.31	57.32
TiO_2	0.10	3.70	5.63	-
Al_2O_3	2.77	14.68	14.55	26.70
FeO	27.70	12.48	15.14	nd
MnO	0.8	nd	0.15	-
MgO	18.66	17.22	14.51	nd
CaO	nd	nd	nd	9.45
Na_2O	nd	0.08	0.10	5.83
K_2O	nd	10.04	9.95	0.44
F	-	2.09	1.92	-
Cl^f	-	0.06	0.06	-
Total	100.73	98.24	99.32	99.74
Si	1.918	5.558	5.484	2.576
Ti	-	0.409	0.622	-
Al	0.124	2.538	2.520	1.414
Fe	0.876	1.531	1.861	-
Mn	0.028	-	0.018	-
Mg	1.051	3.766	3.178	-
Ca	-	-	-	0.455
Na	-	0.022	0.030	0.508
K	-	1.878	1.866	0.025
F	-	0.972	0.894	-
Cl^f	-	0.014	0.015	-
Total	3.997	16.688	16.488	4.978
MF	54.54	71.10	63.07	$Ab_{51.4}$ $Or_{2.6}$ $An_{46.0}$

1E: Representative mineral analyses for biotite-orthopyroxene leucoparagneiss F8256 (n=19)

	Opx3	Bt1	Kfs3	Pl 1	Ilm3
SiO_2	50.63	37.90	37.83	64.90	60.80
TiO_2	nd	4.15	5.13	-	-
Al_2O_3	1.70	13.99	14.10	18.28	24.70
FeO	28.13	14.02	16.07	nd	nd
MnO	1.50	0.12	0.19	-	-
MgO	17.73	15.16	13.86	nd	nd
CaO	0.35	nd	nd	nd	6.82
Na_2O	nd	0.08	0.09	1.56	7.15
K_2O	nd	9.76	9.51	14.37	0.43
F	-	1.86	1.68	-	-
Cl^f	-	nd	nd	-	-
Total	100.04	97.04	98.46	99.11	99.90
Si	1.947	5.650	5.559	3.003	2.704
Ti	-	0.466	0.571	-	-
Al	0.077	2.459	2.458	0.997	1.295
Fe	0.905	1.747	1.988	-	-
Mn	0.049	0.016	0.023	-	-
Mg	1.016	3.368	3.056	-	-
Ca	0.014	-	-	-	0.325
Na	-	0.023	0.025	0.140	0.616
K	-	1.855	1.794	0.848	0.024
F	-	0.879	0.788	-	-
Cl	-	-	-	-	-
Total	4.008	16.463	16.298	4.988	4.964
MF	52.89	65.84	60.59	$Ab_{14.1}$ $Or_{85.6}$ $An_{0.3}$	$Ab_{63.8}$ $Or_{2.5}$ $An_{33.7}$

1F: Representative mineral analyses of biotite-orthopyroxene leucoparagneiss FB96 (n=33)

	Opx3	Bt8	Opx4	$Bt9^p$	$Bt3^e$	Kfs1	Pl1
SiO_2	50.33	37.37	50.85	36.47	37.42	64.56	60.01
TiO_2	nd	4.98	nd	4.43	4.83	-	-
Al_2O_3	3.55	14.55	3.35	14.76	14.64	18.65	24.83
FeO	21.75	12.72	22.23	14.77	13.39	nd	nd
MnO	2.98	0.24	2.78	0.44	0.34	-	-
MgO	20.75	15.80	20.44	15.81	15.15	nd	nd
CaO	0.20	nd	0.21	nd	0.10	0.15	6.91
Na_2O	nd	0.07	nd	0.15	0.15	1.32	7.13
K_2O	nd	9.88	nd	7.85	9.67	14.22	0.30
F	-	2.10	-	1.31	2.03	-	-
Total	99.56	97.77	99.86	95.99	97.72	98.90	99.18
Si	1.899	5.527	1.913	5.451	5.544	2.992	2.690
Ti	-	0.554	-	0.498	0.538	-	-
Al	0.158	2.537	0.149	2.601	2.556	1.019	1.311
Fe	0.686	1.573	0.700	1.856	1.659	-	-
Mn	0.095	0.030	0.089	0.056	0.043	-	-
Mg	1.167	3.483	1.147	3.522	3.346	-	-
Ca	0.008	-	6.009	-	-.016	0.007	0.332
Na	-	0.021	-	0.043	0.044	0.199	0.620
K	1.865	-	1.497	1.828	0.840	0.017	
F	-	0.981	-	0.621	0.950	-	-
Total	4.013	16.586	4.000	16.135	16.524	4.97	4.970
MF	62.98	68.89	62.10	65.60	66.86	$Ab_{12.3}$ $Or_{87.0}$ $An_{0.7}$	$Ab_{64.0}$ $Or_{1.7}$ An_{343}

1G: Representative mineral analyses from biotite-orthopyroxene leucoparagneiss F84 (n=40)

	Opx1	Bt1	Opx7	Bt7	Bt4[e]	Bt5[e]	Pl1	Kfs1	Mgt3	Ilm2
SiO_2	50.78	37.48	51.19	37.92	36.80	38.21	60.40	64.12	nd	nd
TiO_2	0.14	4.52	0.05	4.53	5.17	5.09	-	-	nd	46.24
Al_2O_3	2.97	15.12	2.38	14.99	14.24	14.27	24.84	nd	nd	nd
FeO	22.64	11.22	22.05	11.11	13.04	12.95	nd	nd	99.54[b]	38.80[b]
MnO	2.14	0.19	1.93	0.22	0.21	0.19	-	-	nd	3.63
MgO	21.41	17.57	22.07	17.63	16.36	15.77	nd	nd	nd	0.05
CaO	0.23	nd	0.27	nd	nd	nd	7.10	0.05	nd	0.05
Na_2O	nd	0.06	nd	0.06	0.05	0.08	7.00	0.96	-	-
K_2O	nd	9.73	nd	9.92	9.53	9.82	0.30	15.08	-	-
F	-	1.90	-	1.59	2.00	1.67	-	-	-	-
Total	100.31	97.79	99.94	97.97	97.40	98.05	99.64	98.35	99.54	98.77
Si	1.905	5.479	1.920	5.512	5.464	5.598	2.694	3.001	-	-
Ti	0.004	0.497	0.001	0.496	0.518	0.561	-	-	-	0.925
Al	0.131	2.605	0.105	2.567	2.491	2.464	1.306	1.000	-	-
Fe	0.710	1.372	0.692	1.351	1.620	1.587	-	-	3.987	1.062
Mn	0.068	0.024	0.061	0.027	0.027	0.024	-	-	-	0.082
Mg	1.197	3.827	1.234	3.820	3.621	3.444	-	-	-	0.002
Ca	0.009	-	0.011	-	-	-	-	0.339	-	0.001
Na	-	0.016	-	0.016	0.015	0.024	0.606	0.087	-	-
K	-	1.815	-	1.840	1.806	1.835	0.017	0.900	-	-
F	-	0.878	-	0.732	0.937	0.773	-	-	-	-
Total	4.024	16.513	4.024	16.361	16.559	16.310	4.962	4.900	3.987	2.072
MF	62.89	73.69	64.1	73.96	69.1	68.5	Ab_{63} Or_2 An_{35}	Ab_9 Or_{91} An_0	$F_{2.21}$[b]	$F_{0.29}$[b]

1H: Representative mineral analyses from biotite-orthopyroxene leucoparagneiss F81 (n=16)

	Opx4	Bt1	Bt4	Bt5[e]	Kfs1	Pl1	Mgt1
SiO_2	50.83	38.01	38.48	37.88	65.30	60.24	nd
TiO_2	nd	4.64	3.59	5.02	-	-	nd
Al_2O_3	3.44	14.96	15.08	14.84	18.67	25.54	0.23
FeO	22.02	11.25	10.21	12.49	nd	nd	99.46
MnO	2.48	0.23	0.25	0.25	-	-	nd
MgO	21.57	17.26	18.68	16.14	nd	nd	-
CaO	0.14	nd	nd	nd	0.13	7.47	-
Na_2O	nd	0.07	0.08	0.09	1.96	6.90	-
K_2O	nd	9.93	9.76	9.71	14.02	0.45	-
F	-	1.76	2.59	1.87	-	-	-
Total	100.56	98.11	98.79	98.29	100.08	100.60	99.69
Si	1.898	5.531	5.571	5.534	2.988	2.667	-
Ti	-	0.508	0.391	0.552	-	-	-
Al	0.151	2.565	2.572	2.555	1.007	1.332	0.014
Fe	0.687	1.368	1.236	1.526	-	-	3.961
Mn	0.079	0.028	0.031	0.031	-	-	-
Mg	1.200	3.743	4.031	3.515	-	-	-
Ca	0.006	-	-	-	0.007	0.354	-
Na	-	0.019	0.022	0.027	0.173	0.592	-
K	-	1.843	1.902	1.809	0.818	0.025	-
F	-	0.808	1.186	0.862	-	-	-
Total	4.021	16.435	16.836	16.411	4.993	4.970	3.980
MF	63.59	73.23	76.53	69.73	$Ab_{17.4}$ $Or_{82.0}$ $An_{0.7}$	$Ab_{60.9}$ $Or_{2.6}$ $An_{36.5}$	$F_{2.20}$

1J: Representative mineral analyses from K-feldspar-free biotite orthopyroxene leucoparagneiss DWN544 (n=20)

	Opx3	Bt1	Opx5	Bt5	Bt4	Pl4	Mgt2
SiO_2	51.42	38.42	51.81	38.14	38.18	56.06	nd
TiO_2	0.09	4.63	0.08	4.98	4.80	-	0.23
Al_2O_3	2.80	14.58	2.59	14.65	15.27	27.88	0.13
FeO	21.52	11.64	21.00	10.97	9.54	nd	98.20[b]
MnO	1.14	nd	1.04	0.17	nd	-	0.04
MgO	22.62	17.29	23.03	16.92	18.00	nd	nd
CaO	0.23	nd	0.23	nd	nd	10.83	nd
Na_2O	nd	0.08	nd	0.09	0.09	4.98	-
K_2O	nd	9.54	nd	9.58	9.88	0.23	-
F	-	1.77	-	1.88	1.94	-	-
Total	99.82	97.95	99.78	97.38	97.70	99.98	98.78
Si	1.917	5.585	1.927	5.577	5.532	2.518	-
Ti	0.003	0.507	0.002	0.547	0.523	-	0.009
Al	0.123	2.497	0.114	2.525	2.607	1.476	0.008
Cr	-	-	-	-	-	-	0.007
Fe	0.671	1.415	0.653	1.342	1.156	-	3.955
Mn	0.036	-	0.033	0.002	-	-	0.002
Mg	1.257	3.747	1.277	3.688	3.888	-	-
Ca	0.009	-	0.009	-	-	0.521	-
Na	-	0.022	-	0.026	0.026	0.434	-
K	-	1.768	-	1.787	1.826	0.013	-
F	-	0.813	-	0.868	0.888	-	-
Total	4.016	16.354	4.015	16.380	16.446	4.962	3.981
MF	65.2	72.6	66.2	73.3	77.1	Ab_{45} Or_1 An_4	$F_{2.18}$[b]

1K: Representative mineral analyses from pyroxene granulite gneiss DWN545 (n=29)

	Opx	Cpx	Hbl	Bt[j]	Ilm	Pl
SiO_2	51.91	51.06	43.33	38.89	nd	58.82
TiO_2	0.07	0.19	2.20	449	50.99	-
Al_2O_3	1.06	2.18	10.78	13.88	nd	26.34
Cr_2O_3	nd	nd	0.08	nd	nd	-
FeO	25.19	10.77	14.41	14.10	45.2[b]	0.11
MnO	0.79	0.36	0.21	nd	2.48	-
MgO	20.40	13.23	12.54	15.88	0.06	nd
CaO	0.60	21.42	12.03	nd	nd	9.33
Na_2O	nd	0.41	1.24	0.07	-	5.75
K_2O	nd	nd	1.97	9.39	-	0.43
F	-	-	1.07	0.51	-	-
Total	100.02	99.62	99.86	97.21	99.45	99.98
Si	1.964	1.931	6.334	5.680	-	2.599
Ti	0.002	0.005	0.242	0.493	0.982	-
Al	0.047	0.097	1.857	2.388	-	-
Fe	0.797	0.340	1.762	1.722	0.978	0.004
Mn	0.025	0.011	0.026	-	0.054	-
Mg	1.150	0.746	2.732	3.457	0.003	-
Ca	0.024	0.868	1.884	-	-	0.448
Na	-	0.030	0.351	0.020	-	0.500
K	-	-	0.367	1.749	-	0.025
F	-	-	0.256	0.234	-	-
Total	4.009	4.028	15.743	2.017	4.967	
MF	59.1	68.0	60.8	66.8	$F_{0.062}$[b]	Ab_{51} Or_3 An_{46}

1L: Representative mineral analyses from aluminous quartzofeldspathic gneiss FB266A (n=18)

	Grt1	Grt2[k]	Grt2[m]	Bt5	Pl1	Ilm1
SiO_2	37.30	37.07	36.47	36.97	60.18	nd
TiO_2	nd	nd	nd	3.42	-	49.14
Al_2O_3	21.79	21.71	21.74	15.44	23.78	nd
Cr_2O_3	nd	nd	nd	nd	-	0.16
FeO	33.22	34.15	33.53	14.46	nd	48.15[b]
MnO	1.10	1.15	1.22	nd	-	0.37
MgO	5.59	5.04	5.30	14.25	nd	nd
CaO	0.20	0.40	0.23	nd	6.48	-
Na_2O	0.05	0.04	nd	0.07	7.21	
K_2O	-	-	-	9.72	0.44	-
F	-	-	-	1.70	-	-
Total	99.25	99.55	98.49	96.03	98.09	97.82
Si	2.973	2.963	2.943	5.569	2.725	-
Ti	-	-	-	0.387	-	0.969
Al	2.047	2.045	2.068	2.742	1.269	-
Cr	-	-	-	-	-	0.003
Fe	2.214	2.283	2.263	1.822	-	1.046
Mn	0.074	0.078	0.083	-	-	0.008
Mg	0.665	0.601	0.638	3.199	-	-
Ca	0.017	0.034	0.020	-	0.314	-
Na	0.018	0.006	-	0.002	0.633	-
K	-	-	-	1.868	0.025	
F	-	--	--	0.809	-	-
Total	7.998	8.010	8.015	16.418	4.966	2.019
MF	23.09	20.83	21.98	63.71	$Ab_{65.1}$ $Or_{2.6}$ $An_{32.3}$	$Fo_{0.10}$[b]

1M: Representative mineral analyses from garnet-biotite metapelitic gneiss DUN673 (n=55)

	Grt5[k]	Bt5	Grt6[k]	Bt8	Bt1[e]	Kfs2	Pl1	Ilm3
SiO_2	37.13	36.78	37.30	36.89	36.00	64.42	59.82	nd
TiO_2	nd	5.53	nd	5.02	5.20	-	-	47.68
Al_2O_3	21.74	15.10	21.93	14.99	15.20	18.13	23.93	nd
FeO	33.38	15.76	32.80	14.38	17.43	nd	nd	51.83[b]
MnO	0.76	nd	0.70	nd	nd	-	-	0.25
MgO	5.21	12.99	5.74	14.26	11.79	nd	nd	nd
CaO	1.56	nd	1.42	nd	nd	0.24	6.66	-
Na_2O	nd	0.15	nd	0.17	0.15	1.90	7.49	-
K_2O	-	9.63	-	9.63	9.54	13.64	0.18	-
F	-	2.04	-	2.75	1.67	-	-	-
Total	99.72	97.98	99.97	97.80	96.98	98.33	98.08	99.76
Si	2.954	5.485	2.952	5.504	5.449	3.001	2.711	-
Ti	-	0.620	-	0.563	0.592	-	--	0.938
Al	2.039	2.653	2.046	2.636	2.712	0.996	1.278	-
Fe	2.221	1.965	2.171	1.794	2.206	-	-	1.113
Mn	0.051	-	0.047	-	-	-	-	0.006
Mg	0.618	2.886	0.667	3.170	2.660	-	-	-
Ca	0.128	-	0.120	-	-	0.012	0.324	-
Na	-	0.043	-	0.049	0.045	0.172	0.659	-
K	-	1.832	-	1.832	1.842	0.810	0.010	-
F	-	0.961	-	1.163	0.799	-	-	-
Total	8.011	16.482	8.018	16.711	16.305	4.991	4.982	2.060
MF	21.77	59.70	23.78	63.86	54.66	$Ab_{17.3}$ $Or_{81.5}$ $An_{1.2}$	$Ab_{66.4}$ $Or_{1.0}$ $An_{32.6}$	$F_{0.002}$[b]

1N: Representative mineral analyses from garnet-cordierite metapelitic gneiss RW39 (n=48)

	Grt	Crd
SiO_2	38.39	48.73
Al_2O_3	21.66	33.18
FeO	30.30	6.92
MnO	1.54	nd
MgO	7.47	8.87
CaO	0.92	nd
Total	100.28	97.70
Si	2.995	5.008
Al	1.991	4.020
Fe	1.977	0.595
Mn	0.102	-
Mg	0.869	1.359
Ca	0.076	-
Total	8.010	10.982[h]
MF	30.5	69.6

1P: Representative mineral analyses for hercynite-sillimanite cordierite-garnet-biotite metapelitic gneiss FB210 (n=27)

	Grt4[k]	Crd4	Bt1	Hc5	Pl1
SiO_2	38.20	49.20	38.01	nd	60.18
TiO_2	nd	nd	4.81	nd	-
Al_2O_3	22.28	34.27	15.15	55.90	23.78
FeO	32.18	6.03	12.99	36.12[b]	nd
MnO	1.58	0.12	nd	nd	-
MgO	6.53	9.71	15.19	6.26	nd
CaO	0.66	nd	nd	nd	6.48
Na_2O	nd	0.10	0.17	-	7.21
K_2O	-	nd	9.36	-	0.44
F	-	-	1.98	-	-
Total	101.43	99.43	97.66	98.68	98.09
Si	2.966	6.332	5.586	-	2.725
Ti	-	-	0.532	-	-
Al	2.039	5.198	2.624	1.875	1.269
Fe	2.089	0.649	1.596	0.859	-
Mn	0.104	0.013	-	nd	-
Mg	0.756	1.864	3.328	0.266	-
Ca	0.055	-	-	-	0.314
Na	-	0.024	0.049	-	0.633
K	-	-	1.756	-	0.025
F	-	-	0.918		-
Total	8.009	14.080	16.389	3.000	4.966
MF	26.58	74.18	67.58	23.6 $F_{0.16}$[n]	$Ab_{65.1}$ $Or_{2.6}$ $An_{32.3}$

1Q: Representative mineral analyses from magnesian gneiss RW49 (n=27)

	fspl1[i]	fsp2[i]
SiO_2	64.26	64.23
Al_2O_3	21.03	19.61
FeO	0.06	0.14
MgO	nd	0.12
CaO	3.15	1.83
Na_2O	5.96	4.12
K_2O	5.68	9.33
Total	100.14	99.38
Si	2.880	2.930
Al	1.110	1.054
Fe	0.005	0.005
Mg	-	0.009
Ca	0.151	0.089
Na	0.517	0.364
K	0.325	0.544
Total	4.988	4.995
	$Ab_{52.1}$	$Ab_{36.5}$
	$Or_{32.7}$	$Or_{54.6}$
	$An_{15.2}$	$An_{8.9}$

1R: Representative mineral analyses from magnesian gneiss DWN552 (n=57)

	Opx2[a]	Bt1	Grt7[a]	Crd1	Pl1	Kfs1	Bt4	Hc4	Mgt1	Fsp
SiO_2	48.46	38.51	38.22	49.14	61.48	65.36	37.80	nd	nd	64.48
TiO_2	0.04	2.95	nd	nd	-	-	3.77	nd	nd	-
Al_2O_3	6.75	15.66	22.17	33.19	24.20	18.87	15.50	61.62	0.14	20.97
Cr_2O_3	nd	nd	nd	nd	-	-	nd	nd	0.08	-
Fe	23.28	10.65	28.20	4.94	0.21	0.11	13.75	28.27[b]	98.42[b]	nd
MnO	0.37	nd	1.50	0.07	-	-	nd	0.09	nd	-
MgO	20.79	18.50	8.98	10.60	nd	nd	16.17	9.81	nd	nd
CaO	0.04	nd	0.77	nd	6.10	nd	nd	-	-	2.06
Na_2O	nd	0.16	nd	0.05	7.80	1.97	0.15	-	-	3.94
K_2O	nd	9.59	-	nd	0.14	13.39	9.09	-	-	8.75
F	-	2.33	-	-	-	-	1.76	-	-	-
Total	99.73	98.84	97.99	99.93	99.70	97.90	99.79	98.74	100.20	
Si	1.820	5.574	2.964	1.665	2.731	2.994	5.535	-	-	2.903
Ti	0.001	0.322	-	-	-	-	0.416	-	-	-
Al	0.299	2.672	2.026	1.326	1.267	1.019	2.675	1.974	0.009	1.113
Cr	-	-	-	-	-	-	-	-	0.003	-
Fe	0.731	1.289	1.829	0.140	0.008	0.004	1.684	0.639	3.977	-
Mn	0.012	-	0.099	0.002	-	-	-	0.002	-	-
Mg	1.164	3.992	1.038	0.535	-	-	3.529	0.397	-	-
Ca	0.002	-	0.064	-	0.290	-	-	-	-	0.099
Na	-	0.045	-	-.003	0.672	0.175	0.043	-	-	0.344
K	-	1.771	-	-	0.008	0.782	1.699	-	-	0.503
F	-	1.066	-	-	-	-	0.895	-	-	-
Total	4.092	16.731	8.020	3.671	4.976	4.973	16.396	3.012	3.989	4.962
MF	61.4	75.6	36.2	79.3	Ab_{69} Or_1 An_{30}	Ab_{18} Or_{82} An_0	67.7	38.3 $F_{0.05}$[n]	$F_{2.21}$[b]	Ab_{36} Or_{53} An_{11}

1S: Representative mineral analyses from magnesian gneiss DWN554 (n=15)

	Opx1	Bt3	Grt2	Crd1	Kfs2
SiO_2	48.36	38.25	38.40	48.58	66.93
TiO_2	0.12	4.34	nd	nd	-
Al_2O_3	6.34	15.26	22.46	33.04	19.77
FeO	26.30	13.25	27.93	5.31	0.11
MnO	0.34	nd	0.92	0.07	-
MgO	18.17	16.14	9.32	9.93	nd
CaO	nd	nd	0.33	nd	0.96
Na_2O	nd	0.15	nd	0.15	6.14
K_2O	nd	8.79	-	nd	6.29
F	-	1.82	-	-	-
Total	99.63	98.00	99.36	97.08	100.20
Si	1.842	5.575	2.975	1.665	2.976
Ti	0.003	0.457	-	-	-
Al	0.285	2.621	2.050	1.335	1.036
Fe	0.838	1.615	1.809	0.152	0.004
Mn	0.011	-	0.061	0.002	-
Mg	1.031	3.507	1.076	0.507	-
Ca	-	-	0.027	-	0.045
Na	-	0.043	-	0.010	0.530
K	-	1.634	-	-	0.357
F	-	0.840	-	-	-
Total	4.010	16.310	7.998	3.671	4.948
MF	55.2	68.5	37.3	76.9	Ab_{57} Or_{38} An_5

APPENDIX 2 MODAL PROPORTIONS OF MIGMATITES

The modal proportions of leucosome assemblages are affected by a variety of natural processes, discussed in the text and by Waters (1988). Their estimation is affected by methods of sampling and analysis.

In many cases, centimetre-scale leucosomes can be satisfactorily sampled. However, many leucosomes are texturally and compositionally inhomogeneous and occur as coarse-grained metre-scale bodies. Leucosomes also occur as lenticular bodies with a preferred orientation parallel to the regional mineral foliation and have an associated inhomogeneous mineral distribution. These inhomogeneous leucosomes cannot be easily sampled.

The modal proportions of thin sections of fine- and medium-grained matrix and centimetre-scale leucosomes were determined using an electronic SWIFT point counter. 300 - 1000 points were counted on a range of 0.5 - 2.0 mm grids.

Polished rock slabs of coarse-grained, centimetre-scale leucosomes were etched with 10% hydrofluoric acid (HF) and stained with a saturated solution of sodium cobaltinitrite ($Na_3Co[NO_2]_6$). The technique is used by Pattison and Harte (1988) to distinguish between K-feldspar (bright yellow) and plagioclase (white or lemon yellow). in the samples from this study, biotite as also stained yellow, but was distinguished from K-feldspar by

hardness contrast. Modal proportions were determined manually using transparent 1 mm-grid overlays and 1000 - 5000 points.

A single analysis of a metre-scale leucosome of garnet-biotite metapelitic gneiss FBM2 was performed by tracing the distribution of matrix, quartzofeldspathic leucosome and garnet onto a transparent overlay (Fig. 11). Modal proportions of these components were determined manually (and laboriously!) on a 1 mm grid of 172 760 points.

It is not possible to determine meaningful estimates of analytic error (at any confidence level) on modal estimates using binomial or Poisson theory (Dixon and Massey, 1969, p. 245-251; Cheeney, 1981, p. 69-71) for large or small proportions, respectively. Both the statistical methods depend on sample homogeneity, i.e. the random distribution of components in the sample population. This is not true for compositionally and texturally inhomogeneous leucosomes. However, the determination of a constant garnet:leucosome ratio for the different zones of FBM2 (Fig. 5.12), suggests that homo-geneity may exist within leucosomes at and above a critical sample area, depending on grain size. It would be useful to know this critical sample area in order to optimize the estimation of the modal proportions of leucosomes in future work. Detailed image analysis and strict statistical treatment is required. It is likely that the minimum sample area is greater than the areas of the smaller zones marked on Fig. 5.11, because these zones were not randomly selected (A.O.

Fuller, pers. comm.). The strict statistical treatment of the modal counting leucosome assemblages is difficult, because of their inhomogeneity. This does not invalidate the estimation of their modal proportions. It only invalidates the treatment of the uncertainty of modal pro-portions.

This study qualitatively assesses the reliability of the various mode counting techniques used. The results of thin section point counting (n = 300 - 800) can only be consistently repeated for samples of fine- and medium-grained, centimetre-scale matrix and leucosome. The consistency of garnet:leucosome ratios between zones of a coarse-grained, metre-scale leucosome (Fig. 5.12), suggests that large sample populations produce reasonably accurate estimations with low error. Tests were not repeated for stained rock slab point counting (n = 1000 - 5000). It is suggested that this technique, intermediate in scale between the other two methods, produces estimates of modal proportions that are sufficiently representative for the purposes of mass and volume balance calculations (Appendix 3). The efficiency of individual estimations is vastly improved by selecting point count intervals that are equal to the average grain size of the finest grain size mineral or component to be included in the estimate.

APPENDIX 3 MASS AND VOLUME BALANCE CALCULATIONS

This Appendix sets out the method of balancing the biotite dehydration and dehydration melting reactions for natural mineral compositions in four rocks, respectively with granitic (FB48, FB256) and peraluminous (FB266A, DWN673) bulk compositions. The results are discussed in section 5.5 and, for dehydration melting, represented on Figs. 5.13a, b. These results are representative of calculations performed on other rocks.

Assumptions and Constraints

a) The natural mineral compositions used are listed in Appendices 1C, 1E, 1L and 1M. Minor components Ti, Mn and Fe^{3+} are not considered. The modal abundances of each rock are shown on Table 7.

b) H_2O-CO_2 fluid mixtures are considered ideal and are estimated for the two bulk compositions from Figs. 5.7 and 5.10, respectively, at the appropriate P-T conditions.
H_2O density = 0.7 gcm^{-3} and CO_2 density = 0.9 gcm^{-3}.

c) Liquid composition is assumed constant, except for water content. For melting in granitic compositions, the liquid composition is estimated from the following sources:

Brown and Fyfe (1970), Gupta and Johannes (1982), Grant (1985a, b) and Pitcher (1983).

For melting in peraluminous compositions, liquid composition is estimated from:

Clemens and Wall (1981), Clemens and Vielzeuf (1987) and Keppler (1989).

Liquid compositions are calculated on the basis of 10 oxygen units. Water contents of the liquids are taken from Johannes (1985, Fig. 2.3). Liquid density = 2.2 gcm^{-3}.

d) Molar volumes of all minerals from, Robie et al. (1978), are:

biotite = 300 cm^3mol^{-1}, garnet = 115 cm^3mol^{-1}, K-feldspar = 109 cm^3mol^{-1}, plagioclase = 100 cm^3mol^{-1}, orthopyroxene = 64 cm^3mol^{-1}, sillimanite = 50 cm^3mol^{-1}, and quartz = 23 cm^3mol^{-1}.

Liquid molar volume is estimated at 150 cm^3mol^{-1}.

e) Fe-Mg exchange is ignored.

f) Molecular H_2O (=OH) in 22 oxygen unit biotite is calculated using the expression

$$(F + OH) = 4.$$

g) Sillimanite composition is estimated as pure Al_2SiO_5 with 5 oxygens per unit formula.

APPENDIX 3A BIOTITE DEHYDRATION IN FB48

FB48 is a biotite-orthopyroxene leucoparagneiss without leucosomes. FB1 is an adjacent Bt-Opx gneiss with abundant orthopyroxene. The following dehydration reaction was responsible for the transformation of matrix biotite in FB48 to matrix orthopyroxene in FB1.

	Bt	+ Qtz	+ Pl	= Opx	+ Kfs	+ V	+ residuals
Si	5.63	1.00	2.77	1.93	3.02	-	-0.01
Al	2.48	-	1.26	6.09	1.00	-	+0.18
(Fe+Mg)	5.13	-	-	1.93	-	-	-
Ca	-	-	0.28	0.01	0.005	-	-0.01
Na	0.16	-	0.57	-	0.08	-	+0.04
K	1.82	-	0.02	-	0.83	-	-
OH	2.68	-	-	-	-	2.00	-

Mass balance factors (mole coefficients)

1.00	5.80	0.11	2.66	2.19	1.34

Predicted volume balance (percent consumed or produced)

10.0%	4.4%	0.2%	5.7%	4.6%	1.7%

Predicted volume decrease by this reaction = 0.4%.

The predicted volume balance of the reaction is applied to the modal analysis A of Opx-poor gneiss FB48. The predicted result of partial dehydration is compared with the modal analysis C of adjacent Opx-rich gneiss FB1.

	A	B	C (volume %)
Bt	6.5	5.2	5.7
Opx	tr	0.7	0.7
Qtz	27.1	26.5	31.2
Pl	37.9	38.0	33.0
Kfs	25.9	27.0	28.3
Mag	2.6	2.6	1.1

APPENDIX 3B BIOTITE DEHYDRATION MELTING IN FB256

FB256 is a biotite-orthopyroxene leucoparagneiss with leucosomes. The following vapour-absent melting reaction was responsible for the migmatization of its biotite-rich matrix to form orthopyroxene-bearing leucosomes.

	Bt	+ Qtz	+ Pl	= Opx	+ Kfs	+ L	+ residuals
Si	5.60	1.00	2.70	1.95	3.00	4.09	-
Al	2.46	-	1.30	0.077	1.00	0.89	-0.22
(Fe+Mg)	5.04	-	-	1.29	-	1.09	-0.11
Ca	-	-	0.33	-	-	0.054	-0.02
Na	0.025	-	0.62	-	0.14	0.35	-0.59
K	1.79	-	0.024	-	0.85	0.41	-0.03
OH	2.30	-	-	-	-	1.33	-

Mass balance factors (mole coefficients)

1.00	9.58	0.28	2.53	1.31	1.73

Predicted volume balance (percent consumed or produced)

10.0%	7.3%	0.9%	5.4%	4.8%	8.6%

Predicted volume increase by this reaction = 2.9%

The predicted volume balance is applied to the modal analysis A of a biotite-rich matrix portion of this rock. The predicted result of dehydration melting after crystallization B is compared to the modal analysis C of an orthopyroxene-bearing leucosome in the rock. The result is also shown on Fig. 5.13a, showing relative gains and losses.

	A	B	C (volume %)
Bt	9.8	3.1	3.1
Opx	0.4	4.0	6.2
Qtz	47.2	44.8	44.8
Pl	27.4	27.3	29.0
Kfs	13.0	18.6	14.8
Mag	2.2	2.2	2.1

APPENDIX 3C BIOTITE DEHYDRATION IN FB266A

FB266A is a garnet-biotite aluminous quartzofeldspathic gneiss without coarse-grained leucosomes. Garnet occurs in anhydrous compositional bands, as in FB266B, adjacent to fine- and medium-grained biotite-rich compositional bands. The presence or absence of sillimanite (section 5.4.3) in certain compositional bands largely controlled the dehydration of biotite-rich horizons similar to FB226A to form anhydrous bands abundant in garnet such as FB266B by the reaction:

	Bt	+ Qtz	+ Pl	+ Sil	= Grt	+ Kfs	+ V	+ residuals
Si	5.57	1.00	2.73	1.00	2.96	3.00	-	-
Al	2.74	-	1.27	2.00	2.05	1.00	-	-
(Fe+Mg)	5.02	-	-	-	2.88	-	-	-
Ca	-	-	0.31	-	0.034	-	-	+0.06
Na	0.022	-	0.63	-	-	0.17	-	-0.21
K	1.87	-	0.025	-	-	0.81	-	+0.22
OH	2.30	-	-	-	-	-	2.00	-

Mass balance factors (mole coefficients)

1.00	3.88	0.19	1.31	1.74	2.04	1.15

Predicted volume balance (percent consumed or produced)

10.0%	3.0%	0.6%	2.2%	6.7%	7.4%	0.5%

Predicted volume decrease by this reaction = 7.5%

The predicted volume balance is applied to the modal analysis A of biotite-rich horizon FB266A. The predicted result of complete dehydration B is compared to the modal analysis C of adjacent, anhydrous, garnet-rich horizon FB266B. Note that the 'negative' quantity of sillimanite in B refers to the amount consumed with 15.0% biotite in FB266A to produce 16.1% garnet in the model. Quartzofeldspathic metapelite horizons with <5% sillimanite are common in supracrustal packages metamorphosed in the amphibolite facies of the western Bushmanland Subprovince (e.g. Moore, 1986; Waters, 1986a; McStay, in prep.).

	A	B	C (volume %)
Bt	15.0	0.0	0.0
Grt	0.0	10.2	9.4
Sil	0.0	(-3.3)	0.0
Qtz	40.0	34.5	35.4
Pl	17.0	16.1	17.1
Kfs	28.0	39.2	38.1

APPENDIX 3D BIOTITE DEHYDRATION MELTING IN DWN673

DWN673 is a garnet-biotite metapelitic gneiss with numerous, ovoid centimetre-scale garnet-rich leucosomes that truncate the biotite-rich rock matrix. Some of the garnet poikiloblasts are embayed by coarse-grained skeletal biotite-quartz intergrowths, reflected in modal analysis C below. The following vapour-absent melting reaction (involving sillimanite in a precursor assemblage) was responsible for the migmatization of certain biotite-rich matrix portions of DWN673 to form the garnet-rich leucosomes.

	Bt	+ Qtz	+ Pl	+ Sil	= Grt	+ Kfs	+ L	residuals
Si	5.48	1.00	2.71	1.00	2.95	3.00	3.79	-
Al	2.67	-	1.28	2.00	2.04	1.00	0.76	-0.01
(Fe+Mg)	4.84	-	-	-	2.84	-	0.08	-
Ca	-	-	0.32	-	0.13	0.012	0.06	-0.01
Na	0.034	-	0.66	-	-	0.17	0.30	+0.01
K	1.83	-	0.01	-	0.051	0.81	0.31	-
OH	2.29	-	-	-	-	-	1.87	-

Mass balance factors (mole coefficients)

1.00	5.53	0.95	1.07	1.67	1.70	1.22

Predicted volume balance (percent consumed or produced)

10.0%	4.2%	3.2%	1.8%	6.4%	6.2%	6.1%

Predicted volume decrease by this reaction = 2.7%

The predicted volume balance is applied to the modal analysis A of biotite-rich matrix metapelitic gneiss DWN673. The predicted result of partial dehydration melting after crystallization B is compared to the modal analysis C of a garnet-rich leucosome in DWN673. The 'negative' sillimanite abundance refers to the amount that would react with 17.0% matrix biotite to form 10.5% garnet and the leucosome assemblage in the model. Retrograde, skeletal biotite constitutes 13.3% of the leucosome assemblage. The model does not account for this amount.

	A	B	C (volume %)
Bt	19.0	2.0	2.1 (+13.3 skeletal)
Grt	0.0	10.5	18.5
Sil	0.0	(-3.0)	0.0
Qtz	34.5	32.0	33.2
Pl	33.0	30.1	8.7
Kfs	12.2	25.4	23.5
Mag	1.3	0.0	0.7

Appendix 4

4A

Abstract (Baars, 1988) of oral and poster presentation at the 7th International Gondwana Symposium, Sao Paulo, Brazil, 19 July 1988

PARTIAL MELTING IN SUPRACRUSTAL AND GRANITIC GNEISSES OF THE CENTRAL NAMAQUALAND METAMORPHIC COMPLEX, SOUTH AFRICA.

Frankie J. Baars, Department of Geology and Mineralogy, University of Cape Town, Rondebosch, 7700, South Africa.

The Bushmanland Subprovince of the Namaqua Province comprises narrow E-W trending belts of supracrustal gneisses (age 1.7 Ga), set in granitic gneisses of varying ages. The complex displays an isobaric thermal zonation pattern of a central granulite facies core zone (200 km wide), flanked to the North and South by amphibolite facies rocks. There is good field evidence for a peak metamorphic (age 1.2 - 1.1 Ga) partial melting event in granulite facies granitic, pelitic, and mafic gneisses. Temperature estimates for this zone are well constrained by mineralogic thermometry at between 770 and 820^{o}C. Mineralogic pressure calibrations are consistent around 4.0 - 5.0 kbar (15 - 20 km depth) for the entire region.

The initial stages of migmatization are expressed in outcrop as discordant quartzofeldspathic patches, often with a significant ferromagnesian mineral content. Textural analysis and mineral

chemistry suggest that dehydration melting locally produced small amounts of water-undersaturated silicate liquid and crystal solids. The degree of partial melting was limited by the amount of water available from the dehydration of amphibolite facies minerals. The melt-rock residue system was closed with respect to all major oxides, except H_2O and often K_2O.

Supercritical H_2O from the supracrustal gneisses that was channelled along pre-existing structural discontinuities was responsible for intense local migmatization. This is represented by a wide compositional range of granitic sills and dykes. Viscous, water-undersaturated silicate melt movement along these channelways was limited.

Major, repeated episodes of crustal reworking, under the influence of a high geothermal gradient and local fluid activity gradients, produced a wide chronologic and mineralogic variety of granitic augen and migmatitic gneisses in the Proterozoic crust of Central Namaqualand. The absence of any major retrograde metamorphism with respect to all migmatization phenomena suggests that H_2O was ultimately lost to presently eroded upper crustal levels.

WATERS, D. J., University of Cambridge, Cambridge, U.K.

Baars FJ Univ. Cape Town

Melt Extraction from Granulite Facies Migmatites

Migmatitic rocks in granulite facies terrains commonly consist of coarse anhydrous patches, stringers or vein networks (mobilizates) in a finer-grained, foliated matrix. We interpret these features as the result of incongruent dehydration melting reactions (Waters, 1988). The mobilizates do not represent the composition of segregated melt, but rather represent varying proportions of (i) melt, (ii) solid products of incongruent melting and (iii) excess phases not consumed during the reaction. In metapelites and biotite gneisses, where the near-solidus melt composition is granitic and its water content can be estimated as a function of T, the melting reactions can be balanced and relative volumes of product phases predicted.

We have compared the calculated products with the observed distribution and abundance of phases in granulite facies migmatites from Namaqualand, South Africa. At the amphibolite-granulite transition (c.750 °C), the modal composition of mobilizates indicates that 10–15 vol% melt was produced, but was not extracted from its site of generation. At higher grade (≥ 800 °C) some mobilizate patches are dominated by solid products (e.g. garnet, K-feldspar) implying the loss of 10–20 vol% melt. The existence within a small outcrop area of an apparently complete gradation from garnet-or pyroxene-rich patches to elucogranitic stringers and sheets suggests the the extracted liquid has not migrated far.

A second set of predictions follows from an estimation of the physical properties of water-undersaturated silicic melts. The dihedral angle for melt in a quartzofeldspathic aggregate is probably less than, though close to, 60°. Therefore, if textural equilibrium is approached, the melt phase should be interconnected. The efficiency of melt extraction will be critically dependent of the viscosity of the melt (McKenzie, 1985; Wickham, 1987). Calculated values for the water-undersaturated case are several orders of magnitude greater than those for water-saturated melts, and fall in the range 10^6 - 10^8 Pa.s. These values correspond to a length scale for compaction on the order of centimetres, which is similar to that of the mobilizates, but imply a long time scale of 10 - 1000 Ma. In the absence of deformation, short-range controls such as the minimization of surface energy may determine the distribution of the melt phase. If this is the case, the matrix regions are predicted to contain a few percent melt in an equilibrium distribution along grain boundaries, while the mobilizates contain pooled excess melt.

Many, but not all, of these predictions are supported by the observations on natural rocks. The solid products of incongruent melting are concentrated in the mobilizates, and are not distributed through the rock. Commonly, evidence suggests that mobilizates develop along compositional or structural inhomogeneities in the rock. For example, at the granulite transition, small mobilizates appear to have nucleated on pre-existing matrix garnets. These features indicate that melt is generated within, and is perhaps confined to, the mobilizate volumes. The matrix regions of rocks are texturally similar to their amphibolite facies equivalents, and give no indication that the melt has penetrated the grain boundary network outside the mobilizates. Possibly, textural equilibrium is not achieved on the time scale of the melting event, or else the true dihedral angle is greater than 60°. Elsewhere, some mobilizate follow earlier fabric elements, or are aligned in the hinge zones of decimetre-scale crenulations and in minor shear zones. The structural control of mobilizates, particularly those with more leucocratic compositions, suggests that melt extraction is assisted by deformation or tensional fracturing. In summary, field evidence suggests that some mobilizates represent sites of melt generation, while others represent structurally controlled zones where melt has locally accumulated.

Amphibolite facies migmatites, in contrast, commonly show leucosomes whose compositions are similar to minimum melts, and are markedly different to the matrix (palaeosome) composition. A melanosome is commonly also present. These features imply a much more efficient separation of solids from melt at low melt fractions, consistent with the lower viscosity predicted for melts nearly saturated in H_2O.

We conclude that water content has a critical effect on the viscosity (and/or possibly the dihedral angle) of siliceous melt, so that small melt fractions are even less likely to be extracted from partially melted granulite facies rocks at about 800 °C than from amphibolite facies migmatites. Large, mobil magma bodies will result only when the melt fraction becomes large enough to cause disaggregation and convective instability of the whole rock mass. A higher melt fraction may result from higher temperature, a higher initial proportion of hydrous minerals, or an external source of H_2O. In the case of Namaqualand, the region of magma generation lay at hotter, deeper levels in the crust. The magmas are represented in part by late-tectonic, approximately synmetamorphic granitoids, which intrude the migmatites, and which probably assisted in the transfer of heat to the exposed levels.

REFERENCES

McKenzie, D. p., 1985, Earth Planet Sci Lett 74: p. 81–91.
Waters, D. J., 1988, J. Metamorphic Geol. 6: p. 387–404.
Wickham, S. M., 1987, J. Geol Soc London 144: p. 281–297.

STOP PRESS: Paul Whelan and Charles Basson are thanked for their efforts and assistance with production.